Sandstone reservoir quality: assessing the negative and positive controls: a study of the eodiagenetic Corallian sandstones of the Weald Basin

A thesis submitted in partial fulfilment of the requirements for the degree of Doctor of Philosophy at the University of Liverpool

School of Earth Ocean and Ecological Sciences by

Dinfa Vincent Barshep

January 2022

Dedication

For my late Mum and Dad.

Declaration

I declare that this thesis, which I submit for the degree of Doctor of Philosophy at the University of Liverpool, is my work, except where acknowledgment is made in the text, and not substantially the same as any work which has previously been submitted at this or any other institution for any degree, diploma or other qualification.

Note on publications included in this thesis

At the time of submission, two chapters of this thesis have been published in peer-reviewed journals and one chapter has been submitted for peer review and publication.

Chapter 3: Hinterland environments of the Late Jurassic Northern Weald Basin, England.

This chapter has been prepared for publication in the Journal of The Geological Society of London**.**

Chapter 4: This chapter has been published in the journal Marine and Petroleum Geology: Barshep, D.V., Worden, R. H. 2022. Reservoir quality and sedimentology in shallow marine sandstones: Interplay between sand accumulation and carbonate and clay minerals. *Marine and Petroleum Geology*, **135**, 105398,

http://doi.org/https://doi.org/10.1016/j.marpetgeo.2021.105398.

Chapter 5: This chapter has been published in the journal Geosciences. Barshep, D.V.; Worden, R.H. Reservoir Quality of Upper Jurassic Corallian Sandstones, Weald Basin, UK. *Geosciences* **2021**, *11*, 446, https://doi.org/10.3390/geosciences11110446

All work presented in this thesis is the author's original contribution.

January 2022

Abstract

Shallow marine sediments are at the transient boundary between continent and ocean and are affected by an interplay of mechanisms that control sediment deposition including tectonism, relative sea level rise and climate. Consequently, shallow marine environments present varied sedimentological, mineralogical, and stratigraphic properties which makes reservoir quality prediction challenging. Assessment of diagenetic controls and their interlinking relationships is important for effective reservoir quality prediction hence in this study, shallow marine Corallian sandstone reservoir rocks from Palmers Wood and Bletchingley fields were investigated to understand the controls on porosity and permeability (reservoir quality). This study involves wireline analysis, core analysis, sedimentary core log analysis, optical petrography, SEM-EDS analysis and geochemical analysis techniques to understand the provenance, depositional and diagenetic controls on reservoir quality. The results show that these shallow marine sandstones have low evidence of compaction but low to moderate porosity for their relatively shallow burial depths of less than 1700m during their maximum burial. Their porosity ranges from 0.8 to 30% (average of 12.6%) and permeability range from 0.01 to 887 mD (average of 31 mD). The Corallian sandstones also show a unique composition of medium to coarse grained siliciclastic sandstones with abundant bioclasts and Fe-ooids deposited during a tectonic active phase undergoing sea level rise. Provenance analysis revealed a mixed mafic-felsic provenance which supplied sediments extensively enriched in quartz and Fe by sedimentological processes especially hydrological sorting. Tectonism influenced water depth, controlled the quantity of detrital bioclasts and the resulting calcite cement and clay matrix distribution. Early bioclast-derived calcite cement retarded compaction and together with calcite from organically derived CO_2, is the dominant cause of porosity loss. Other cements include berthierine, pyrite, siderite, dolomite, apatite, illite, kaolinite and quartz. The reservoir quality of the Corallian sandstones have no significant depositional controls; reservoir quality was reduced by cementation and pore-filling clays, locally preserved by authigenic quartz-inhibiting berthierine grain coats and enhanced by detrital grain dissolution as well as cement dissolution. Reservoir quality in the Corallian sandstones can therefore be predicted by considering abundance of calcite cement, pore-filling clay and Fe-clay coats. This research presents a potential first sandstones reservoir quality study in the Palmers Wood and

Bletchingley which are relatively poorly studied hence paucity of data to predict reservoir quality away from wells. This study can be used to understand eodiagenetic conditioning of sediments for mesodiagenetic processes such as chlorite grain coats formation from berthierine as these sandstones straddle the conditions between surface controls on eodiagenesis and mesodiagenesis.

Acknowledgements

Firstly I would like to say a big thank you to my supervisors Professors Richard H. Worden (primary supervisor), Dan Faulkner (secondary supervisor), and Dr. Pete Armitage (industry supervisor). I remember my first month as a PhD student, Richard told me “do not believe everything you read just because it is published, think about it and decide for yourself if it makes sense”. These words have stayed with me throughout my studies and Richard has patiently guided me to value critical thought, precise analysis and clear and concise communication of results. On a personal note, Richard was patient with me when I had to work to support myself during my studies and helped me through the challenges that came with combining work and research. I am eternally grateful to Richard and hope that someday I will be a great mentor to someone as Richard is to me. I would like to thank Professor Dan Faulkner for teaching me the fundamentals of rock deformation and granting me precious time on his rigs in the Rock Deformation Laboratory. I would like to thank Dr. Pete Armitage for providing core plugs from BP’s tight gas project in Wamsutter and supporting data. Though my project has evolved in a way that has not involved much rock deformation analysis, I have learnt a lot from Dan and Pete and will forever be grateful to them.

Special thanks to my sister Yahkat Barshep who always believed in me even when I doubted myself: you are my greatest inspiration. Many thanks to my sisters Bolcit, Byencit, Yacit and Julbyen as well as my brother Jidiya and my niece Freda for their support. I would especially like to thank my stepmother Mrs. Nancy Barshep who raised me as her own and ensured I was raised in a healthy and stable environment.

I like to thank Dahiru Muhammad and Naboth Simon for their constructive discussions during my studies. I would also like to thank Dr. Auwalu Yola Lawan for the numerous journals. I thank James Utley for his support with analysis and Gary for maintaining the rigs I worked with in the Rock Deformation Laboratory. I would like to thank Michael Allen and John Bedford for teaching me how to use the rigs in the Rock Deformation lab and showing me how to analyse my data. I would like to thank Maggie Williams, Rob Duller, Liz Rushworth and Charlotte Jefferey for always being available to discuss sedimentology during our teaching sessions as well as regarding my research.

I would also like to appreciate the Petroleum Technology Development Fund (PTDF) for sponsoring this research.

Table of contents

List of Figures

Figure 3.8: (a) QtFL plot for PW7, PW3 and BL5 showing the relative proportion in percent of total detrital quartz (Qt), feldspars (F), and lithic grains (L). The plot shows a dominant quartz –rich lithology for the sandstones with minor feldspars and lithic grain fragments. This is indicative of a mature sediment source typical of long sediment transport and/or reworked sediments which has undergone intense hydrologic sorting. (b) QmFL compositional plot of the Corallian sandstones: after Dickinson 1985 to show source-area tectonic setting. Monocrystalline quartz shows a dominant proportion above 60% relative to feldspars and lithic grain components (Igneous +sedimentary +metamorphic rock fragments). The sample points plot dominantly in the quartzose recycled orogen region with BL5 having more monocrystalline quartz than PW3 and PW7. Sandstone package BL5-3 has more feldspars and clusters close to the craton interior orogen. (c) The lithic fragments plot dominantly in the metamorphic zone (>90%) with minor sedimentary clasts (<5%) and no igneous grains. The dominance of quartzose sediments and low feldspar content suggests an intensely weathered hinterland. 59

Figure 3.9: Boxplots for selected point count data for the Corallian sandstones (a) shows box plots for grain size measured from point counting analysis with grain sizes highlighted according to the Wentworth (1922) scale. The plots show medium-grained fractions in PW7-1 to PW3-2 and finer-grained fractions in BL5-1 to BL5-3 (b) shows more monocrystalline quartz in BL5-1 to BL5-3 with the highest occurrence in BL5-1 (c) shows less polycrystalline quartz in BL5-1 to BL5-3. 63

Figure 3.10: Boxplots of SEM-EDS mineralogy for the Corallian sandstones as a function of sand packages. The plots have been normalised for porosity, bioclasts and diagenetic components: calcite, siderite, dolomite, Fe-dolomite and pyrite with the detrital grain percentages expressed in the boxplots. (a) Shows high quartz content from ~65% to ~97% with sand packages BL5-2 and BL5-3 having the least sand content. (b) and (c) show K-feldspar and plagioclase feldspar respectively with BL5-2 and BL5-3 showing the highest feldspar content. (d) Shows trace amounts of zircon in PW7-1 to PW3-1 with increase in PW3-2 and the highest content in BL5-1, BL5-2 and BL5-3. Rutile shows varied levels in the sand packages with BL5-1, BL5-2 and BL5-3 showing the highest quantity of rutile. (e). Illite (f) and muscovite (g) shows the highest content in BL5-2 with lesser content in BL5-3, BL5-

List of tables

Chapter 1: Introduction

1.1 Project context

Sandstone porosity and permeability (reservoir quality) determine the amount of fluid a rock can store and the rate at which the rock will allow the fluid to flow (Bloch 1994; Gluyas & Swarbrick 2004). Reservoir quality is critical to the success of many geoscience and engineering applications including Carbon Capture and Storage (CCS), hydrocarbon exploration, groundwater development, geothermal exploration, waste management design, earthquake studies and other environmental management applications, such as slope stability and dewatering analysis. In hydrocarbon exploration, reservoir quality is important throughout the life cycle of a field from basin modeling, exploration, appraisal and field development, hence reservoir quality is a key risk factor in the viability of any hydrocarbon prospect (Taylor et al. 2010; Worden et al. 2018c). It is therefore important to understand the factors that control reservoir quality as this will enable accurate pre-drill prediction of porosity and permeability in sandstone reservoirs (Bloch 1994; Byrnes 1994; Kupecz et al. 1997a).

The factors that control reservoir quality can be broadly divided into depositional characteristics: e.g. provenance inherited mineralogy, texture and depositional environment and diagenetic (post-depositional) factors (Scherer 1987). Diagenesis involves a variety of physical chemical and biological changes that cause a primary sedimentary assemblage to approach chemical and textural equilibrium with their ambient environment through burial (Burley & Worden 2003a). Many studies of reservoir quality have identified diagenetic factors such as calcite cement, clay coats, quartz overgrowth, micro-quartz, compaction, detrital clay, grain dissolution and grain replacement as factors that could destroy, enhance or preserve reservoir quality (Wilson 1994; Kupecz et al. 1997b; Burley & Worden 2003a; Worden et al. 2018c). These factors are subject to interdependent controls including sediment provenance, depositional environment, rate of burial, depth of burial, material flux, effective stress, geothermal gradient and fluid pressure (Morad et al. 2013; Worden et al. 2018c). Hence diagenesis represents a continuum of processes from deposition through to maximum burial, with depositional environment and provenance being especially important in shallow buried sandstones that have not been significantly buried (Worden et al. 2018d). Assessment of conditions under which diagenetic processes occur, and any interlinking relationship, is critical

in advancing reservoir quality prediction (Taylor et al. 2010). As diagenesis is a continuum from depositional to maximum burial processes, shallow burial diagenesis (eodiagenesis) plays a pivotal role in conditioning sediments for deep burial diagenesis (mesogenesis).

The carbonate community has widely acknowledged the importance of eodiagenetic processes in conditioning sediments for mesodiagenesis with the sandstone community taking longer to acknowledge processes that condition sediments before mesodiagenesis (Worden et al. 2018d). There is increasing interest in how sandstones are conditioned before mesodiagenesis e.g. the formation of grain coating clays (Daneshvar & Worden 2017; Wooldridge et al. 2017) with increasing acknowledgement of the importance of studying how sediments are conditioned before deep burial (Griffiths et al. 2018; Griffiths et al. 2019a; Worden et al. 2020b) there is need for more studies to investigate how sediments are altered during eodiagenetic.

In addition clastic and carbonate reservoir quality prediction has been undertaken by different communities with many assumptions from both communities that contradict each other (Worden et al. 2018c). Mixed carbonate-clastic systems such as the study area here provides opportunities to bring these communities together to identify overlaps and advance reservoir quality prediction for carbonate, clastic and unconventional systems (Worden et al. 2018c).

A full understanding of the controls on reservoir quality with a view to the pivotal role of shallow buried rocks will therefore involve a non-routine approach of integrating depositional and stratigraphic controls (Griffiths et al. 2019c; Henares et al. 2020) to a more traditional approach involving petrography, wireline analysis and geochemistry to predict reservoir quality. This thesis investigates the relative importance of depositional and diagenetic factors in the reservoir quality evolution of shallow-marine, shallow buried, Corallian sandstones of the Weald Basin, UK. This study will take the non-routine approach of linking sedimentology and sequence stratigraphy with transport systems and diagenesis (Caracciolo 2020; Henares et al. 2020). This research focuses on the Upper Jurassic Corallian sandstones of the UK's Weald Basin via study of the Palmers Wood and Bletchingley petroleum fields (Figs. 1.1 and 1.2). The two fields are potentially important as they are relatively close to populous parts of southeast England and may be re-purposed in the future for carbon-neutral development such as carbon capture and storage, compressed air storage or hydrogen storage. The Corallian sandstones in both fields are an example of eodiagenetic sandstones and are buried less than 1000 m but have relatively low porosity for their depths of burial. They are composed of

intensely cemented shallow marine, shallow-buried siliciclastic reservoir rocks hence they straddle conditions between surface controls on eodiagenesis and mesodiagenesis. The reservoir sandstones were deposited during an era of tectonic activity and sea level rise (Hawkes et al. 1998; Barshep & Worden 2021, 2022) and present a unique combination of petrophysical, eustatic, tectonic and burial conditions that makes them prime candidates to study the links between depositional and diagenetic controls on reservoir quality. Given the importance of these fields, there is no known research (apart from published work arising from this study) dedicated to the reservoir quality of the Corallian sandstones in the Weald Basin, and necessarily a paucity of data to predict reservoir quality away from the areas of well control.

1.1.1 Research questions

This thesis will specifically address the following research questions:

1. How did provenance affect the supply of siliciclastics in the Upper Oxfordian Weald Basin?
2. What are the controls on Corallian sediment transport, deposition and redistribution in the Weald Basin and how did this affect reservoir quality?
3. What were the consequences of syn-sedimentary tectonism on reservoir architecture and reservoir properties (especially porosity)?
4. What controls reservoir quality in these sandstones?
5. What are the key aspects of diagenesis to consider in assessment and prediction of reservoir quality in shallow buried, shallow marine siliciclastic rocks?

To answer the questions above this study will systematically:

1. Describe the source area for the Corallian sandstones.
2. Describe the depositional facies and depositional controls in the Corallian sandstones.
3. Describe the mineralogy and diagenetic relationships in the Corallian sandstones.
4. Describe the extent of depositional and diagenetic controls on reservoir quality.
5. Understand how the implications for the positive and negative effects of diagenesis on reservoir quality in these fields can be applied to similar reservoirs during exploration and development.

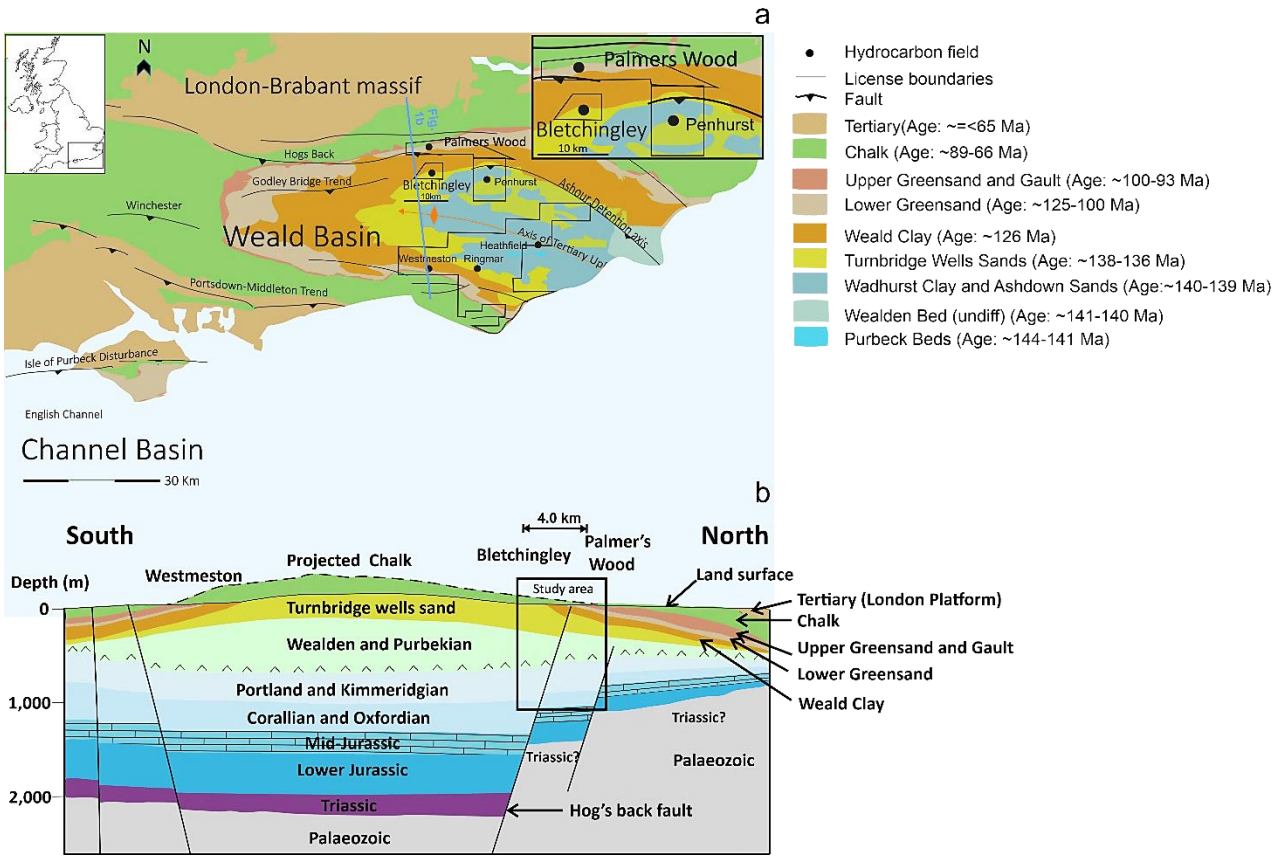

Figure 1.1: (a) Location map of the Weald basin showing selected hydrocarbon fields, structural features as well as surface geology. (b) Shows a schematic section of the Weald Basin highlighting the study area as well as subsurface geology (Barshep & Worden 2022) as modified from Butler & Pullan (1990); Trueman (2003a); Andrews (2014)

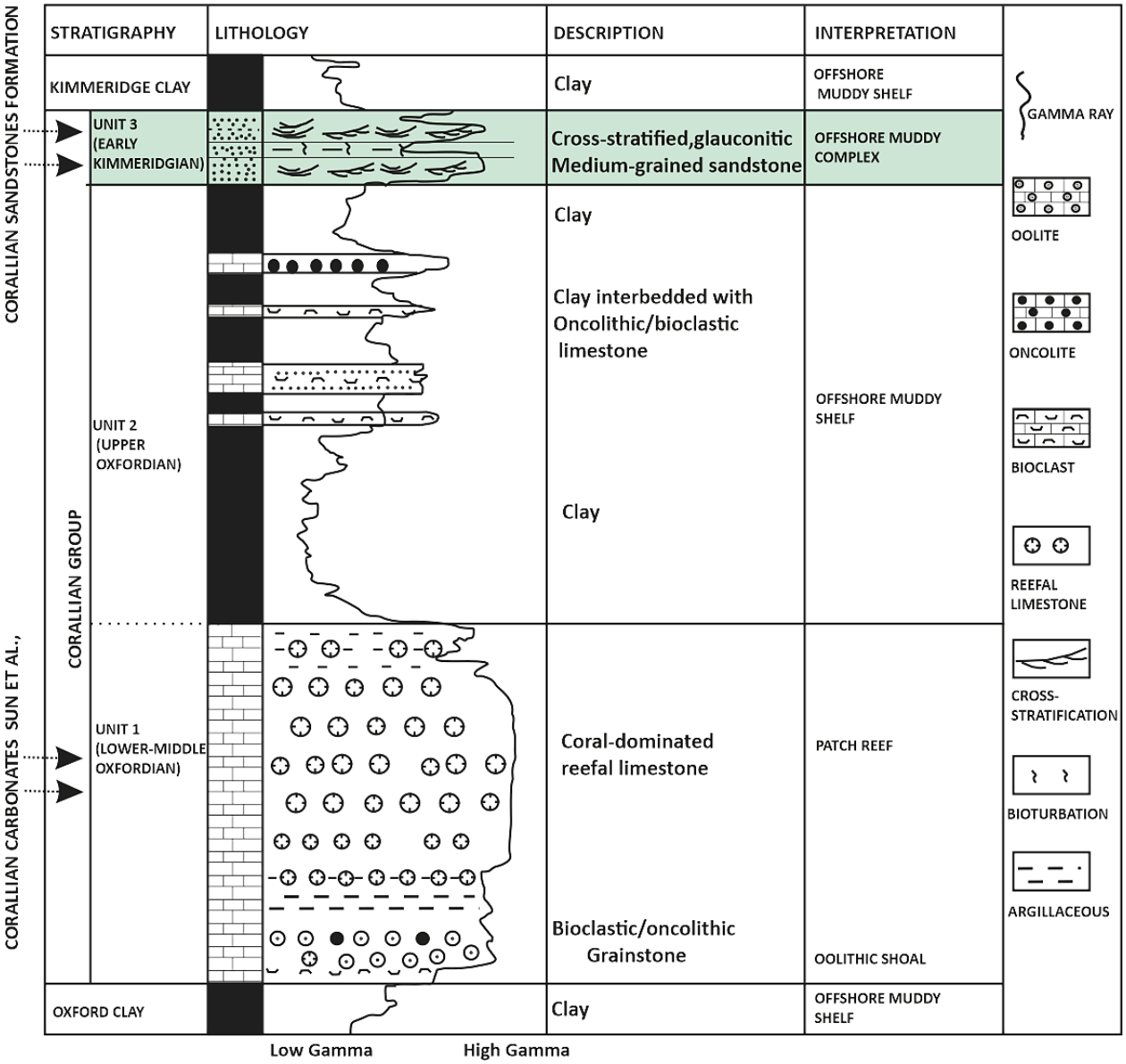

Figure 1.2: is a stratigraphic section of the Upper Jurassic Weald Basin showing the Corallian sandstones Barshep & Worden (2022): after Sun (1992).

1.1.2 Thesis structure

This thesis comprises six chapters. Chapter 1 is an introduction of the thesis aims and objectives as well as a general introduction of reservoir quality. Chapter 2 describes the materials and methods used in this study. Chapters 3 to 5 are presented as standalone chapters, two of which have been published and one already submitted for publication in a peer-review international journal. Each of chapters 3 to 5 has its own structure based on the requirements of the publishing/target international journal. The co-author for each of the articles presented in

chapters 3 to 5 is my primary supervisor, who has provided advice on project conceptualisation, design, scientific content, analysis and editorial guidance. I am the main author of the work presented in chapters 3, 4 and 5 and have carried out most of the primary data collection, analysis, interpretation and write-up.

Chapters 1-6 are described as follows:

- **Chapter 1** is a desk-based review of existing literature on sandstone reservoir quality. It introduces the fundamental factors and controls on reservoir quality. Chapter 1 also highlights the main objectives and research questions addressed in this study.
- **Chapter 2** is the experimental design and methods section which describes the analytical techniques applied in this study.
- **Chapter 3** describes the provenance of the Corallian sandstones outlining the palaeogeographic, palaeoclimatic and palaoetectonic as well as sedimentological influences on sediment accumulation. This chapter incorporated petrographic analysis, geochemical analysis, wireline analysis and core analysis. This manuscript is prepared for submission to the Journal of the Geological Society of London for peer-review and publication.
- **Chapter 4** applies sequence stratigraphic methods to link sedimentological controls to reservoir quality distribution in the Corallian sandstones. Chapter 4 is based on wireline analysis, facies analysis, petrographic analysis and interpretation of the depositional controls: eustasy, climate and tectonism. This Chapter is published in Marine and Petroleum Geology, https://doi.org/10.1016/j.marpetgeo.2021.105398.
- **Chapter 5** investigates depositional as well as diagenetic controls on reservoir quality of the Corallian sandstones. Chapter 5 analyses authigenic mineral development, diagenetic evolution and their overall effect on reservoir quality. Chapter 5 has been published in Geosciences, https://doi.org/10.3390/geosciences11110446.
- **Chapter 6** is a synthesis and discussion of the major research questions with key conclusions from this thesis.

1.2 Sandstone reservoir quality

1.2.1 Introduction

Sandstone reservoir quality is controlled by many sedimentary, depositional and diagenetic processes (Bloch & McGowen 1994; Burley & Worden 2003a; Ajdukiewicz & Lander 2010; Taylor et al. 2010). The sediment source area (hinterland) and transport characteristics controls the sediment mineralogy, grain size and texture (Bloch & McGowen 1994; Ajdukiewicz & Lander 2010). Initial porosity and permeability are determined by sediment grain size, sorting and matrix content, all controlled by the depositional conditions, and factors such as rate of overburden loading (Rahman & Worden 2016a). The initial porosity and permeability of deposited sediments is then modified through eodiagenesis and burial, controlled by the changing ambient conditions (Tucker 1985; Burley & Worden 2003a). Deposited sediments could have initial porosity of up to 40-50% and permeability of 10 to 2,000 Darcies; the porosity- and permeability-loss with burial may reflect depositional controls in some sandstones but may not reflect, or even reverse, depositional controls in others (Wilson & Stanton 1994). The different depositional controls on reservoir quality can therefore combine in different ways during burial to produce varied and sometimes unpredictable diagenetic end products. There is, however, some degree of agreement of how reservoir quality evolves under certain conditions, e.g., porosity loss with compaction (Gluyas & Cade 1997; Ramm et al. 1997a; Rahman & Worden 2016a), quartz cementation during burial (Walderhaug 1994a, b; Bjørkum et al. 1998b; Lander & Walderhaug 1999; Morad et al. 2000; Walderhaug 2000) and carbonate cementation (Scholle & Ulmer-Scholle 2003; Worden et al. 2019) as well as porosity-enhancement by unstable mineral dissolution (Surdam & Crossey 1985; Emery et al. 1990), porosity preservation by microquartz or clay coats (Pittman et al. 1992; Ehrenberg 1993; Aase et al. 1996; Worden & Morad 2000; Ajdukiewicz & Lander 2010), hydrocarbon emplacement (Worden et al. 2018a), as well as cement dissolution and replacement (Worden et al. 2019; Barshep & Worden 2021). All the factors listed above are controlled by one or more of provenance, depositional environment, structural evolution, fluid wettability, and diagenesis (Barclay & Worden 2000; Zhang et al. 2018). Of all the controls listed above, diagenesis plays a dominant role and will be discussed in a section of its own. The other factors are discussed below.

1.2.2 Provenance

The primary mineralogical compositions of sandstones in a basin is controlled by provenance and the weathering characteristics that evolve during transport from sediment hinterland to the site of deposition (Ingersoll 1990). Provenance can be understood and predicted using geochemical and mineralogical techniques (Potter 1978; Valloni & Maynard 1981; Nesbitt et al. 1996) with modal mineralogy commonly applied in many studies e.g. Dickinson & Suczek (1979); Dickinson (1985); Dickinson (1988);Milliman et al. (1975);Valloni & Maynard (1981);Blatt (1967). Provenance-controlled compositionally-driven differences, in turn, significantly influence how sandstone reservoirs behave under varied conditions e.g., burial, effective stress, fluid composition and fluid pressure (Dickinson & Suczek 1979; Tobin & Schwarzer 2013; Nguyen et al. 2016). Different provenances produce sediments of varied composition depending on primary mineralogy, tectonic setting and climate (Basu et al. 1975; Schwab 1975; Dickinson & Suczek 1979; Dickinson 1985; Dickinson 1988). These sediments will evolve within their depositional environment based on the inherited characteristics from their source-areas. An example come from Tobin & Schwarzer (2013), where provenance was used to interpret sediment transport fairways and also show how provenance-controlled compositional differences affected reservoir quality prediction under different effective and thermal stress conditions.

1.2.3 Primary depositional environment

Most reservoir properties, from large scale to small scale variations, can be traced to variations within the depositional environment (Bloch & McGowen 1994; Taylor et al. 2015). Different depositional environments have sand bodies with different compositional and textural properties as well as sedimentary structures (Ehrenberg 1997). In addition, with the exception of stable minerals, such as quartz, it is common for minerals in their primary depositional environment to be unstable under a range of oxidation states, temperature, pressure, water composition and pH from transport and depositional processes (Burley & Worden 2003a). Diagenetic alterations will thus commence on these sediments at the surface, within their depositional environment (Emery et al. 1990; Nguyen et al. 2016). These surface conditions ultimately prepare the sediment for later diagenetic alteration through burial (Bloch & McGowen 1994; Wooldridge et al. 2017).

1.2.4 Structural evolution

Structural deformation can cause syn-kinematic diagenesis which may improve or destroy reservoir quality (Johansen et al. 2005; Rice-Birchall et al. 2021). Indurated rocks subjected to mechanical stress are susceptible to fracturing and brecciation when mechanical stress exceeds rock strength (Herwanger et al. 2015) thereby altering their reservoir quality (Johansen et al. 2005; Zahm & Hennings 2009). Brittle rocks have high Young's modulus and low Poisson's ratio values; these rocks also typically have high quartz content and low ductile grain content e.g. clay mineral, content (Herwanger et al. 2015) and are not susceptible to plastic deformation (Zoback & Kohli 2019). Brecciation may be triggered along a fracture and increase reservoir quality (Kitamura et al. 2010). Conversely, shear stresses in sandstones can cause fine-grained gouge in the axis of a fault (Worden et al. 2018c). Thus rocks with a high natural fracture density will have a higher effective porosity and permeability. However, if mineralisation fills natural fractures, pores are sealed and pore connectivity reduced to result in poor reservoir quality (Worden et al. 2016). Pressure induced quartz diagenesis may also produce deformation bands along faults that can result in locally very low porosity (Johansen et al. 2005).

1.2.5 Fluid wettability

Wettability is the ability of a fluid to adsorb onto a solid surface in the presence of another immiscible fluid and is used to describe the affinity of a rock for water or oil (Crocker & Marchin 1988). By definition, this means that one liquid phase will preferentially adsorb or adhere to a solid surface at the expense of another liquid phase. Quartz cement is the major cause of porosity-loss in deeply buried sandstone reservoirs (Worden & Morad 2000; Nguyen et al. 2016). The rate of quartz development depends on the supply rates of silica, the transport rates of silica and the precipitation rate of quartz from silica on a nucleating surface (Worden et al. 1998; Barclay & Worden 2000; Walderhaug 2000). Oil wet grains will be preferentially coated with oil, hence aqueous phases rich in silica will not be able to precipitate quartz on their surface as the oil will hinder contact between the silica-rich fluid and grain surfaces (Worden et al. 1998; Barclay & Worden 2000). Conversely, if a water wet mineral grain has its surface coated with silica-rich fluid, quartz cement will be able to nucleate and develop on the grain surface (Worden et al. 1998; Barclay & Worden 2000; Worden & Morad 2000; Worden et al. 2018a).

1.3 Some applications of reservoir quality

Porosity and permeability apart from being important properties of rocks in hydrocarbon exploration can also play important roles in carbon capture and storage. Some applications of reservoir quality are outlined below:

Basin modelling: Porosity and permeability are critical for modelling flow and thermal conductivity in sedimentary basins (Waples 1998). Permeability is critical for modeling convective heat transfer, pressure regimes, flow rates and fluid migration pathways (Bloch 1994).

Calculation of hydrocarbon content using the volumetric method: Initial hydrocarbon-in-place is estimated by the volumetric method using porosity as an input.

$$0IP = 7758AhΦS_o \frac{1}{B_o} \qquad \text{(Bloch 1994)}$$

(Equation 1.1)

Where OIP is original oil in place in stock tank barrels (STB), 7758 is the number of barrels in 1 acre-foot, A is the reservoir area in acres, h is the average thickness of the reservoir in feet, Φ is the average reservoir porosity fraction, S_o is initial oil saturation fraction and B_o is the formation volume factor in bbl/STB.

For gas, the formula becomes:

$$GIP = 43560AhΦS_g\ 1/B_g \qquad \text{(Bloch 1994)}$$

(Equation 1.2)

Where GIP is original gas in place in standard cubic feet (SCF), S_g is initial gas saturation fraction and B_g is initial gas formation volume factor (ft^3/SCF).

Thermal conductivity: Thermal conductivity is both lithology- and porosity-dependent and typically has an inverse relationship with porosity (Goff et al. 1984; Bloch 1994). Thermal conductivity is also inversely proportional to thermal gradient for a given heat flow. Porosity input data are therefore important for the accurate estimation of rock temperature, organic matter maturation and hydrocarbon expulsion window (Goff et al. 1984).

Fluid migration: Basinal fluid movements are important for geological phenomena such as hydrocarbon migration as well as the mineralization, diagenesis and cementation of potential

reservoir units (Worden et al. 2016). Pore spaces in rocks are affected by a system of static and dynamic pressures that cause migration of petroleum (and other fluids) (Beckmann 1976). Accurate estimates of permeability are essential in modelling fluid movement from lower porosity source rocks to higher porosity reservoir rocks (Bloch 1994).

Carbon Capture and storage (CCS): The long-term effectiveness of geological storage of CO_2 depends on the integrity of caprocks to seal natural storage sites (Armitage et al. 2011; Worden et al. 2020a) as well as the storage characteristics of the reservoir rocks, the economic feasibility of the projects and the safety of the site over geologic time (Alcalde et al. 2021). CO_2 is buoyant relative to the dominant aqueous pore fluids, hence its migration is driven by capillary entry pressure, diffusion through fluid saturated pore space, permeability and relative permeability (Armitage et al. 2011). In the absence of tectonic deformation or seal rupture, CO_2 will travel through a reservoir by diffusion or when pore capillary entry pressure is exceeded and will breach the trapping structure unless it is trapped by caprock of significantly low permeability or relative permeability to hinder CO_2 migration (Armitage et al. 2011). Consequently, for any CCS site to successfully store CO_2 both the vertical and horizontal permeability of the trapping structure (s) must be low enough to prevent vertical or horizontal leakages from the storage site.

1.4 Diagenesis

Some of the most important physical processes in diagenesis are compaction and pressure solution but note that important chemical diagenetic processes include dissolution of unstable grains, precipitation of new minerals and replacement of grains by other minerals (Tucker 1981). Diagenetic processes start at the site of weathering and transport in the source-area, oxidation in the water column and compaction during burial (Fig. 1.4). Other early processes include biogenic alteration of loose sediments, water expulsion and cementation of grains at, or slightly below, the sediment-water interface with consequent porosity-loss (Boggs 2009b). Further diagenetic modifications with burial include formation of authigenic minerals such as calcite and quartz as well as dissolution of unstable minerals and grains (Boggs 2009b). Diagenetic alterations are primarily controlled by depth, temperature, fluid composition, mineral composition , and effective stress (Worden et al. 2018c), and will continue until the sediments reach the threshold of metamorphism (Fig. 1.3). Metamorphism commences at a broad temperature range of >180-250°C (Burley & Worden 2003a). The driving force for

diagenesis is the temperature-related instability of framework components, matrix and interstitial pore waters under dynamic temperature and pressure conditions (Wilson & Stanton 1994; Morad et al. 2000; Burley & Worden 2003a). The net result of diagenesis is the evolution of sediments from chemical and textural disequilibrium towards chemical and textural (e.g. compaction) equilibrium with their diagenetic environments (Boggs 2009b). During diagenesis, sediments will change their porosity, texture, strength and even bulk composition as they undergo post-depositional alteration (Pettijohn et al. 1973).

Several processes occur during diagenesis. These include the following: (i) Authigenesis: which is the in-situ mineral growth related or unrelated to lithification. (ii) Compaction: describes processes leading to the loss of pore space. Compaction can include physical reduction in pore-size from confining stress or chemical cementation. (iii) Cementation: which is the precipitation of minerals in pore spaces including both intergranular and intragranular pores with accompanying lithification. (iv)Dissolution: The disintegration of a mineral by interacting with a fluid (solute). (v) Dehydration: thermally induced loss of water in clays and organic matter. (vi) Decarboxylation: the thermally induced loss of CO_2 by organic matter. (vii) Neomorphism: the transformation of a mineral into its polymorph(s), involving the replacement and recrystallization of one mineral into another mineral of the same chemistry. (viii) Replacement: which occurs when a chemically-distinct mineral grows within a pre-existing mineral. (ix) Recrystallization: dissolution followed by precipitation of a specific mineral accompanied by changes in crystal size and habit. The above-mentioned processes occur during the three stages of diagenetic evolution of a sedimentary basin. These stages are divided into eodiagenesis, mesodiagenesis and telodiagenesis (Burley & Worden 2003a).

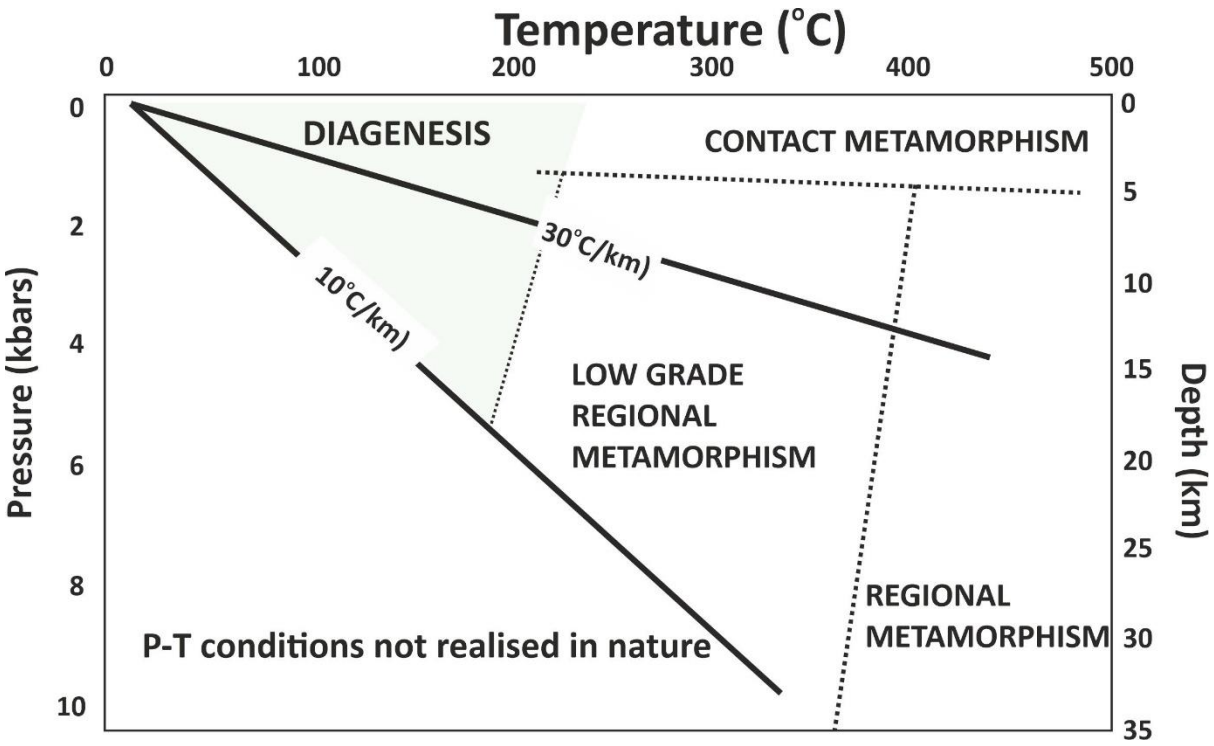

Figure 1.3: Temperature-pressure diagram showing typical geothermal and pressure gradients and how they relate to diagenesis and metamorphism (Modified from Burley and Worden 2003).

Eodiagenesis: Eodiagenesis, also known as early diagenesis or eogenesis, refers to diagenesis that occurs under the influence of surface pore waters and the depositional environment (Burley & Worden 2003a; Boggs 2009b) (Fig. 1.4). Eogenetic processes typically occur at temperatures less than about 60-70°C and at depths less than 1 to 2km (Worden et al. 2018c). The definition of eodiagenesis, with emphasis on 0 to 2 km depth is based on inferences to temperature and applies the geothermal gradient of 20 to 30°C for most basins thereby constraining eodiagenesis to 30 and 70°C (Morad et al. 2000). Definitions should however not rely heavily on maximum temperature of burial as diagenetic reactions are subject to kinetic controls and temperature boundaries for diagenetic regimes may not take into account the residence time of sediments within a temperature range (Burley & Worden 2003a; Ehrenberg et al. 2009). Eodiagenesis occurs as sediments attempt to reach physical and chemical equilibrium soon after initial depositional (Worden et al. 2018c). Despite attempts to constrain eodiagenesis by depth and temperature, authors such as Choquette & Pray (1970) suggested that the boundary between eodiagenesis and mesodiagenesis is not clear, but based the boundary on the occurrence of

mesogenetic alterations such as burial quartz cementation, stylotisation and clay mineral transformation reactions (Morad et al. 2000).

Eodiagenesis includes processes under the influence of continental weathering and soil development, as well as bioturbation and marine bacterially mediated reduction reactions (Burley & Worden 2003a; Boggs 2009b; Worden et al. 2018c). In marine environments, eodiagenesis may be characterized by oxidizing or reducing pore waters while non-marine environments may have arid-oxidizing or wet-reducing pore waters (Boggs 2009b). The influence of surface pore-water chemistry in eodiagenesis may extend from a few metres in low permeability rocks or one or two thousand metres in more permeable rocks, depending on the arrangement and permeability of aquifers as well as geometry and position of syn-sedimentary faults (Burley & Worden 2003a).

Eogenetic alterations in sediments are predominately controlled by depositional facies, detrital composition, climate, and relative sea level change (Morad et al. 2000). Important processes in continental eodiagenesis include development of calcrete, dolocrete, and silicate mineral alteration to form kaolinite and smectite (Morad et al. 2000). Under marginal marine and marine conditions eogenetic minerals include carbonates, Fe-clay silicates, opal, microquartz, sulphates and zeolite (Morad et al. 2000). Eodiagenesis is important as, during this stage, sediments are conditioned before the onset of mesodiagenesis (Morad et al. 2000; Worden et al. 2018c). Compaction starts during eodiagenesis as overburden thickness increases. Compaction involves conversion of random grain fabrics at the time of deposition, with porosity of about 48%, into rhombohedrally packed grain fabrics with a porosity of about 26%. Compaction can also include ductile compaction of weak grains, bending of plastic grains and grain fracturing. Compaction continues into mesodiagenesis.

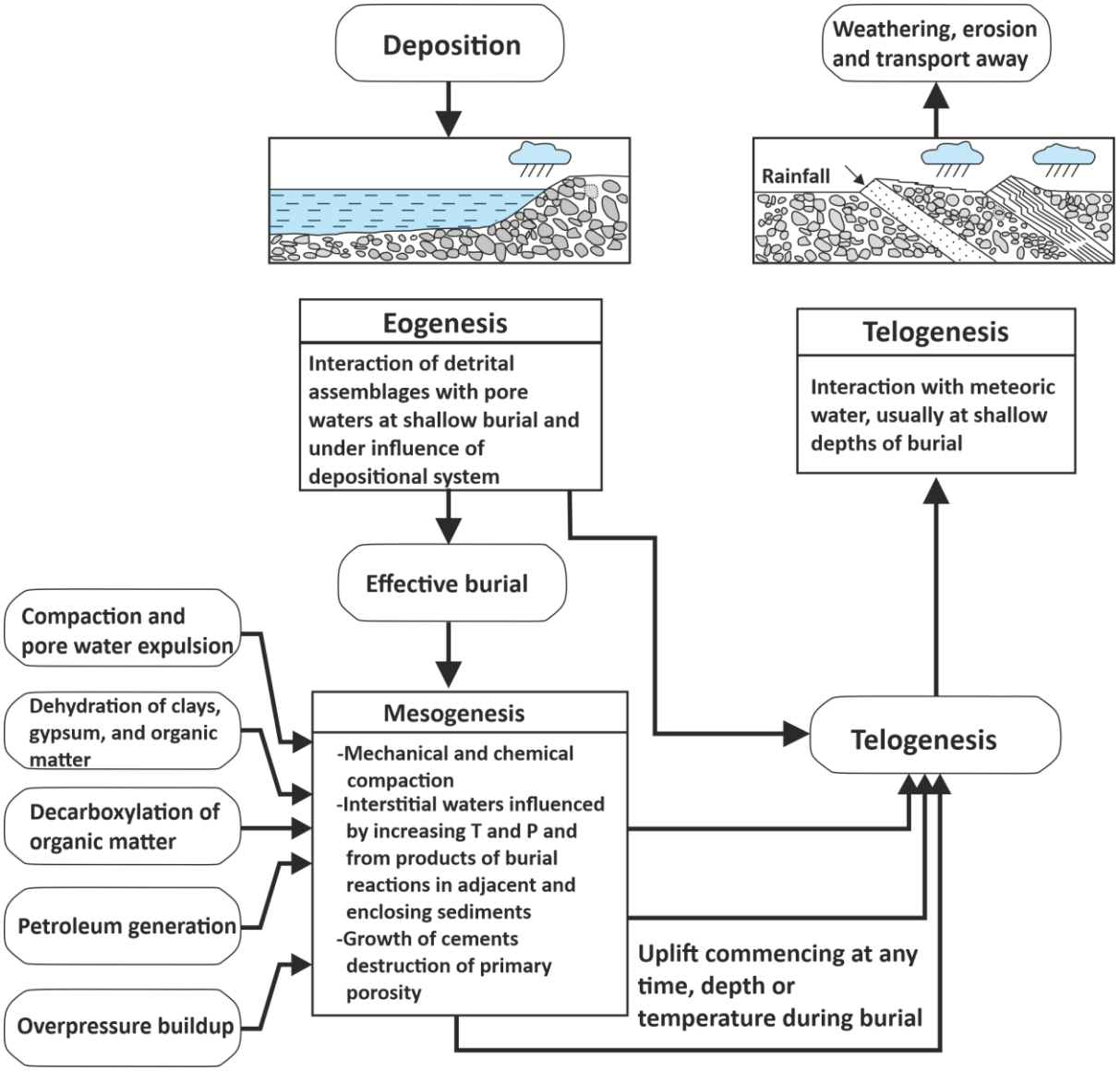

Figure 1.4: The flow chart illustrates diagenetic regimes related to different stages of basin evolution after Burley & Worden (2003a)

Mesodiagenesis: Mesodiagenesis, also called burial diagenesis or mesogenesis, occurs at depths greater than about 2 km, away from the influence of surface waters, and where temperatures exceed 60-70°C. It extends through to the onset of low grade metamorphism, or uplift caused by basin inversion (Morad et al. 2000; Burley & Worden 2003a; Worden et al. 2018c). Although the boundary between mesodiagenesis and eodiagenesis is not distinct, mesodiagenesis is characterised by high temperatures beyond the range of bacterially mediated mineral reactions (Worden et al. 2018c). Mesodiagenesis is therefore strongly influenced by temperature, pressure and basinal brines (Morad et al. 2000) and can be identified based on

isotopic, textural and mineralogical parameters (Burley & Worden 2003a). Compaction that started during eodiagenesis, continues into the mesogenetic realm.

Rather few chemical changes typically occur to sandstones during eodiagenesis, unless the sandstone is rich in reactive minerals, there are major changes in stress or there is an unusual influx of material from outside the sandstone (Tucker 1981; Boggs 2009b). Mesodiagenesis is characterised by common mineralogical and chemical changes. With increase in burial there are changes in temperature, pressure and pore water chemistry which can cause alterations from smectite to illite, K-feldspar reaction with kaolinite to form illite, berthierine to chlorite, alteration of plagioclase to albite and development of zeolites from volcanic grains (Tucker 1981; Worden et al. 2018c). Other processes include pressure dissolution, quartz overgrowths, development of dolomite, ankerite, stylotite formation, minor barite, minor fracturing and K-feldspar overgrowths (Worden & Burley 2003a; Worden et al. 2018c).

Telodiagenesis: also called telogenesis only occurs when buried rocks are uplifted and exhumed and thus exposed to surface (meteoric) waters, that are clearly different to the waters present at the time of deposition (Burley & Worden 2003a; Boggs 2009b) (Fig. 1.4). In extreme cases, rock overburden is completely stripped off and previously buried rocks are exposed to surface processes such as oxidation of chemically-reduced phases e.g. pyrite and dissolution of feldspars (Worden et al. 2018c). Where overburden has not been completely eroded, the telodiagenetic realm can extend to a few metres in the case of non-brittle, low permeability rocks (Armitage et al. 2016) but can also extend to hundreds of metres in the case of aquifers (Worden et al. 2018c). The typical characteristic of this regime is the displacement of connate water (interstitial water during rock formation) by surface water (Boggs 2009b). Physically, surface waters are able to penetrate and displace connate water due to the pressure head created by rainfall on upland regions (Burley & Worden 2003a). The surface waters are typically of low salinity and have the capacity to cause changes including oxidation of iron-rich minerals, feldspar alteration to clay minerals and dissolution of carbonate cements (Burley & Worden 2003a). Others alterations include oxidation of sulphide minerals and iron carbonates (Tucker 1981; Parnell et al. 2002). Bacterial sulphate reduction can also occur during telodiagenesis causing biodegradation of hydrocarbons and dissolution of sulphates (Worden et al. 2018c). During uplift, near-surface brittle fracturing may occur, which may be unfavourable for hydrocarbon prospects due to the possibility of surface water influx but may also be favourable

for fracture bound fluid flow (increase permeability) as well as remigration of hydrocarbons to peripheral traps, especially as gas expands and condensate dropout occurs (Parnell 2002). Although mesogenetic strain is considered to be irreversible, a physical effect of telodiagenesis is the development of decompaction joints caused by the erosion of overburden material during uplift. These decompaction joints allow penetration of meteoric water up to tens of metres deep (Neuzil 2003; Worden et al. 2018c).

The controls on diagenesis can combine in diverse ways to produce a wide range of diagenetic minerals and fabrics. Diagenetic processes and fabrics are discussed in detail in various text (Heald & Baker 1977; Glasmann et al. 1989; Scotchman et al. 1989; Gehring 1990; Ehrenberg 1997; Bjørlykke 1998; Swarbrick 1999; Morad et al. 2000; Parnell et al. 2002; Burley & Worden 2003a; Tada & Siever 2003; Worden & Burley 2003a; Aase & Walderhaug 2005) which are too numerous to cover here. This study will therefore focus on the diagenetic processes and minerals that are relevant in the study locations discussed here.

1.4.1 Compaction

Compaction is the progressive loss of porosity with increasing depth due to overburden stresses, with consequent loss of water and bulk rock volume (Burley & Worden 2003a; Gluyas & Swarbrick 2004). With the exception of fluid overpressure zones, compaction generally increases with depth (Gluyas & Swarbrick 2004; Ehrenberg et al. 2009). Overpressure zones occur where fluid pressure is higher than hydrostatic pressure, overpressure lowers the effective stress caused by overburden loading, retards mechanical compaction and produces anomalously high porosity for that depth (Worden & Burley 2003a; Gluyas & Swarbrick 2004). There are two types of compaction, mechanical and chemical compaction; mechanical compaction is controlled by effective stress and rock volume is reduced in response to vertical shear-compressional stresses caused by overburden weight (Worden & Burley 2003a; Bjorlykke et al. 2009; Worden et al. 2018c). Chemical compaction, or pressure solution, is the dissolution and precipitation of solids and is controlled by thermodynamics and kinetics (Bjorlykke et al. 2009) (Fig. 1.5). Both mechanical and chemical compaction are dependent on the depositional, compositional and textural properties of the rock as well as the rock properties during shallow burial (Ramm & Bjørlykke 1994; Bjørlykke 2014; Rahman & Worden 2016a).

At depths less than 2 to 3 km, and temperatures below 70-80 °C, mechanical compaction is dominant due to low chemical reaction rates of silicate minerals at low temperatures (Fig. 1.5) (Ramm 1992; Ramm & Bjørlykke 1994; Bjørlykke 2014). Mechanical compaction involves grain rotation, sliding and brittle grain fracture or crushing (Sheldon et al. 2003). At depths were mechanical compaction is dominant, quartzose sands are sensitive to grain size and sorting with coarse-grained and lithic sands more susceptible to brittle fracture and porosity loss than finer-grained monocrystalline sands (Chuhan et al. 2002). Grain fracturing produces smaller sand fractions and thus reduces grain sorting; these poorly sorted sands show less porosity-loss than coarser-grained more sorted sands (Chuhan et al. 2002; Fawad et al. 2010). In addition, mechanical compaction is dependent on mechanical properties, quantity of framework clastic particles as well as the magnitude and orientation of 3D stress distribution in the absence of pore-filling material (Worden et al. 2018c).

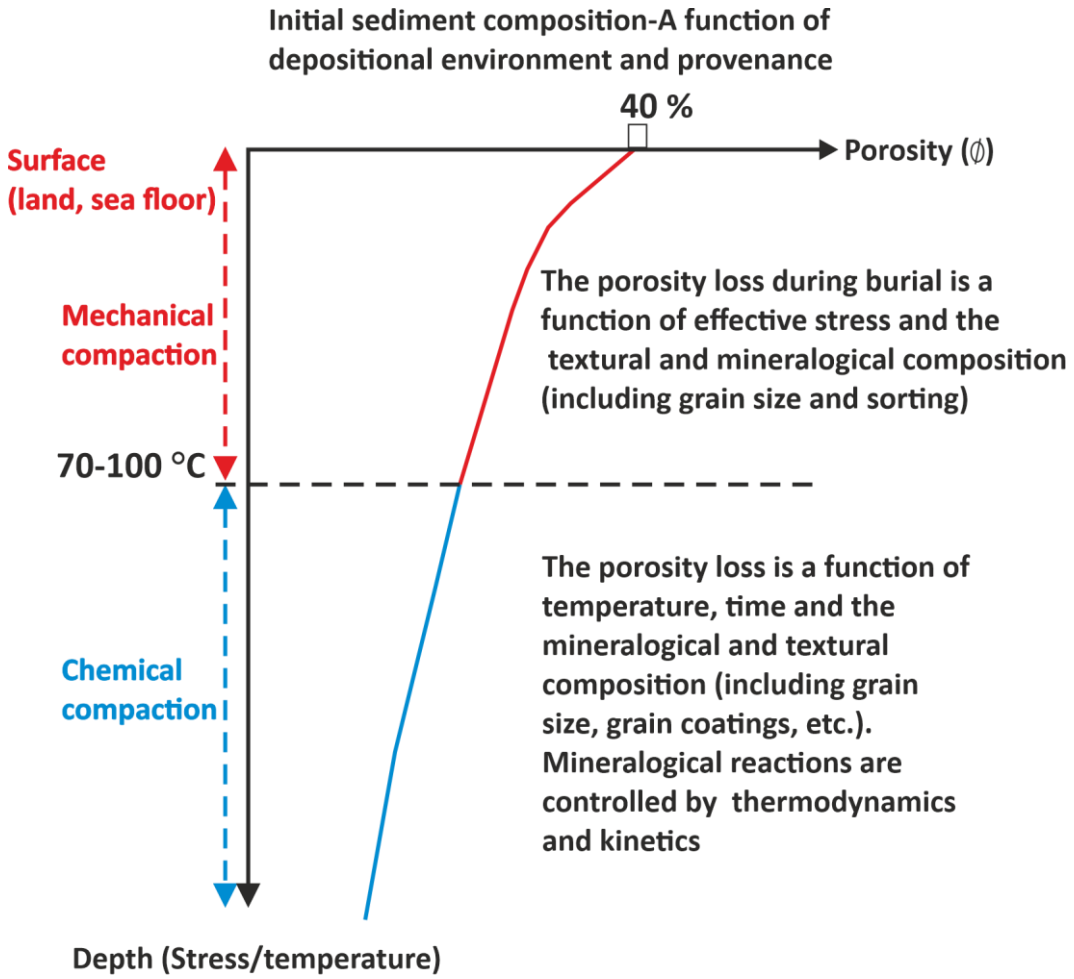

Figure 1.5: Porosity-depth curve showing the principal causes of compactional porosity-loss with burial, as modified from Bjørlykke (2014). Porosity-loss due to mechanical compaction is controlled by sediment composition and the effective overburden stress while chemical compaction is controlled by mineralogy, time and temperature.

As burial progresses, temperature increase cause mineral reaction rates to increase (Fig.1.5). This takes sandstones into the region of chemical compaction where thermodynamic and kinetically controlled mineral reactions are dominant controls on porosity loss (Bjørlykke 2014). Chemical compaction involves the dissolution of minerals along grain contacts as well as diffusive transport of mineral elements into pore space (Wilson & Stanton 1994; Sheldon et al. 2003; Baron & Parnell 2007). The solutes may precipitate on free grain surfaces, be involved in other chemical reactions or be removed from pore fluid by advection or diffusion (Sheldon et al. 2003). Two types of dissolution can occur due to pressure, stylolitisation which is due to contact from many grains or intergranular pressure solution between two grains (Tada & Siever

2003). Chemical compaction causes porosity-loss in two ways: dissolving grain contacts and bringing the centres of grains closer together as well as precipitating the dissolved material on other sites (Sheldon et al. 2003). Chemical compaction is dominant at depths greater than 2 km and where temperatures are > 80° C; at these depths, a rigid framework of quartz overgrowths infills primary pore space and retards further mechanical compaction (Paxton et al. 2002).

Chemical compaction involves dissolution, transport and precipitation. The rate of chemical compaction can be affected by a sequence of events, the slowest of which is the rate-controlling step. Processes include dissolution at grain contacts, diffusion along the grain contacts and removal of dissolved matter from pore-fluid either by precipitation or flow (Tada & Siever 2003). After pressure solution has been initiated, dissolution rate increases with increasing temperature, diffusion rate increases with effective pressure and precipitation rate increases with decrease in grain size (Tada & Siever 2003).

There are controversies about the causes of chemical compaction, for instance Heald (1959) found a positive correlation for clay content and intergranular pressure solution for the St Peter sandstone, with a similar trend reported by Sibley & Blatt (1976). Thomson & Ireland (1959) similarly suggested that clays films have an important role in pressure solution. It has been hypothesized that clay films between grains increases the rate of diffusion transfer, and hence increases the rate of pressure solution (Weyl 1959). It has been suggested that the increase in the rate of diffusion is achieved by sheet silicates' high surface charge, causing a thicker fluid layer to be trapped between grains (Renard & Ortoleva 1997). It has also been suggested that clays and sheet silicates increase the pH along grain contacts and increase quartz grain solubility (Sheldon et al. 2003). Conversely, no correlation between clay content and intergranular pressure solution intensity was found by Siever (1959), in the clay-rich lithic-bearing Pennsylvanian sandstones of north eastern USA. Siever (1959) attributed the lack of correlation of clay and chemical compaction to cushioning effect by clay matrix and ductile lithic fragments. The cases mentioned above have effects on the rate of dissolution and diffusion, but in the end, chemical compaction must be driven by effective stress between grain contacts and pores; which is the only means to create and maintain a gradient in chemical potential to drive diffusion (Sheldon et al. 2003).

It is also worth mentioning that clay coats, and especially chlorite, on grain surfaces can inhibit porosity loss by quartz cementation in deep reservoirs (Sibley & Blatt 1976; Worden & Morad

2000; Worden & Burley 2003a; Ajdukiewicz & Lander 2010; Worden et al. 2020b). Large amounts of clay matrix, ductile fragments and early calcite cement also inhibits chemical compaction (Sibley & Blatt 1976; Tada & Siever 2003). Early diagenetic quartz also inhibits chemical compaction by equalising the distribution of stress along grain surfaces (Sibley & Blatt 1976).

1.4.2 Pyrite

Pyrite is an iron sulphide mineral formed under reducing conditions (Tucker 1981; Canfield & Raiswell 1991; Goldhaber 2003). It is the dominant solid-phase form of sulphur in organic-rich marines sediments (Goldhaber 2003). Pyrite abundance in organic-rich sediments is due to bacterially-mediated reduction during decomposition of organic matter (Tucker 1981; Worden et al. 2018c). Pyrite morphologies include framboidal, aggregate, bladed and equant morphologies (Canfield & Raiswell 1991). Pyrite morphologies provide indications of their depositional setting e.g. framboidal and equant pyrite commonly formed due to eogenetic microbial activity (Canfield & Raiswell 1991; Worden et al. 2018c) and coarser pyrite morphologies are typical of burial diagenesis (Goldhaber 2003). Pyrite is more common in marine sediments as sea water contains more dissolved sulphates than freshwater (Tucker 1981).

1.4.3 Apatite

Apatite contains phosphorus which is scarce in plants but is a major component of vertebrate skeletons and invertebrate hard parts, such as teeth (Tucker 1981). Phosphate is an abundant nutrient in sea water and is an important control on organic productivity, hence apatite in sedimentary environments is closely related to organic activity (Lucas & Prevot-Lucas 1997). In marine sediments and sedimentary rocks, phosphate is present as apatite as well as bone fragments and coprolites (Tucker 1981; Macquaker et al. 1996). Apatite occurs in marine environments in areas of negligible clastic sedimentation and may range in shape from slabs, nodules, ooids and irregular masses (Tucker 1981). Apatite occurs as trace cements in sandstones and carbonates and typically does not significantly affect reservoir quality (Worden et al. 2018c).

1.4.4 Berthierine

Berthierine is a common eogenetic mineral that develops in Fe-rich pore waters with an abundant supply of iron (Worden & Morad 2003b; Worden et al. 2018c). Berthierine is an iron-rich, aluminous, 1:1 phyllosilicate mineral in the kaolinite-serpentine series (Worden & Morad 2003b). It is a trioctahedral clay mineral with general composition $Y_6Z_4O_{10}(OH)$, where Y represents combination of Fe^{2+}, Mg, Fe^{3+}, Al; Z represents combinations of Si, Al, Fe^{3+} (Bhattacharyya 1983). Berthierine forms <5 µm lath-shaped grain coats on detrital grains, it also forms as pellets, ooids or replacing silicate and carbonate bioclasts (Worden & Morad 2003b). Fe-ooids typically develop as tangential rings around a nucleus composed of mineral grains, glaucony, pellet, other berthierine mud or skeletal debris (Macquaker et al. 1996; Worden & Morad 2003b).

Berthierine forms during shallow burial under reducing conditions below the sediment-water interface in estuarine- deltaic deposits (Fritz & Toth 1997; Williams 2003) in nutrient –rich tropical to sub-tropical seas (Odin 1990). Berthierine has also been reported to form from other precursor clays such as kaolinite (Bhattacharyya 1983; Fritz & Toth 1997).

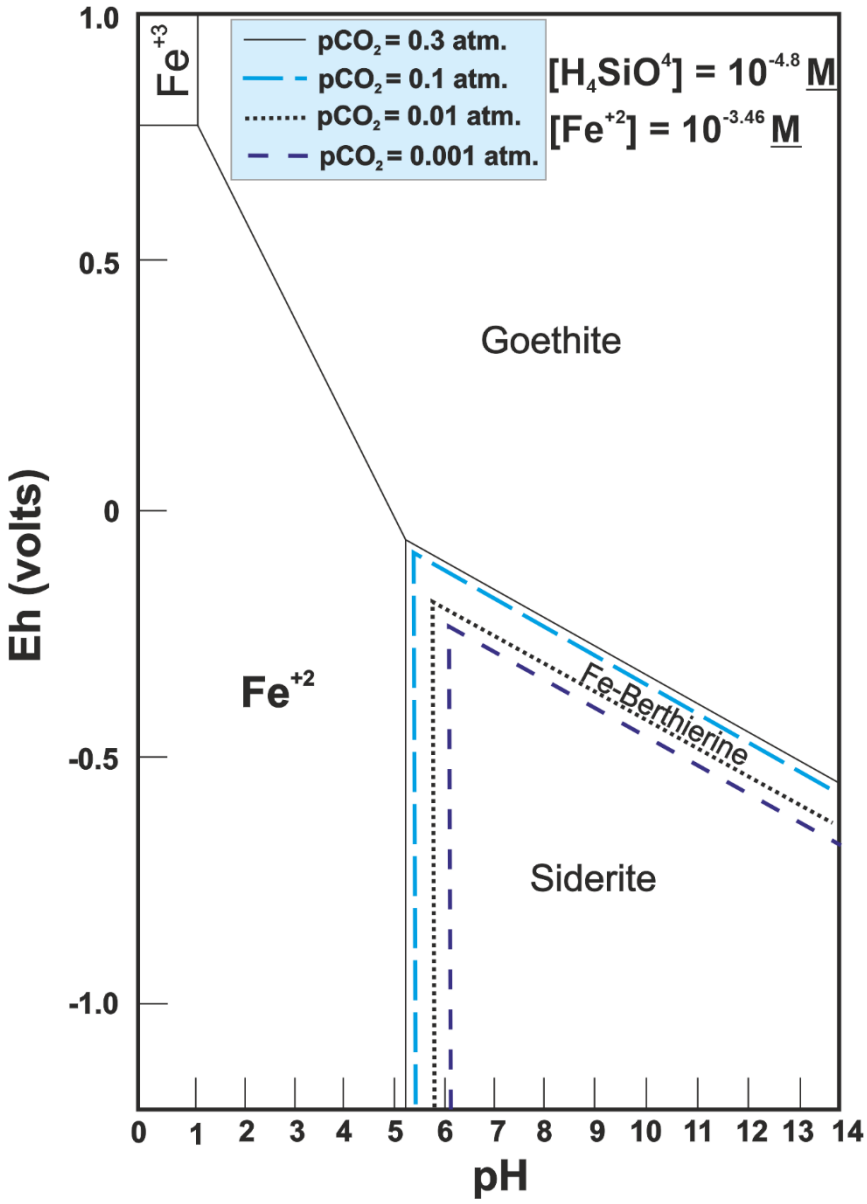

Figure 1.6: Eh / PH diagram showing stability fields for berthierine, goethite and siderite as a function of CO_2 partial pressures (PCO_2) modified from Fritz & Toth (1997). H_4SiO_4 and Fe^{2+} are fixed at PCO_2 of 0.3 at concentrations where siderite, kaolinite, berthierine, goethite and gibbsite are in equilibrium.

Geochemical modelling work by Fritz & Toth (1997) investigated the conditions under which berthierine is stable (Fig. 1.6). The model showed that berthierine development occurs under conditions with low $[Mg^{2+}]/[Fe^{2+}]$ ratio, high PCO_2, low silica concentration, low sulphate content before reducing conditions and moderate reducing conditions (Eh around 00.5 V). The low $[Mg^{2+}]/[Fe^{2+}]$ ratio is necessary because higher concentrations of Mg would preferentially

develop amesite ($Mg_2Al_2SiO_5(OH)_4$). A high Eh (oxidising conditions) leads to goethite instead of berthierine as ferric iron is stable. Very low Eh conditions leads to siderite growth. An intermediate Eh can lead to berthierine growth if the PCO_2 is low. Under reducing and acidic conditions, reduced iron would occur but would preferentially combine with sulphite (reduced sulphate) to form pyrite rather than berthierine. Finally, very high silica concentration in pore waters will favour the development of Fe-clays with higher silica content than berthierine e.g. clinochlore or greenalite (Fritz & Toth 1997).

Berthierine is important during diagenesis as it has been recognized as the early diagenetic precursor to the 1.4 nm mineral chlorite (Aagaard et al. 2000; Worden & Morad 2003b; Worden et al. 2018c). Berthierine and chlorite have similar chemical composition and stoichiometry especially with the ferrous end-member chamosite (Macquaker et al. 1996). They cannot be differentiated by routine backscattered scanning electron microscopy (BSEM) and conventional energy-dispersive spectrometry (EDS) but they can be discerned by X-ray diffraction (XRD) as berthierine has a 0.7 nm basal spacing and chlorite has a 1.4 nm basal spacing (Taylor 1990; Macquaker et al. 1996; Worden et al. 2018b).

1.4.5 Calcite

Calcite is one of the most common cements in sandstones and may occur in sandstones as local segregations, patchy distribution and concretions, and is found over the whole diagenetic spectrum from eogenetic arid continental sediment to sea floor environments and through to deep burial (Tucker 1981; Milliken 2003). Calcite formation occurs when there is increase in the activity of carbonate ion; in shallow reservoirs, this may be through evaporation and in deeper reservoirs by an increase in pH or temperature (Tucker 1981). Ca^{2+} for calcite cementation can be sourced from biogenic sources e.g. bioclasts (Walderhaug & Bjørkum 1998; Scholle & Ulmer-Scholle 2003; Worden et al. 2019; Barshep & Worden 2021, 2022) and inorganic sources e.g. plagioclase and sea water (Morad & De Ros 1994; Milliken 2003). $\delta^{13}C$ values show that organic carbon is common at shallow depths but inorganic carbon makes up about 50% of carbon with burial (Milliken 2003), indicating a decrease in biogenic influence with depth.

The two main types of calcite cement are single large poikilotopic crystals and drusy spar (Tucker 1981). Poikilotopic calcite is composed of a large crystal which can extend up to several centimetres and cement multiple grains (Tucker 1981). Drusy calcite is made of equant

crystals which grow into pore space and increase in size in the direction of growth (Scholle & Ulmer-Scholle 2003).

1.4.6 Siderite

Siderite is common in both Precambrian and Phanerozoic Fe-rich sediments (Tucker 1981). Siderite was reported to occur exclusively in brackish to non-marine pore fluids but it is now known that it also occurs in marine environments in association with decomposing organic matter (Scholle & Ulmer-Scholle 2003). Siderite commonly forms in association with chamosite ooids, skeletal grains and as a replacement mineral for many grains (Tucker 1981). Modern siderite is currently forming in muds, deltaic and lacustrine sediments as small disseminated crystals or as nodules and rounded groundmass (Ho & Coleman 1969). Siderite in thin section includes the following textures, coarse crystals with rhombohedral cleavages common in oolitic and bioclastic ironstones; fine-grained equant rhombic crystals found interbedded with chert in Precambrian iron formations and thirdly, as fibrous crystals which forms spherulites commonly formed in the water column (Tucker 1981; Vuillemin et al. 2019).

Siderite forms under reducing conditions (Fig. 1.6), oxidation of organic matter produces CO_2 as well as reduces iron to Fe^{2+} for siderite formation (Fritz & Toth 1997). In contrast to pyrite, siderite is more common in non-marine sediments, this is because siderite requires low sulphide activity and sea water is abundant in dissolved sulphates (Tucker 1981). When there is sufficient reduced Fe^{2+} over Ca^{2+}, siderite will therefore form in preference to calcite and where there is more carbonates over sulphides siderite will develop instead of pyrite (Tucker 1981; Worden et al. 2018c). Siderite can be an important indicator of iron-rich hinterland conditions (Hallam 1975; Vuillemin et al. 2019).

1.4.7 Quartz

Quartz cement is the most common cement that causes porosity and permeability loss in deeply buried, quartz-rich and clay-poor sandstones (Pettijohn et al. 1973; Tucker 1981; McBride 1989; Walderhaug 1994a; Worden & Morad 2000; Worden et al. 2018c). Quartz cement forms syntaxial overgrowths on detrital quartz grains and is recognised by its euhedral faces, iron oxide rims lining detrital grains, fluid inclusions at grain-cement boundaries and, most reliably, by cathodoluminiscence analysis (Tucker 1981). Quartz cementation typically occurs during burial diagenesis at temperatures above 70-80 °C (Morad et al. 2000; Ajdukiewicz & Lander

2010; Worden et al. 2018a). Quartz cementation requires a source of silica, a transporting medium and a substrate to nucleate on (Walderhaug 2000) with the slowest of these requirements serving as a rate-limiting factor (Worden & Morad 2000). There are many debates on the origin of silica for quartz cements as well as the temperature and timing of cementation. Some authors have claimed that silica transport over long distances is required to generate adequate volumes of quartz cement (McBride 1989). Quartz cement however requires a large volume of water as silica solubility is low (Land & Dutton 1978; Worden & Morad 2000). The large volume of water required for quartz cementation cannot be accounted for by simple compaction in the absence of flowing meteoric water (Milliken 2003). To explain the volume of cement present from external sources in most sandstones, evidence of significant convective recycling of formation waters will have to be illustrated (McBride 1989).

A number of possible sources for silica have been advocated, including pressure solution, clay mineral transformations (e.g. illitisation of smectite), feldspar alteration and dissolution of opaline tests of organisms in shales (McBride 1989; Worden & Morad 2000). In sandstones, the predominant sources include clay mineral transformations (e.g. illitisation of smectite), pressure solution at grain contacts of detrital quartz and stylolites, carbonate replacement of silicate minerals and margins of quartz grains and alteration of feldspars (McBride 1989) . Many workers favor illitisation of smectite , pressure solution, dissolution of volcanic glass, dissolution of feldspars and dissolution of siliceous microfossils (Tucker 1981; Wilson & Stanton 1994). Many early workers noticed pervasive quartz cement in quartzose rock and mistakenly interpreted it as an early diagenetic event (McBride 1989), it has now been shown that quartz cementation predominantly develops in late diagenesis (Lander & Walderhaug 1999; Barclay & Worden 2000; Worden & Morad 2000; Goldstein & Rossi 2002; Aase & Walderhaug 2005; Lander et al. 2008).

Factors that inhibit quartz cement include early formed grain coats (Pittman et al. 1992; Worden & Morad 2003b; Worden et al. 2020b), calcite cement (Ajdukiewicz & Lander 2010; Ajdukiewicz & Larese 2012), overpressure conditions before compaction (Bjørlykke et al. 1979; Bloch et al. 2002; Paxton et al. 2002), oil emplacement (Worden et al. 1998; Wilkinson & Haszeldine 2011; Worden et al. 2018a) and microcrystalline quartz (Ehrenberg 1993; Aase et al. 1996).

1.4.8 Dolomite

Dolomite is a rhombohedral mineral which commonly occurs as a secondary mineral (Tucker 1981; Scholle & Ulmer-Scholle 2003) although primary dolomite can also occur from direct precipitation during diagenesis (Tucker 1981; Adams & Mackenzie 1998; Worden 1998). Dolomite cement is mainly recognised during burial diagenesis however pedogenic dolomite has been reported by Worden (1998) in the Chaunoy Formation sandstone hence dolomite cement is also formed during early diagenesis.

Dolomite in thin section occurs as euhedral rhombohedra often recognisable as a replacive grain (Adams & Mackenzie 1998). To aid identification of dolomites from calcite, carbonate thin sections are etched and stained (Adams & Mackenzie 1998; Scholle & Ulmer-Scholle 2003). During burial diagenesis, pre-existing calcite can reprecipitate in the presence of increasing aqueous Fe content to create Fe-dolomite (Burley & Worden 2003a). In the absence of pre-existing carbonates, an influx of source rock-derived CO_2 and alkaline earth elements, from sand-grain decomposition, evaporates and mudstones, can combine to form dolomite (Burley & Worden 2003a).

1.4.9 Illite

Illite is the most common clay mineral in sediments and commonly occurs in sediments where the intensity of leaching is limited e.g. temperate soils (Tucker 1981). Diagenetic illite is a major cause of reservoir quality degradation in many reservoirs (Ehrenberg & Nadeau 1989; Giles et al. 1992; Nguyen et al. 2016; Worden et al. 2018c). Diagenetic illite results from alteration of precursor neoformed clays e.g. kaolinite, smectite and mixed layer smectite-illite; alteration of detrital kaolinite and smectite, alteration of feldspars and direct precipitation from solution (neoformation) (Wilson & Stanton 1994; Worden & Morad 2000). Authigenic illite can form grain-concentric coats with dense mats of randomly oriented thin ribbons (Giles et al. 1992; Wilson et al. 1992), or as flakes that extend away from grain surfaces to form stubbly hair-like ribbons that extend into pore spaces (Wilson & Stanton 1994). Other illite morphologies include acicular, fibrous and platy morphologies (Giles et al. 1992). Although illite abundance can show a relationship with depth (Ehrenberg & Nadeau 1989; Giles et al. 1992), there are controversies about the formation temperatures of illite. Some have reported illite growth temperatures ranging from as low as 50 °C (Bjorkum & Gjelsvik 1988) while Ehrenberg & Nadeau (1989) reported illite began developing at temperatures between 130-140

°C. Reviewing the controversies in temperature for illite development Giles et al. (1992) concluded that time-temperature exposure is the cause of illite formation and not temperature alone.

1.4.10 Kaolinite

There is a general consensus that most kaolinite is formed from open system, freshwater flushing (Bjørlykke et al. 1979; Worden et al. 2018c) as well as from neoformation or replacement of detrital alumino-silicate minerals (Glasmann 1992; Wilson & Stanton 1994; Worden et al. 2018c; Worden et al. 2019). Kaolinite is characteristic of tropical soils where intense acidic leaching occurs (Tucker 1981). Kaolinite occurs in two forms, the low temperature vermiform kaolinite and the blocky form (dickite) (Giles et al. 1992) and has been reported to form from pore waters at low temperatures of about 45-60 °C (Glasmann et al. 1989). Kaolinite crystals can range from 5-30 µm with some vermiform aggregates reaching up to 2500µm (Wilson & Stanton 1994). In many diagenetic environments, kaolinite content reduces with depth due to the increasing stability field of illite and kaolinite gets converted to illite (Giles et al. 1992; Glasmann 1992; Worden et al. 2018c). When there is no K-feldspar to supply potassium, kaolinite transforms into dickite; a high temperature polymorph of kaolinite (Worden et al. 2018c), which has greater crystallinity and stability at higher temperatures (Wilson & Stanton 1994).

Chapter 2: Materials and methods

The materials and techniques used in this study are selected to provide insight into pre-depositional sedimentary processes that conditioned the Corallian sandstones for diagenesis as well as diagenetic processes that modified the Corallian sandstones after burial. Overall the materials used in this study are based on core from wells drilled at Palmers Wood-3 (PW3), Palmers Wood-7 (PW7) and Bletchingley-5 (BL5) by Star Energy, and predecessors. The cores from the wells were stored at the British Geological Survey (BGS) core store in Keyworth, Nottinghamshire (Fig. 2.1). These cores were analysed for sedimentological, petrographic, geochemical and petrophysical data. Supporting data from Igas was also used for burial modelling as well as wireline analysis. In this study, there is no single method unique to each research question, rather, a combination of complementary methods are selected to answer the research questions.

To understand the provenance and distribution of sediments in the Corallian sandstones, a combination of petrographic, sedimentological and geochemical data is analysed. These analyses provide insight into the source of the Corallian sandstones as well as how the siliciclastic Corallian sediments were conditioned and redistributed during transport and deposition.

Core analysis provided insight to Corallian sediment transport, deposition and redistribution in the Weald Basin. Core description combined with wireline lithological and petrophysical analysis was employed to investigate patterns in reservoir quality distribution from a sedimentological perspective.

Identification of sequence stratigraphic surfaces during core analysis aided in the identification of allogenic and autogenic influences on sediment distribution and reservoir architecture. This is useful in understanding reservoir architecture and the relative effects of tectonism on reservoir quality and reservoir quality distribution. The sequence stratigraphic approach also investigate the effects of syndepositional tectonism on sediment distributing and reservoir quality distribution in the Weald Basin.

Petrographic data combined with core logging data provided insight into the extent of depositional controls and diagenetic controls on reservoir quality. Results from petrographic analysis will enable the analysis of micro-scale reservoir quality controls and investigate any such links on a larger scale using depositional units from core analysis.

Considering the uplift in the Weald Basin, burial history modelling was carried out to constrain the maximum burial depth as well as temperature profiles with time. This is important to understand the temperature range for mineral formation as well as constrain the diagenetic regime of these sandstones.

The materials and methods applied in this study are outlined below in greater detail. Chapters 3, 4 and 5 have a detailed methods section specific to the research questions answered in each chapter. The reader may at their discretion, choose to skip this section here or the methods section in each chapter.

2.1 Sedimentary core logging

High resolution sedimentary logs were created during this research at a resolution of 1:24 from 175.5 ft of core with 56.1 ft (17.9 m) of core from PW3, 54.5 ft (16.6 m) of core from PW7 and 64.9 ft (19.8 m) of core from BL5. As the wells are deviated to varying degrees, measured depths were converted to true vertical depths to give a representative idea of reservoir thicknesses and absolute present-day depths of burial. Each core was logged for lithology, grain size, sedimentary structures, ichnology, bed contacts, cement types, hydrocarbon stains and degree of cementation. Ichnofabrics were described using the approach defined by Pemberton et al. (2012a). Lithology, grain size and sedimentary structures were recorded to determine primary depositional conditions. Bed contacts and ichnology were recorded to give indications of both primary depositional conditions as well as significant sequence stratigraphic surfaces such as discontinuities.

Figure 2.1: Core logging at the BGS core store, Keyworth, Nottinghamshire.

The 1:24 logs were subsequently summarised and digitised at a resolution of 1:120, with their facies classified based on texture and lithological attributes as proposed by Farrell et al. (2012). Facies associations were based on the proposed schemes by Hampson & Storms (2003) and Kamola & Van Wagoner (1995) for shallow marine shoreface to shelf depositional environments.

2.2 Wireline analysis

Wireline logs were collected by Duke engineering services for Star Energy Ltd from the three wells in this study. The suite of logs includes, gamma ray, neutron porosity, compressional

sonic velocity as well as density and resistivity logs. Wireline data were used to calculate shale volume, wireline porosity, water saturation and neutron-density crossover plots were used to determine pay and non-pay zones. The wireline log depths were depth-matched to core depths where core and wireline attributes required comparison as well as correlation of core and wireline derived petrophysical properties. A detailed presentation of analysis and calculations carried out on wireline logs is presented in the methods section of each chapter based on the objectives of each chapter.

Gamma ray signals were also used to identify lithologic units for correlation sandstones and mudstones. This in combination with stratigraphic surfaces (Hampson & Storms 2003; Jordan et al. 2016) was used to develop a sequence stratigraphic framework from core logging to identify the spatial and stratigraphic extent of reservoir units, their depositional controls as well as the effect of these controls on reservoir architecture and reservoir quality distribution.

2.3 Handheld X-ray fluorescence (XRF) analysis

For decades, X-ray fluorescence (XRF) analysis has been a standard technique for generating quantitative bulk geochemical data (Potts & Webb 1992; Rowe et al. 2012). XRF analysis is popular due to a number of characteristics: analysis is made on solid samples without the need for dissolution, it has a reputation for precision and it is also a nondestructive technique (Potts & Webb 1992). The principle behind XRF analysis is high energy bombardment of samples by X-rays which causes ionization of inner shell electrons (photo-electric effect) (Fig. 2.2). This causes instability in the electron orbitals in the atom and an outer shell electron transitions to fill the vacancy caused by the ionization of the inner electron (Fig. 2.2). Excess energy produced from the drop in an electron's potential energy gradient towards the nucleus is released as secondary X-rays (or fluorescence) (Potts & Webb 1992; Lentz et al. 2014). The wavelength of the secondary X-rays depends on the atom present and the intensity of the fluorescence is proportional to the atomic concentration (Tucker 1988; Potts & Webb 1992; Worden 2005). XRF is insensitive to the oxidation state of an element as XRF analysis involves inner electrons (Potts & Webb 1992).

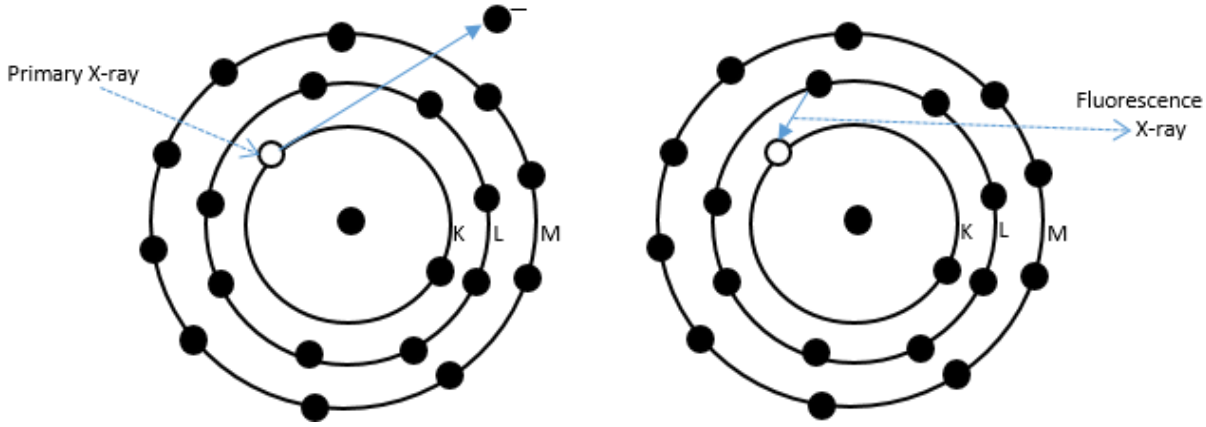

Figure 2.2: Photoelectric ionisation of an inner shell. Modified from Potts & Webb (1992)

Recent advancements have led to the production of portable handheld XRF devices suitable for quick and accurate collection of bulk geochemical data from rock, drill cutting and mine material (Rowe et al. 2012; Brand & Brand 2014; Lentz et al. 2014). Geochemical X-ray data were collected for this study using a Thermofisher Niton XL3T GOLDD (Geometrically Optimized Large Area Drift Detector) handheld X-ray Fluorescence spectrometer with a variable intensity X-ray source (6–50 kV, 0–200 μA Ag anode) and a proprietary GOLDD (Geometrically Optimized Large Area Drift Detector). The device analyses elements including (in order of atomic number): Al, Si, P, S, Cl, K, Ca, Sc, Ti, V, Cr, Mn, Fe, Co, Ni, Cu, Zn, As, Se, Rb, Sr, Zr, Nb, Mo, Pd, Ag, Cd, Sn, Sb, Te, Cs, Ba, Hf, Ta, W, Re, Au, Hg, Pb, Bi, Th, and U. The important elements Na and Mg cannot be analysed by pXRF as the X-rays have too low energy to be detected.

Before sampling, the spectrometer was tested for precision by taking ten readings from the same point for 50 seconds, 100 seconds, 150 seconds and 200 seconds and the standard deviations calculated to test for repeatability. The standard deviations were calculated for silicon, iron, aluminium, calcium, zircon and titanium. The least deviations were observed at 150 seconds and 200 seconds durations, consequently, a sampling time of 150 seconds was chosen for the whole core analysis to optimise precision and measurement duration. Forty three (43) elements were analysed with some local readings, especially in trace elements, below detection. One hundred and ninety-four (194) data points were analysed from BL5, PW3 and PW7 with sixty five (65) points from PW7, forty (40) points from PW3 and eighty nine (89) points from BL5.

2.4 Core analysis

Porosity and permeability data were provided by Igas along with the wireline logs. Porosity and permeability were measured by industry core laboratories, from one and a half inch diameter core plugs which were cleaned in hot refluxing solvents to remove hydrocarbons and residual brines. Helium porosity was determined using a Boyle's Law porosimeter. Permeability was measured using a nitrogen permeameter, with samples mounted in a "Hassler" type core holder. Permeability was measured using a steady state flow of nitrogen gas through core plugs; flow rate, temperature and differential pressure were recorded and used in conjunction with core dimensions to calculate permeability from Darcy's Equation.

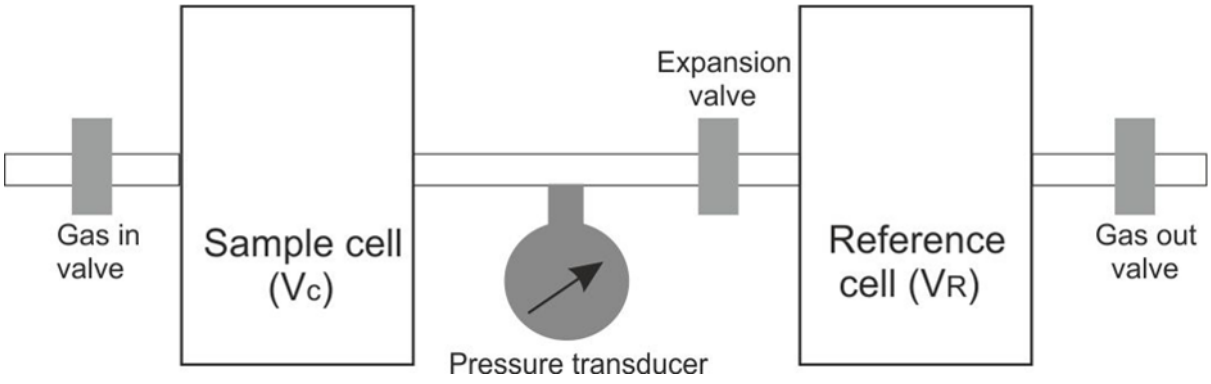

Figure 2.3: Schematic illustration of a pycnometer

The porosities of six additional core plugs from PW3 and PW7 were measured at the Rock Deformation Laboratory University of Liverpool using a Quantachrome pycnometer. The Quantachrome pycnometer is capable of carrying out non-destructive analysis for a variety of sample volumes and configurations using a small volume of gas, capable of being pressurised up to ~20 psig. It measures the density of the rock material using Archimedes principle of fluid displacement, Boyle's law of gas expansion and employs an inert gas-helium- which can penetrate through pore spaces of up to 1 Å diameter. The basic operating principle for the pycnometer is Boyle's law where the pressure of an ideal gas is inversely proportional to its volume. Hence, gas pressure drops starting from a known volume and known pressure will give an indication of porosity.

The density of a material is measured by passing a known quantity of helium gas under known pressure conditions from a reference cell (V_R) into a sample cell (V_c) (Fig. 2.3) containing the rock sample. The pore volume of the sample is deduced from the pressure drop in the sample cell using Boyle's law (eq. 2.1).

From Boyle's law

$P_1V_R=P_2V_c$

(Equation 2.1)

V_c=Volume of cell

V_R=Reference volume

P_1= Initial pressure (Reference cell)

P_2=Final pressure (Sample cell)

2.5 Optical microscopy

Fifty one (51) polished sections were prepared to a thickness of 30 μm in the standard manner for water-sensitive plugs and impregnated with blue-dyed resin for easy pore identification (Miller & Tucker 1988). Light microscopy was undertaken using an Olympus BX51 microscope under plane and cross-polarised light. The analysis was carried out to provide insight into detrital compositions, authigenic compositions, and textural relationships and to screen samples for Scanning electron microscopy (SEM), Backscattered Scanning Electron Microscopy (BSEM) and modal analysis.

2.6 Modal analysis

Modal analysis of polished sections (point counting) was carried out using an Olympus BX53M microscope fitted with a Conwy Valley Systems Petrog stage and software. For point counting, appropriate grid spacing was chosen to enable representative sampling of 300 compositional points with a X10 magnification objective. Attention was paid to cement types, cement stratigraphy and replacive cements to reveal the order of diagenetic events (i.e., paragenetic sequence). A further 250 points were analysed with a X5 objective to reveal grain size and sorting by measuring the long and short grain axes.

2.7 X-ray diffraction analysis (XRD)

Samples were crushed to a powder in a mechanical disk mill and then ground to a fine powder using an agate mortar and pestle. The powder was then sieved to < 52 μm. Water was used to clean the mortar and pestle and then dried after each sample to avoid cross-contamination after which samples were loaded into cavity holders.

X-ray diffraction (XRD) analyses were undertaken at the University of Liverpool's Diagenesis Research Group lab. The analyses were undertaken using randomly oriented powders in the PANalytical X'Pert Pro MPD X-ray diffractometer (Malvern PANalytical, UK) with a Copper X-ray tube and Ni filter to select for Cu k-α radiation. XRD Analysis and quantification was carried out by James Utley with the aid of the "HighScore Plus®" analysis software. Minerals were quantified by the relative intensity ratio (RIR) method (Chung 1974). XRD analysis was carried out to determine bulk rock mineralogy with specific interest on identifying berthierine. Berthierine was tested for by heating samples to temperature ranges from ambient, 300°C, 400°C and 550°C.

2.8 Scanning electron microscopy

Backscattered Scanning Electron Microscopy (BSEM) was carried out using a Hitachi TM3000 table-top SEM equipped with an energy-dispersive spectroscopy detector (EDS). The Hitachi TM3000 is capable of electron-optical magnification to a range of 15x-30,000x. To prevent build-up of electrical charges on the surface of the polished sections, avoid thermal damage and ensure optimal secondary electron signals, the polished sections were carbon-coated. Images were acquired at an accelerated voltage of 5-15kV in a vacuum generated by a vacuum pump. This was carried out to ascertain mineralogy, mineral/cement growth relationships and textural relationships.

2.9 Scanning electron-microscopy energy dispersion spectroscopy (SEM-EDS)

Automated mineralogy data were acquired using SEM-EDS technology developed by FEI (Worden et al. 2018b); SEM-EDS is basically a scanning electron microscope (SEM) equipped with high speed Energy Dispersive X-Ray Spectroscopy detectors (EDS) (Armitage et al. 2011). SEM-EDS identifies minerals using Species Identification Protocols (SIPs) which represents an extensive mineral chemical database archived in a library to produce a quantitative evaluation of mineral proportions (Pirrie et al. 2004; Armitage et al. 2010). SEM-EDS analysis produces quantitative mineral proportions, grain and pore space morphology and distribution to a minimum resolution of about 1 to 2 μm (i.e., equal to the diameter of the smallest beam-sample interaction volume). SEM-EDS analyses were undertaken with a user-defined resolution depending on the level of detail required and analysis time. In this study, SEM-EDS analyses were carried out at the University of Liverpool, using a tungsten-filament, operating at 15 kV, equipped with two Bruker EDS detectors (Wooldridge et al. 2018). The

ideal minimum practical spacing resolution of 2 µm was used for higher resolution and 20 µm spacing resolution was used where average mineralogy across a polished section was required.

2.10 Burial history modelling

Burial history modelling was carried out with BasinMod software, courtesy of Platte River Associates. The stratigraphic data are from well completion reports for BL5, where depths are reported as true vertical depths subsea (TVDss) in metres and formation tops defined from cuttings, measurement while drilling (MWD) gamma ray and Rate of Penetration (ROP) data. The TVDss were converted to true vertical depths (TVD) in metres to account for surface elevation above mean sea level before burial analysis was carried out. The missing uppermost stratigraphic section, eroded during the Aptian to Turonian (Cenozoic) inversion, was modelled using the Dartford area north of the Weald Basin as Upper Cretaceous (Chalk) and Cenozoic deposits above the Weald Clay have been eroded. The ages of the various stratigraphic intervals were derived from the British Geological Survey's (BGS) lexicon of named rock units (The British Geological Survey 2020) and the age for erosion inferred by calculating the duration of erosion from the deposit thicknesses and a maximum erosion rate of 14.7 metres/Ma. The erosion rate was deduced by dividing the total eroded thicknesses by the number of years since erosion started (55Ma). Bottom-hole temperatures used here were from BL5 well temperature profile as provided in the company report.

Chapter 3: Hinterland Environments of the Late Jurassic Northern Weald Basin, England

This chapter investigates the provenance of the Corallian sandstones using geochemical, mineralogical as well as sedimentological techniques with the aim of deducing the palaeogeology, palaeoenvironment and sediment distribution in the northern parts of the Weald Basin. This chapter aims to deduce how provenance has affected the supply of siliciclastics to the study area as well as address the relegation of sedimentological analysis in provenance studies. This chapter also aims to disentangle the effects of sedimentary processes during sediment transport and deposition and how they can affect provenance analysis.

This Chapter is prepared for submission to the Journal of the Geological Society of London for peer-review and publication.

ABSTRACT

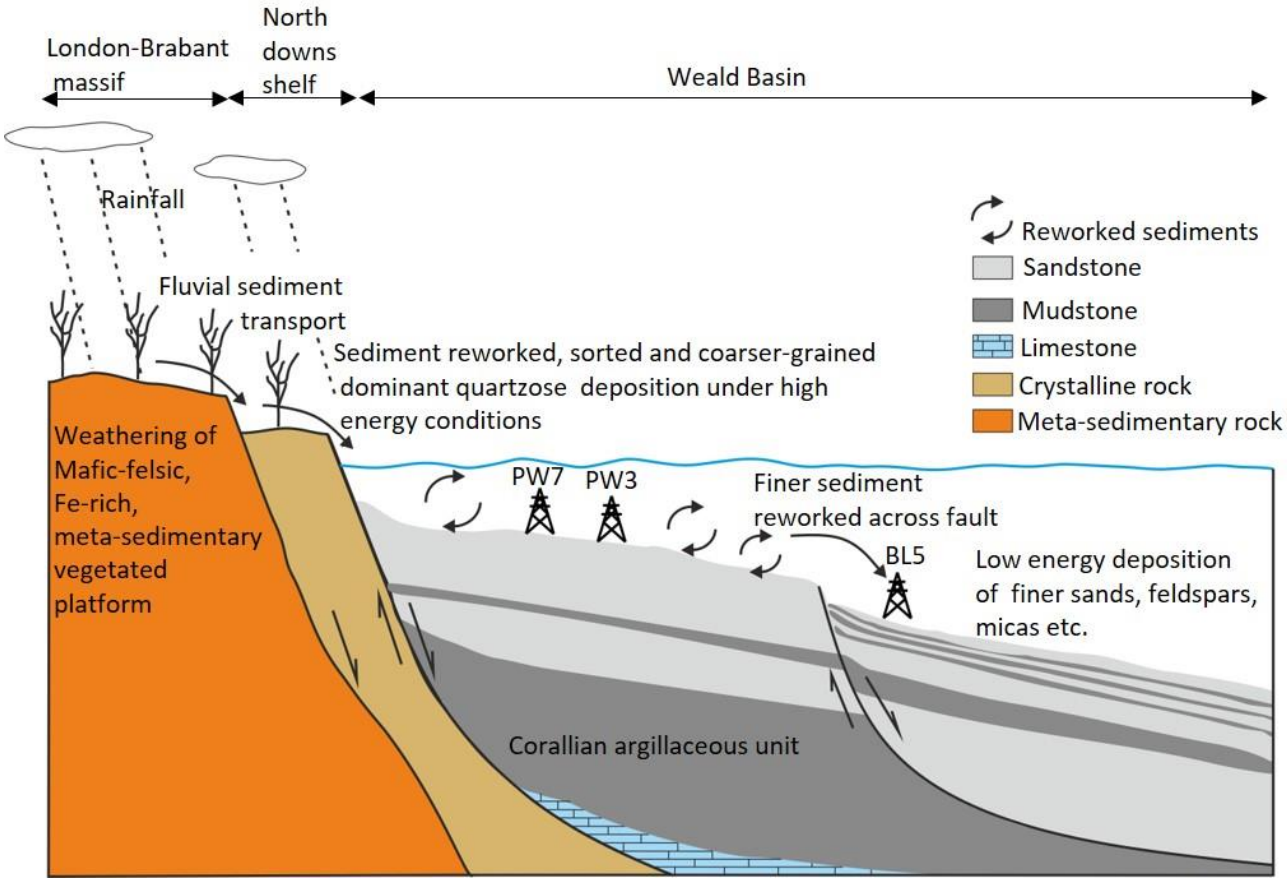

Graphical abstract showing conceptual model of sediment supply from source area and deposition in the Weald Basin. Not to scale.

Little is known about the palaeogeologic and palaeoclimatic conditions in the Upper Oxfordian Weald Area. Reconstructing provenance in sandstones can be a challenge, especially when the hinterland palaeogeology is unknown due to burial and diagenesis or weathering of outcrops. A multi-proxy approach to provenance, including detrital mineralogy and bulk geochemistry can reduce the uncertainty in provenance analysis as they can complement as well as supplement each other. Integrating depositional controls on textural and mineralogical distribution in a basin could potentially enhance reconstruction of buried or eroded hinterlands as sedimentary processes continue to modify sediments in the depositional environment. This study applied petrography, X-ray fluorescence geochemistry and sedimentology to understand the provenance of the Weald Basin's shallow marine Corallian sandstones, with the aim of deducing the palaeogeology, palaeoenvironment and sediment distribution within the northern parts of the Weald Basin during part of the Upper Jurassic. Corallian sandstones had a mixed mafic-felsic (intermediate) metasedimentary recycled orogen source. The hinterland had significant physical and chemical weathering under humid conditions, conducive to produce mineralogically mature sediments, as well as iron oxidation and transport to the basin. This study has revealed that depositionally up-dip sediment was more chemically-weathered, whereas depositionally down-dip the sediment was more texturally mature. Sedimentological analysis has highlighted potential for the concentration of both chemically unstable and heavy minerals in slightly more distal locations. Sedimentologically-controlled mineral distributions highlight potential errors which may be made in estimating source-area maturity. This study underscores the importance of a multi-proxy approach to accurate provenance analysis in shallow marine siliciclastic rocks.

3.1 Introduction

In ancient sandstones, direct evidence for palaeoenvironmental conditions in the sediment source-area are typically scarce and hence are commonly inferred, either from the characteristics of sediment from adjacent basins (Sladen & Batten 1984). Sandstone mineralogy and textural maturity are functions of their hinterland mineralogy, the dispersal paths that link the hinterland to the depositional basin, climate, and the sedimentary processes within the depositional basin (Pettijohn et al. 1973; Potter 1978; Dickinson & Suczek 1979; Tobin & Schwarzer 2013). It therefore follows that understanding sandstone provenance will potentially unlock information about conditions in the source-area, especially when the palaeogeology cannot be directly studied due to outcrop weathering or burial diagenetic

obliteration of primary sedimentary character (Odom et al. 1976; Dickinson 1988). Understanding sediment source-areas is important as it enhances knowledge of the palaeogeography of an area, including palaeocurrent and palaeoslope directions which advances prediction of sediment movement (Pettijohn et al. 1973). Provenance studies can be practically applied to problems including basin evolution and tectonics (Dickinson 1985), climate and relief (Folk 1980; Ruffell & Rawson 1994), discrimination of sandstone petrofacies and source-areas (Ingersoll 1990), as well as palaeo-drainage and sediment dispersal patterns (Lowe et al. 2011). Other practical applications of provenance analysis recognise that varied sand framework grain compositions typically have diverse diagenetic pathways which can affect porosity during burial; hence provenance studies are applied in hydrocarbon exploration, mining and groundwater studies (Pettijohn et al. 1973; Dickinson & Suczek 1979; Boggs 2009a; Tobin & Schwarzer 2013).

Many provenance analyses are carried out using element geochemistry (Middleton 1960; Potter 1978; Middelburg et al. 1988; Nesbitt et al. 1996) and detrital mineralogy (Dapples et al. 1953; Blatt 1967; Basu et al. 1975; Dickinson 1985; Nesbitt et al. 1996; Lowe et al. 2011; Reinson et al. 2015) complemented by other techniques such as facies analysis, wireline log analysis, and palynology. Most studies focus heavily on mineralogical and bulk geochemical analysis e.g. Nesbitt et al. (1996) Basu et al. (1975); Dickinson & Suczek (1979). With few studies incorporating sedimentological processes within the depositional basin (Odom et al. 1976), sedimentary processes such as hydrologic sorting which could cause mineralogical as well as textural redistribution of sediment (Kroonenberg 1992; Dokuz & Tanyolu 2006) can be overlooked in analysing provenance and source area evolution. This may potentially lead to errors in provenance analysis as sedimentological processes continue to modify sediments and influence their distribution in depositional basins (Odom et al. 1976).

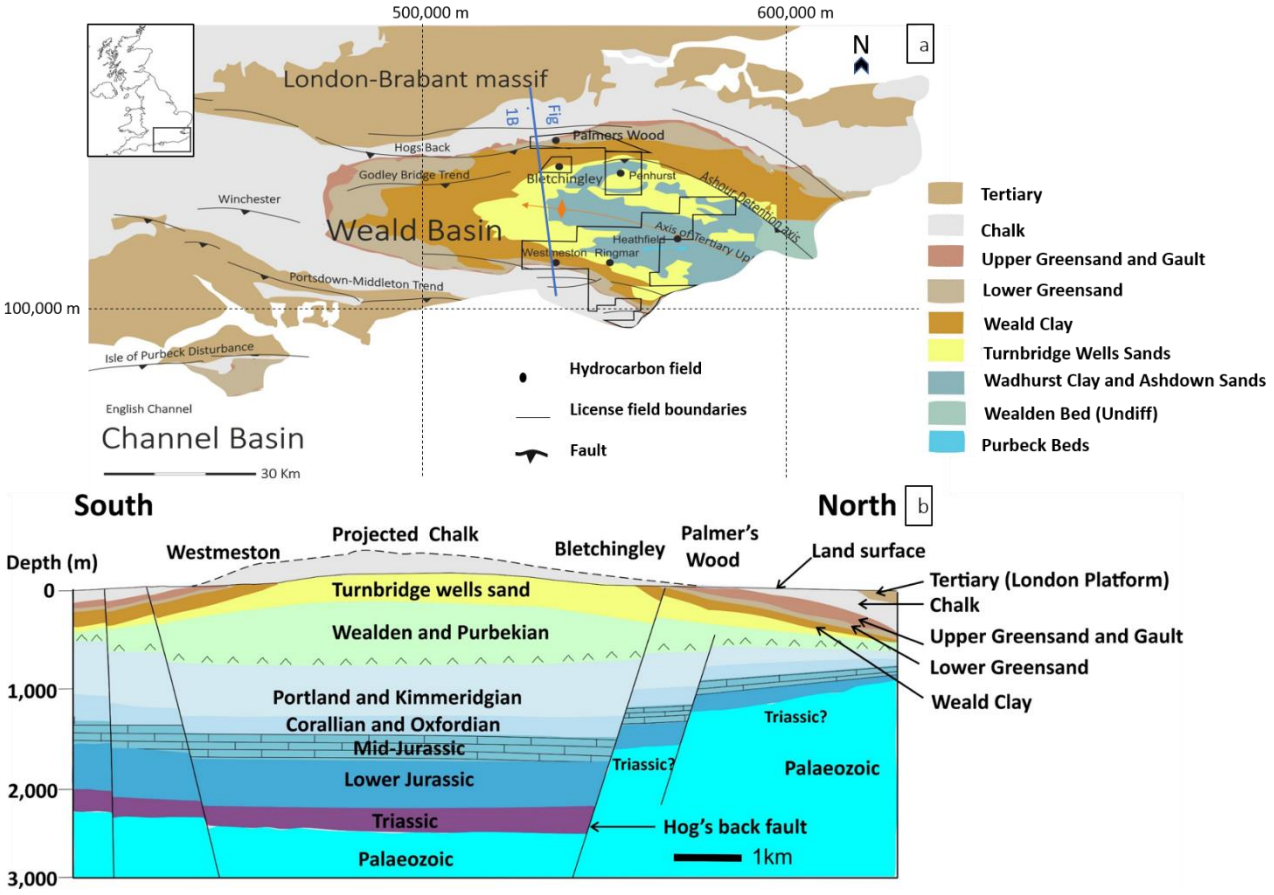
500,000 m
600,000 m
100,000 m
N
a
London-Brabant massif
Fig. 1b
Hogs Back
Godley Bridge Trend
Winchester
Weald Basin
Palmers Wood
Bletchingley
Penhurst
Ashour Detching axis
Axis of Tertiary Up
Heathfield
Westmeston
Ringmar
Portsdown-Middleton Trend
Isle of Purbeck Disturbance
English Channel
Channel Basin
30 Km
Hydrocarbon field
License field boundaries
Fault
Tertiary
Chalk
Upper Greensand and Gault
Lower Greensand
Weald Clay
Turnbridge Wells Sands
Wadhurst Clay and Ashdown Sands
Wealden Bed (Undiff)
Purbeck Beds
South
North
b
Depth (m)
0
1,000
2,000
3,000
Westmeston
Projected Chalk
Bletchingley
Palmer's Wood
Land surface
Tertiary (London Platform)
Chalk
Upper Greensand and Gault
Lower Greensand
Weald Clay
Turnbridge wells sand
Wealden and Purbekian
Portland and Kimmeridgian
Corallian and Oxfordian
Mid-Jurassic
Lower Jurassic
Triassic
Palaeozoic
Triassic?
Triassic?
Palaeozoic
Hog's back fault
1km

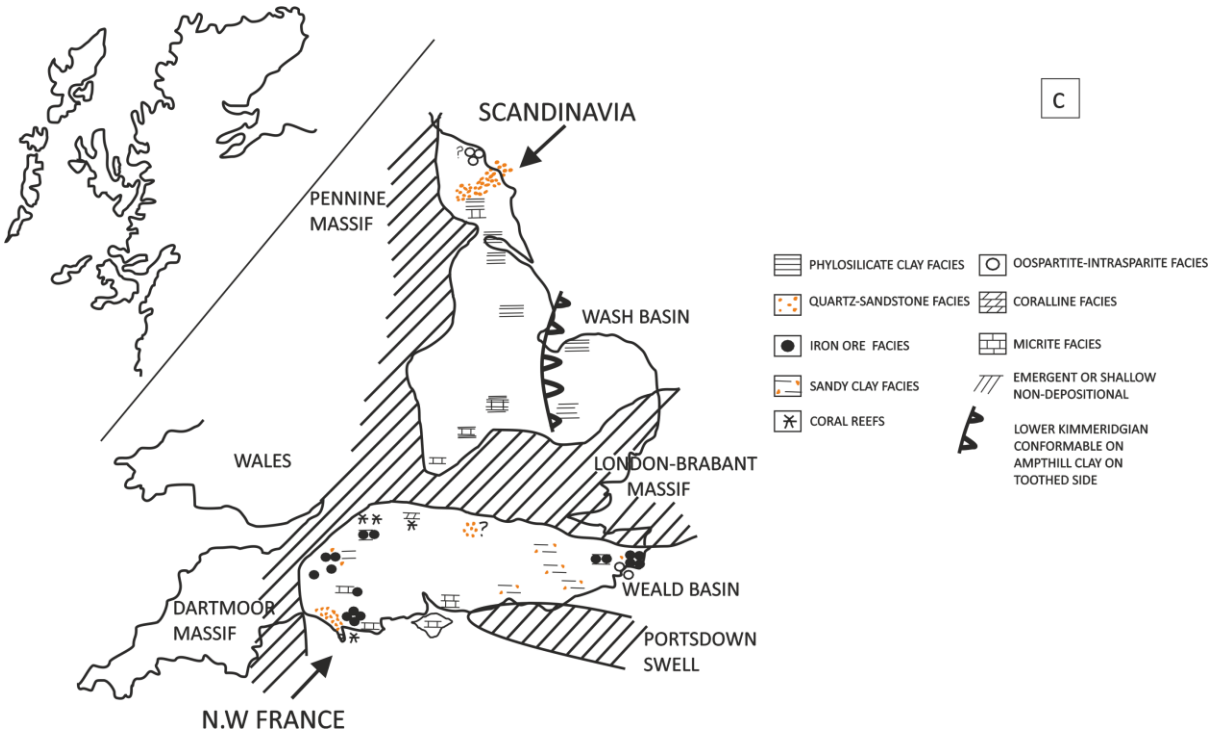

Figure 3.1: Geological map of the Weald Basin showing surface geology major structural trends as well as the London-Brabant massif. (a) Shows the location of the Palmers Wood and Bletchingley fields which are separated by a fault to the North of the Weald Basin. (b) Schematic cross-section of (a) showing faults and subsurface geologic units. (c) Palaeogeographic map of the Upper Oxfordian of England after Brookfield (1973) showing some facies distribution as well as the Weald Basin and London-Brabant Massif.

This study applied mineralogical, geochemical, wireline and sedimentological analyses to investigate the provenance of the Weald Basin's Upper Jurassic Corallian sandstones. These techniques have been chosen as framework grains are generally inherited from the source area hence composed of provenance inherited mineralogy which can be analysed by mineralogical and geochemical analysis to deduce source-area mineralogy, weathering and climate (Pettijohn et al. 1973; Potter 1978; Ruffell & Rawson 1994; Nesbitt et al. 1996). Sedimentological analysis will deduce potential controls of sediment redistribution and mineralogical enrichment in the basin while wireline logs will allow an unbiased separation of sand-rich from clay-rich zones. The study focused on the sand-rich portions of the Corallian sandstones as defined by neutron-density crossover plots because precise identification of detrital components by point counting is best achieved in sand-grade sediments compared to mud-grade sediments (Dickinson 1985). This case study has taken data from the Palmers Wood and Bletchingley

petroleum accumulations from the northern margin of the Weald Basin, close to the London-Brabant massif (LBM) (Fig. 3.1a and 3.1c). The Corallian contains producible oil in these two accumulations and several wells have been cored and most wells have good quality downhole wireline log data. The LBM has been identified by several authors as the likely source-area for the Weald Basin (Sladen & Batten 1984; Butler & Pullan 1990; Hawkes et al. 1998) but Oxfordian section and sediment supply to the Weald Basin has not been extensively studied. The Palmers Wood and Bletchingley fields are separated by a syn-sedimentary fault with subtly contrasting high and lower energy hydrodynamic regimes, sedimentology and sediment dispersal patterns updip and downdip of the fault (Barshep & Worden 2022). The two fields are also relatively close to the London-Brabant massif (~ 15 km) (Fig. 3.1). The Corallian sandstones are at shallow present-day depths (< 1000 m true vertical depth) and have not been buried deeper than about 1,500 m, hence they are not significantly altered by mesodiagenesis (Barshep & Worden 2021, 2022). These qualities make the case study suitable for the reconstruction of the palaeogeology, palaeoclimate and palaeotectonic setting of the Jurassic LBM area, as well as for the investigation of the effects of sedimentological controls on provenance analysis. To do this, this study will answer the following research questions:

- What was the source-area palaeogeology for the Corallian sandstones from the north part of the Weald Basin?
- Is there evidence of source-area migration?
- What were the palaeoclimatic conditions in the Upper Jurassic in the source-area?
- What was the Upper Jurassic tectonic setting of the source-area?
- What are the effects of tectonism on sediment distribution?

3.2 History and sediment source

The Weald Basin located in Southeast England is bound to the north by the London-Brabant massif (LBM), the Hampshire-Wessex Basin to the west and the Portsdown-Middleton trend to the south (Lake & Karner 1987; Butler & Pullan 1990; Hansen et al. 2002) (Fig. 3.1). The geologic history of the Weald Basin can be summarised into three phases (i) Palaeozoic deformation of basement rocks (ii) Early Jurassic to Lower Cretaceous basin subsidence and (iii) Tertiary uplift.

The Palaeozoic deformation of basement rocks occurred during the Variscan (also known as Hercynian) orogeny (Hansen et al. 2002; Trueman 2003b) with resulting east-west trending compressional fault development (Fig. 3.1). These faults evolved to become extensional faults and formed the structural controls along which Mesozoic incipient basin formation occurred due to thermal subsidence accompanied by block faulting (Butler & Pullan 1990). Basin formation was accompanied by the Rhaetic transgression and the deposition of the White Lias, Lower Lias, Middle Lias and Upper Lias units in the Lower Jurassic (Fig. 3.2) (Sellwood et al. 1986; McLimans & Videtich 1989; Andrews 2014). The Inferior Oolite and Great Oolite were deposited in the Bajocian and Bathonian respectively on a carbonate platform formed due to uplift (Talbot 1973; Lake & Karner 1987). The Callovian to Lower Oxfordian experienced continued rifting and deposition of the transgressive Oxford Clay Formation, Corallian Group, Kimmeridge Clay Formation and the Tithonian Portland sandstones (Fig. 3.2). Sea level fell causing the sabkha-type Purbeck Group to be deposited at the end of the Jurassic through to the Lower Cretaceous (Butler & Pullan 1990; Hansen et al. 2002; Radley 2006). Deposition of the Purbeck Group was followed by Valanginian Wealden Group Clastic sediments (Radley 2006).

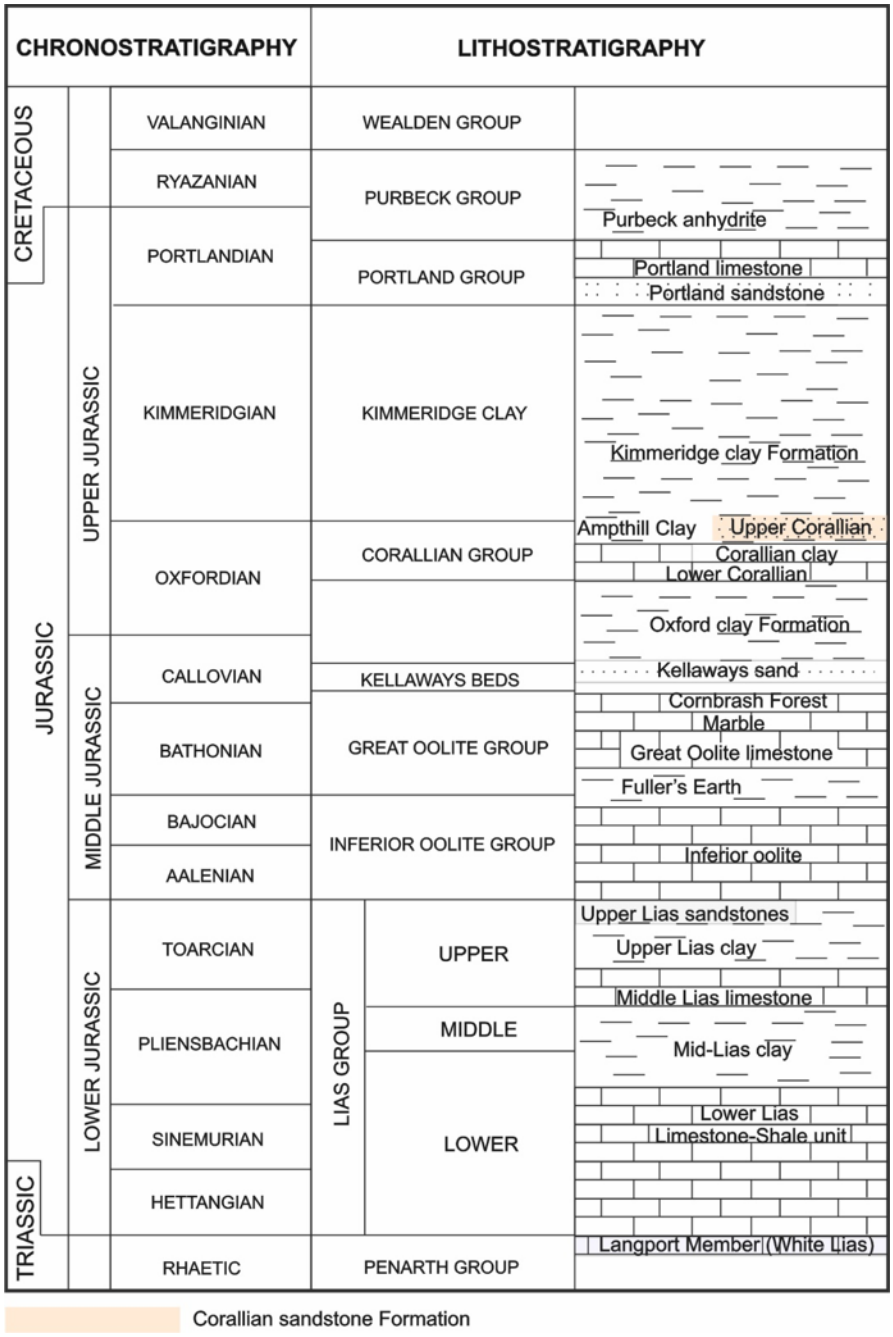

Figure 3.2: Generalised stratigraphic section for the Jurassic of the Weald basin as modified from Andrews (2014). The Corallian sandstone Formation is highlighted in brown.

Cenozoic uplift was caused by compressive forces from the south of the basin during the opening of the North Atlantic (Jones 1999b). This episode has been attributed to the Pyrenean orogeny (Parrish et al. 2018b), based on the dating of calcite veins. Cenozoic uplift caused

erosion and removal of sediments, younger than the Wealden Group (Sellwood et al. 1985), presumably Chalk, Upper and Lower Greensand, and Palaeogene clastic sediments.

The main source-area for the Weald Basin was the London-Brabant Massif (LBM), also known as London Platform (Fig. 3.1a and 3.1c). Rocks from the LBM were weathered and sediments transported southward into the Weald Basin (Allen 1975; Sladen & Batten 1984; Butler & Pullan 1990; Hawkes et al. 1998). The LBM consists of Precambrian crystalline basement and metasedimentary rocks, as well as Ordovician and Silurian volcanic and clastic sedimentary rocks (Rijkers et al. 1993). The LBM is an east-west trending stable structure located beneath southeast England, extending across the southern North Sea and into Belgium (Rijkers et al. 1993; Pharaoh 2018). The LBM is thus the easterly extension of the Anglo-Brabant Massif which has a lengthy geologic history extending from the Neoproterozoic as comprehensively discussed in Pharaoh (2018). Unlike the Weald Basin to the south, the LBM did not subside as it has minimal Variscan-induced internal structures like the Weald Basin (Chadwick 1985a). The LBM thus remained as a structural high to the north of the Weald Basin and was the source for the Upper Jurassic Corallian sandstones (Hawkes et al. 1998).

3.3 Data and Methods

3.3.1 Core log analysis

High resolution core logging recording centimetre and mm scale features was carried out on core from three wells, Bletchingley 5 (BL5), Palmers Wood 3 (PW3) and Palmers Wood 7 (PW7) at the British Geological Survey (BGS) core store, Keyworth, Nottinghamshire. BL5 was drilled in 2008, PW3 was drilled in 1984 and PW7 was drilled in 1990. All depths were recorded in feet and have been converted to meters in this study. The wells were initially logged at a resolution of 1:24, recording grain size, lithology, sedimentary structures, and bioturbation. 56.1’ (17.1m) of core was logged from PW3, with 54.5’ (16.6m) from PW7 and 65’ (19.8m) from BL5. The logs were summarised and digitised to a scale of 1:240 for comparison to wireline log data. All reported depths are measured depths except where otherwise stated.

3.3.2 Wireline analysis

Neutron-density cross-over plots were plotted using Rstudio to define sand-rich areas i.e. sand packages in the logs similar to pay zones in conventional petrophysical analysis (Tiab & Donaldson 2012). Core to log depth shifts were corrected by optimising the match of both core

porosity to density logs and the sedimentary log-determined presence of mudstones to gamma ray logs (Fig. 3.3).

3.3.3 Handheld XRF analysis

One hundred and eighty-nine sample points were analysed from the sand packages in BL5, PW3 and PW7 using a Thermofisher Niton XL3T GOLDD (Geometrically Optimized Large Area Drift Detector) handheld X-ray Fluorescence (XRF) device. The XRF sample points include 37 from PW7, 60 from BL5 and 27 from PW3. XRF analysis points were directly matched to core analysis plug points to allow XRF data to be related to core analysis data.

Before measurements, the handheld XRF was tested for precision by taking ten readings on the same sample point for a duration of 50 seconds, 100 seconds, 150 seconds and 200 seconds and the data compared for repeatability. Repeatability was calculated by comparing the standard deviations for all ten readings for silicon, iron, aluminium, calcium, zircon and titanium. The analysis showed the least deviations at ≥150 seconds sampling duration, consequently, a sampling time of 150 seconds was chosen for the whole core measurements to optimise precision and measurement duration. Forty three elements were analysed with some readings, especially trace elements, below detection.

3.3.4 Optical petrography

Optical microscopy was carried out on 51 polished sections from PW7, PW3 and BL5 using an Olympus BX51 transmitted light microscope. Analysis was carried out to determine mineralogy, textural relationships and cement types. Thirty three samples from the sand-rich zones were selected for point counting using an Olympus BX53M microscope aided by the Conwy Valley systems Petrog software with samples mounted on a Petrog stage. The samples analysed include 18 polished sections from BL5, 5 from PW3, and 10 from PW7. 300 points were analysed for each polished section using a x10 objective, for a statistically representative analysis of each polished section. Point counting focused on identifying diagenetic minerals from detrital minerals with emphasis on polycrystalline and monocrystalline quartz, feldspars, lithic grains and cement types.

3.3.5 SEM Analysis

A table-top Hitachi TM3000 was used to carry out Back Scattered Scanning Electron Microscopy (BSEM) at the University of Liverpool's Central Teaching Labs (CTL). The

BSEM analysis was carried out to determine mineralogy, mineral/cement types and textural relationships.

3.3.6 SEM-EDS

SEM-EDS analysis was carried out for automated quantitative mineral analysis (Worden et al. 2018b). The SEM-EDS instrument used in this study was an FEI WellSite QEMSCAN, at the University of Liverpool, using a tungsten-filament, operating at 15 kV and equipped with two Bruker EDS detectors (Wooldridge et al. 2018). The technique makes use of a Scanning Electron Microscope (SEM) equipped with two or more high speed Energy Dispersive X-Ray Spectroscopy (EDS) detectors (Armitage et al. 2011; Worden et al. 2018b; Barshep & Worden 2021) to give a quantitative proportion of mineral assemblages. In this study, the ideal minimum practical spacing resolution of 2 µm was used for higher resolution analyses and 20 µm spacing was used where average mineralogy across a whole polished section was required. The identification and quantification of minerals was determined using a pre-defined mineral database, known as Species Identification Protocol (SIP) archived in a mineral library (Pirrie et al. 2004; Armitage et al. 2010). Each mineral was assigned a colour for identification, and modal compositions were collated based on the areas they occupied in the polished section.

3.3.7 Wireline log and core analysis data

A suite of modern conventional wireline logs was available for each well including caliper, gamma, compressional sonic, bulk density, neutron and deep and shallow resistivity logs. Wireline data were reported every 15 cm, as this reflects the minimum resolution of the suite of logging tools. Core analysis data were also available for each well, including porosity, permeability, and grain density data.

3.4 Results

3.4.1 Core description and wireline

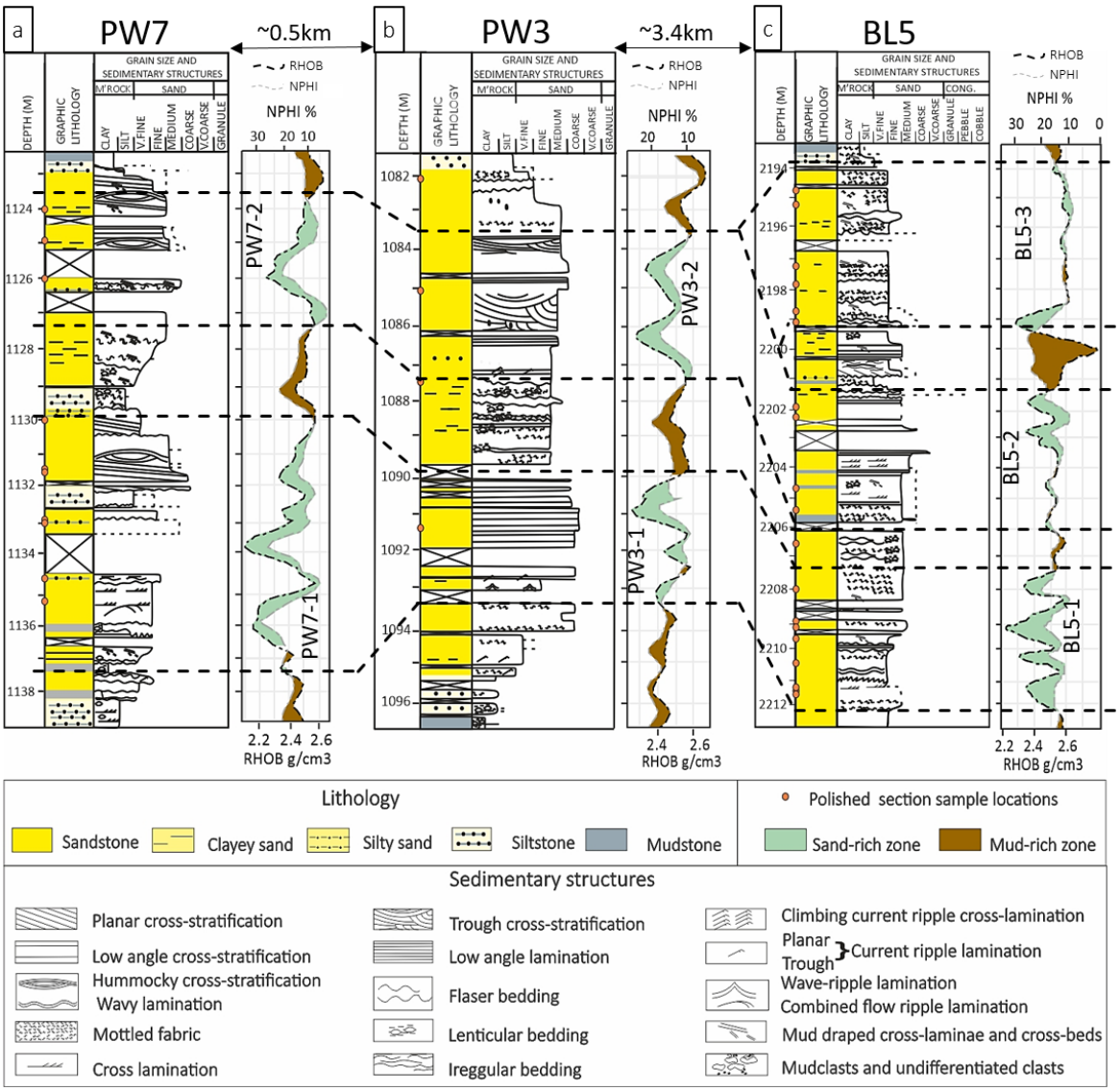

Figure 3.3: shows sedimentary logs from PW7 (a) PW3 (b) and BL5 (c). The sedimentary logs show the lithology and sedimentary structures in the Corallian sandstones. The NPHI_RHOB cross-over plots separate the sand-rich from the clay-rich sections of the sedimentary logs. The sand-rich sections are labelled by well as PW7-1, PW7-2, PW3-1, PW3-2, BL5-1, BL5-2 and BL5-3. Lithostratigraphic correlation show that none of the sand packages correlate with sand package BL5-3 which suggests that BL5-3 has a different genetic relationship to the other sand packages.

The Corallian clastic sediments are composed of sandstones and siltstones with local intermittent argillaceous intervals (Fig. 3.3). Sandstones comprise the main lithology with siltstones and mudstones making up minor portions of the basal, mid and top parts of the Corallian clastic section (Fig. 3.3). PW7 and PW3 are composed of medium grained sands with minor fine-grained sand, silt and clay (Fig. 3.3). BL5 is predominantly composed of medium grained sand and upper fine-grained sand, with minor very fine–grained sand, silt and clay (Fig 3.3). The sandstones have abundant sedimentary structures including low angle cross-stratification, planar cross-stratification, trough cross-stratification, low angle lamination, mud drapes, massive bedding, as well as hummocky cross-stratification. Other sedimentary structures include flaser bedding, lenticular bedding, wave ripple lamination, current ripple lamination, cross lamination and climbing current ripple lamination (Figure 3.3). Planar cross-stratification (Fig. 3.3a at 1131.4 m), hummocky cross-stratification (Fig. 3a at 1123.4 m) and trough-cross-stratification (Fig. 3.3b at 1085.4) are more common in PW3 and PW7; in contrast flaser beds (Fig. 3.3c at 2206.8 m), mud drapes (Fig. 3.3c at 2196.9) and argillaceous intervals mottled by bioturbation (Fig. 3.3c at 2207.4 m) are more common in BL5.

To objectively delineate sand-rich, from the clay-rich, intervals, neutron-density cross-over plots (Rider 1986) were used in conjunction with the sedimentary logs (Fig. 3.3), leading to the identification of seven sand packages. These are labelled PW7-1, PW7-2, PW3-1, PW3-2, BL5-1, BL5-2 and BL5-3; all are separated by argillaceous zones (Fig. 3.3). The sand packages have been correlated across the three wells. PW7-1, PW3-1 and BL5-1 can be easily correlated across all wells. Similarly, PW7-2, PW3-2 and BL5-2 can be correlated across all wells (Fig. 3.3). In contrast, BL5-3 cannot be correlated to any other sand package (Fig. 3.3).

3.4.2 Geochemical analysis

To compare the composition of sediments in the various sand packages, we have defined numerous element cross plots as well as geochemical indices. Indices and ratios are better than elemental concentration for studying clastic sediments as indices remove the effects of variable dilution by dominant minerals such as calcite. Indices are preferred to ratios as they vary from 0 to 1 rather than infinitely small to infinitely large values. Indices provide proxies for bulk lithology, mineralogy, and weathering characteristics. The geochemical indices have been calculated using the parts per million (ppm) values of the elements being compared. Lines have been drawn on the cross plots to indicate the range for granite and basalt (Figs. 3.4a-3.4e) which

are indicators of mafic and felsic provenance from endmember values reported in Krauskopf (1979). The granite and basalt lines are derived from molar proportions calculated from granite and basalt values as reported in Krauskopf (1979).

Ti and Al were compared as proxies for mafic or felsic provenance respectively (Andersson & Worden 2004). A cross plot of Ti and Al indicates a maximum Ti atomic fraction below 0.07 and aluminium has an atomic fraction of up to 0.9 (Fig. 3.4a). The sample points plot predominantly between the trajectories for basalt and granite suggesting a mixed mafic-felsic (intermediate) provenance for the Corallian sandstones (Fig. 3.4a).

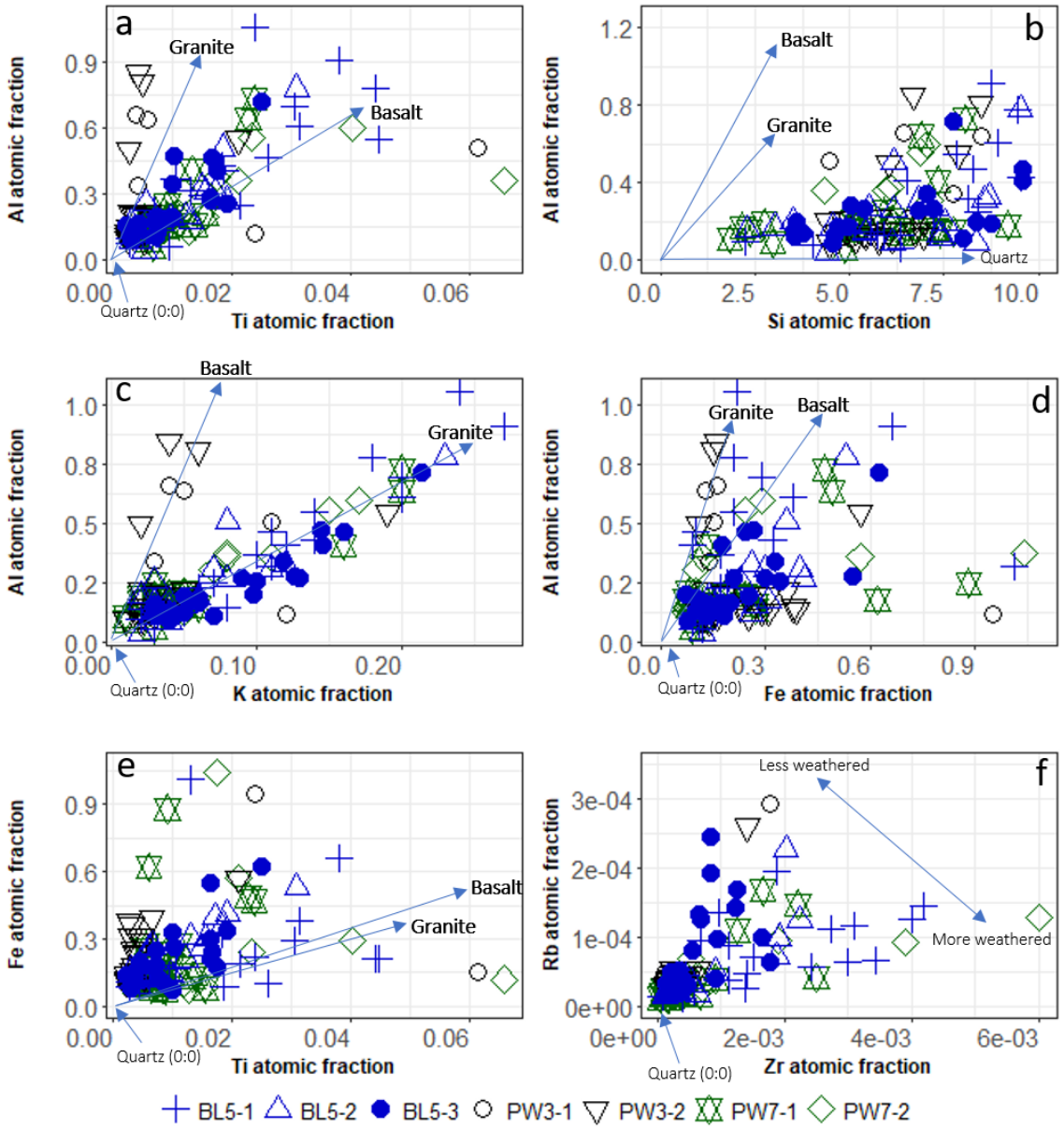

Figure 3.4: shows proxies for provenance, bulk lithology, mineralogy and weathering in the Corallian sandstones. The elements are expressed in atomic fractions to discount for quartz dilution and vector points have been included for granite and basalt using molar proportions calculated from Krauskopf (1979). (a) Compares Ti and Al content as proxies for mafic vs. felsic provenance. Sample points plot between the basalt and granite lines to indicate a source-area lithology of mixed mafic-felsic (intermediate) composition. Sample points cluster close to the origin to suggest hydrologic enrichment of quartz. (b) Sample points plot predominantly away from the basalt and granite line and cluster closer to the quartz line to underscore vast

quartz enrichment by hydrologic processes. (c) Vast sample points cluster around the graph's origin to indicate hydrologic enrichment of quartz. The elevated Al content is indicative of intense weathering. (d) Reflects local Fe enrichment in the sediments. The samples that plot away from the granite and basalt lines suggest Fe-enrichment by secondary processes such as weathering and diagenesis. (e) The Ti-Fe plot shows many sample points clustered along the basalt and granite lines to indicate significant mafic input to the sediments regardless of protolith. The plot indicates elevated Fe-rich rather than Ti-rich mafic influence on the sediments. (f) Is a proxy for weathering with elevated Zr as well as the clustering of sample points at the origin indicates enrichment of quartz by intense weathering.

The distribution of Ti to Al in the sand packages does not show a systematic pattern and suggest a general intermediate origin for the Corallian sandstones (Fig. 3.5e). Sample points however cluster around the origin of Figure 3.4a to suggest significant quartz enrichment in these compositionally intermediate rocks.

The cross plot of Si versus Al (Fig. 3.4b) as well as the high Si to Al index (Fig. 3.5a) indicates a high proportion of Si relative to Al suggesting that quartz is vastly dominant over feldspars micas, or other clay minerals which contain Al. The sample points plot closer to the Si axis and away from the basalt and granite lines to suggest significant quartz enrichment by secondary processes such as weathering and hydrologic sorting (Kroonenberg 1992). The cross plot of K versus Al confirms the enrichment of Si (note the dominance of samples near the origin) and also indicates the enrichment of Al relative to K as Al has an atomic fraction of up to 0.85 while K has a maximum atomic fraction less than 0.3. A significant proportion of samples plot along the granite line to suggest the presence of felsic minerals common in granites such as K-feldspar, and muscovite. Few samples cluster around the basalt line to indicate either minor occurrence of K-deficient minerals such as illite (Figs. 3.4c). The K versus Al plot approximates the chemical index of alteration (CIA) of Nesbitt & Young (1982) where the relatively stable oxide of Al is compared with the sum of oxides of Al and relatively unstable oxides of Na, K, and Ca. The Al to K index in Figure 3.5b indicates intense weathering with mean values greater than 0.5. BL5-1, 2 and 3 have the lowest mean values compared to the Palmers Wood sand packages.

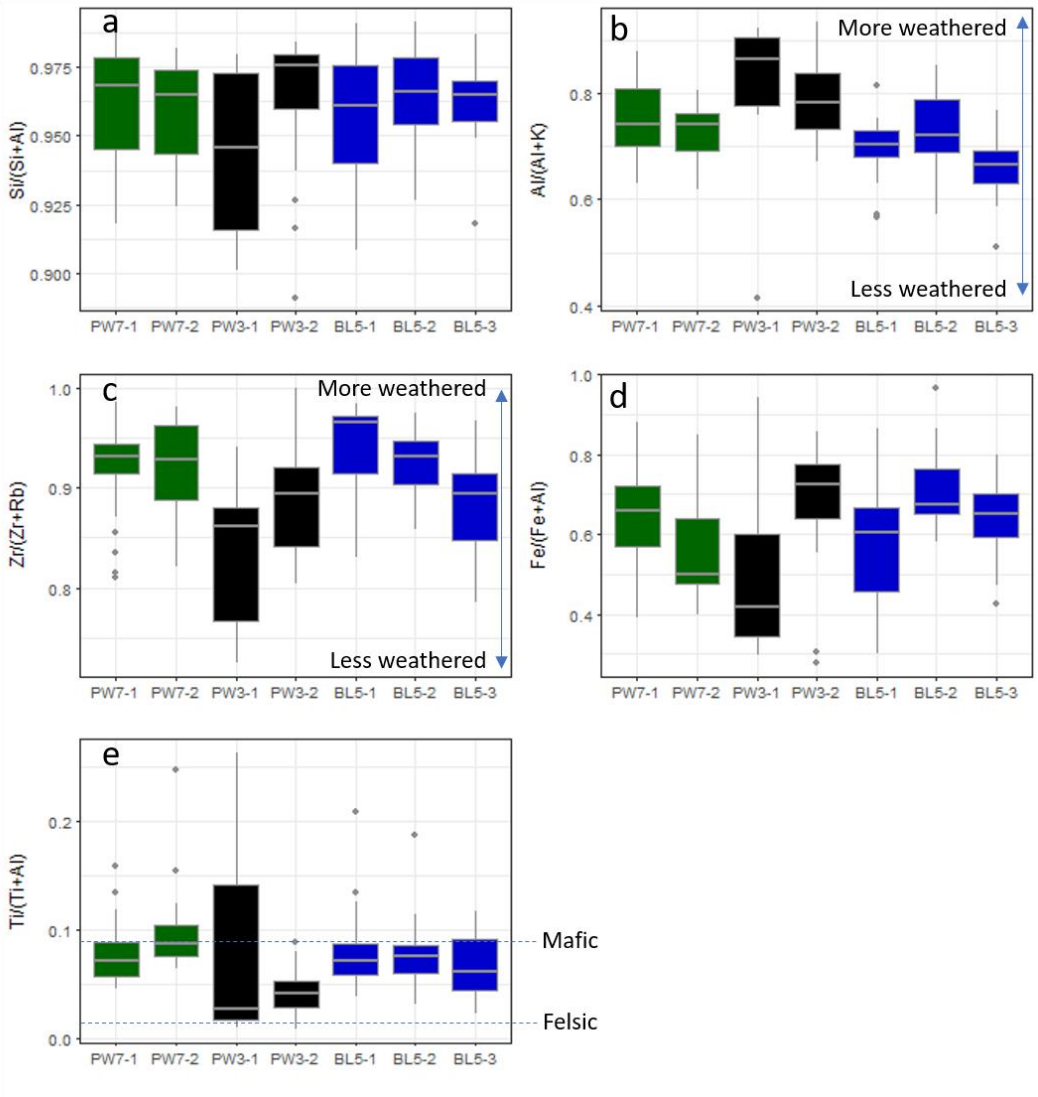

Figure 3.5: the box plots show selected element indices by sand packages calculated using their ppm concentration. The grey lines in the boxes are the mean values for each well. (a) shows high silica index for all sand packages indicative of vast quartz enrichment due to hydrological sorting. (b) indicates elevated Al content due to intense weathering in the sand packages similar to the chemical index of alteration of Nesbitt & Young (1982). BL5-1,2 and 3 have elevated K values which suggests less intense weathering in the Bletchingley area (c) also emphasizes intense weathering by the enrichment of the more resistant Zr relative to the more mobile Rb (d) shows differential sedimentological Fe-enrichment in the sand packages (e) the Ti-Al index shows dominant intermediate mean values between the mafic and felsic lines. The mafic and felsic lines are drawn based on ppm concentration of elements in basalt and granite respectively as reported in Krauskopf (1979).

Fe is present in significant quantities in these rocks (Fig. 3.4d) and Fe-Al relationship suggests the presence of Fe-rich Alumino-silicates such as berthierine and biotite. A significant proportion of samples plot away from the granite and basalt lines closer to the Fe axis to suggest enrichment by processes not typical for formation of basalt and granite (Fig. 3.4d). Fe is not enriched in specific sand packages and there is no suggestion of different Fe source-areas (Fig. 3.5d). Samples in Figure 3.4d similarly cluster around the origin to suggest quartz enrichment. Fe could have been transported in Fe-rich minerals such as Fe-clay, biotite and ilmenite, as indicated in the elevated Fe atomic fractions compared to Ti atomic fractions in (Fig. 3.4e). Titanium could have been transported as rutile, ilmenite, biotite or muscovite. The samples also concentrate closer to the Fe axis away from the granite and basalt lines (Fig. 3.4e).

Rb versus Zr has been used as a weathering indicator as both are present in sediments and have different stability Rubidium typically occurs in K-feldspars which are relatively unstable during weathering while Zr occurs in zircon, which is a stable mineral during weathering (Everett et al. 2019). The cross plot of Rb versus Zr shows that the Corallian sandstones are depleted in rubidium relative to zirconium to indicate significant weathering (Fig. 3.4f). BL5-3 has an elevated Rb content suggesting elevated feldspar input and less intense weathering of the sediment source material (Fig. 3.4f). Boxplots of Zr-Rb index also indicate slightly elevated Zr in BL5-1 and 2 as well as PW7-1 and PW7-2 (Fig. 3.5c) to indicate elevated weathering in these sandstones.

3.4.3 Optical mineralogy

3.4.3.1 Detrital mineralogy

The Corallian sandstones packages are composed of fine to medium-grained, predominantly moderately- to moderately-well-sorted sands with local poorly sorted sand intervals (Figs. 3.6, 7 and table 3.1). The detrital components of the Corallian sandstones include monocrystalline quartz, polycrystalline quartz, K-feldspar, plagioclase feldspar, Fe-ooids and bioclasts (Figs. 3.6 and 3.7). Monocrystalline quartz is present as rounded to subrounded grains (Fig. 3.6a), which locally show undulose extinction under cross-polarised light (Fig. 3.6a). Polycrystalline quartz is present as angular to sub-rounded grains (Fig. 3.6a) and is recognised under cross-polarised light as a single grain composed of several interlocking crystals each of which presents a distinct undulose extinction under cross-polarised light (Fig. 3.6a). Quartz grains

have embayments filled by early calcite (Fig. 3.6a) which suggests pre-diagenetic or early diagenetic corrosion and embayment.

K-feldspar and plagioclase feldspars are present in small quantities as angular grains in both the coarser-grained as well as finer-grained samples (Fig. 3.6 and Fig. 3.7). The K-feldspar grains occur as both altered and unaltered grains (Figs. 3.6a and 7a). Feldspars are more abundant in the fine-grained sand to clay-size fractions (Fig. 3.6c and 6d).

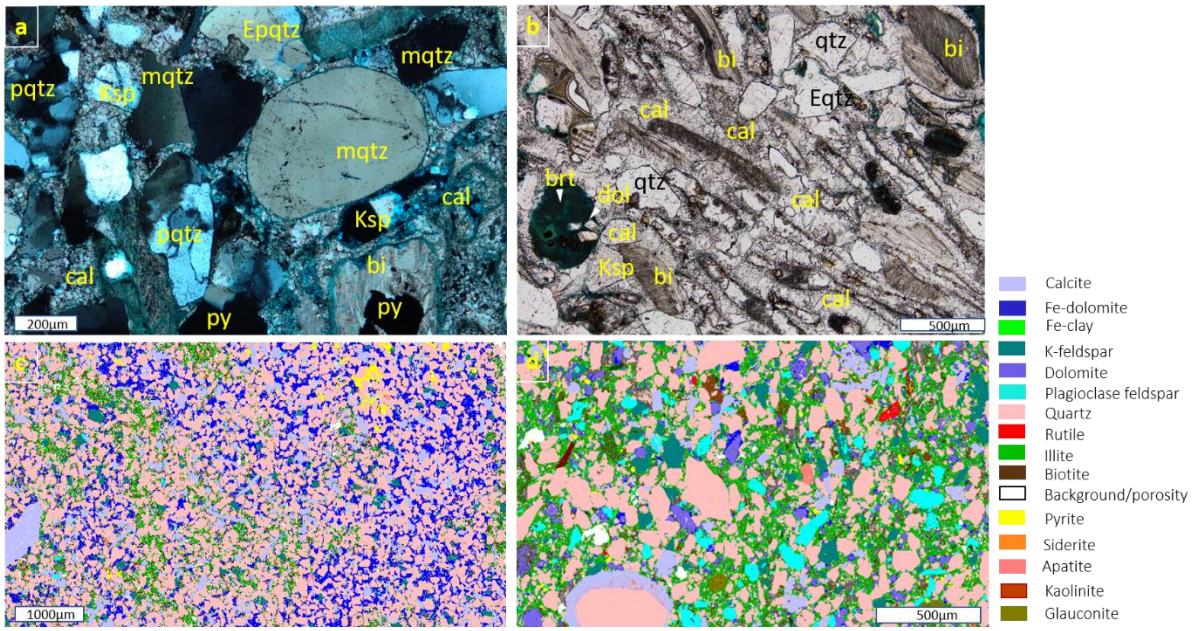

Figure 3.6: shows petrographic images which highlight the main mineralogy in the Corallian sandstones. (a) Is a cross-polarised image from PW3 (1083.1) highlighting monocrystalline and polycrystalline quartz, calcite cement, pyrite cement and a bivalve bioclast. The monocrystalline quartz at the top center-left shows undulose extinction typical of metamorphic quartz. (b) Is from PW7 (1131.9) showing pervasive calcite cement and several bivalve bioclasts under different stages of neomorphism and/or dissolution to form calcite cement. (c) BL5 (2197.9) intense cementation by Fe-rich minerals Fe-dolomite, and pyrite. (d) PW7 (1124.3) highlights the diverse mineralogy in the detrital clays as well as shows authigenic dolomite, Fe-dolomite and calcite.

Qtz: quartz, mqtz: monocrystalline quartz, pqtz: polycrystalline quartz, Epqtz: embayed polycrystalline quartz, Eqtz: embayed quartz; cal: calcite, py: pyrite, ksp: K-feldspar, dol: dolomite, brt: berthierine, bi: bivalve. Optical petrography suggests a felsic origin with potential significant sediment transport or reworking before deposition. The occurrence of iron-

rich minerals also suggests significant input of iron from the source-area or sedimentological Fe-enrichment.

Fe-ooids occur as detrital grains with cement aligned along their outer grain boundaries (Fig. 3.7b). Other minor detrital grains include biotite, illite, kaolinite, glauconite, rutile, apatite, muscovite and zircon (Figs. 3.6 and 7) as well as smectite and ilmenite.

The average total quartz (Qt), feldspar (F) and lithic grain (L) compositions of the sandstones are typical of quartz arenites with average composition $Qt_{97.2}F_{2.3}L_{0.6}$ (Fig. 3.8a). The average proportion of monocrystalline quartz (Qm), feldspar (F) and lithic grains plus polycrystalline quartz (Lt) is $Qm_{76.5}F_{2.3}Lt_{21.2}$ typical of a quartzose recycled orogen after Dickinson (1985) (Fig. 3.8b) where sediments are recycled and transported from deformed uplands such as fold-thrust systems. BL5 has more monocrystalline quartz and plots closer to the craton interior orogen than PW3 and PW7 (Fig. 3.8b). The monocrystalline quartz is more abundant in the BL5 sandstones with BL5-1 and BL5-3 having the greatest abundances (Fig. 3.9b).

BL5 has a slightly higher feldspar content than the other wells, especially in sandstone package BL5-3 which plot closer to the craton interior orogen (Fig. 3.8b). The lithic grain fragments are dominantly of metamorphic origin (Fig. 3.8c) with minor sedimentary grains and no igneous grains present (Fig. 3.8c). Polycrystalline quartz comprises an average of about 16.1% with minor extrabasinal chert, extrabasinal quartzite, extrabasinal mudstone and extrabasinal sandstone making up less than 2% of total rock volume (Table 3.1). Polycrystalline quartz is more abundant in the Palmers Wood sand packages PW7-2, PW3-1, PW7-1 and PW3-2 in order of abundance and less abundant in BL5-1, BL5-3 and BL5-2 in order of abundance (Fig. 3.9c).

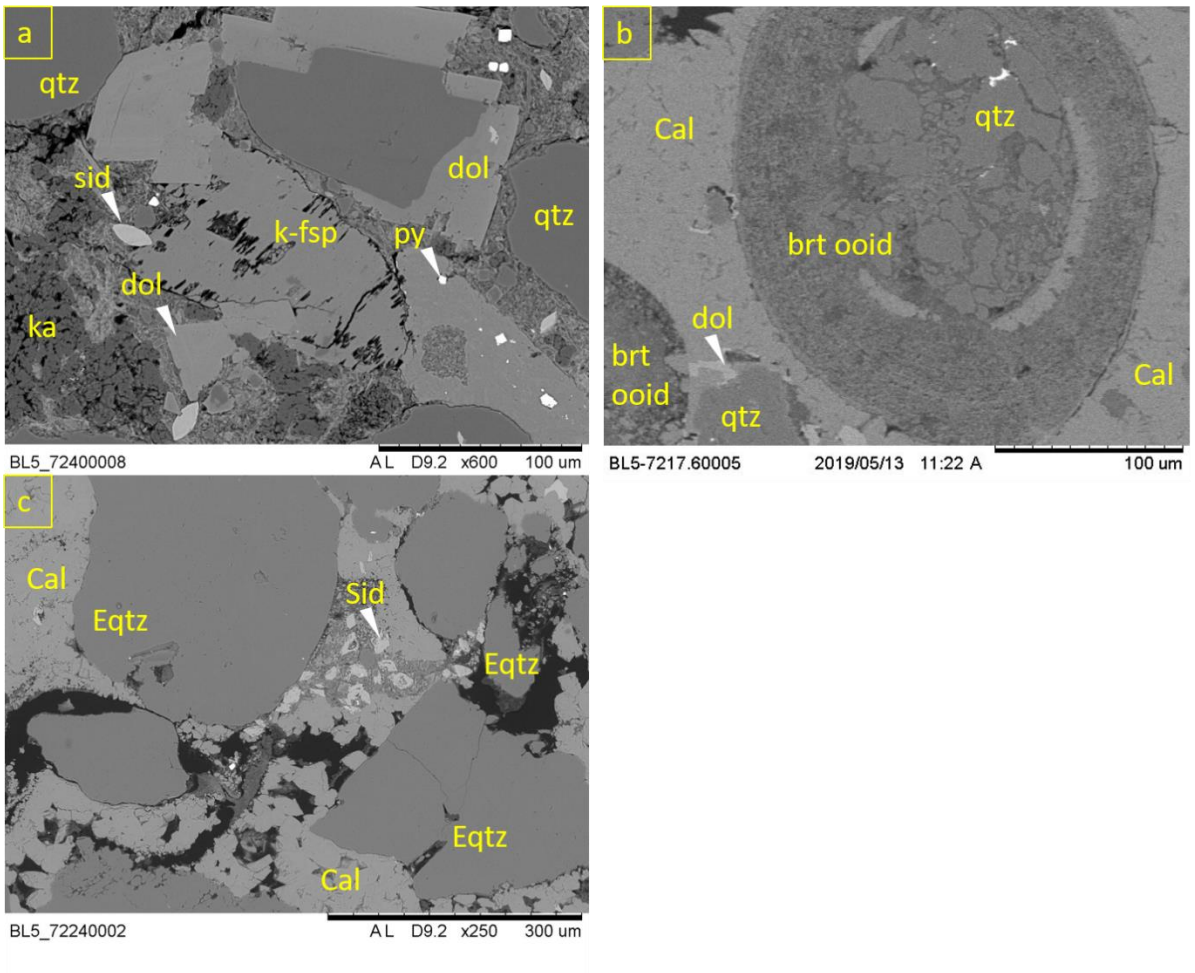

Figure 3.7: SEM-EDS micrograph showing mineralogy of the Corallian sandstones. (a) Shows slightly altered K-feldspar, siderite, kaolinite, pyrite, dolomite and quartz. (b) Shows a berthierine ooid in calcite cement. The ooid is held in the rock fabric by calcite cement, typical of detrital grains. (c) shows embayed quartz in a calcite cemented rock. py: pyrite, k-fsp: potassium feldspar, qtz: quartz, Eqtz: embayed quartz; dol: dolomite, ka: kaolinite, brt: berthierine.

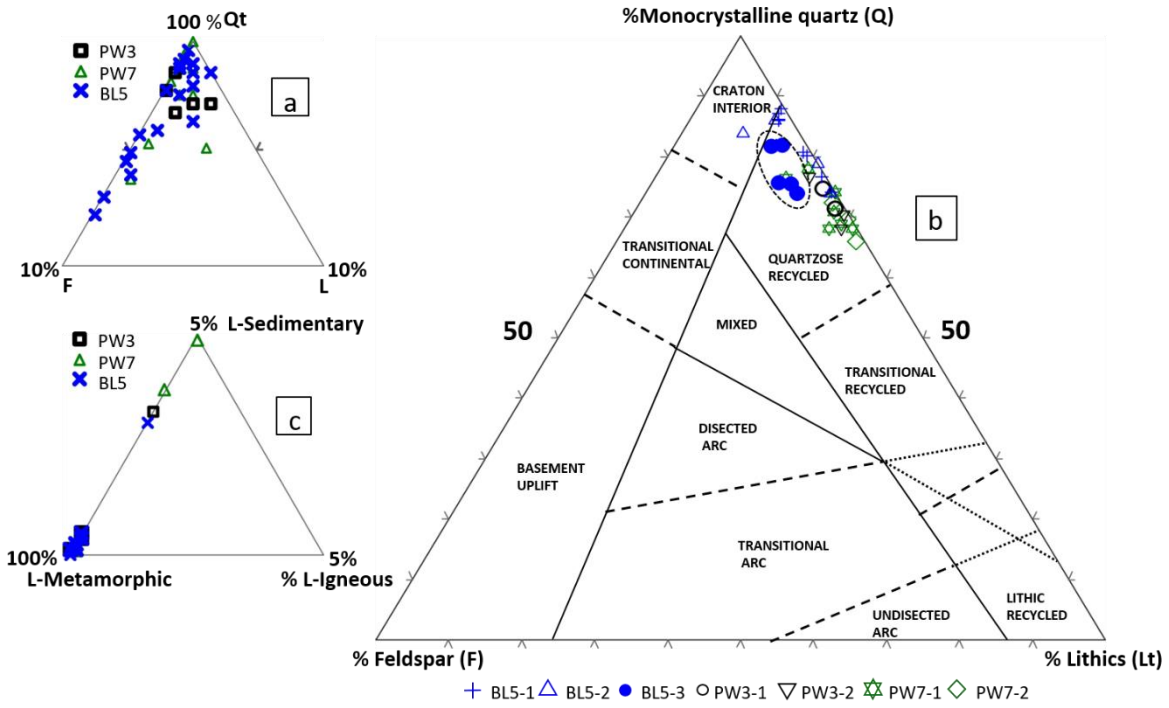

Figure 3.8: (a) QtFL plot for PW7, PW3 and BL5 showing the relative proportion in percent of total detrital quartz (Qt), feldspars (F), and lithic grains (L). The plot shows a dominant quartz –rich lithology for the sandstones with minor feldspars and lithic grain fragments. This is indicative of a mature sediment source typical of long sediment transport and/or reworked sediments which has undergone intense hydrologic sorting. (b) QmFL compositional plot of the Corallian sandstones: after Dickinson 1985 to show source-area tectonic setting. Monocrystalline quartz shows a dominant proportion above 60% relative to feldspars and lithic grain components (Igneous +sedimentary +metamorphic rock fragments). The sample points plot dominantly in the quartzose recycled orogen region with BL5 having more monocrystalline quartz than PW3 and PW7. Sandstone package BL5-3 has more feldspars and clusters close to the craton interior orogen. (c) The lithic fragments plot dominantly in the metamorphic zone (>90%) with minor sedimentary clasts (<5%) and no igneous grains. The dominance of quartzose sediments and low feldspar content suggests an intensely weathered hinterland.

Grain size analysis indicate that the Palmers Wood sand packages have coarser grain sizes than the Bletchingley sand packages (Fig. 3.9a). This systematic difference in grain size suggests different processes were responsible for deposition of sandstones in the two fields.

SEM-EDS boxplots analysis confirms the high quartz content of ≥ 90% of the detrital grains in all the sand packages (Fig. 3.10a). SEM-EDS also confirms elevated quantities of K-feldspar, plagioclase feldspar, zircon, rutile, illite, muscovite, biotite, Fe-clay and kaolinite in BL5 relative to the Palmers Wood area (Fig. 3.10). Illite, muscovite and biotite show a similar relationship by sand packages. SEM-EDS analysis shows the highest K-feldspar content in BL5-2 and BL5-3 (Fig10b) and the highest plagioclase feldspar content in BL5-1, BL5-2 and BL5-3 (Fig.10c).

Table 3:1: Summary of detrital mineralogy for the Corallian sandstones from point counting

Well	Depth (m)	Monocrystalline quartz	Polycrystalline quartz	Poly+Monocrystalline quartz	Extrabasinal Chert	Extrabasinal quartzite	Extrabasinal sandstone	K-feldspar	Plagioclase feldspar	Bioclasts	Muscovite	Biotite	Fe ooids	Glauconite	Apatite	Extrabasinal mudstone	Matrix	Grain size (mm)	Sorting (Trask)
PW3	1082.3	22.0	9.0	31.1	0.3	0.3	0.0	0.7	0.0	3.0	0.0	0.0	0.3	0.0	0.3	0.0	2.0	0.4	Moderate
PW3	1085.1	33.4	12.8	46.2	0.0	1.0	0.0	0.3	0.0	0.7	0.0	0.3	0.6	0.0	0.3	0.0	0.3	0.4	Moderate
PW3	1087.5	35.4	9.7	45.1	0.0	0.0	0.0	1.0	0.0	1.7	0.0	0.0	0.0	0.0	0.0	0.0	0.3	0.2	moderate well
PW3	1091.4	38.8	11.7	50.5	0.0	0.7	0.0	0.7	0.0	0.0	0.0	0.0	0.0	0.0	0.3	0.0	0.0	0.3	Moderately well
PW3	1091.5	38.5	14.8	53.2	0.0	0.0	0.0	0.7	0.0	0.0	0.0	0.0	0.3	0.0	0.0	0.0	0.0	0.3	Moderately well
PW7	1124.0	35.9	15.1	51.0	0.0	0.3	0.0	0.0	0.3	1.0	0.0	0.0	0.0	0.0	0.0	0.0	0.0	0.3	Moderately well
PW7	1124.9	35.5	12.4	47.9	0.0	0.0	0.3	0.3	0.3	0.3	0.0	0.0	0.0	0.0	0.0	0.3	0.0	0.3	Moderately well
PW7	1126.0	32.9	16.4	49.4	0.0	0.0	0.0	0.3	0.3	0.9	0.0	0.0	0.0	0.0	0.0	0.0	0.0	0.3	Moderate
PW7	1130.0	18.1	6.3	24.4	0.0	0.0	0.0	0.0	0.0	4.6	0.0	0.0	0.3	0.0	0.0	0.0	0.7	0.4	Moderate
PW7	1131.6	33.5	15.4	48.9	0.0	0.0	0.0	0.3	0.0	3.4	0.0	0.0	0.0	0.0	0.0	0.0	0.0	0.3	Moderately well
PW7	1131.7	28.5	11.1	39.6	0.0	0.0	0.0	0.7	0.0	2.3	0.0	0.0	0.7	0.0	0.0	0.0	0.0	0.3	Moderately well
PW7	1132.9	33.1	13.4	46.5	0.0	0.3	0.0	1.6	0.3	0.0	0.0	0.0	0.0	0.0	0.0	0.0	0.0	0.3	Moderately well
PW7	1133.0	33.1	8.0	41.1	0.3	0.3	0.0	0.7	0.0	0.7	0.0	0.0	0.0	0.0	0.3	0.0	0.0	0.3	well
PW7	1134.6	36.5	8.3	44.8	0.0	0.3	0.0	2.3	0.3	0.3	0.0	0.3	0.0	0.3	0.0	0.0	18.8	0.2	Moderately well
PW7	1135.2	38.4	14.7	53.2	0.0	1.6	0.0	1.0	0.0	0.0	0.0	0.0	0.0	0.0	0.0	0.0	0.0	0.2	Moderately well
BL5	2194.7	41.7	11.4	53.1	0.0	0.0	0.3	2.7	0.3	1.3	0.0	0.0	0.0	0.0	0.3	0.0	2.3	0.3	Moderate
BL5	2195.2	38.5	6.3	44.8	0.0	0.0	0.0	2.0	0.3	0.0	0.0	0.0	0.0	0.0	0.0	0.0	6.3	0.2	Moderately well

BL5	2197.9	28.7	7.3	36.0	0.0	0.0	0.0	2.0	0.0	1.0	0.0	0.0	0.0	0.0	0.0	0.0	13.3	0.2	Moderately well
BL5	2198.8	39.1	6.7	45.8	0.0	0.3	0.0	1.3	0.3	1.6	0.0	0.0	0.0	0.3	0.0	0.0	0.0	0.2	Moderate
BL5	2199.1	43.9	10.0	53.9	0.0	0.0	0.0	4.0	0.0	0.0	0.0	0.0	0.0	0.7	0.0	0.0	0.3	0.2	Moderate
BL5	2201.9	31.3	10.7	42.0	0.0	0.0	0.0	0.3	0.0	1.3	0.0	0.0	0.0	0.0	1.0	0.0	0.0	0.3	Moderately well
BL5	2202.2	37.2	9.3	46.5	0.0	0.7	0.0	0.0	0.0	0.3	0.0	0.3	0.0	0.0	0.0	0.0	0.3	0.3	Moderately well
BL5	2204.7	51.5	7.0	58.5	0.0	0.0	0.0	1.0	0.3	0.6	0.0	0.0	0.0	0.0	0.0	0.0	0.0	0.2	Moderate
BL5	2205.8	39.0	6.7	45.8	0.0	0.0	0.0	2.0	0.0	0.7	0.7	5.0	0.0	0.0	0.0	0.0	4.7	0.2	Moderately well
BL5	2206.6	32.8	3.3	36.1	0.0	0.0	0.0	2.7	0.3	0.0	0.3	0.3	0.0	0.3	0.0	0.0	10.0	0.2	Moderate
BL5	2208.0	47.1	5.7	52.9	0.0	1.0	0.0	1.0	0.0	0.0	0.0	0.0	0.0	0.0	0.0	0.0	13.4	0.2	Moderate
BL5	2208.9	35.9	4.7	40.6	0.0	0.3	0.0	0.7	0.0	0.6	0.0	0.0	0.0	0.0	0.0	0.0	0.0	0.2	Moderately well
BL5	2209.2	53.3	6.7	60.0	0.0	0.3	0.0	0.3	0.0	0.0	0.0	0.0	0.0	0.3	0.0	0.0	1.0	0.2	Moderate
BL5	2209.5	52.2	12.4	64.6	0.0	0.0	0.0	0.6	0.0	1.3	0.0	0.0	0.0	0.0	0.0	0.0	0.3	0.2	Moderately well
BL5	2210.4	34.8	10.0	44.9	0.0	0.3	0.0	0.0	0.3	0.0	0.0	0.0	0.0	0.0	0.0	0.0	2.7	0.2	Moderate
BL5	2211.4	54.6	7.3	62.0	0.0	0.0	0.0	0.7	0.0	0.9	0.0	0.0	0.0	0.0	0.0	0.0	0.0	0.2	Moderately well
BL5	2211.5	46.2	15.8	62.0	0.0	0.0	0.0	0.0	0.3	0.0	0.0	0.0	0.0	0.0	0.0	0.0	2.9	0.2	Moderate
BL5	2211.6	50.2	10.7	60.9	0.0	0.6	0.0	0.3	0.3	0.3	0.0	0.0	0.0	0.0	0.0	0.0	0.0	0.2	Moderate
	Max.	54.63	16.41	64.56	0.30	1.60	0.30	4.02	0.30	4.62	0.70	5.01	0.71	0.70	1.00	0.30	18.78	0.43	
	Mean	37.93	10.04	47.97	0.02	0.25	0.02	0.98	0.12	0.88	0.03	0.19	0.07	0.06	0.08	0.01	2.42	0.24	
	Min.	18.09	3.31	24.42	0.00	0.00	0.00	0.00	0.00	0.00	0.00	0.00	0.00	0.00	0.00	0.00	0.00	0.15	

3.4.3.2 Authigenic mineralogy

Authigenic mineral volumes were determined by point counting (Table 3.2). The authigenic minerals in the Corallian sandstones include calcite, siderite, Fe-clay, pyrite, dolomite, and kaolinite others include traces of quartz cement, authigenic illite, and authigenic apatite (Figs. 3.6, 7 and Table 3.2). Calcite is the main authigenic mineral in these sandstones, making up to 62% (average of 28.7%) of total rock volume (Table 3.2). Calcite filled intergranular and

moldic pore spaces as well as separated detrital grains from each other, which indicates an

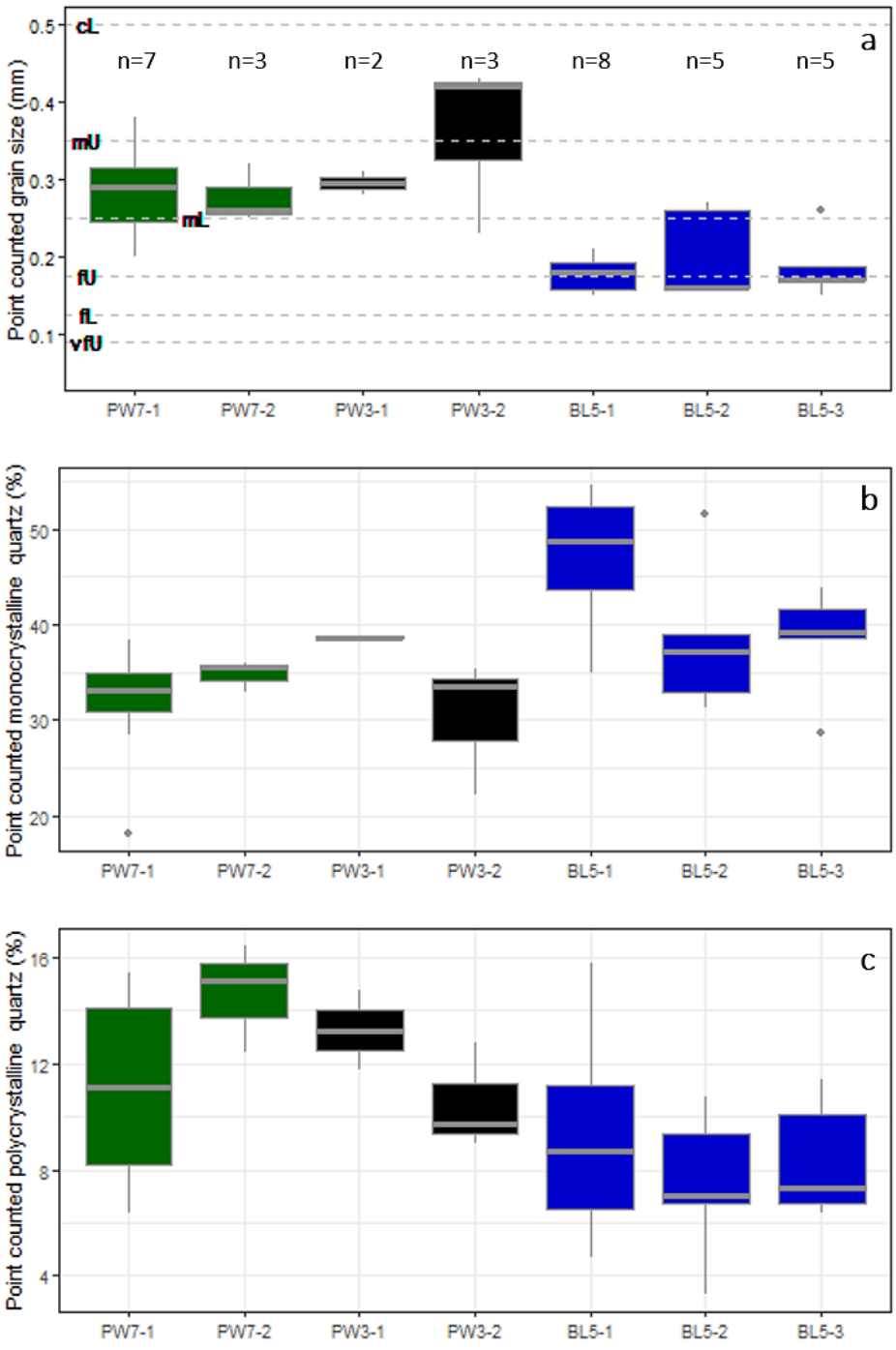

Figure 3.9: Boxplots for selected point count data for the Corallian sandstones (a) shows box plots for grain size measured from point counting analysis with grain sizes highlighted according to the Wentworth (1922) scale. The plots show medium-grained fractions in PW7-1 to PW3-2 and finer-grained fractions in BL5-1 to BL5-3 (b) shows more monocrystalline

quartz in BL5-1 to BL5-3 with the highest occurrence in BL5-1 (c) shows less polycrystalline quartz in BL5-1 to BL5-3.

early origin (Figs. 3.6a, 6b and 7b) (Barshep & Worden 2021, 2022). Calcite cement is present at different stages of neomorphism from bivalve shells in Figure 3.6b with the outline of the bivalve shells locally preserved by micrite envelopes.

The other cements include dolomite: up to 17.7% (average of 1.59%), siderite, up to 5% of total rock volume (average of 1.3%); Fe-clay, up to 3.6% (average of 0.9%); and pyrite, up to 2.7% (average of 0.6%) (Table 3.2). Other cements include illite, up to 22.3% (average of 2.4%), quartz, up to 7.9% (average 0.6%) and kaolinite, up to 1.0 % (average of 0.09%).

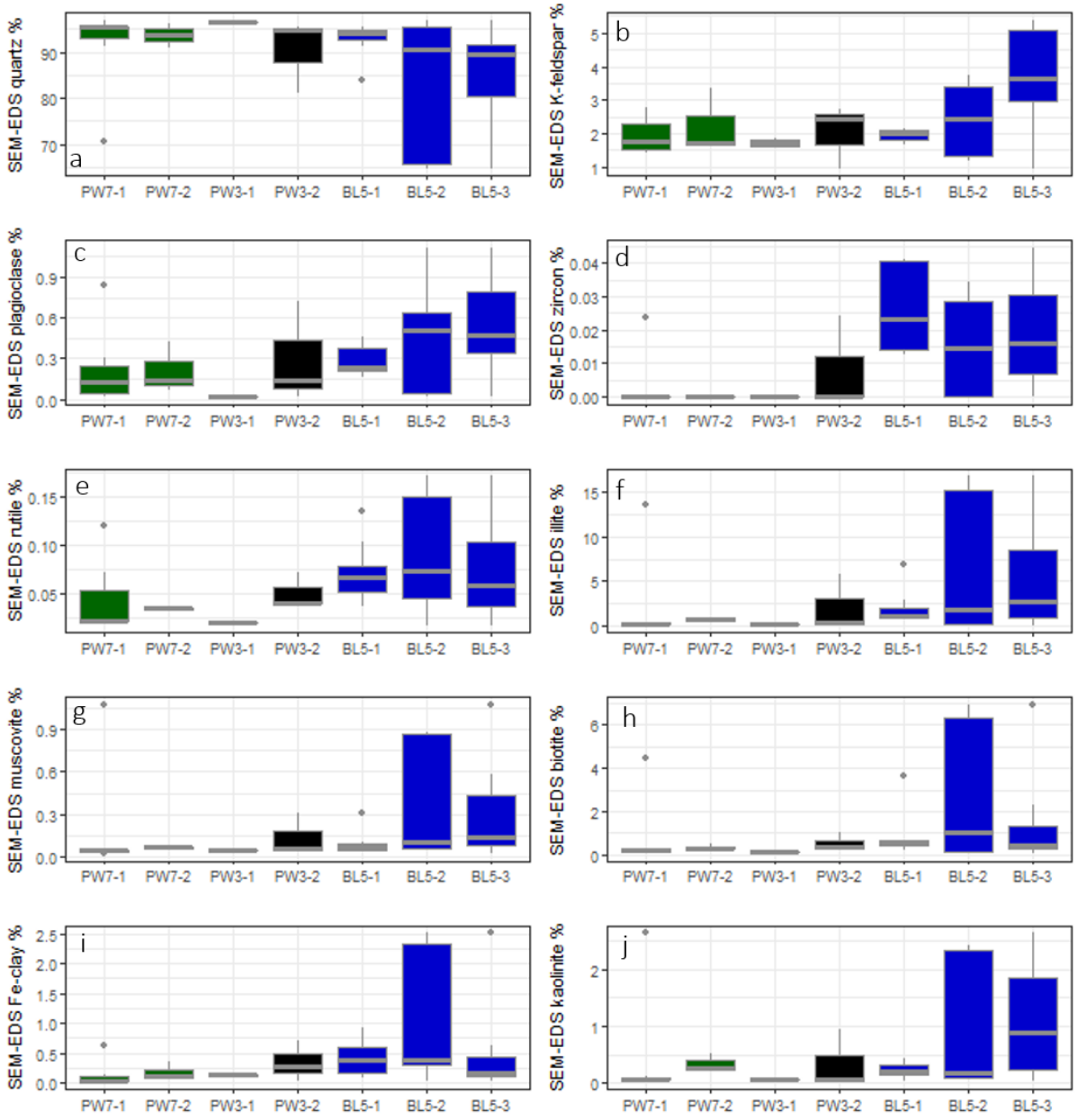

Figure 3.10: Boxplots of SEM-EDS mineralogy for the Corallian sandstones as a function of sand packages. The plots have been normalised for porosity, bioclasts and diagenetic components: calcite, siderite, dolomite, Fe-dolomite and pyrite with the detrital grain percentages expressed in the boxplots. (a) Shows high quartz content from ~65% to ~97% with sand packages BL5-2 and BL5-3 having the least sand content. (b) and (c) show K-feldspar and plagioclase feldspar respectively with BL5-2 and BL5-3 showing the highest feldspar content. (d) Shows trace amounts of zircon in PW7-1 to PW3-1 with increase in PW3-2 and the highest content in BL5-1, BL5-2 and BL5-3. Rutile shows varied levels in the sand

packages with BL5-1, BL5-2 and BL5-3 showing the highest quantity of rutile. (e). Illite (f) and muscovite (g) shows the highest content in BL5-2 with lesser content in BL5-3, BL5-1, PW3-2 and PW7-1, PW7-2 and PW3-1 having trace quantities. (h) Biotite has the highest content in BL5-2, similar to Fe-clay (i) and kaolinite (j). The mineralogical differences in BL5 suggests either a source-area evolution or tectonic controls on sediment distribution and transportation.

3.5 Discussion

3.5.1 Provenance

The QmFL composition of the Corallian sandstones within the quartzose recycled orogen (Fig. 3.8b) suggests a provenance of stratified rocks that were deformed, uplifted and eroded (Dickinson & Suczek 1979; Dickinson 1985). Sediments from a recycled orogen are susceptible significant reworking and can be from different sources (Dickinson 1985; Dickinson 1988). The medium-grained monocrystalline quartz grains here (Table 3.1, Fig. 3.6a, 3.8b) indicate an original plutonic igneous or metamorphic source-area (Pettijohn et al. 1973). The sediment maturity observed in the Corallian sandstones (Fig. 3.8a and 8b) however is not typical for the relatively short transport distance (~15km from the LBM to the study area) for plutonic rocks as such maturity results from intense weathering, significant transport-e.g. up to 3000km in Damuth & Fairbridge (1970)- or sediment recycling (Pettijohn et al. 1973; Milliman et al. 1975; Potter 1978; Tucker 1981; Kroonenberg 1992). Original plutonic rocks would require significant alteration such as hydrologic sorting to reach the level of maturity observed in the Corallian sandstones. Hydrologic sorting typically causes separation of grain size of specific minerals, sorting of minerals by density and enrichment in quartz content (Kroonenberg 1992). Evidence for hydrologic sorting in the Corallian sandstones include significant quartz enrichment (Figs. 3.4a-4f and 8a), elevated heavy minerals zircon and rutile content in BL5 (Figs. 3.10d and 10e), elevated micas in BL5, separation of coarser-grained fractions and finer-grained fractions between the Palmers Wood area and Bletchingley area (Fig. 3.9a), and concentration of feldspars in the Bletchingley area (Figs. 3.10b and 3.10c).

Lithic grains present in the Corallian sandstones such as polycrystalline quartz and minor quartzite (Figs. 3.6a, 3.8c, 3.9c and Table 3.1) are indicative of metamorphic rocks in the source-area (Blatt 1967; Pettijohn et al. 1973; Basu et al. 1975). Polycrystalline quartz is

susceptible to mechanical weathering and disintegrates into monocrystalline quartz in mature sediments (Basu et al. 1975; Dickinson 1985) hence polycrystalline quartz content is expected to be low in mature sediments (Pettijohn et al. 1973). The high polycrystalline quartz (up to 16%) in the mature Corallian sandstones suggests a much higher original polycrystalline quartz fraction hence a significant metamorphic influence on provenance. The presence of lithic grains of sedimentary and metamorphic origin in the Corallian sandstones (Table 3.1) suggests reworking of sedimentary or metamorphic rocks (Dickinson & Suczek 1979). Given the evidence for sedimentary and metamorphic input as well as sediment recycling and the absence of igneous grains (Fig. 3.8c), the Corallian sediments were thus most likely sourced from a metasedimenary source-area.

Ti-Al cross plot indicates vast sample points between the granite and basalt trajectories to indicate a predominant mixed mafic-felsic provenance (Fig. 3.4a). Ti and Al are useful indicators of mafic and felsic provenance (Andersson & Worden 2004) as Ti is relatively enriched in basaltic rocks and Al is slightly enriched in felsic rocks (Krauskopf 1979; Bhattacharjee & Mondal 2021). Ti and Al are both relatively stable and immobile elements under conditions of weathering and transport hence are useful indicators of provenance in sediments (Hallberg 1984). The distribution of Ti to Al does not show a specific pattern by sand packages (Fig. 3.5e); and predominantly plot within the intermediate provenance to indicate a general intermediate provenance for all the sand packages.

Elevated iron content in these sandstones relative to Al indicates a significant iron input from Fe-Al minerals such as biotite and berthierine (Fig. 3.4d and 3.5d). In sedimentary rocks, Fe-Ti minerals such as ilmenite are depleted in Fe during their alteration due to the oxidation of iron in the ilmenite lattice (Morad & Adin 1986). The elevated Fe in the Corallian sandstones indicates that Fe-rich minerals predominate over Ti-rich minerals in the source-area (Fig. 3.4e) such that sedimentary oxidation did not significantly elevate the relative concentration of Ti to Fe. Fe was possibly sourced from protolith or sediment pathways, the occurrence of Fe-rich minerals such as biotite (Fig. 3.10h) strongly suggest an iron-rich hinterland. Vast sample points plot away from the granite and basalt trajectories, close to the Fe-axis and near the origin of Figure 3.4d to suggest that Fe was concentrated by processes outside of the primary mineralogy in the source-area. Berthierine ooids are Fe-rich minerals of sedimentary origin and their occurrence in the Corallian sandstones (Fig. 3.7b) suggests weathering of Fe-rich

sediment pathways, hence sedimentological concentration of Fe. The presence of diagenetic Fe-minerals such as pyrite, siderite and dolomite also suggests significant diagenetic concentration of Fe in the Corallian sandstones.

Table 3:2: Summary of authigenic mineralogy for the Corallian sandstones from point counting

Well	Depth (m)	Quartz	Calcite	Dolomite	Siderite	Illite	Kaolinite	Fe-Clay	Pyrite	Apatite
PW3	1082.3	0.0	54.1	0.3	5.0	0.3	0.0	0.0	1.0	1.3
PW3	1085.1	0.0	42.5	0.0	0.3	0.0	0.0	1.0	0.0	0.3
PW3	1087.5	0.0	43.8	0.0	2.2	0.0	0.0	0.0	0.3	0.0
PW3	1091.4	0.0	34.3	0.7	2.3	0.0	0.0	0.3	0.0	0.3
PW3	1091.5	0.3	32.7	0.3	4.0	0.0	0.0	1.5	0.7	0.0
PW7	1124.0	0.0	27.3	0.7	0.3	0.0	0.0	2.2	0.0	0.0
PW7	1124.9	0.0	43.2	0.3	0.0	0.3	0.0	0.3	0.0	0.0
PW7	1126.0	0.0	19.1	1.2	0.0	0.0	0.0	0.3	0.3	0.0
PW7	1130.0	0.0	62.9	0.0	1.2	0.0	0.0	0.3	0.0	0.0
PW7	1131.6	0.3	26.1	0.3	4.6	0.7	0.0	1.5	0.3	0.0
PW7	1131.7	0.0	24.5	1.2	4.3	0.0	0.0	1.6	0.3	0.0
PW7	1132.9	0.0	43.1	0.0	2.3	0.0	0.0	0.0	0.0	0.0
PW7	1133.0	0.0	51.8	0.0	0.6	0.9	0.0	0.0	0.3	0.3
PW7	1134.6	0.0	5.9	0.7	2.0	8.3	1.0	1.0	1.0	0.0
PW7	1135.2	0.0	39.4	0.0	0.3	0.0	0.0	0.0	0.3	0.0
BL5	2194.7	0.7	24.9	7.1	0.3	2.3	0.0	0.7	2.0	0.6
BL5	2195.2	1.3	37.8	1.0	1.3	1.3	0.3	0.0	1.3	0.0
BL5	2197.9	0.7	22.4	17.7	2.0	0.3	0.0	0.0	2.7	0.0
BL5	2198.8	0.0	42.0	2.1	0.6	2.0	0.0	0.7	1.7	0.0
BL5	2199.1	7.9	6.4	1.0	0.3	0.7	0.3	2.5	1.7	0.0
BL5	2201.9	0.0	48.8	0.0	0.9	0.0	0.0	0.6	0.3	1.0
BL5	2202.2	0.3	39.4	1.3	1.7	0.3	0.0	1.4	0.0	0.0
BL5	2204.7	0.7	10.2	1.0	1.0	2.7	0.0	3.6	1.0	0.0

BL5	2205.8	1.0	6.3	0.7	0.7	22.3	0.3	1.3	0.7	0.0
BL5	2206.6	0.7	22.4	8.3	1.7	12.0	0.0	1.3	0.6	0.0
BL5	2208.0	0.7	3.0	0.3	0.7	10.6	0.0	0.6	1.0	0.0
BL5	2208.9	0.0	46.0	0.9	0.7	2.6	0.0	1.6	0.3	0.0
BL5	2209.2	0.3	16.0	0.0	0.0	3.9	0.3	1.0	0.0	0.0
BL5	2209.5	0.0	9.2	0.7	0.0	1.0	0.0	1.0	0.0	0.0
BL5	2210.4	0.0	38.7	0.3	1.3	1.0	0.3	0.0	1.0	0.0
BL5	2211.4	3.0	1.9	1.3	0.3	2.3	0.0	1.3	1.6	0.0
BL5	2211.6	0.6	9.0	2.7	0.7	2.0	0.3	0.3	0.0	0.0
BL5	2211.6	2.0	7.3	0.3	0.0	1.7	0.3	2.3	0.7	0.0
	Max	7.9	62.9	17.7	5.0	22.3	1.0	3.6	2.7	1.3
	Mean	0.6	29.2	1.6	1.4	2.4	0.1	0.9	0.6	0.1
	Min.	0.0	1.9	0.0	0.0	0.0	0.0	0.0	0.0	0.0

3.5.2 Tectonic settings

The average $Qm_{76.5}F_{2.3}L_{21.2}$ composition of the Corallian sandstones is indicative of the foreland uplift provenance (a subdivision of recycled orogens) where elevated foreland thrust-fold belts supply sediments directly into adjacent foreland basins (Dickinson & Suczek 1979). This is consistent with the history of the London Platform which remained stable hence was elevated relative to the subsiding Upper Jurassic Weald Basin (Hawkes et al. 1998; Pharaoh 2018). Foreland basins are described by Dickinson & Suczek (1979) to flank collision or arc orogens such that their elevated fold-thrust uplands typically act as a barrier to sediments from magmatic arc or suture belts. Consequently sediment supply to foreland basins is predominantly from recycled sedimentary successions (Dickinson & Suczek 1979). The interpretation of recycled sedimentary successions is consistent with the Corallian sandstones here as they are composed mainly of recycled sediments without significant magmatic input (Figs. 3.8a and 8c).

Sediments from BL5 show more monocrystalline quartz and cluster closer to the craton interior orogen boundary (Fig. 3.8b) which may indicates tectonic evolution in the source-area. The stratigraphically youngest sand package in BL5, BL5-3, has more feldspars and clusters closest to the craton interior orogeny. As BL5-3 was deposited during a period of accelerated fault

movement (Barshep & Worden 2022) typified by increased feldspar supply to depositional areas (Dapples et al. 1953; Pettijohn et al. 1973); higher feldspar in BL5-3 is therefore indicative of evolution of source-area and/or sediment supply caused by tectonism. This is because subsidence increases the gradient with the hinterland thereby increasing erosion rates and sediment supply (Leeder et al. 1998; Mack 2003).

3.5.3 Climate and weathering

Mineralogical proxies in the Corallian sandstones show warm, humid, conditions with high precipitation rates capable of fluvial recharge. These mineralogical proxies include (i) detrital kaolinite (Figs. 3.6c and 3.6d), (ii) iron-rich minerals, pyrite, Fe-dolomite, siderite and berthierine (Figs. 3.6a, 3.6b, 3.6c, 3.7a), (iii) the dominance of quartz over feldspars (Figs. 3.4a, and 3.8a) (iv) embayed quartz grains (Figs. 3.6a, 3.6b, 3.6d and 3.7c).

Kaolinite is indicative of warm tropical to sub-tropical climates with high rainfall rates and vegetation (Burley & Worden 2003b). This is because, the decay of organic matter under humid conditions creates acidity which enhances chemical weathering of alumino-silicate rocks to produce kaolinite (Hallam 1975; Burley & Worden 2003b). Evaporite minerals e.g. gypsum and anhydrite are developed under arid conditions with subaerial exposure conducive for dissolved salts to concentrate and form minerals (Tucker 1981; Ruffell & Rawson 1994). The presence of kaolinite in detrital clay and almost no smectite or evaporate minerals such as gypsum/anhydrite (Fig. 3.6) indicates humid conditions in the Upper Jurassic hinterland (Barshep & Worden 2022).

Fe-dolomite, siderite, pyrite and berthierine in marine sediment indicates warm, humid, continental weathering as development of these iron-rich minerals in shallow marine environments involves terrigenous weathering under humid conditions to form lateritic soils, which when eroded transports iron to the marine environment (Tucker 1981; Hallam 1984).

The intense chemical weathering and iron enrichment in the source-area is emphasised by the low fraction and index of K relative to Al (Figs. 3.4c and 3.5b) as enrichment of aluminium is typical of intense chemical weathering (Middleton 1960; Krissek & Kyle 2001). Enrichment of Al in the Palmers Wood wells is indicative of intense chemical weathering capable of depleting K-rich minerals and enrichment of Al e.g.(Emery et al. 1990). Other indicators of intense weathering include the dominance of quartz over feldspars (Fig. 3.8a), depletion of Rb to Zr (Fig. 3.4f) and presence of altered K-feldspar (Fig. 3.7a) (Damuth & Fairbridge 1970;

Milliman et al. 1975; Dickinson 1985). Rb and Zr have different mobility during weathering with Zr (in Zircon and sphene) relatively more stable compared to the Rb (in K-feldspars)(Everett et al. 2019). The elevated Zircon and feldspars in BL5 suggests intense mechanical weathering which typically does not completely remove feldspars from sediments but causes reduction in feldspar grain-size (Odom et al. 1976). The mechanical stability of zircon also causes zircon enrichment during physical weathering (Hubert 1962) thereby indicating intense mechanical weathering of sediments in the BL5 area.

Embayments and evidence of corrosion (Figs. 3.6a, 3.6b, 3.6d and 3.7c) have been interpreted as evidence for tropical and subtropical environments (Cleary & Conolly 1971; Potter 1978) as well as volcanic provenance (Folk 1968). The sediments here do not have volcanic lithic grains (Fig. 3.8c) and locally occur with rounded edges (Fig. 3.6a, 3.6b and 3.6c) typical of sedimentary transport (Potter 1978) and precluding volcanic origin to embayments and corrosion. Embayments are therefore interpreted to be formed in sediments under tropical to subtropical conditions.

3.5.4 Sediment reworking and redistribution

The Corallian sandstones present mineralogical and textural differences between the Bletchingley and Palmers Wood areas which indicate either or all of tectonic evolution, changes in source-area weathering characteristics (Dickinson 1985) or changes in depositional processes (Odom et al. 1976). Hydrologic sorting during transportation and deposition of sediments may have significantly affected the distribution and texture of Corallian sandstones sediments in the study area. BL5 has elevated: K-feldspar (Fig.3.10b), plagioclase feldspar (Fig. 3.10c), zircon (Fig.3.10d), rutile (Fig. 3.10e), muscovite (Fig. 3.10g), biotite (Fig. 3.10h) Fe-clay (Fig. 3.10i) and monocrystalline quartz (Fig. 3.9b). BL5 also has smaller grain size fractions (Fig. 3.9a) and less polycrystalline quartz than PW7 and PW3 (Fig. 3.9c). The two fields are separated by a fault with evident up-dip and down-dip differences in hydrodynamic conditions (Barshep & Worden 2021, 2022). Sedimentary structures such as planar cross-stratification, hummocky cross-stratification, trough cross-stratification and stacked massive beds predominate up-dip in PW3 and PW7 (Figs. 3.3a and 3.3b) and indicate deposition under relatively high energy. Down-dip, relatively lower energy conditions prevailed in the Bletchingley area as evident from frequent bioturbated intervals and sedimentary structures such as mud drapes (Fig. 3.3c) (Barshep & Worden 2022). The textural and mineralogical

differences across the fault are most likely due to the hydrodynamic differences which are capable of causing differences in sediment characteristics and distribution (Folk 1956; Odom et al. 1976; Kroonenberg 1992). It is not uncommon for mature sandstones to have elevated feldspar content in their finer-grained fractions as observed in BL5. This is because feldspars are not destroyed when abraded during mechanical weathering but become finer-grained, hence maturity might be due to grain size and sorting rather than mineralogy or hinterland climates (Odom et al. 1976). In addition, fine-grained feldspars can be carried as suspension for long distances in large water bodies (Milliman et al. 1975). The high energy nearshore setting of the Palmers Wood area is susceptible to intense mechanical sediment reworking hence hydrological sorting would cause (i) deposition of coarser-grained fractions in the higher energy Palmers Wood area (Fig. 3.9a) (ii) potential mechanical breakdown of feldspars to finer-grains which remain in suspension in the higher energy Palmers Wood area, hence lower feldspar content (Figs. 3.10b and 3.10c) (iii) less mica, detrital illite and kaolinite in the Palmers Wood area as they would remain in suspension under high energy conditions (Figs. 3.10f to 3.10i). The larger grain sizes in the Palmers Wood area and elevated polycrystalline quartz content indicates intense chemical weathering capable of retaining coarser-grained sizes, diminished feldspar content and retain polycrystalline grains that did not mechanically disintegrate during transport (Potter 1978). Conversely, finer-grained mechanically unstable grains such as feldspars can be transported in suspension and deposited under lower energy conditions in the Bletchingley area. This will increase the feldspar content (Figs. 3.5b, 3.5c, 3.10b and 3.10c) as well as fine-grained mineral fractions present in detrital clay e.g. illite, muscovite, biotite, and kaolinite (Figs. 3.10f, 3.10g, 3.10h and 3.10j). Evidence of intense physical weathering in the Bletchingley sediments include elevated monocrystalline quartz (Fig. 3.9b), zircon (Fig. 3.10d) and rutile (Fig. 3.10e). Zircon and rutile have a high resistance to weathering and unlike unstable minerals like feldspars can be relatively enriched especially in the fine-grained fractions of weathered, transported and recycled sediments (Carroll 1953; Hubert 1962; Pettijohn et al. 1973; Hallberg 1984; Kroonenberg 1992; Dokuz & Tanyolu 2006). Their abundance in the finer-grained sediments in BL5 is thus attributed to intense recycling and sorting e.g. Dokuz & Tanyolu (2006). The elevated zircon, rutile, K-feldspar, plagioclase feldspar, biotite, muscovite, monocrystalline quartz and finer-grained sizes in the Bletchingley area are therefore not caused by source-area migration but hydrological sorting.

It is therefore critical that sedimentological processes be applied in provenance analysis to improve interpretation of depositional processes as related to provenance.

In summary, the comparison of mafic-felsic geochemical endmembers to investigate provenance and hydrological sorting is novel and improves on results derived from petrographic analysis as well as highlights hydrologic sorting. The incorporation of sedimentological analysis in this study highlighted the importance of sedimentary processes which caused redistribution of sediments in the basin which would otherwise have been attributed to source area migration hence a misinterpretation of the effects of provenance on sediment supply.

The study is limited by its geographic extent as it is based on the Bletchingley and Palmers Wood area in the northern part of the Weald Basin. The study is also limited by the availability of heavy mineral data for heavy mineral analysis. Results from this study has broad implications for identifying and separating the effect of sedimentary processes such as hydrologic sorting from provenance analysis. In addition the application of geochemical mafic-felsic endmembers can enhance the interpretation of sediment weathering and mineral enrichment by sedimentary processes. The approach applied here has wider implications for provenance analysis in any sedimentary basin where surface outcrops are not available for direct correlation with depositional mineralogy.

3.6 Conclusion

- The Corallian sandstones are composed of recycled coarse siliciclastic sands from a source-area with intermediate mineralogy. The source-area has many Fe sources which supplied Fe to the basin. Fe was probably enriched through transport over Fe-rich pathways and concentrated in the basin by diagenetic development of Fe-rich minerals.
- Reference to a Dickinson & Suczek (1979) type provenance model suggests the Corallian sandstones were sourced from a quartzose recycled orogen where stratified rocks are deformed, uplifted and eroded.
- Petrographic evidence shows major sediment input from a sedimentary as well as metamorphic source-area with no evidence of igneous input. This has led to the conclusion of a metasedimentary provenance for the Corallian sandstones.

- Paleoclimate indicators suggest a humid source-area capable of chemically-weathering feldspars creating kaolinite and oxidising iron compounds. The humid climate produced sufficient rainfall capable of transporting coarse siliciclastic to the basin.
- Spatial compositional and textural differences in sediment distribution was caused by hydrodynamic sorting not source-area migration. Tectonic evolution caused changes in depositional energy and enhanced the effects of hydrodynamic sorting.
- Integrating deposition controls in provenance analysis could enhance understanding of source-area geology, source-area migration, estimation of hinterland sediment maturity, and generally enhance results from bulk mineralogy and geochemical analysis.

Chapter 4: Reservoir quality and sedimentology in shallow marine sandstones: interplay between sand accumulation and carbonate and clay minerals

Chapter four is focused on depositional processes within the study area to extend the analyses in chapter three which focused on provenance. Chapter four decouples the relative influence of climate, sea level change and tectonism on sediment supply and investigates how these factors affect reservoir quality, reservoir quality distribution and reservoir architecture. Traditional approaches to reservoir quality prediction focus on diagenesis and underplay the effects of depositional controls thereby limiting the range of reservoir quality prediction away from well control points. This chapter aims to highlight the effect of depositional controls on reservoir quality distribution as a useful tool for reservoir quality analysis and prediction. Rather than focusing on the traditional approach of analysing diagenetic controls on reservoir quality, this chapter focuses on depositional controls on sediment supply and distribution then links them to reservoir quality. The study applies a sedimentological and sequence stratigraphic approach to correlate good and poor reservoir quality zones also to understand the controlling factors for the differences in reservoir quality during shallow burial.

This chapter is published in the Journal of Marine and Petroleum Geology:

Barshep, D.V. & Worden, R.H. 2022. Reservoir quality and sedimentology in shallow marine sandstones: Interplay between sand accumulation and carbonate and clay minerals. *Marine and Petroleum Geology*, **135**, 105398,

http://doi.org/https://doi.org/10.1016/j.marpetgeo.2021.105398.

ABSTRACT

Sedimentological studies are important in understanding and predicting reservoir quality, especially in shallow buried sandstones that are dominated by eogenetic processes. Understanding the sedimentological controls on siliciclastic depositional environments will enhance the knowledge and prediction of reservoir architecture and reservoir quality, both of which are essential to resource exploitation and future CCS and hydrogen storage projects. Here, a study of sedimentology and depositional mineralogy, as well as controls on the deposition of siliciclastic sandstones, from the shallow-buried, Upper Jurassic Corallian marine sandstones of the Weald Basin, UK is presented. These sandstones host small oil accumulations

and, being close to large centres of population, are possible gas storage or carbon capture and storage sites. The study employs wireline log analysis, high resolution core logging, optical petrography, and SEM-EDS imaging to investigate reservoir architecture and the relative importance of depositional versus secondary diagenetic controls on reservoir quality. Shallow marine conditions, adjacent to a continent experiencing a warm humid climate, are interpreted based on ichnofabrics and mineralogy. Tectonic processes influenced water depth which subsequently controlled both the quantity of detrital bioclastic material (and the resulting calcite cement), and the amount of detrital clay matrix. The eustatic influence on deposition led to the development of a relatively thin intra-Corallian mudstone which compartmentalises the reservoir into discrete upper and lower sand bodies. The results of this study underline the importance of integration of detailed sedimentological and wireline log analysis in improving the prediction of reservoir quality in tectonically active environments for shallow buried, eogenetic-dominated sandstones.

Keywords:

Weald Basin, Corallian sandstone, transgressive sandstones, reservoir quality prediction, eodiagenesis, tectonism, wireline log lithology

4.1 Introduction

Siliciclastic shallow-marine environments are one of the settings that mark the boundaries between continent and ocean. The transient nature of the boundaries between continent and ocean is due to the interplay of the mechanisms that control deposition, including relative sea level, tectonic processes such as fault movement, sediment flux and climate (Dailly 1975; Burton et al. 1987; Posamentier & Vail 1988; Wagoner et al. 1990; Lawrence 1993; Andrieu et al. 2016). The interplay of these four controls produces a wide range of possible depositional sedimentological characteristics (Walker & James 1992; Kupecz et al. 1997b) which in turn control reservoir quality, especially in shallow buried reservoir rocks (Worden et al. 2018d). It follows that reservoir quality prediction must involve sedimentological analysis of primary sand characteristics as well as petrophysical analysis of the effects of diagenetic processes and their evolution with time during burial, compaction and heating (Kupecz et al. 1997b).

Many studies have applied depositional mineralogy, facies and facies associations as key elements to unlock an appreciation of the depositional controls on reservoir quality (Schmid et

al. 2004; Rahman & Worden 2016b). Some studies have also considered the effects of primary depositional controls on reservoir quality (Griffiths et al. 2019b) but this approach is not routine with many studies overlooking regional sedimentological factors. The application of sequence stratigraphic techniques to disentangle and understand the relative influence of sea level change, tectonics, sediment supply and climate, together with depositional processes and subsequent diagenetic controls will lead to improved reservoir quality interpretations which in turn will enhance the prediction of reservoir quality away from, and between, well control points.

This study investigated the influence of depositional processes on the reservoir quality of shallow-buried siliciclastic reservoir rocks in the Weald Basin. The current burial depth is less than 1000 metres, but burial restoration by Palci et al. (2018a) has the Upper Jurassic buried as deep as 1500 m in the northern flank of the Weald Basin, before uplift to current depths. These Upper Jurassic rocks in the Weald Basin are dominated by eogenetic processes as they have not been buried very deeply, so that the physical and chemical processes that result from mesodiagenesis, and typically obscure depositional and eogenetic signals, have not occurred. This study focuses on sandstones from the Upper Jurassic Corallian Group (Fig. 4.1c), which were deposited during a period of active tectonism and sea level rise. The Corallian Group is dominated by carbonate lithologies across much of the UK (Arkell 1933b) but there are Corallian sandstones at outcrop on the Dorset coast (Allen & Underhill 1989; Goldring et al. 1998) and in Calne, Wiltshire (de Wet 1987). The Corallian sandstones are locally-important oil-bearing rocks in the Weald Basin (Trueman 2003a). The study aimed to understand the relative contributions of eustasy, tectonism and climate on sediment supply and deposition in this shallow marine depositional environment with the aim of appreciating their relative impacts on reservoir quality. The two oil fields employed in this study, Palmers Wood and Bletchingley, are relatively close to London and other populous parts of the SE of the UK. Given the proximity of these oil fields to energy-hungry areas and the UK's progressive drive to carbon-neutrality, it is possible that these relatively old petroleum discoveries could be re-purposed, in the near future, for one or other of carbon capture and storage, compressed air storage or hydrogen storage. Understanding the sedimentology, internal architecture and distribution of reservoir quality of Corallian sandstones may become increasingly important as the energy transition advances. This study addressed the following questions:

1. What were the tectonic, eustatic and climate conditions prevalent during the deposition of the Corallian sandstones in the Weald Basin?
2. What were the consequences of syn-sedimentary tectonism on reservoir architecture and reservoir properties (especially porosity)?
3. What controls reservoir quality in the Corallian sandstones in the Weald Basin?

To answer these questions, analyses were carried out on primary and secondary sedimentary structures in core, defined depositional facies and looked for links between sedimentological expressions and reservoir quality. Relationships were looked for between wireline log data, sedimentology and reservoir quality.

The results from this study show that sediment supply was controlled by tectonism under a warm humid climate that supported fluvial transport. Tectonism also caused differences in bioclast derived calcite development which controlled porosity differences between the two fields. The reservoir unit was stratigraphically separated into two distinct sand bodies by a transgressive flooding surface caused by sea level rise outpacing sediment supply. These results have implications for predicting reservoir quality in tectonically active shallow marine depositional environments similar to the case study locations.

4.2 The Weald Basin

4.2.1 Background geology and tectonism

The Weald Basin is bound to the north by the London-Brabant platform, to the south by the Portsdown-Paris Plage ridge (Portsdown-Middleton trend), the Hampshire and Wessex Basins to the west and it merges into the Paris Basin to the east (Butler & Pullan 1990; Hansen et al. 2002) (Fig. 3.1). The basement of the Weald Basin includes extensively-deformed later Palaeozoic (Middle Devonian to Lower Carboniferous) rocks whose deformation occurred during the Variscan orogeny (Butler & Pullan 1990; Taylor et al. 2001) (Figs. 3.1b and 4.1a). The Variscan deformation event was characterised by north-south compressional forces with resultant east-west thrusts (Fig. 3.1b) in the basement rocks (Butler & Pullan 1990; Hansen et al. 2002; Trueman 2003a).

The Weald Basin formed as a result of thermal subsidence after late Triassic to early Jurassic extensional faulting (Lake & Karner 1987), when north-south crustal extension, utilising earlier Variscan east-west faults, caused the Weald area to subside south of the stable London-Brabant

Platform (Hansen et al. 2002; Trueman 2003a). Sherwood Sandstone Group sediments, important geothermal and petroleum reservoirs in the Wessex Basin to the west (Downing et al. 1983; Hogg et al. 1996), do not typically extend into the Weald Basin as Mesozoic sedimentation in the Weald generally commenced with Rhaetian-Hettangian transgression over Devonian and Carboniferous basement (Andrews 2014).

The Lower Jurassic experienced the deposition of the transgressive limestone-shale units of the Lower Lias over the Palaeozoic basement which was followed by Middle Lias shale and Upper Lias shale-sandstone units (Sellwood et al. 1986; Andrews 2014). The presence of sandstones in the Upper Lias has been attributed to regression by Sellwood et al. (1986). Extensive carbonate ramp structures in the Middle Jurassic led to the deposition of the Inferior Oolite and the oil-bearing Great Oolite Formations (Butler & Pullan 1990; Heasley et al. 2000) whose passage into quieter conditions are marked by the muddy and ferruginous units towards the centre of the Weald Basin (Sellwood et al. 1986). Isopach maps from Sellwood et al. (1986) show the deposition of the upward-coarsening, intensely-bioturbated transition muddy sandstones of the Kellaways Beds with clays at the base and sand at the top (Ebukanson 1984).

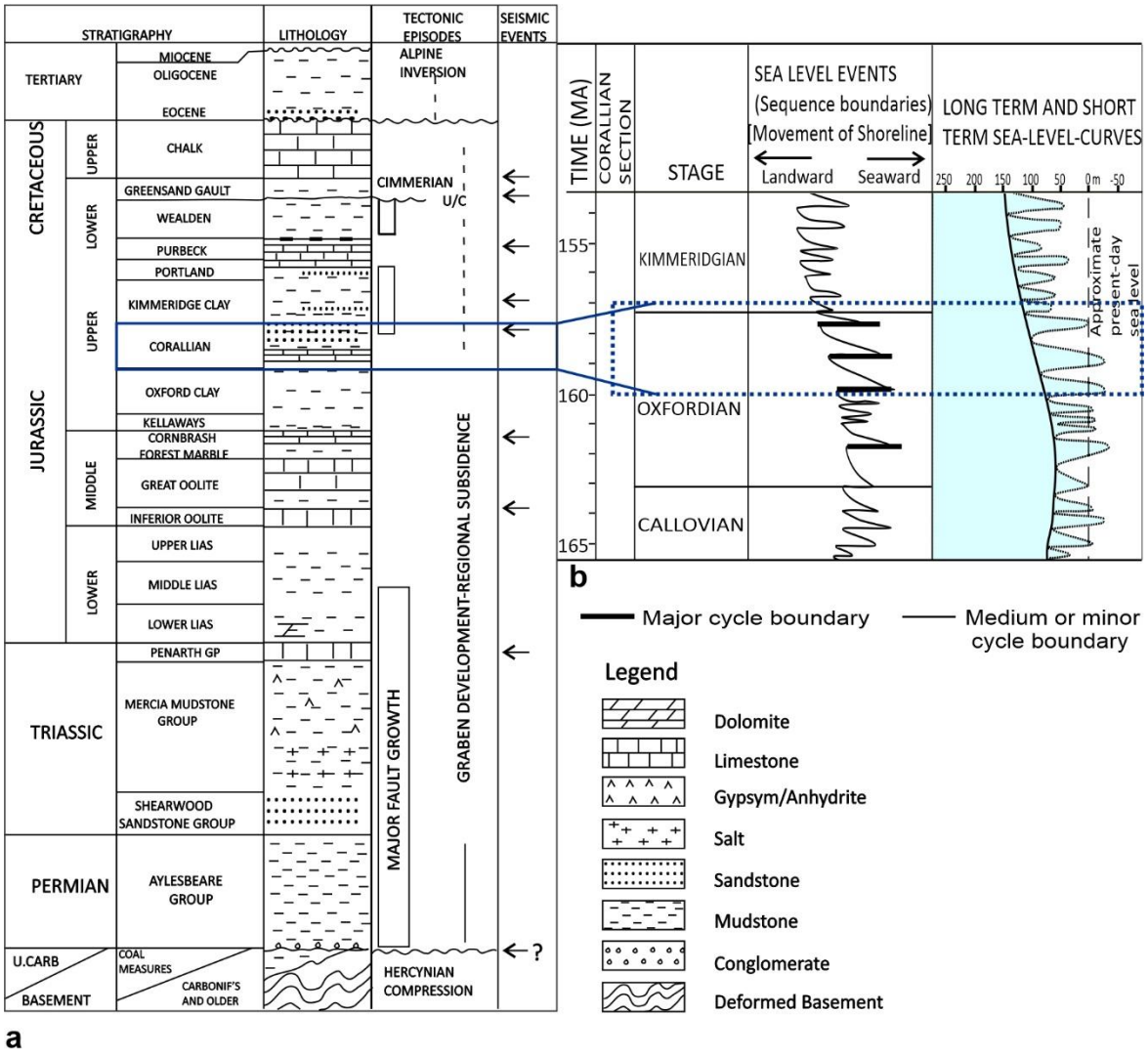
STRATIGRAPHY
LITHOLOGY
TECTONIC EPISODES
SEISMIC EVENTS
TERTIARY
MIOCENE
OLIGOCENE
EOCENE
ALPINE INVERSION
CRETACEOUS
UPPER
CHALK
LOWER
GREENSAND GAULT
WEALDEN
CIMMERIAN U/C
PURBECK
PORTLAND
KIMMERIDGE CLAY
UPPER
CORALLIAN
OXFORD CLAY
JURASSIC
KELLAWAYS
MIDDLE
CORNBRASH
FOREST MARBLE
GREAT OOLITE
INFERIOR OOLITE
LOWER
UPPER LIAS
MIDDLE LIAS
LOWER LIAS
PENARTH GP
TRIASSIC
MERCIA MUDSTONE GROUP
SHEARWOOD SANDSTONE GROUP
PERMIAN
AYLESBEARE GROUP
U.CARB
BASEMENT
COAL MEASURES
CARBONIF'S AND OLDER
MAJOR FAULT GROWTH
GRABEN DEVELOPMENT-REGIONAL SUBSIDENCE
HERCYNIAN COMPRESSION
?
a
TIME (MA)
CORALLIAN SECTION
STAGE
SEA LEVEL EVENTS
(Sequence boundaries)
[Movement of Shoreline]
Landward
Seaward
LONG TERM AND SHORT TERM SEA-LEVEL-CURVES
250 200 150 100 50 0m -50
Approximate present-day sea level
155
160
165
KIMMERIDGIAN
OXFORDIAN
CALLOVIAN
b
Major cycle boundary
Medium or minor cycle boundary
Legend
Dolomite
Limestone
Gypsym/Anhydrite
Salt
Sandstone
Mudstone
Conglomerate
Deformed Basement

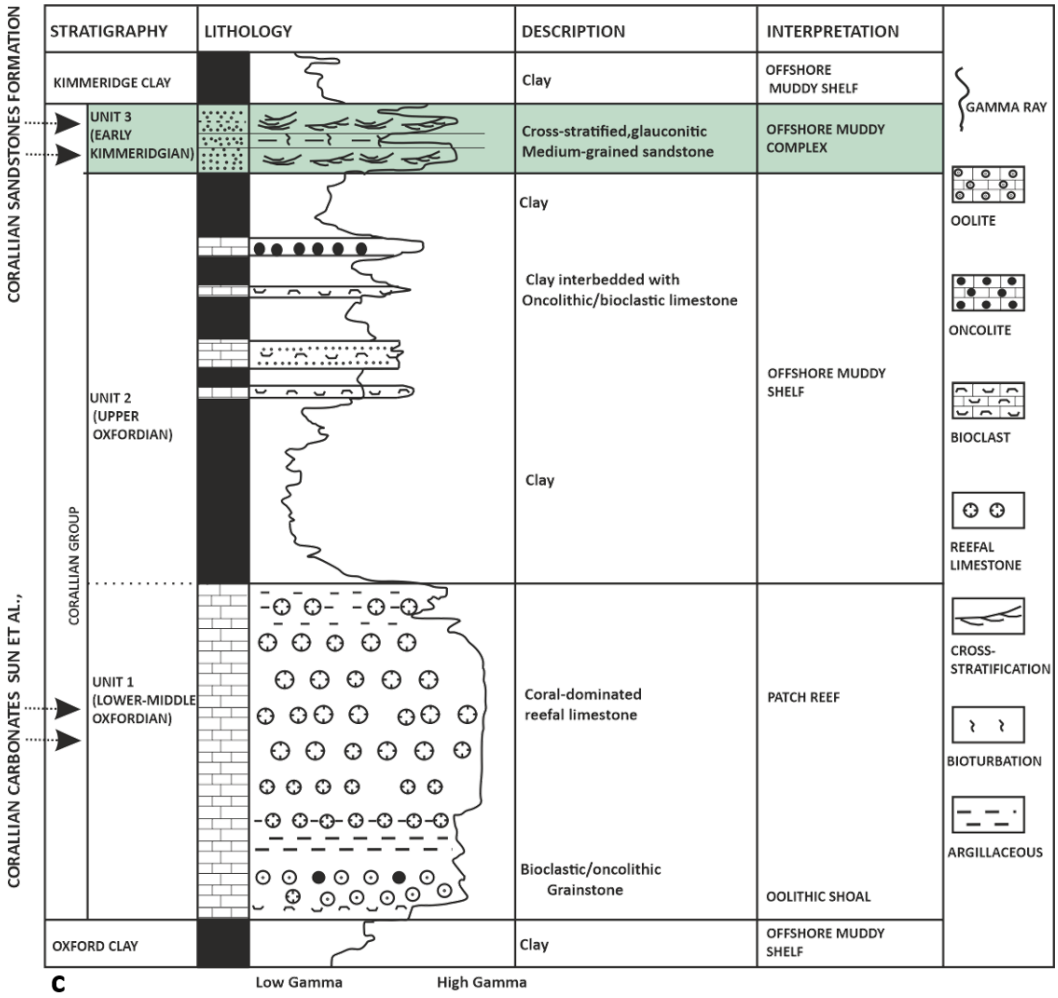

Figure 4.1: (a) Stratigraphy of the Weald Basin, modified from Butler & Pullan (1990),showing major tectonic episodes and lithologic units with the Corallian section highlighted by the rectangle in the Upper Jurassic. The section show the Corallian sandstones deposited during a period of tectonic activity accompanied by graben development and regional subsidence. The Corallian has been described as both a group (Wright 1981) and a formation (de Wet 1998). Here the term Corallian Formation is adopted to match the naming of the under- and overlying Oxford Clay and Kimmeridge Clay Formations. (b) Jurassic sea level curves, modified from Haq (2017), show dominant sea level rise through the late Jurassic with the dotted rectangle showing the time that the Corallian sandstone was deposited. Sequence boundaries define rapid seaward shoreline movements corresponding to minor sea level falls punctuating an overall landward shoreline movement. (c) This is a stratigraphic section summarising the Corallian Group as modified from Sun (1992). The Corallian sandstone Formation is highlighted at the top of the Corallian Group.

Through the Upper Jurassic to Lower Cretaceous, the Weald Basin became a significant depocentre during continued thermal subsidence, with associated active faulting and deposition of the basinal, black, and commonly laminated Oxford Clay Formation (Sellwood et al. 1986; Butler & Pullan 1990; Hansen et al. 2002) (Fig. 4.1). The Oxford Clay Formation was followed by the deposition of the shallow marine Corallian Group (Fig. 4.1c), the subject of this study, in the Upper Jurassic Oxfordian stage, during a period of marine transgression and tectonic activity (Sellwood et al. 1986; Sun 1992). Sun (1992) placed Corallian sandstones, at the top of the Corallian Group, in the Early Kimmeridgian, which was a period of marine transgression (Fig. 4.1b and 4.1c). Deposition of the Corallian Group was also a time of the development of extensional east-west, low angle faults (Hawkes et al. 1998; Hansen et al. 2002) that now separate Palmers Wood and Bletchingley oil fields. The Corallian Group was followed by marine deepening and deposition of the Kimmeridge Clay Formation (Hallam 1978) during a period of sea level rise and increased seismicity, with evidence indicating contemporaneous fault activity during the deposition of the Kimmeridge clay (Fig. 4.1).

Deposition of the bioturbated, glauconitic Portland sands during the Tithonian marks the uppermost Jurassic unit (Andrews 2014) which was sourced from the London-Brabant massif to the north (Hawkes et al. 1998). The Portland sands deposition was succeeded by a relative sea-level fall, during hot arid conditions, and the consequent deposition of sabkha-type, anhydrite-bearing lower Purbeck sediments (Upper Portlandian to Ryazanian) signalling a regressive episode (Butler & Pullan 1990; Hansen et al. 2002; Andrews 2014). The Wealden clay then succeeded the Ryazanian Purbeck group during the Lower Cretaceous Valanginian stage (Andrews 2014). Sellwood et al. (1986) interpreted the zero isopachyte for the Weald as a result of erosion from Cimmerian tectonic activity (Fig. 4.1) and lowstand sea level.

The overlying thin Gault-Upper Greensand succession has been interpreted to signal the gradual cessation of fault movements and transgression (Butler & Pullan 1990) or post-Cretaceous erosion (Sellwood et al. 1986). Although well-exposed along the south and north margins of the Weald Basin (i.e., the South and North Downs), the overlying Chalk Group is absent, or too thin for seismic identification, in the Weald Basin (Sellwood et al. 1986); it is not possible to be definitive about seismic activity during its deposition. Chadwick (1985b) suggested that the Chalk Group was deposited during compaction-subsidence of underlying sediments (Chadwick 1985a; Butler & Pullan 1990).

The Cenozoic experienced fault reactivation and uplift in the Weald Basin, including Palmers Wood and Bletchingley oil fields, due to regional-scale compression (Hawkes et al. 1998; Hillis et al. 2008a). The uplift has been attributed to two factors, the opening of the North Atlantic which led to regional uplift in the Paleogene and a second phase in the Miocene associated with the Alpine tectonism (Jones 1999b) or possibly the Pyrenean Orogeny (Parrish et al. 2018a). Cenozoic inversion was discussed by Hillis et al. (2008a); in the Weald, it manifested as a large scale N-S anticline. Uplift has been estimated to range from as little as 701.4 m (2300 ft), based on mapping and extrapolating a base chalk surface (Chadwick 1993), to as much as 2276.7 m (7470 ft), based on the analysis of sonic logs compared to normal compaction trends of the Oxford Clay Formation (Law 1998). The basin inversion and uplift led to the formation of broad, dome-shaped hanging wall anticlines, with subsidence of the London Basin to the north and the linked Hampshire-Weald-Dieppe Basins to the south, during the late Palaeocene-Eocene (Hansen et al. 2002).

4.2.2 Conditions during the deposition of the Upper Jurassic in the Weald area

The Jurassic was a greenhouse period with no polar ice caps, and tropical and subtropical zones that were wider than present day ranges (Talbot 1973; Hallam 1975; Hallam 1977, 1984). In the Oxfordian, when the Corallian was deposited, the palaeolatitude of Britain is estimated to have been in the subtropical range between 31^{o} N and 37^{o} N (Hallam 1975) or alternatively about 24°N (Scotese 2001). The climate was generally warm with peak temperatures in present-day NW Europe (Britain) occurring in the Kimmeridgian (Haq 2017). However, Ruffell & Rawson (1994) concluded that the aridity/humidity of the local land-masses of southern and eastern England, England, NW Europe and southern France during the deposition of the Corallian (in the Oxfordian) have not been well documented. Nonetheless, a study by Hallam (1984) suggested the occurrence of a humid Jurassic climate in eastern, central and north-western Europe up until the Kimmeridgian.

It has been concluded that Jurassic sea levels were not significantly different to present day sea levels, as suggested by Hallam (1981); Hardenbol et al. (1998); Haq (2017) (Fig. 4.1b); it was inferred, by these authors, that the Upper Jurassic was a period of overall sea level rise. A modified curve of Upper Jurassic sea levels (Fig. 4.1b), as documented by Haq (2017), presents a eustatic rise in sea level from the Lower Oxfordian through to the Kimmeridgian, as well as several short-term sea level falls of uncertain magnitude.

4.3 Datasets and methodology

4.3.1 Sedimentary logs

This study focused on the examination of Corallian cores from three wells, Palmers Wood-3 (PW3), and -7 (PW7) and Bletchingley-5 (BL5), from the Weald Basin, onshore SE England (see Fig. 3.1). The cores are held at the British Geological Survey (BGS) core store in Keyworth, Nottinghamshire. The three wells were initially logged at high resolution (1:24). PW3 had 17.1 m of core, PW7 had 16.6 m of core and BL5 had 19.8 m of core. Measured depths from the cores were converted into true vertical depth by taking well deviation into account. The present-day true vertical depths to the top of the Corallian sandstones are BL5: 844.2 m, PW7:875.4 m and PW3: 904.1 m. Each core was logged for lithology, grain size, sedimentary structures, ichnology, bed contacts, cement types and degree of cementation. Ichnofabrics were described using the approach defined by Pemberton et al. (2012a). Lithology, grain size and sedimentary structures were recorded to determine primary depositional conditions. Bed contacts and ichnology was recorded to give indications of primary depositional conditions and sequence stratigraphic surfaces such as discontinuities.

Sedimentary logs were summarised and digitised at a resolution of 1:120, with their facies classified based on texture and lithological attributes following Farrell et al. (2012). Facies associations were interpreted to help determine depositional environments, using methods described by Hampson & Storms (2003) and Kamola & Van Wagoner (1995) relevant for shallow marine shoreface to shelf depositional environments.

4.3.2 Petrography

Petrographic analysis of the Corallian sandstones was carried out using automated Scanning Electron Microscopy-Energy Dispersive Spectroscopy (SEM-EDS) and optical microscopy. Fifty-one polished thin sections (30 μm thickness) were prepared from rock samples from the three cores with samples first injected with blue dyed resin to highlight any porosity. Twenty-three samples were from BL5, nine were from PW3, and 19 were from PW7.

Optical petrography, using an Olympus BX51 transmitted light microscope, was carried out to investigate lithology, micro-textures, cement types and mineralogy. Samples were point counted, using a CVS Petrog stage, for 300 counts per section.

SEM-EDS was undertaken to provide a quantitative evaluation of mineral proportions as well as grain and pore space morphology. The equipment used in this study was an FEI WellSite QEMSCAN, at the University of Liverpool, equipped with a tungsten-filament, operating at 15 kV and two Bruker EDS detectors (Wooldridge et al. 2018). The QEMSCAN is made up of a scanning electron microscope equipped with energy dispersive X-ray spectrometers and is capable of automated mineral identification from an extensive mineral database known as Species Identification Protocols (SIPs) (Pirrie et al. 2004; Armitage et al. 2010). SEM-EDS has spatial resolution of about 1 μm, thus it cannot identify minerals grains or pore space less than 1 μm. Mineral quantification with SEM-EDS is accurate to within fractions of a percent.

4.3.3 Wireline logs

Gamma ray, neutron porosity, sonic velocity, density and resistivity logs from PW7, PW3 and BL5 were available for analysis. For the overall interpretation of lithology and fluid saturation, porosity was derived from the density log using:

$$\text{Porosity}\left(\phi_{\text{RHOB}}\ \%\right) = 100\,.\frac{\rho_{\text{meas}} - \rho_{\text{b}}}{\rho_{\text{matrix}} - \rho_{\text{fl}}}$$

(Equation 4.1)

Where ρ_{matrix} is the assumed matrix (rock) density, ρ_{meas} is the reported log (bulk) rock density (ρ_b) and ρ_{fl} is the assumed fluid density for the invaded zone of the near well-bore region.

The fluids in the pore space were divided into water and petroleum using the deep resistivity log (R_d) and equation 4.2, the Archie equation:

$$S_w = \sqrt[n]{\frac{a\,.\,R_w}{\phi_{\text{RHOB}}^{m}\cdot R_d}}$$

(Equation 4.2)

Where S_w is the fractional water saturation, a, m and n are the Archie constants (default values: 1, 2 and 2 but modified here to fit the S_w to as close to 1.00 as possible in the water leg), ϕ_{RHOB} is the porosity determined using the density log (equation 4.1) and R_d is the deep resistivity of the formation. Formation water salinity was assumed to be between 85,000 and 100,000 ppm, resulting in an in-situ resistivity (R_w) of about 0.06 ohm.m (Trueman 2003a).

The solid part of the rock was split into proportions of shale and sand using gamma log data and the Vshale calculation:

$$\text{Vshale} = \frac{\text{GR}_{\text{meas}} - \text{GR}_{\text{min}}}{\text{GR}_{\text{max}} - \text{GR}_{\text{min}}}$$

(Equation 4.3)

Where GR_{max} is the maximum gamma value for the reservoir-top-seal section of interest, GR_{meas} is the measured gamma value for the depth of interest and GR_{min} is the minimum gamma value for the reservoir-top-seal section of interest.

The computed wireline lithology and neutron-density cross-over plots were used to define pay and non-pay zones and to help deduce correlations between wells. Gamma ray logs were used for correlations across facies associations to determine the lateral continuity of facies associations between wells and tectonic structures. Core-to-log depth-shifts were applied to allow comparison of core and log data and true vertical depths calculated to put the porosity data into context of the present-day depth of burial and possible extent of uplift.

4.4 Results

4.4.1 Sedimentary logs

In the following sections, where depth is referred to in text or on figures, all depths are reported in terms of measured (as opposed to true vertical) depth in metres (m-md) but were originally reported in units of feet. We also have used a single key to represent the logged data from cores (Fig. 4.2) as shown in Figure 4.3 for the sedimentary logs in Figures 4.4, 4.5 and 4.6. All cores were dominated by light grey to brown sandstones, siltstone and minor dark brown to black mudstones (Fig. 4.2). Bivalve clasts are common and appear as white and grey, thin curved shells in core (Fig. 4.2), especially in the coarser grained sections. Grain size varies from clay, through silt to coarse sand with beds showing repeated coarsening upward cycles. Some of the coarsening upward cycles then reverse into fining upward cycles (Figs. 4.4-4.6).

The Mudstones are predominantly highly bioturbated (Fig. 4.5 at 1096.7-1097.9 m) and mainly occur as thin beds or laminae within the sandstones (Fig. 4.5 at 1089.6 m), or at the boundary with the underlying Corallian argillaceous unit (Fig. 4.4 at 1138.0 m) and overlying Kimmeridge Clay (Fig. 4.4 at 1122.5 m). Typical sedimentary structures include lenticular

bedding, cross-lamination, mottled fabrics where bioturbation has obscured primary depositional features, and massive featureless beds that may be wholly bioturbated. Mudstones in core are apparently free of bioclasts (Fig. 4.2e).

The siltstones are present adjacent to mudstones at the upper boundary of the Corallian argillaceous unit and the lower boundary of the Kimmeridge Clay, and in the middle section of PW7 (Figs. 4.4, 4.5 and 4.6). Sedimentary structures in the siltstones include lenticular bedding (BL5 at 2193.6 m), mud drapes, mottled fabric (PW7 at 1128.9 -1129.6 m) and massive bedding (PW3 at 1081.4 m).

Sandstones are the dominant lithology in the Corallian section with a range of sedimentary structures including: planar-, trough- and hummocky-cross-stratification, massive-bedding, lenticular- and flaser-bedding, as well as current-, wave- and climbing-current ripple lamination (Figs. 4.4, 4.5 and 4.6). Bed types seem to be randomly stacked over short vertical intervals (Figs. 4.2c, 4.4, 4.5 and 4.6). Bivalve clasts are common and appear as white and grey pin-shaped, curved shells in core (Fig. 4.2), especially in the coarser grained sections.

Secondary features in the Corallian sandstones include cementation, bioturbation, erosional surfaces and hydrocarbon staining. The cores have variable degrees of carbonate cementation as well as hydrocarbon staining (Fig. 4.2), with dark brown hydrocarbon staining found in the poorly cemented, more porous zones (Fig. 4.2b) and negligible hydrocarbon staining in highly cemented zones (Figs. 4.2a and 4.2c). Bioturbation is common but with varying intensity and diversity. Intense bioturbation has resulted in a mottled fabric (Fig. 4.2c) as well as mixing clean sands beds with more clay-rich beds (PW3 at 1087.5-1089.4 m). Bioturbation intensity is here described on a scale of 0-6 using the Taylor & Goldring (1993) index. Common ichnofabrics include Skolithos ichnofacies (Seilacher 1967) with *Skolithos*, *Ophiomorpha* and *Diplocraterion* (Fig. 4.2, 4.4, 4.5 and 4.6); the Cruziana ichnofacies (Seilacher 1967) with *Rhizocorallium, Rosellia, Teichichnus, Thalasinoides* as well as Zoophycos ichnofacies (Pemberton et al. 2012a) with *Chondrites* (Fig. 4.2d and 4.2e). Some non-graded bed boundaries were erosive with sharp changes in grain size locally accompanied by abrupt increases or decreases in the degree of bioturbation (Fig. 4.4, 4.5 and 4.6).

4.4.2 Interpretation of sedimentary logs

The localised variations of grain size and sedimentary structures in the Corallian sandstones in the three wells (Figs. 4.4, 4.5 and 4.6) indicates variable energy conditions during deposition. Abrupt decreases in grain size can be interpreted in different ways. For example, reductions in grain size in PW7 (at 1122.8 m), PW3 (at 1082.0 m) and BL5 (at 2193.9 m) are here interpreted as flooding surfaces as they are succeeded by a change in lithology to shale, signifying an increase in water depth (Walker & James 1992) while changes in grain size above scours (e.g. Fig. 4.2d) represent erosional surfaces which have here been interpreted as erosional or non-depositional (hiatal) discontinuities (Hampson & Storms 2003) (Figs. 4.4-4.6).

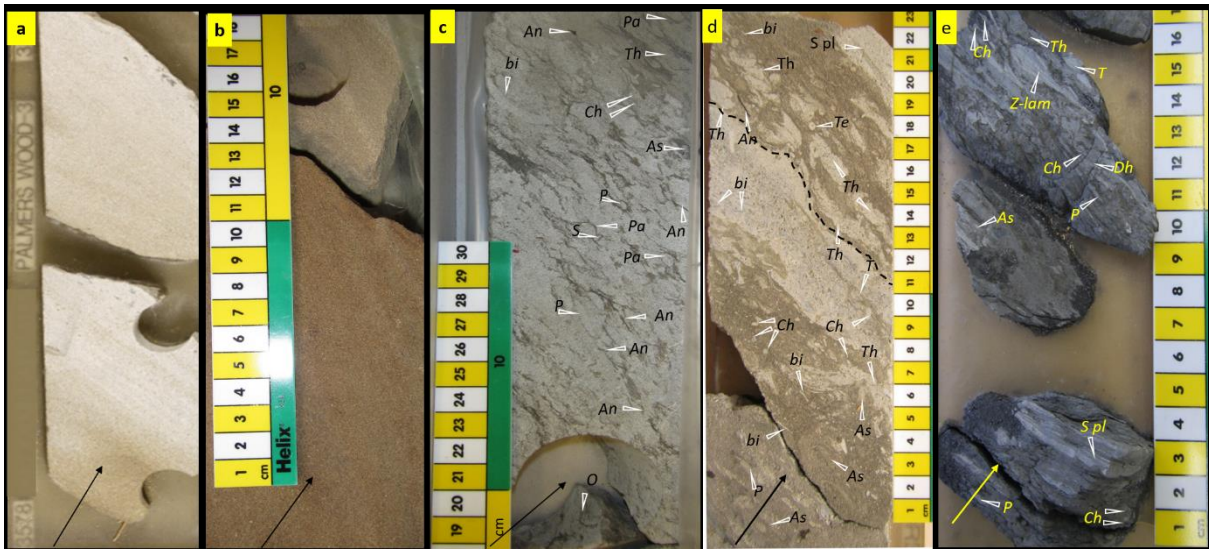

Figure 4.2: (a) PW3 (1090.6-1090.9 m) highly cemented foreshore sandstone with no visible bioturbation (b) PW7 (1131.6 m) loosely cemented medium-grained, massive bedded upper shoreface sandstone with no visible bioturbation. The brown colour is from intense (significant) hydrocarbon staining. (c) BL5 (2207.5 m to 2207.9 m) proximal lower shoreface sandstones has been intensely bioturbated obscuring original fabric (BL5 is deviated at an angle of about 50°, explaining the great difference in measured depths). (d) PW3 (1087.9 m) distal lower shoreface sandstones, beds show rapid colonisation after a storm event. The broken line shows an erosional surface at the top of the storm bed. The non-amalgamated coarse-grained bed at the middle is succeeded by an argillaceous low energy section with parallel lamination (S pl) and increase in bioturbation. (e) PW3 (1098.5 m) offshore muds with laminated silty lenses. Lenses have parallel lamination (S pl) and wave ripple lamination (S r-lam). *Anconichnus* (An), *Asterosoma* (As),bivalve (bi) shells, *Chondrites* (Ch), *Ophiomorpha* (O), *Paleophycus* (Pa),

Planolites(P),*Diplocraterion habichi*(Dh), *Skolithos* (S), *Teichichnus* (T), *Terebellina* (Te) and *Thalasinoides* (Th).

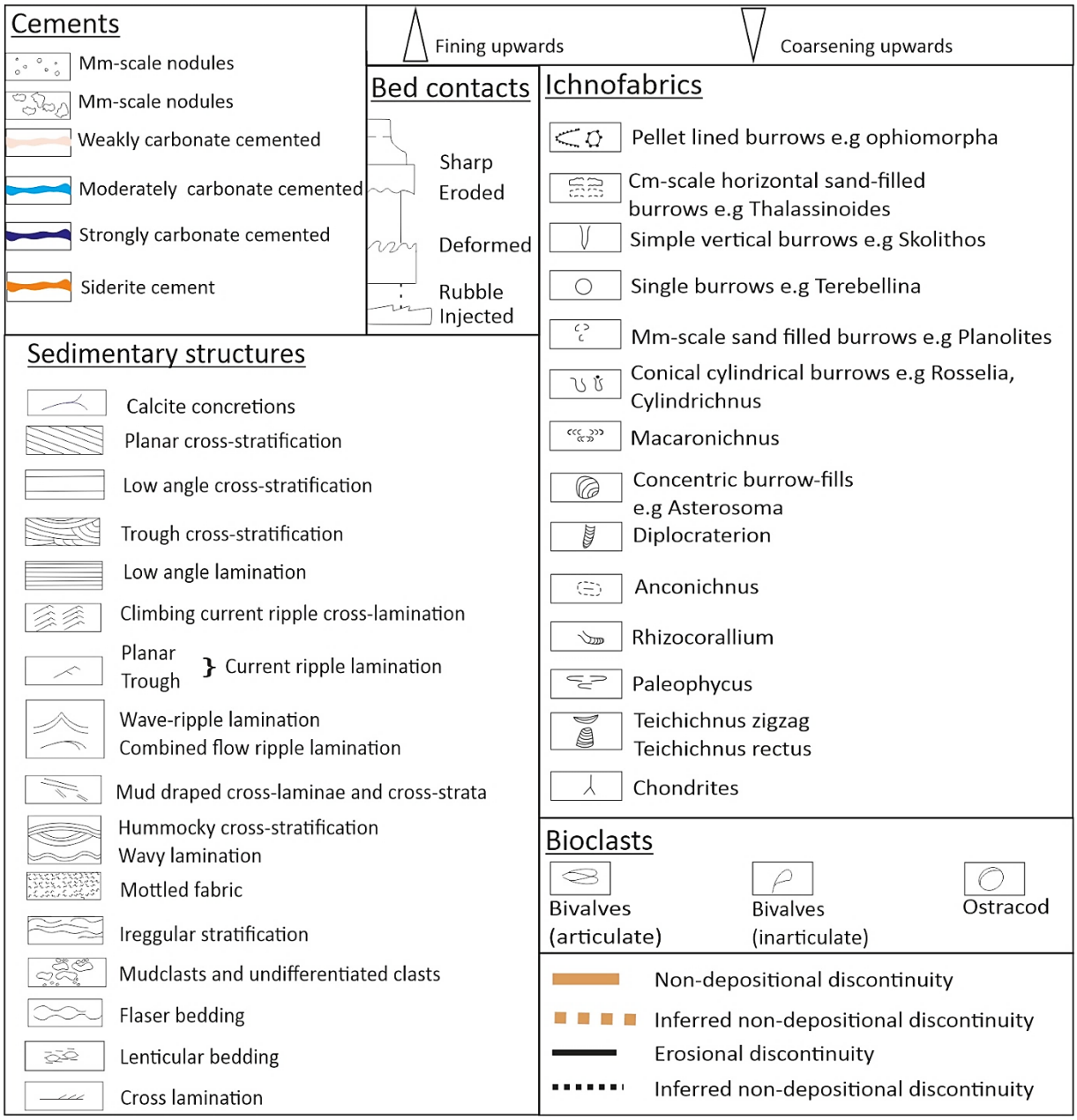

Figure 4.3: The key for the sedimentary logs in Figures 4.4, 4.5 and 4.6.

Based on grain size and both primary (bed-relationships) and secondary (bioturbation) sedimentary structures, a total of 12 facies have been identified (Table 4.1). The ichnofacies in the Corallian sandstones indicates varied energy conditions during deposition. *Skolithos, Ophiomorpha and Diplocraterion* of the Skolithos ichnofacies are typical of episodic high energy erosion and sedimentation events (Seilacher 1967) while the Cruziana and Zoophycos

ichnofacies are typical of deposition under lower energy conditions (Seilacher 1967; Pemberton et al. 2012a). The occurrence of both the Skolithos and Cruziana ichnofacies re-emphasises the varied energy conditions during the deposition of these sandstones. The diversity of the facies suggests varied energy conditions during marine deposition. For example, the massive mudstone facies (Mm) was deposited from suspension under low-energy, sediment-starved conditions (Walker & Plint 1992) with a slow rate of deposition under quiescent conditions conducive for sediments to be reworked by fauna (Gowland 1996). Sandstone facies represent deposition in relatively high energy conditions; for example, planar cross-bedded sandstones, trough cross-bedded sandstones and low angle cross-bedded sandstones of the cross-bedded sandstone facies (Sx) are products of dune migration under high energy condition (Vakarelov et al. 2012) and hummocky cross-bedded sandstone represent deposition by storm events in shoreface to offshore settings (Pemberton et al. 2012a; Vakarelov et al. 2012).

From a reservoir quality perspective, the dominance of sand in this part of the Corallian is an indicator of potential reservoir zones. Although there is no simple relationship between cementation and depositional facies, the occurrence of hydrocarbon staining only in the less-cemented intervals indicates that porosity has been destroyed by cementation (Fig. 4.3a and 4.3b). Reservoir presence has also been affected by homogenisation of sand and clay beds and laminae by bioturbation which has locally reduced the net clean sand fraction in some bioturbated sections of core (Fig. 4.3c and 4.3d).

4.4.3 Wireline logs

The wireline logs were converted to fractions of sand, shale, water and oil using equations 4.1, 4.2 and 4.3 (Figs. 4.4b, 4.5b, 4.6b). The interpreted lithology logs reveal sand- and shale-rich sections in the Corallian, including relatively coarse beds that contain abundant clay minerals due to bioturbation (Fig. 4.5 at 1088.9 m). The interpreted lithology logs have good relationships with the neutron density cross-over logs, delineating sections with potentially good reservoir. The neutron-density cross-over plots together with the lithology logs reveal the dominantly sand-rich lithology of the Corallian sandstones evolving from the underlying shale-rich Corallian argillaceous unit and into the overlying shale-rich Kimmeridge Clay (Figs. 4.4b, 4.4c, 4.5b, 4.5c, 4.6b and 4.6c). All three wells show a decrease in sand- and increase in shale

in the middle of the Corallian section, representing an intra-Corallian shale horizon. In addition, BL5 also has an extra clay-rich section at 2199.0 -2201.5 m.

The wireline-derived lithology, the neutron-density cross-over plots and the gamma ray logs show the intra-Corallian argillaceous section correlates across all three wells (Figs. 4.7 and 4.8). The two deepest sandstone packages (S1 and S2) seem to correlate from PW3 and PW7 to BL5. However, by reference to the true vertical depths, there is a distinct thickening (of more than 4.27 m) of the Corallian sandstones southward from Palmers Wood to Bletchingley (Fig. 4.7). The sandstone package at the top of BL5 (labelled S3 in Fig. 4.7) does not correlate with any of the sandstone packages in the Palmers Wood wells and accounts for the southward thickening of the whole Corallian sandstones (Fig. 4.8).

The correlated sandstones, above and below the intra-Corallian mudstone, all show variable, but locally fair to good, porosity (Figs. 4.4, 4.7); in contrast, the top-most sandstone in BL5 seems to be different, having uniformly low porosity (Figs. 4.6 and 4.7).

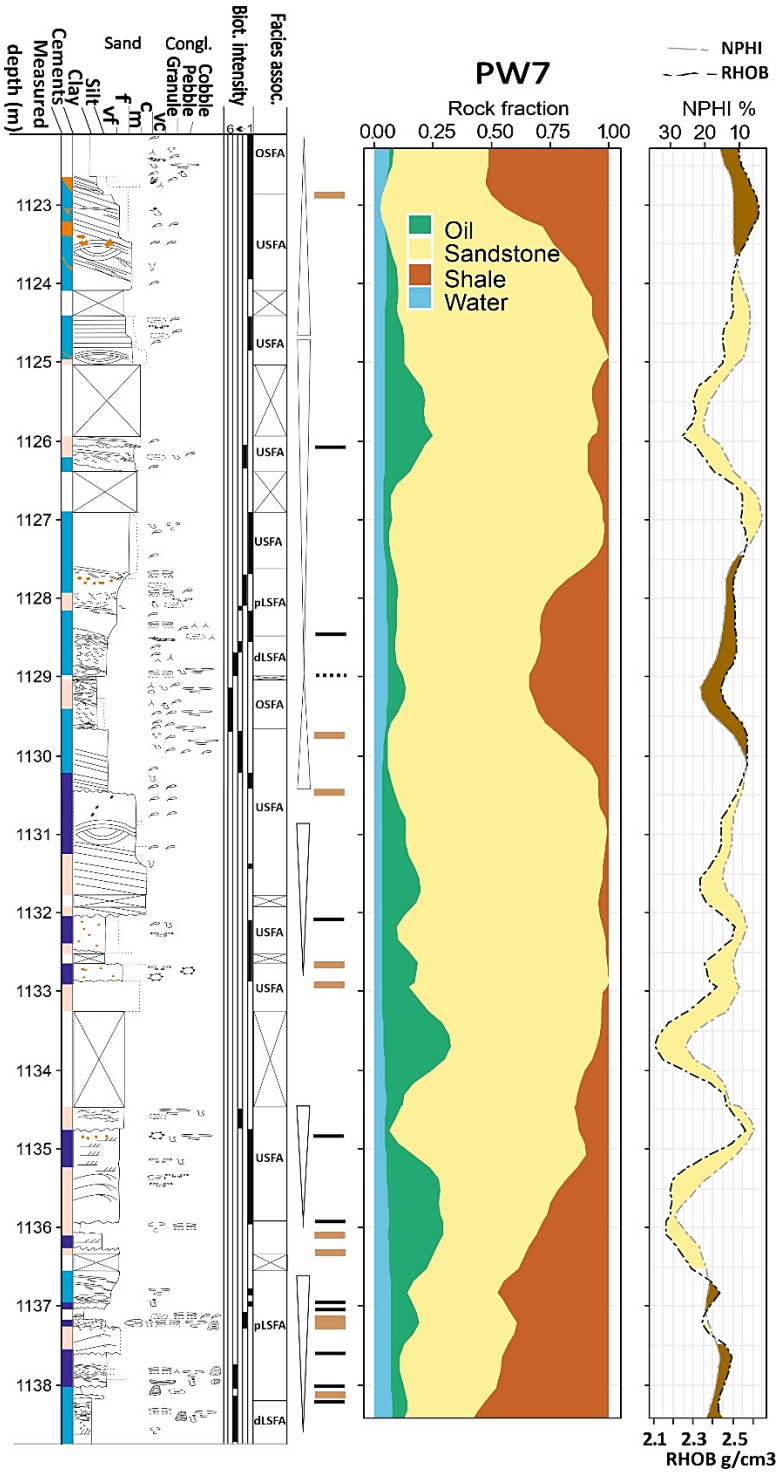

Figure 4.4: sedimentary log, wireline lithology log, and neutron-density cross-over plots for PW7: (a) sedimentary structures, extent of cementation, facies associations, bioturbation and discontinuities. (b) the lithology interpretation from wireline logs with relative proportions of oil saturation, sandstone, shale and water. (c) a neutron-density cross-over plot with non-pay zones coloured brown and pay zones coloured yellow. The sedimentary log shows the Corallian

sandstones separated by a local argillaceous section. The sedimentary logs also show coarsening upward cycles interrupted by a fining upward cycle (top of b and lower part of a). Common discontinuities point to a varied interplay of energy levels and/or sediment source. The lithology log shows good sand/shale correlation with grain size variation and bioturbation (when grain size does not change). Also note the increase in porosity in the top and bottom argillaceous sections. Wireline depths have been shifted to match core.

4.4.4 Petrographic data

Optical microscopy and SEM-EDS data help support interpretation of the conditions during deposition; they reveal that the Corallian is locally quartz-rich with minor feldspars, berthierine-ooids, phosphate ooids, bioclasts and minor clay-rich lithic grains (Figs. 4.9a, 4.9c and 4.10a). Sandstone grain sizes range from coarse- and medium- (Figs. 4.9a and 4.9c) to fine-grained (Figs. 4.11a and 4.11b). The cements include calcite, dolomite, siderite, pyrite, berthierine, quartz and kaolinite (Figs. 4.9, 4.10 and 4.11). There is no evidence for the development of evaporitic cements, such as gypsum.

Pore-filling detrital clay minerals are composed of illite, berthierine and kaolinite (Fig. 4.11). Other poor-filling, fine-grained minerals include biotite, K-feldspar, plagioclase feldspar and rutile (Fig. 4.11).

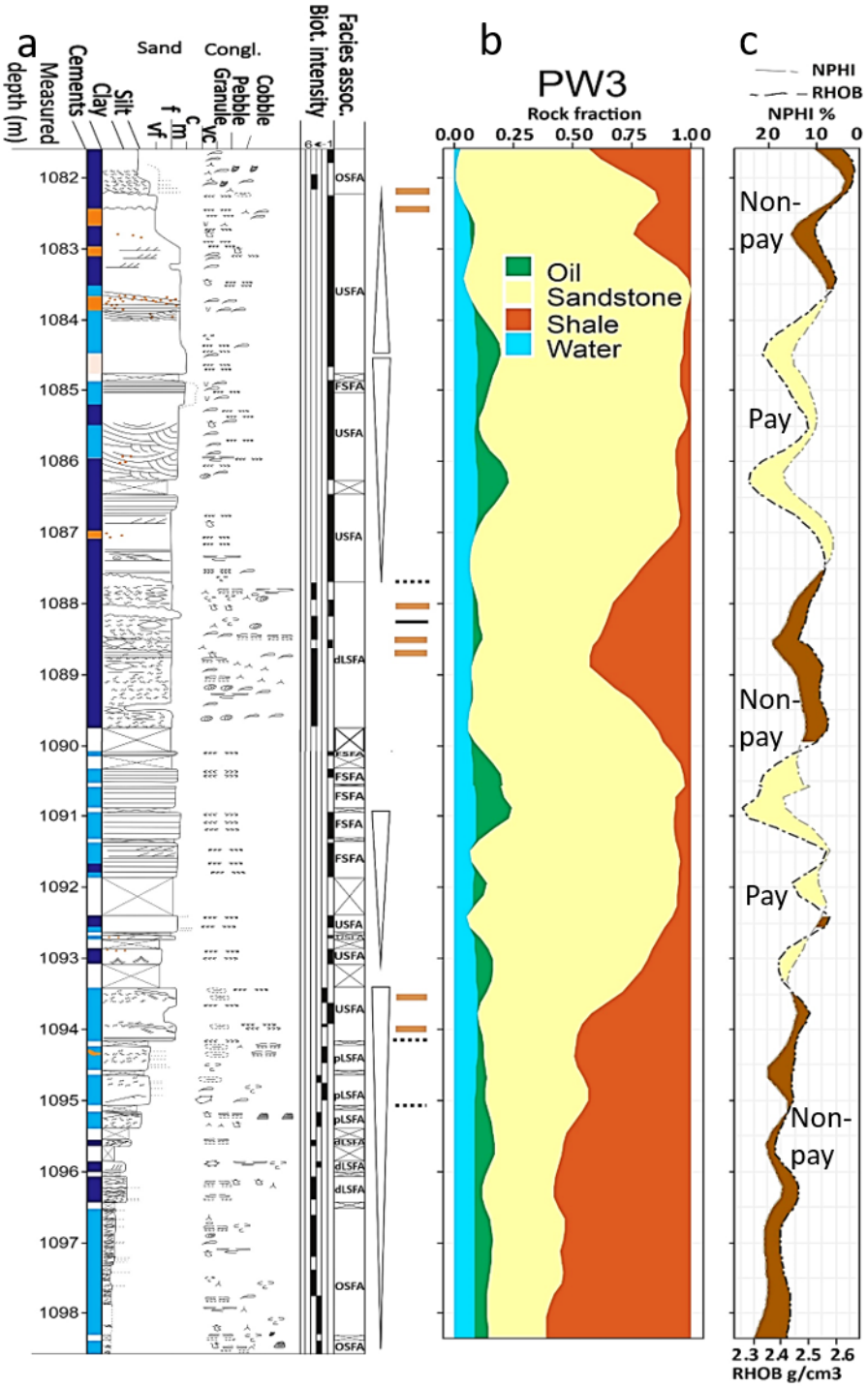

Figure 4.5: Detailed sedimentary log, wireline lithology log, and neutron-density cross-over plots for PW3: (a) sedimentary structures, extent of cementation, facies associations, bioturbation and discontinuities. (b) the lithology interpretation from wireline logs with relative proportions of oil saturation, sandstone, shale and water. (c) a neutron-density cross-over plot with non-pay zones coloured brown and pay zones coloured yellow. In the sedimentary log

beds show frequent short-range facies shifts with mostly upper shoreface facies association truncated by lower energy facies associations. The middle argillaceous section does not show change in grain size but has been highly bioturbated. Wireline depths have been shifted to match core depths.

Petrographic images reveal a relatively uncompacted texture where grains are separated from each other by cement or pore spaces (Figs. 4.9 and 4.10). In cases where the detrital grains are in contact, they dominantly have face-to-edge contacts (Fig. 4.9c). Sandstones range from coarse- and medium- (Figs. 4.9a and 4.9c) to fine-grained (Figs. 4.10a and 4.10c). Disarticulated bivalve clasts are most common in the coarsest grained fractions (Fig. 4.9a and 4.9c). Acicular cement occurs around bivalve fragments, suggesting marine cementation (Scholle & Ulmer-Scholle 2003) (Figs. 4.9a and 4.9c). Bioclasts show a great degree of micritisation of their edges (Tucker 1981; Adams 1998), even in completely neomorphosed bioclast grains (Fig. 4.9), confirming that the Corallian was deposited in the marine photic zone.

Modal analysis (point count) data are shown in a ternary plot (McBride 1963), in Figure 4.11c with Q representing the sum of polycrystalline and monocrystalline quartz. F is the sum of plagioclase and K-feldspars and L is the sum of all lithic fragments including extrabasinal mudstone, extrabasinal chert, extrabasinal sandstone, extrabasinal quartzite, muscovite, berthierine and bioclasts. The ternary plot shows a composition typical of a quartz arenite, with minor subarkoses and sublitharenites (Fig. 4.11c). The plots show no distinct distribution of QFL by facies association except for the offshore facies association, which has slightly elevated feldspars and the upper shoreface which shows a high lithic content.

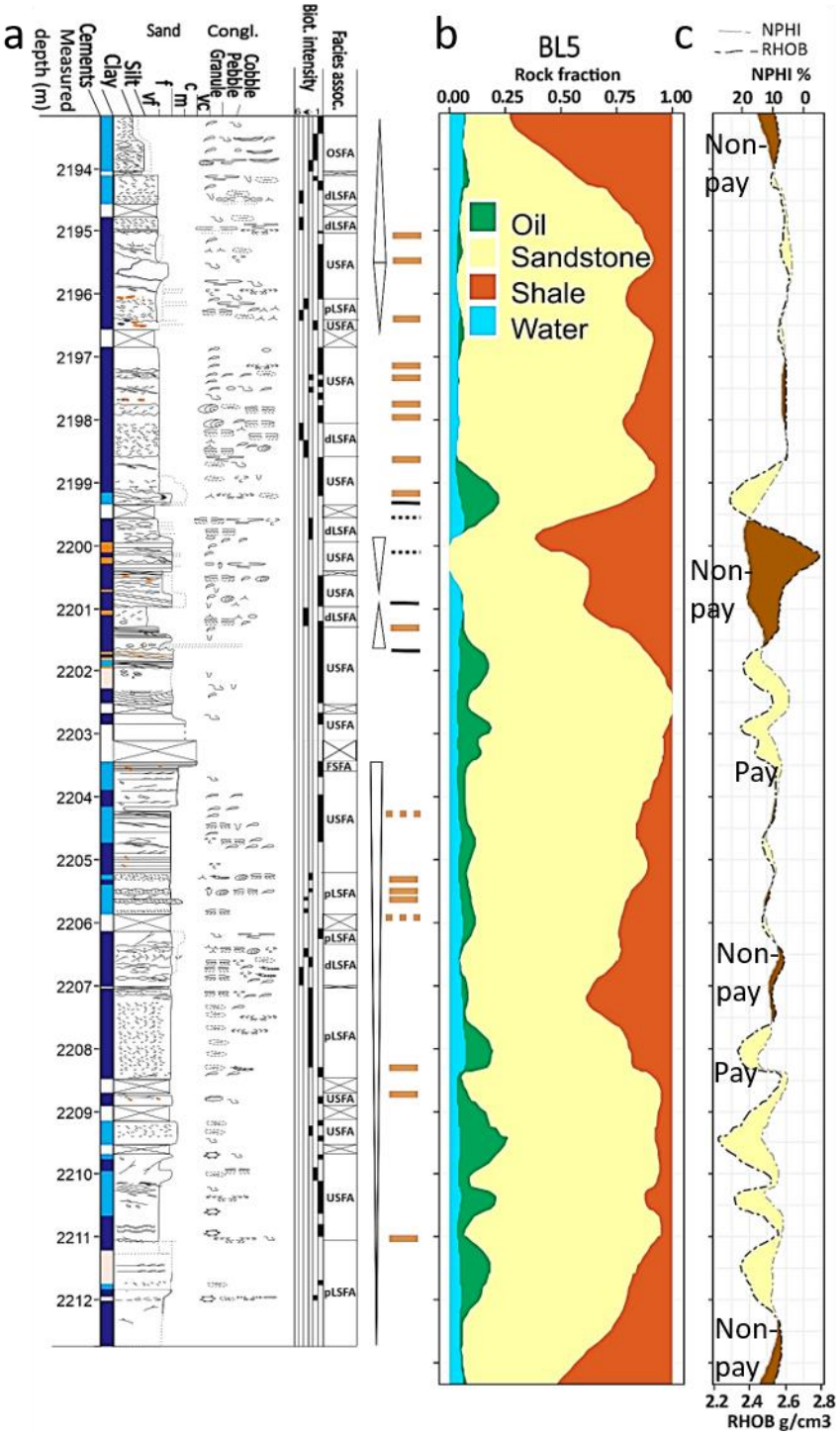

Figure 4.6: Detailed sedimentary log, wireline lithology log, and neutron-density cross-over plots for BL5: (a) sedimentary structures, extent of cementation, facies associations, bioturbation and discontinuities. (b) The lithology interpretation from wireline logs showing relative proportions of oil saturation, sandstone, shale and water. (c) a neutron-density cross-over plot with Non-pay zones coloured brown and pay zones coloured yellow. Note that BL5

has another argillaceous section from 2201.9 m to 2199.4 m. Several coarsening and fining upwards cycles are observed and argillaceous sections are more common in this well compared to the Palmers Wood wells. The log also shows common erosional and non-depositional discontinuities, and short-range vertical heterogeneity in cementation and sedimentary structures. Wireline depths have been shifted to match core depths.

The distribution of feldspars in the offshore facies association is due to the abundance of fine-grained feldspars in the lower energy, argillaceous zones (Figs. 4.10b and 4.11b). Lithic fragments are abundant in the upper shoreface facies association because the high density larger bioclasts and ooids can settle under high energy upper shoreface environments.

SEM analysis revealed that calcite is the main cement, with an average of up to 39% (Fig. 4.12b). Dominant calcite cement can be seen in images where the SEM image is next to an equivalent optical image, e.g., Figs. 4.9 as well as 4.11a and 4.11b with abundant calcite cement evident in samples with elevated bioclast concentrations (Figs. 4.9) and less abundant in samples with fewer bioclasts and clay minerals (Figs. 4.10a and 4.11b). This relationship is also seen at the well-scale where BL5 has fewer bioclasts and clay minerals and more calcite in PW3 and PW7 (Fig. 4.12b, 4.12c and 4.12d). The dominant calcite cement fills pore spaces and separates framework grains from each other, suggesting an early origin (Fig. 4.9). Longitudinal grain contacts are not common in these sandstones as early calcite cementation has filled pores and hindered pore-loss due to compaction (Fig. 4.9a, 4.9b, 4.9c and 4.9d). Calcite-poor samples have higher porosity (Fig. 4.10a and 4.12). It is also worth noting that bioclasts are less abundant in finer-grained, clay-rich samples (Fig. 4.10c) and more abundant in the coarse-grained, clay-poor samples (Fig. 4.9). The relationships between bioclasts, grain-size and clay content suggests a hydrodynamic control on bioclast accumulation.

Table 4:1: Table showing facies in the Corallian sandstone. The number and variety of facies indicates deposition under a wide range of hydrodynamic conditions.

S/n	Facies type	Facies code	Facies description	Ichnofabrics	Interpretation	Facies associations
1	Sandstone	S-lam	**Laminated sandstone**: characterised by very fine to medium-grained trough-laminated, planar cross-laminated and low angle laminated sandstone	Low: *Macharonichnus, Skolithos*	Deposition from high energy storms or waves (Plint, 1992B)	Foreshore, Upper shoreface, Proximal lower shoreface
2		S-rlam	**Wave-laminated sandstone**: characterised by fine-grained wave and flow ripple-laminated sandstone	Rare: *Macaronichnus* with subordinate *Chondrites* and *Teichichnus*	Moderate rate of sand deposition by low energy current and wave transport (Gowland, 1996)	Upper shoreface, proximal lower shoreface
3		Sx	**Cross-bedded sandstone**: composed of medium-grained planar and trough cross-bedded sandstone as well as fine-to medium-grained hummocky cross-bedded sandstone	Absent to trace: *Skolithos* and *Cylindrichnus*	High energy sediment transport capable of causing dune migration (Pemberton et al., 2012; Vakarelov et al., 2012)	Upper shoreface, proximal lower shoreface
4		Sm	**Massive bedded sandstone**: this facies is made up of upper fine-grained to medium-grained massive bedded and low angle bedded sandstone	Absent to trace: *Macaronichnus, Skolithos and Anconichnus*	Rapid deposition of sandstone (Castro et al., 2019)	Upper shoreface, proximal lower shoreface
5		Sbiot	**Bioturbated sandstone**: this facies is composed of mainly fine-grained bioturbated sandstone with minor very fine-grained and medium-grained bioturbated sandstone. Sedimentary structures such as mud drapes and laminae are obscured by bioturbation	High: *Chondrites, Thalasinoides, Palaeophycus, Asterosoma, Rhizocorallium, Cylindrichnus and Rosellia*	Slow to moderate deposition of sand allowing colonisation by fauna (Gowland, 1996)	Proximal lower shoreface, distal lower shoreface, offshore
6		Sl	**Lenticular bedded sandstone**: characterised by very fine-grained to fine-grained sandstone with silt or clay lenses, as well as flaser bedded sandstones.	*Low to high: Thalasinoides, Planolites, Chondrites, Rhizocorallium* and *Terebellina*	Intermittent fluctuations in depositional energy and sediments (Tucker, 1981)	Distal lower shoreface, offshore
7		(m)S	**Muddy sandstone**: this facies is composed of fine to medium-grained mud draped sandstone or clay rich sandstone with irregular muddy beds	*Low: Skolithos, Anconichnus, Cylindrichnus* and rare *Chondrites* in the muddy intervals	Moderate rate of sand deposition. Presence of drapes suggests some tidal influence (Gowland, 1996)	Upper shoreface, proximal lower shoreface

8	Siltstone and mudstone	Zbiot	**Bioturbated siltstone**: this is composed of bioturbated siltstone and mudstone	High: *Chondrites, Teichichnus zig-zag, Teichichnus Rectus, Thalasinoides, Palaeophycus, Asterosoma, Rhizocorallium,* Cylindrichnus and Rosellia	Slow rate of deposition from suspension which allowed sediments to be reworked by fauna (Gowland, 1996)	Distal lower shoreface, offshore
9		Zl	**Lenticular bedded siltstone**: lenticular bedded siltstone as well as siltstone mudstone intercalations	High: *Thalasinoides, Chondrites, Palaeophycus, Terebellina* and *Rosselia*	Slowly deposited silt and mud modified by bottom currents (Gowland,1996)	Distal lower shoreface, offshore
10		Z-lam	**Laminated siltstone**: this facies is made up of low angle laminated siltstone, trough ripple laminated siltstone and planar laminated siltstone	Moderate: *Teichichnus, Thalasinoides, Ophiomorpha* and *Rosselia*	Slowly deposited silt from final stages of waning flow (Gowland,1996)	Offshore, distal lower shoreface
11		Ml	**Lenticular mudstone**: lenticular mudstone composed of mudstone with sand or silt lenses	Moderate to high: *Chondrites, Thalasinoides, Palaeophycus, Planolites and Diplocraterion*	Quiescent deposition from suspension with intermittent increase in energy from waning storms or waves (Tucker, 1981)	Offshore, distal lower shoreface
12		Mm	**Massive mudstone**: this facies is composed of massive bedded mudstone with no discrete sedimentary structures	Low-High: *Teichichnus, Anconichnus, Chondrites, Rhizocorallium, Palaeophycus and Cylindrichnus*	Deposited under low energy conditions from suspension (Plint 1992)	Offshore

4.4.5 Facies associations and depositional environments

Five facies associations (Table 4.2) were derived from the 12 facies (Table 4.1) to help reveal the overall sedimentary environment of these relatively thin bedded, variably bioturbated and complex sediments. These facies associations include foreshore, upper shore face, proximal lower shoreface, distal lower shoreface and offshore shelf/ramp facies associations (Table 4.2). The facies associations are presented below in order of decreasing energy conditions.

4.4.5.1 Foreshore facies association (FSFA)

The foreshore facies association (Table 4.2) is composed of fine- to medium-grained, low angle, planar-parallel laminated sandstones (Fig. 4.2a) mainly of the laminated sandstone facies association with minor cross-bedded sandstone facies association. The foreshore facies association is absent in PW7 (Fig. 4.8) but forms thin beds in PW3 and BL5, with the thickest beds in the lower sandstone unit of PW3. The foreshore facies association has a sharp basal contact with the upper shoreface facies association in PW3 (Fig. 4.5a at 1085.1 m). The

foreshore facies association is commonly non-bioturbated, but where, bioturbated it displays low intensity *Macaronichnus* (Fig. 4.5a at 1090.0 -1091.8 m).

Foreshore facies association sandstones are well-sorted to very well-sorted with sub-rounded to rounded grains (Fig. 4.9a). They show an abundance of disarticulated bivalve shells aligned in one direction suggesting transport of the bioclasts into and within the depositional environment (Fig. 4.9a). The coarser-grain sizes, disarticulated bivalve shells, rare bioturbation and sharp contacts with other facies associations suggest high energy deposition of this facies association similar to lithofacies unit 3 of Sun (1992), who described deposition in a shallow, high energy environment. These sandstones are, however, not glauconitic as described in Sun (1992); instead they contain the Fe-clay mineral berthierine. It seems that Sun (1992) mistook berthierine for glauconite as both are green marine clay minerals.

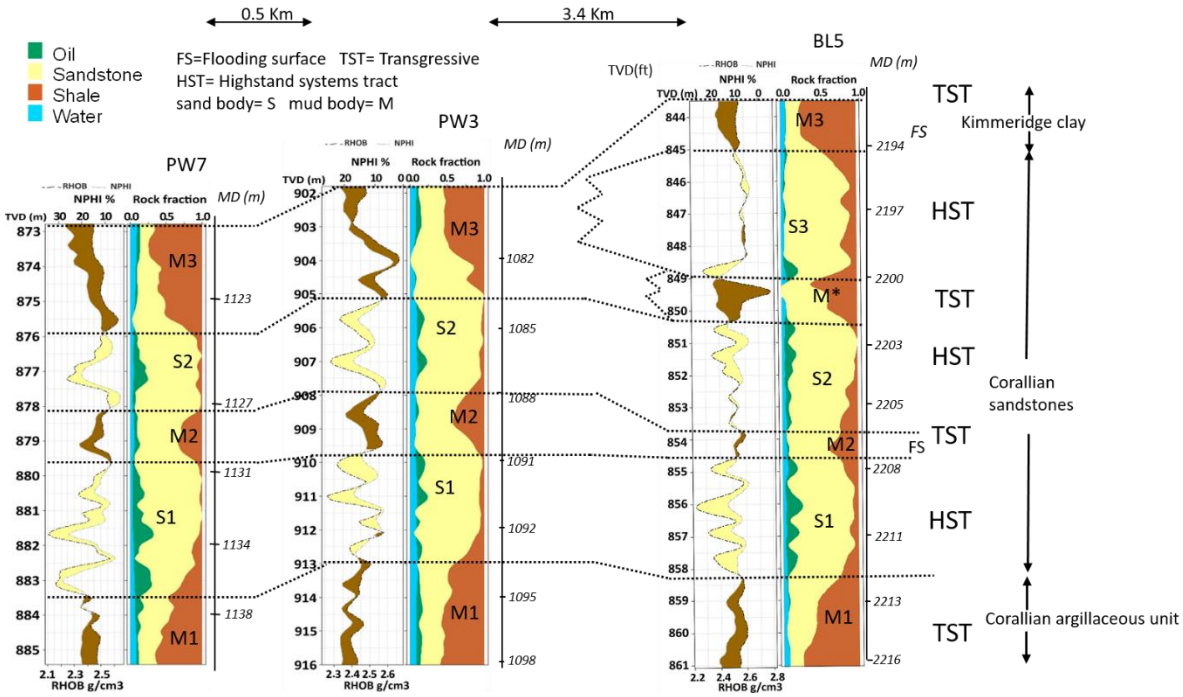

Figure 4.7: Schematic section across the Palmers Wood and Bletchingley fields, showing the stratigraphic framework from the Oxfordian to Early Kimmeridgian. The Corallian argillaceous section is succeeded by highstand conditions and deposition of the Corallian sandstones. The highstand conditions were interrupted by a rise in base level before the resumption of highstand conditions. The Corallian is succeeded by the Kimmeridge Clay Formation deposited during resumption of transgression. The section shows about 14.02 m of Corallian sandstones in BL-5, 9.14 m in PW3 and 9.44 m in PW7. Correlation shows that BL5

has an extra sand and mud package in its upper section. The extra sand package shows lower reservoir quality than the other sand packages.

4.4.5.2 Upper Shoreface facies association (USFA)

The upper shoreface facies association (Table 4.2) is the most common facies association in the three wells; it is characterised by upper fine- to medium-grained sandstone. Massive, structureless bedding is common (Fig. 4.2b) as well as trough cross-stratification, planar cross-stratification and localised low angle cross-stratification (Fig. 4.4a). Minor planar lamination and hummocky cross-stratification (Fig. 4.4a) and wave ripple lamination (Fig. 4.6 at 2210.9 m) are also present. Facies present in this facies association include laminated sandstone, wave laminated sandstone, cross-bedded (cross-stratified) sandstone, and massive bedded sandstone. Sandstone body thicknesses are variable, from less than thirty centimetres (Fig. 4.5a at 1092.5 m) to greater than four metres (Fig. 4.4a at 1129.6 -1135.8 m). Some beds within individual sand bodies display upper and lower erosive contacts within the upper shoreface facies association (e.g., Fig. 4.4a at 1134.8 m) indicating high energy conditions.

Ethological expressions are sparse to moderate probably because of high energy depositional conditions. Where present they include: *Ophiomorpha, Skolithos, Planolites, Cylindrichnus, Anchonichnus* and *Macaronichnus* (Figs. 4.4-4.6) supporting an interpretation of high energy deposition.

Erosive lower contacts occur between the relatively high energy, upper shoreface facies association sediment and underlying lower energy facies associations, e.g., on proximal lower shoreface facies association (Fig. 4.4a at 1135.9 m; Fig. 4.6a at 2211.1 m) and on distal lower shoreface (Fig. 4.5a at 1087.5 m). These erosive contacts reveal sudden, rather than gradational, increases in energy conditions.

Sharp upper contacts are common between the high energy, upper shoreface facies association sediment and overlying finer-grained, lower energy facies associations, e.g., with offshore facies association and with distal lower shoreface facies association (Fig. 4.4a at 1129.6 m). These sharp contacts also represent a sudden, as opposed to gradational, change in energy conditions.

In contrast, gradational upper contacts occur between the high energy, upper shoreface facies association sediment and overlying high energy foreshore facies association (Fig. 4.6a at 2203.6 m).

Carbonate cementation, visible in core in the upper shoreface facies association, is variable and is broadly proportional to the quantity of micritised, detrital, disarticulated bivalve shells (Fig. 4.9c). The pronounced preferential alignment of bivalve shells (Fig. 4.9c) suggests deposition following high energy current transport.

Upper shoreface facies association sediments are interpreted as deposits above fair wave base under the influence of wave activity. The low degree of bioturbation (Figs. 4.2b and 4.4-4.6) implies high energy conditions which were intermittently interrupted by the low energy conditions, in the photic zone, as evidenced by the alignment of micritised bivalve shells (Pemberton et al. 2012a; Salah et al. 2016). The erosively-amalgamated beds within sand bodies occur due to stacking that indicates continuous deposition succeeding erosion, rather than completely eroded older beds (Hampson & Storms 2003). This facies association is similar to lithofacies 3 and 5 of Sun (1992), with medium-grained trough cross-bedded, planar cross-bedded, structureless-bedded and low angle cross-bedded sandstones with many shell fragments typical of high energy depositional environments.

4.4.5.3 Proximal Lower Shoreface facies association (pLSFA)

The proximal lower shoreface facies association (Table 4.2) is characterised by upper fine- to fine-grained amalgamated sandstone beds (Fig. 4.6 at 2211.1 -2212.8 m). Proximal lower shoreface beds commonly have current ripple lamination (Fig. 4.5 at 1095.1 m), cross lamination (Fig. 4.6 at 2211.6 m) and mud-drapes (Fig. 4.4 at 1128.2 m). These sediments are moderately- to intensely-bioturbated with common ichnofossils in argillaceous zones including *Anconichnus, Ophiomorpha, Palaeophycus, Rhizocorallium, Cyclindrichnus, Teichichnus rectus, Thalasinoides* and *Chondrites* (Fig. 4.2c). Bed thicknesses vary from less than centimetre-scale laminae (Fig. 4.6 at 2206.1 m) to beds that are about 2.13 m thick (Fig. 4.4a at 1137.5 m). Facies present in this facies association include wave-laminated sandstone, cross-bedded sandstone, and bioturbated sandstone. Beds in this facies association commonly have erosive lower contacts with distal lower shoreface facies association sediment (Fig. 4.4a at 1128.4 m and 1138.2 m). Carbonate cementation is variable; it seems to be most intense in the most highly bioturbated zones (Fig. 4.2c and Fig. 4.4a at 1137.6 m).

Based on grain size, sedimentary structures and degree and type of bioturbation, the proximal lower shoreface sandstones are interpreted to have been deposited under moderate energy conditions when the influence of wave action above the storm wave base was dominant (Pemberton et al. 2012a). The moderate- to intense-bioturbation suggests that periods of low deposition rate and non-deposition were more prevalent in these proximal shoreface sandstones than in upper shoreface sandstones. The occurrence of bed amalgamation suggests repeated high energy conditions that interrupted ambient moderate energy conditions (Vakarelov et al. 2012), most likely due to storm activity (Hampson & Storms 2003).

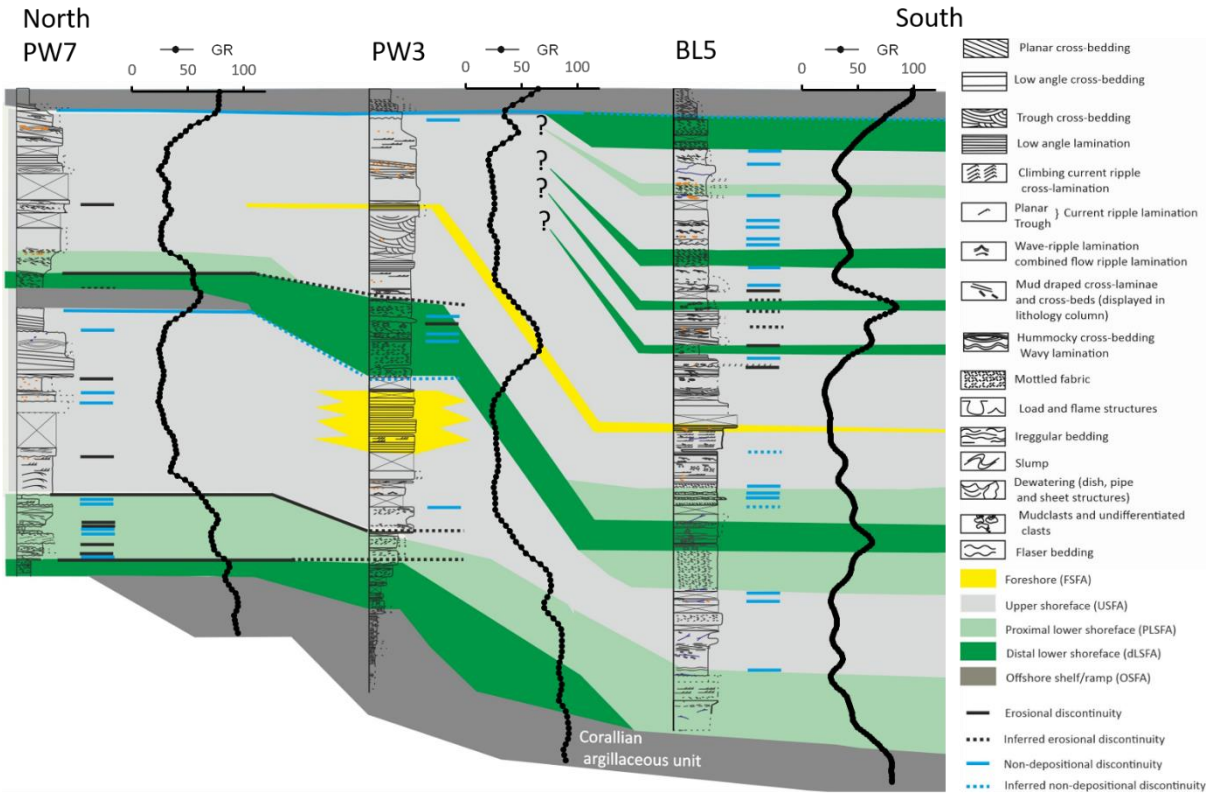

Figure 4.8: Integration of sedimentary logs (Figs 4.4, 4.5 and 4.6) and gamma log data from the three wells with correlation of facies associations. The panel correlates erosional and non-depositional (hiatal) discontinuities across the Palmers Wood wells at the boundaries of facies associations. These discontinuities do not correlate to BL5. The Corallian section is thicker in BL5 than the Palmers Wood wells, with the top section of BL5 showing non-contiguous successions of facies associations possibly suggesting that the normal fault separating the two fields underwent syn-depositional movement. The question marks in the upper section of BL5

indicates the sand package S3 (Fig. 4.7) which do not correlate to the other sand packages/facies associations in PW3 and PW7.

4.4.5.4 Distal Lower Shoreface facies association (dLSFA)

Siltstones and fine-grained sandstones are the dominant lithology in the distal lower shoreface facies association (Table 4.2), which also hosts minor medium grained sandstone (Fig. 4.2d). These sandstones are moderately-sorted to poorly-sorted mostly due to their high clay content and are composed of sub-angular to sub-rounded grains (Fig. 4.10c and 4.10d). Sedimentary structures include hummocky cross-stratification, minor wavy lamination and wave ripple lamination (Figs. 4.4-4.6). Beds are mainly non-amalgamated (Fig. 4.2b). Facies present here include lenticular bedded siltstone, laminated siltstone, and bioturbated sandstone. These distal lower shoreface sediments show moderate to intense bioturbation, suggesting deposition in low energy conditions with low input of sand-grade sediment but in aerobic and nutrient-rich conditions (Seilacher 1967). Erosive amalgamation of non-bioturbated, distal lower shoreface beds is relatively rare (e.g., Fig. 4.5a at 1088.1 m).

Distal lower shoreface sandstones are mostly thin-bedded, typically varying from less than ten centimetres to half a metre (Fig. 4.5a at 1095.6 m) but reaching up to about two metres (Fig. 4.5a). These sandstones are commonly erosively overlain by higher energy facies associations, e.g., proximal lower shoreface (Fig. 4.4a at 1128.4 m) and upper shoreface facies associations (Fig. 4.5a at 1087.5 m).

Ethological expressions in distal lower shoreface sandstones are dominated by the Cruziana ichnofacies and include *Anchonichnus, Chondrites, Ophiomorpha, Planolites, Palaeophycus, Rosellia, Rhizocorallium, Terebellina, Teichichnus rectus* and *Thalasinoides* (Fig. 4.2d and Figs. 4.4 to 4.6). The presence of Cruziana ichnofacies suggests intensive deposit feeding behaviour typical of low energy environments (Pemberton et al. 2012a). These sandstones are similar to lithofacies 2 of Sun (1992) and are composed of very fine to fine-grained intensely bioturbated sand deposited under fluctuating storm activity. The distal lower shoreface facies association is here interpreted to have been deposited below storm wave base, with deposition mostly from suspension, probably between storm events (Hampson & Storms 2003; Pemberton et al. 2012a). The non-amalgamated beds typify low energy deposition from low velocity flow connoting a predominance of low energy regimes with little significant erosion (Vakarelov et al. 2012). Localised erosively-amalgamated non-bioturbated beds suggest high energy pulses

from storm-induced higher energy conditions capable of injecting coarser grains and eroding bed boundaries (Hampson & Storms 2003; Andrieu et al. 2016).

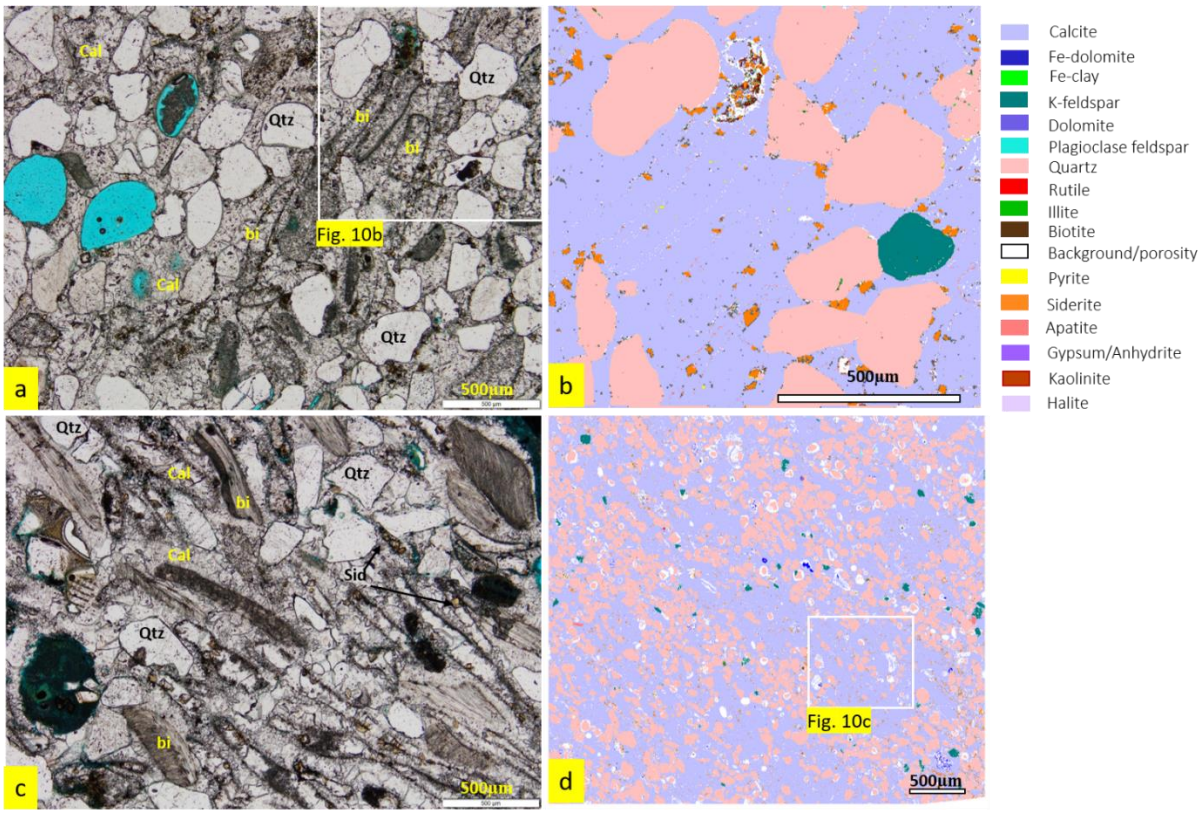

Figure 4.9: (a) PW3 (1091.5 m), optical image of medium- to coarse-grained foreshore sandstone. Calcite cementation is intense with cements around grain surfaces typical of phreatic conditions. Aligned, neomorphosed bivalve shells are outlined by earlier-formed micrite envelopes. (b) is an SEM-EDS image of the rectangle outlined in (a), it shows pervasive calcite cementation. (c) is an optical image of a highly calcite cemented, upper shoreface sandstone from PW7 (1130.0 m). Like (a), bivalve shells are aligned suggesting deposition from suspension during relatively low energy conditions. Also, bivalve shells (e.g., top-left and top-right) have acicular calcite cement lining (d) is also an SEM-EDS image of PW7 (1130.0 m) showing dominant calcite cement with some dolomite cement. Quartz (Qtz), calcite (Cal), bivalve (bi) shells, siderite (sid).

4.4.5.5 Offshore Shelf/Ramp facies association (OSFA)

This facies association is composed of dark mudstone, siltstone, and some thin beds of fine-grained sandstone (Fig. 4.2d; Table 4.2). The main sedimentary structures include wave ripple lamination, current ripple lamination and heterolithic bedding (Figs.4.6 and 4.6). Lenticular

bedding is present but rare in this facies association. Facies present here include bioturbated siltstone, lenticular bedded siltstone, laminated siltstone, lenticular mudstone, and massive mudstone.

Bioturbation tends to be intense and there is wide diversity of ichnofabrics with ichnofossils mostly belonging to the Cruziana ichnofacies. These include *Chondrites, Cylindrichnus, Planolites, Palaeophycus, Terebellina, Teichichnus zigzag, Teichichnus rectus, Thalasinoides* and *Rhizocorallium*.

The offshore shelf/ramp facies association shows a sharp basal contact with the upper shoreface at the top of PW7 (Fig. 4.4); this represents an erosive basal contact with the upper shoreface in the intra-Corallian section, at 1129.6 m. In PW3, the basal contact of the offshore shelf/ramp facies association is erosive (Fig. 4.5a at 1082.2 m) and is interpreted as a flooding surface.

The offshore shelf/ramp facies association is interpreted to have been deposited below storm wave base, mostly from suspension in low energy water as evident by occurrence of siltstone and mudstone as well as the abundance of the Cruziana ichnofacies (Pemberton et al. 2012a).

The offshore shelf/ramp facies association is found mostly in the upper and lower part of the Corallian section (Figs. 4.4, 4.5 and 4.6). Only PW3 contains about half a metre of this facies association in the middle section (Fig. 4.4). The offshore shelf/ramp facies association at the bottom and top boundaries of the Corallian sandstones represent transition from the Corallian argillaceous section and the Kimmeridge Clay, respectively. This facies association is similar to lithofacies Unit 1 of Sun (1992), as it is diagnostic of low energy deposition of mostly fine-grained sediments with sedimentary structures, such as ripple lamination and low energy ichnofabrics such as *Chondrites*.

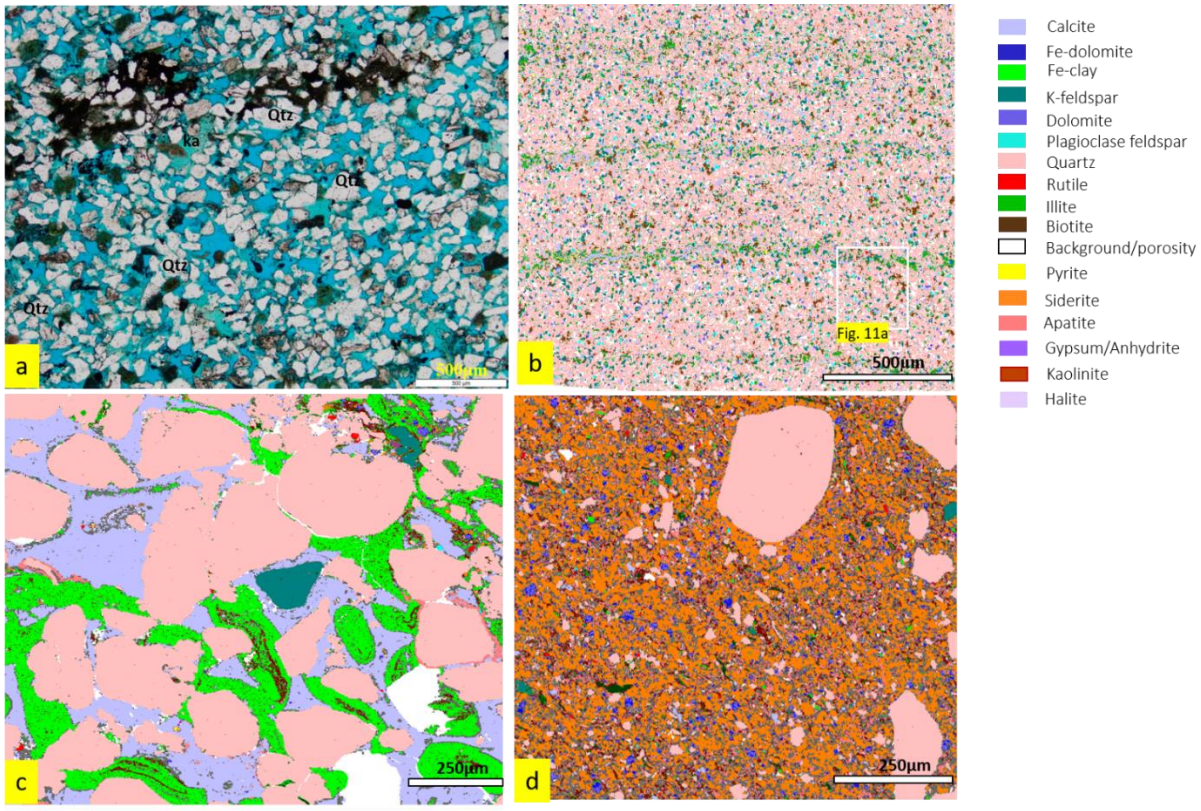

Figure 4.10: (a) this is an optical image of proximal lower shoreface sandstone PW3 (1137.4 m) showing fine grained sandstone with high porosity. Bivalve shells are not common compared to Figure 4.9. (b) Represents an SEM-EDS image (area of 4.10a highlighted in the rectangle). The thin laminae could either be mud drapes or the lining from burrowing organisms. (c) Is a distal lower shoreface sandstone from BL5 (2199.9) m showing Fe-ooids cemented in calcite cement. The degraded Fe-ooids are recognised by their oval shape and relics of their laminae around detrital grains (centre and bottom-left of image). Some of the Fe-clay has recrystallised to fill pores as seen in the top-centre of Fig. 4.10c (d) image of BL5 (2199.9) m showing siderite matrix, fine-grained quartz and kaolinite, suggesting that sediment was sourced from an iron-rich, extensively-weathered environment. Quartz (Qtz), kaolinite (ka)

4.4.6 Breaks in sedimentation

4.4.6.1 Erosional discontinuities

Erosional discontinuities are common throughout the Corallian sandstones. Erosional surfaces may indicate a lowering of storm wave base due to minor fall in sea level or due to storm events (Hampson & Storms 2003). The presence of erosional discontinuities here have been

interpreted where there is an increase in grain size and a reduction in bioturbation intensity in beds overlying an erosional bed contact (Fig. 4.4a at 1126.1 m and 1128.4 m, 1134.8 m, 1137.1 m, 1137.6 m and Fig. 4.5a at 1088.1 m).

Inferred erosional discontinuities (represented by dotted lines on Figs. 4.4, 4.5 and 4.6) have been added where there is either (i) a sharp increase in grain size (but no change in bioturbation) or (ii) a marked decrease in bioturbation intensity (but no increase in grain size). Erosional contacts are common in the high energy, wave-dominated facies associations, e.g., in the upper shoreface facies association in BL5 (Fig. 4.6a), in the proximal lower shoreface facies association in PW7 (Fig. 4.4a) and at the boundary between the distal lower shoreface and the proximal lower shoreface also in PW7 (Fig. 4.4a).

Correlation of erosional discontinuities is represented in Figure 4.8 with PW7 and PW3 having three correlations: two at the base of the Corallian and one at the middle (Fig. 4.8). These correlated discontinuities are at facies boundaries and represent shore-ward shift to higher energy facies associations. Erosional discontinuities are typically succeeded by high energy, storm-related deposits (Fig. 4.4 at 1137.6-1138.1 m).

4.4.6.2 Non-depositional discontinuities

The Corallian sandstones have abundant evidence of non-depositional discontinuities. Non-depositional discontinuities are here recognised by a sharp reduction in grain size, an abrupt increase in bioturbation intensity and anomalous (non-contiguous) successions of facies associations (Hampson & Storms 2003). Non-depositional discontinuities are common in the proximal lower shoreface and upper shoreface facies associations in BL5 and PW7 and are found in the distal lower shoreface and upper shoreface associations in PW3.

The non-depositional discontinuities are here interpreted to be a result of a drop in energy due to sea-level rise, a tectonically-induced break in sediment supply or waning storm-wave conditions (Hampson & Storms 2003).

Except for the flooding surface marking the transition to the Kimmeridge Clay Formation at the top of all three wells, only one other non-depositional discontinuity correlated in the middle section of PW7 and PW3 (Fig. 4.8). The correlated non-depositional discontinuity is at the boundary between the upper shoreface facies association offshore facies association (PW7) and

distal lower shoreface (PW3). The correlated non-depositional surface marks a basinal shift to lower energy facies associations in the middle of the Corallian sandstones.

4.5 Discussion

4.5.1 Relationship between wireline and sedimentary logs

The variations in the relative abundance of sand and shale proportions in the wireline lithology logs and neutron-density cross-over plot show changes in sand and shale sediment deposition as seen when compared with the sedimentary logs in Figures 4.4, 4.5 and 4.6. The sedimentary logs show thick sand bodies in all the wells. High gamma ray values are observed in some thick sand bodies due to small-scale, clay-rich sedimentary structures, such as flaser beds, lenticular beds (Fig. 4.6 at 2206.5 m; Fig. 4.5 at 1088.0 m), mud drapes (Fig. 4.6 at 2210.4 m) and intense homogenisation of sand and clay by bioturbation (Fig. 4.6 at 2207.4-2208.0 m; Fig. 4.5 at 1088.7 m).

The evolution from deposition of the Corallian argillaceous section to deposition of the overlying Corallian sandstones is represented by the elevated sand fraction, shown by the lithology log and the basal sand in the neutron-density cross-over plot (Fig. 4.7). Similarly, the top of the Corallian grades into the Kimmeridge Clay Formation where there is a marked decrease in the sand fraction also shown by the lithology log and neutron-density cross-over plots (Fig. 4.7).

The intra-Corallian mudstone, correlated across this part of the basin, may be the result of a transient increase in sea level (Newell 2000) that exceeded the rate of supply of sand. Considering that the sandstones were deposited during a period of eustatic sea level rise (Fig. 4.1), the deposition of clastic sediment indicates that supply of material outpaced sea level rise (Conybeare 2013). Conversely, the intra-Corallian mudstone and siltstone represents subdued coarse clastic deposition where sea level rise has caused an increase in accommodation space and sediment starvation (Newell 2000).

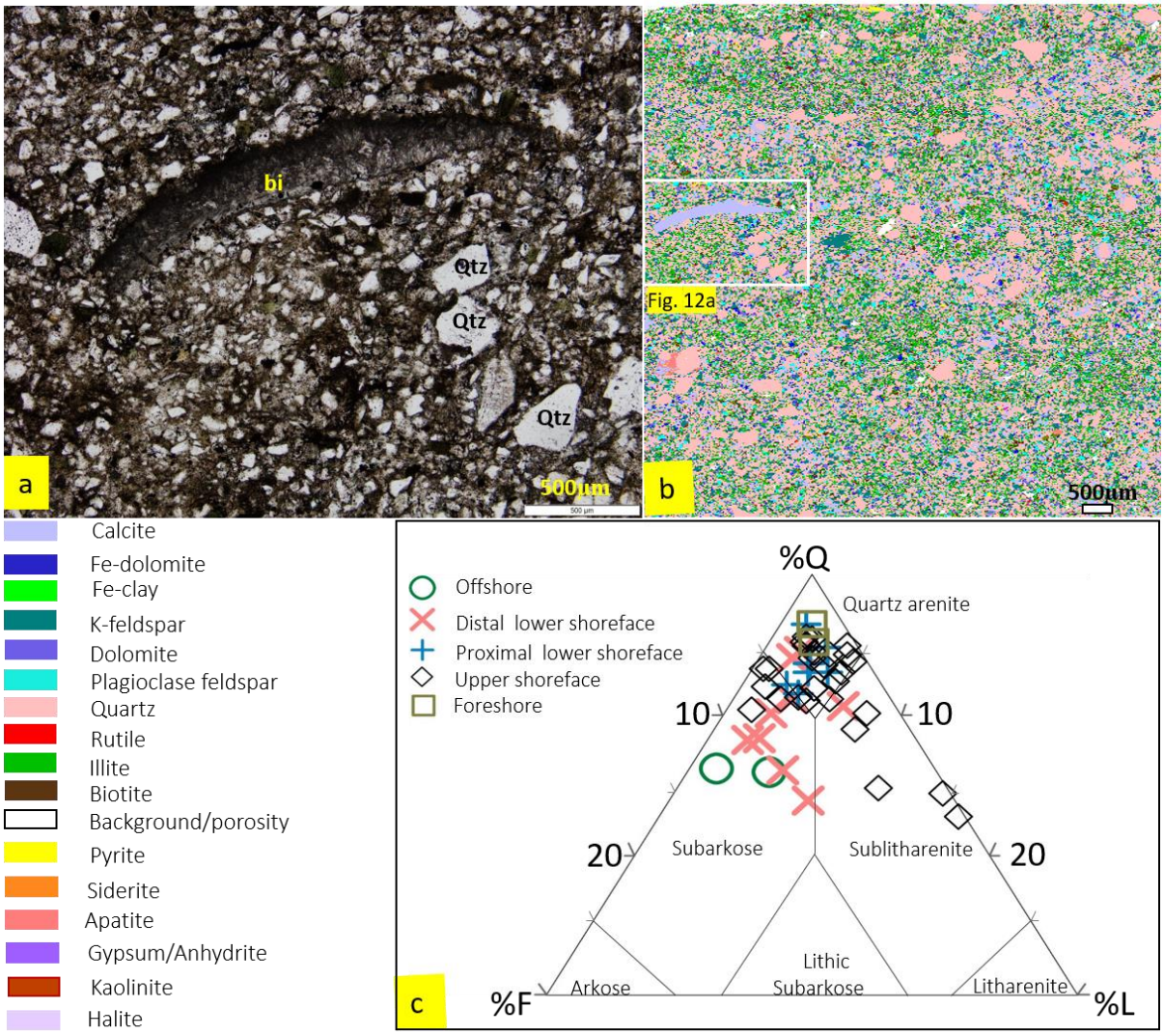

Figure 4.11: Data from PW7 1122.5 m which is an offshore clay-rich siltstone. In (a), the dark areas are detrital clay which is distributed throughout the optical image. The bivalve shell in the centre is highly micritised and calcite cement and clay minerals can be seen filling pore spaces. (b) is an SEM-EDS image revealing the highly bioturbated characteristics of the sediment and includes the area of Figure 4.11a. The SEM-EDS image shows that bivalve clasts are not common in this section and the detrital clay material is mostly composed of illite, with some kaolinite. Some medium grained sand grains are also found within the section suggesting energy conditions were not exclusively low during deposition. (c) Ternary plot, after McBride (1963), showing the relative proportion of quartz (Q) feldspars (F) and lithic grains (L). The plot shows a dominance of a quartz-rich lithology representing a quartz-arenite with minor subarkosic and sublitharenites. Quartz (Qtz), calcite (Cal), bivalve (bi) shells, siderite (sid).

The deposition of the upper and lower Corallian sandstones during a period of sea level rise, makes it similar to the highstand deposition interpreted for the Corallian in the Wessex Basin (Newell 2000). Thus, a highstand systems tract interpretation is also used here for these sandstones.

The sedimentary logs, wireline lithology logs and neutron-density cross-over plots (Figs. 4.4, 4.5 and 4.6) all show agreement in a dominant sand-rich lithology with reservoir potential (pay zones). The correlation of the intra-Corallian section across all three wells splits the reservoir in the Corallian sandstones into an upper and lower unit (Fig. 4.7). The pay zones S1 and S2 have lateral continuity across the three wells (Fig. 4.7) and hence can be predicted away from the wells.

4.5.2 Correlation of Corallian sandstones and intra-Corallian mudstone

Mudstone packages that correlate across all three wells, M1 (Corallian argillaceous section), M2 (intra-Corallian section) and M3 (base of Kimmeridge shale), mark genetically related lithologic units. Similarly, the sandstone package, S1 below the intra-Corallian section and S2 above the intra-Corallian, also correlate across all three wells (Fig. 4.7). The mudstone packages indicate a transient regional reduction in clastic input while the sand packages indicate a regional flux of clastic sediment (Walker & Plint 1992; Conybeare 2013).

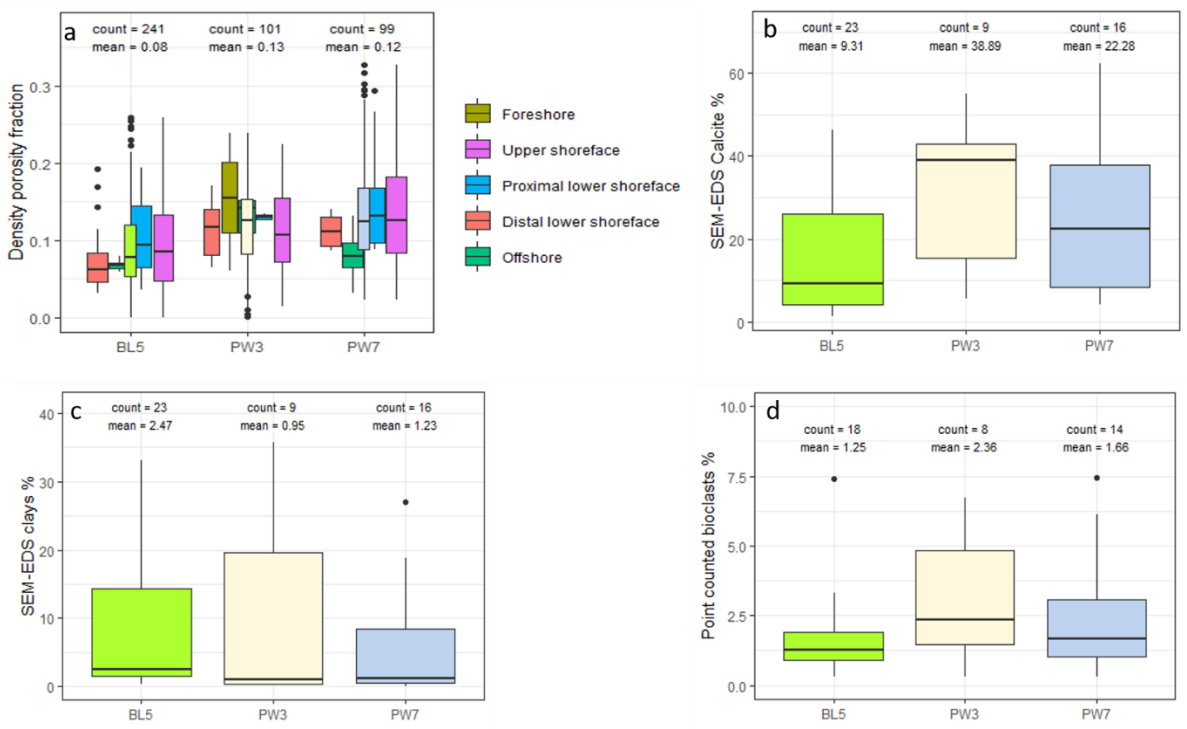

Figure 4.12: Boxplots comparing density porosity by facies associations for PW7, PW3 and BL5 (a), calcite content for PW7, PW3 and BL5 (b), clay content for PW7, PW3 and BL5 (c), and percentage of bioclasts for PW7, PW3 and BL5 (d).

Mudstone package M* and S3 in BL5 do not seem to correlate with any of the sandstone and mudstone packages in Palmers Wood indicating a local control on deposition. In addition, the Corallian section from S1 to S2 does not show significant thickness variation but the increase in thickness in excess of 4.3 m in M* and S3 is typical of fault-controlled deposition (de Wet 1998; Newell 2000; Childs et al. 2003).

Facies associations correlate relatively well between PW7, PW3 and the lower to middle section of BL5 (Fig. 4.8). The upper section of BL5 show non-contiguous juxtaposition of lower energy proximal and distal lower shoreface facies association with upper shoreface facies association. These facies associations at the upper section of BL5, which do not correlate with PW7 and PW3, show anomalous juxtaposition typical of syn-depositional fault control (de Wet 1998; Cecil 2013).

4.5.3 Eustatic controls on sediment supply and deposition

Marine deposition of the Corallian sandstones can be inferred from the marine deposition of both the underlying Oxford Clay and overlying Kimmeridge Clay Formations, which were both deposited during periods of sea level rise (Hallam 1981; Hardenbol et al. 1998; Haq 2017) and the absence of any evidence of significant regression preceding deposition of the Corallian sandstones. Direct evidence of marine deposition of the Corallian includes eogenetic carbonate and phosphate cements (Fig. 4.11b), acicular calcite cement fabrics lining bivalves and framework grains (Scholle & Ulmer-Scholle 2003) (Fig. 4.9c), presence of marine ichnofossils (Fig. 4.2), micritisation of bivalve shells (Figs. 4.9) and the absence of evidence of rhizocretions, paleosols or other signs of emergence surfaces within the Corallian sandstones.

The intra-Corallian mud- and silt-stone, high gamma interval represents a regionally correlated transgressive event (Figs. 4.7 and 4.8). The non-depositional surface identified in core at the base of the intra-Corallian section (Figs. 4.4 to 4.6) suggests that there was a reduction in energy and sediment supply due to sea level rise outpacing sediment supply. Coarse-grained, high-energy facies associations overlay the intra-Corallian (Fig. 4.8) suggesting resumption of sediment supply rate outpacing sea level rise. Analysing the lateral extent of the non-reservoir intra-Corallian and reservoir sandstone packages, beyond the case study location, is limited by the number of wells in this study. However, the intra-Corallian section was previously described as lithofacies unit 4 by Sun (1992) and correlated across PW3, PW5, BL2 and Collendean Farm 1 in the Weald Basin. Similarly, in the Wessex Basin, transgressive events were also noted at the equivalent Oxfordian-Kimmeridgian boundary in the nearby Wessex Basin by Sun (1989). The occurrence of the transgressive events in both the Weald and Wessex Basins suggests an allocyclic influence where sea level rise outpaced sediment supply.

Local conditions influenced deposition. Although non-depositional discontinuities (hiatuses) could mark reduction in marine circulation caused by sea level rise, their frequency and lack of correlation across the three wells suggests localised effects (Fig. 4.8). Similarly, erosional surfaces that do not correlate between wells also suggest local conditions rather than a basin-scale influence expected of sea level rise.

Overall, it is here inferred that eustasy led to the deposition of the intra-Corallian mudstones but played a muted role in controlling deposition of the Corallian sandstones.

Table 4:2: Summary of facies associations, based on a modified version of the facies associations described by Hampson (2003). The facies associations are grouped on the basis of lithology, sedimentary structures and ichnology.

Facies association	**Lithology and sedimentary structures**	**Bioturbation**	**Associated facies**
1. Foreshore (FSFA)	Low angle Planar-parallel laminated, fine to medium-grained sandstone, commonly highly cemented.	Absent, rare *Macaronichnus*	Laminated sandstone
2. Upper shoreface (USFA)	Upper-fine to medium-grained sandstone. Low angle cross beds, trough and tabular cross-bedded with minor planar lamination and hummocky cross-stratification. Cementation is variable.	Sparse to moderate (*Ophiomorpha, Skolithos, Planolites, Cylindrichnus some Anchonichnus and Macaronichnus*)	Laminated sandstone, wave-laminated sandstone, cross-bedded sandstone and massive bedded sandstone
3. Proximal lower shoreface (pLSFA)	Very-fine to fine-grained amalgamated sandstone beds. Wave ripple cross-lamination, current ripple lamination, mud-drapes. Cementation is variable.	Moderate to intense (*Anconichnus, Ophiomorpha, Palaeophycus, Rhizocorallium, Arenicolites,* some *Cyclindrichnus, Teichichnus rectus, Thalasinoides and Chondrites* in argillaceous zones)	Bioturbated sandstone, laminated sandstone, wave laminated sandstone and muddy sandstone
4. Distal lower shoreface (dLSFA)	Clayey siltstone and sandstone with some fine to medium-grained sand. Beds are non-amalgamated with flaser bedding, minor wavy lamination and wave ripple cross-lamination. Cementation is variable.	Moderate to intense (*Anchonichnus, Chondrites, Ophiomorpha, Planolites, Palaeophycus, Rosellia, Rhizocorallium, Terebellina, Arenicolites, Teichichnus rectus, Thalasinoides*)	Bioturbated siltstone, wave ripple laminated sandstone, lenticular bedded sandstone and lenticular bedded siltstone
5. Offshore shelf/ramp (OSFA)	Mudstone, silty mudstone, siltstone with some beds of very fine-to upper fine-grained sandstone. Wave ripple lamination, current ripple lamination, lenticular beds, sand-mud heterolithics beds. Cementation is variable.	Intense (*Chondrites, Cylindrichnus, Planolites, Paleophycus, Terebellina, Teichichnus zig-zag, Teichichnus rectus, Thalasinoides* some *Rhizocorallium*)	Massive mudstone, lenticular mudstone, laminated siltstone and lenticular siltstone

4.5.4 Tectonic controls on sediment supply and deposition

Although deposited during a period of transgression, the Corallian consists of coarse-grained siliciclastics with several coarsening upward sand packages (Figs. 4.4 to 4.6). These cycles observed in core, confirm coarsening upward cycles reported from gamma ray logs by Sun (1992). This pattern can be explained by the net rate of sediment supply exceeding the net creation of accommodation space.

Tectonic activity is capable of increasing the rate of creation of accommodation space and sediment supply such that sedimentary expressions typical of transgression are in one part of a basin and regression in other parts of a basin as a result of the interplay of locally variable subsidence and deposition rates (Lake & Karner 1987; de Wet 1998; Newell 2000).

Evidence supporting syn-tectonic depositional controls on the Corallian sandstones include thickening of the Corallian sandstone section at the upper section of BL5 in excess of 4.3 m, across the fault separating the Palmers Wood wells from BL5 (Figs. 4.7, 4.8 and 4.13). The position of extra sand and mud packages in the upper section of BL5 suggests that syn-depositional faulting occurred in the final stages of Corallian sandstone deposition. Fault-controlled sedimentation of Corallian sediments in the Weald Basin was also proposed by de Wet (1998).

Fault activity led to localised water depth differences and, as a consequence, different styles of sedimentation between the Palmers Wood and Bletchingley (Fig. 4.8 and 4.13) as indicated by the argillaceous, more bioturbated facies associations in BL5 compared to PW7 and PW3. The common occurrence and lack of extended lateral correlation of both erosional and non-depositional discontinuities in all three wells suggests local changes in the creation of accommodation and sediment supply linked to local tectonic activity, rather than global sea level changes. Consequently, basinal facies associations south of the fault in BL5 emphasise the increasing water depth across the fault separating BL5 from PW3 and PW7 (Figs. 4.7 and 4.13).

The overall accumulation of facies in the three wells is typical of fault-controlled, marine sediment accumulation (de Wet 1998; Castro et al. 2019). The irregular arrangement of coarsening and fining upward cycles at the top of the Corallian sandstones as against the bottom of the Corallian section (Figs. 4.4, 4.5 and 4.6), as well as the short-range vertical juxtaposition of facies associations e.g., Sun (1992) in the top sand package S3 in BL5 (Fig. 4.8), suggest transient changes in water depths as coarsening upward zones indicate shoaling while fining upward cycles indicate flooding (Walker & Plint 1992; Newell 2000). The non-contiguous succession of facies associations in S3, as well as the absence of local correlation with other sand packages in the other wells required local variations in accommodation and sediment supply (de Wet 1998), typical of aperiodic, allocyclic, tectonic controls (Cecil 2013).

4.5.5 Climatic controls on sediment supply and deposition

The occurrence of coarse clastic Corallian deposits suggests a significant influence of source-area weathering, run-off, and fluvial discharge into the marine environment (Ruffell & Rawson 1994; Leeder et al. 1998) at the sites of Bletchingley and Palmers Wood. The distance of these fields from the London platform source area (Fig. 3.1), and the presence of products of source-area weathering such as detrital kaolinite (Figs. 4.10 and 4.11), as well as mineralogical and textural maturity, are further indicators of continental weathering and fluvial transport.

Climatic conditions in the hinterland,-the London Platform, - that supplied the sediment are here inferred from mineralogical proxies which suggest warm, humid conditions with high rainfall. These mineralogical proxies include (i) kaolinite in detrital clay (Figs. 4.10b, 4.10d and 4.11b), (ii) presence of the iron-rich minerals, siderite and berthierine (Fig. 4.10d), (iii) the absence of evaporite minerals or alkali-rich clays such as smectite (McKinley et al. 2003a).

Kaolinite typically is produced in warm tropical to sub-tropical climates with high rainfall rates and vegetation (Burley & Worden 2003b). The decay of organic matter under humid conditions creates acidity which enhances chemical weathering of feldspar- and mica-bearing silicate rocks to produce kaolinite (Hallam 1975; Burley & Worden 2003b).

The presence of siderite and berthierine in marine sediment indicates warm, humid, continental weathering because the formation of shallow marine iron-rich minerals requires intense weathering of continental rocks under humid conditions to form lateritic soils, which are then eroded and the iron transported to the marine environment (Tucker 1981; Hallam 1984). The presence of kaolinite (Worden & Burley 2003b) and the abundance of Fe-rich minerals (Worden et al. 2020c), is here taken to show that advanced weathering in the hinterland occurred in organic-rich soils that resulted from lush vegetation.

The absence of evaporite minerals in these marine Corallian rocks precludes deposition on an arid shoreline, because evaporite minerals require subaerial concentration of dissolved salts, typical of arid conditions (Tucker 1981). The absence of Ca^{2+} and Mg^{2+} clays, such as smectite, also seems to preclude arid conditions, as high rainfall typically causes intense leaching of alkaline and alkaline earth cations thereby reducing alkaline conditions and reducing the possibility of the creation and deposition of Ca^{2+} and Mg^{2+} clay minerals (Sladen & Batten 1984; Burley & Worden 2003b).

In summary, the climatic controls on sediment transport further provide an insight into the geology and weathering characteristics of the hinterland London Platform. As the Corallian sandstones are relatively shallow buried, we can infer their source-area characteristics as they have not had their depositional character overprinted by burial (meso) diagenesis (Sladen & Batten 1984). We can therefore infer that the Upper Jurassic London platform created mature sediments which resulted from advanced weathering in a warm humid environment. The material deposited as the Corallian sandstones was transported from a warm vegetated hinterland, with substantial rainfall, capable of causing fluvial transport of sediments which were deposited in a shallow marine environment.

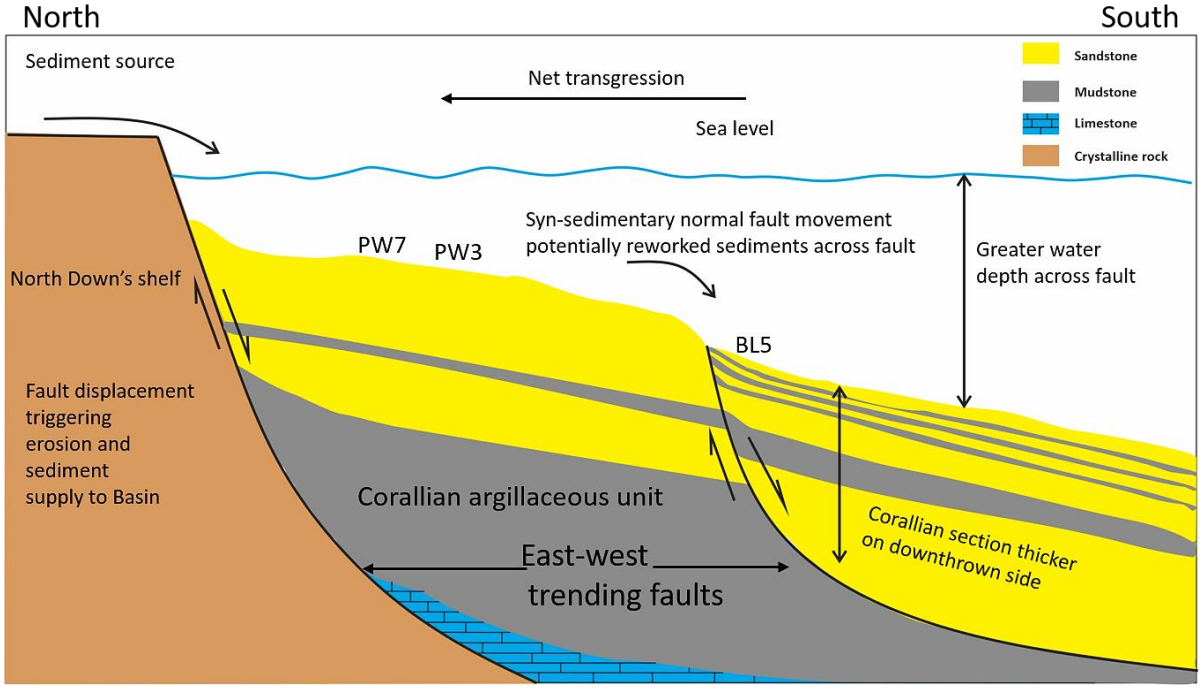

Figure 4.13: Depositional model for the Corallian sandstones showing sediment source and increase of water depth across the main fault separating Palmers Wood and Bletchingley. Not to scale.

4.5.6 Controls on reservoir quality

From a sedimentological perspective, all three wells have well-defined sand packages (Figs. 4.4, 4.5, 4.6, 4.7 and 4.8). From core examination, the elevated degree of hydrocarbon staining in the less cemented sandstone zones (Figs. 4.2a and 4.2b) indicates that calcite cementation is

a significant control on reservoir quality. Calcite cement is present in variable amounts throughout the cores and seems to display no distinct relationship with sedimentary structures, lithology or bioturbation (Figs. 4.4, 4.5 and 4.6). Analysis of log-derived porosity for each well, subdivided by facies association, shows that there is apparently no simple relationship between porosity and depositional facies association (Fig. 4.12a). This is because the trend of high and low porosity is not consistent with facies associations, as seen in Figure 4.12. For instance, the upper shoreface facies association has porosity above the mean value in BL5, below the mean value in PW3 and slightly above the mean value in PW7 (Fig. 4.12a).

Comparison of sedimentary logs to log-derived porosity and oil saturation, for all three wells (Figs. 4.4 to 4.6), confirms that there is no simple relationship between grain size and porosity. For example, the elevated porosity in PW3 at 1090.9m is associated with finer-grained sandstones than the lower porosity-bed immediately below (Fig. 4.5). In all wells, the fluctuations in porosity in the sandstones above and below the intra-Corallian mudstone are not linked to variations in the proportion of clay minerals, as revealed by the interpreted shale volumes in Figures 4.4 to 4.6. The 10 to 20 % variations in Corallian sandstone porosity must be due to another process. The core-derived estimation of intensity of cementation (weakly, moderately or highly calcite cemented) links well with the wireline-log-derived estimation of porosity with the highest porosity values tied to weakly or moderately cemented sandstones. The low porosity beds in the Corallian sandstones are all highly calcite cemented.

The anomalous extra sandstone interval (S3) at the top of the Corallian in BL5 is unusual in that it has uniformly poor reservoir quality; the high porosity values typical of the sandstones either side of the intra-Corallian are absent (Fig. 4.6). There are two possible explanations for the poor reservoir quality. First is that the shale proportion in S3 never gets lower than 10 % and is more typically 20 %. Second is that core description showed that the whole of the anomalous top sandstone layer in BL5 is highly calcite cemented.

The intra-Corallian, defined by the high shale proportion, also tends to be highly calcite cemented (Figs. 4.4 - 4.6) suggesting that this correlatable unit will act as a baffle or a barrier to fluid movement due to the abundance of both clay minerals and carbonate cement.

Petrographic analysis confirms the combined interpretation of core and wireline logs, as it revealed that calcite cement is the dominant pore-filling mineral (Fig. 4.9) with the most porous

samples having the least quantities of calcite cement (Fig. 4.10A). SEM-EDS analysis revealed that median calcite volumes are relatively high (9% to 39%), but the interquartile ranges are large confirming that calcite cement is heterogeneously distributed (Fig. 4.12b). The Corallian sandstones do not display signs of advanced compaction, with an absence of long grain contacts and occurrence of a floating-grain texture (Fig. 4.9b and 4.10A) suggesting that mechanical compaction did not play a major role in porosity-loss and proving the role of cementation in reservoir quality evolution. Petrographic examination revealed that clay minerals occupy pore space as matrix, especially in the finer grained samples (Fig. 4.11) showing that the presence of clay minerals has also caused reduction in reservoir quality. SEM-EDS analysis confirmed that median clay mineral volumes are relatively low (1 % to 2 %) but high upper quartile ranges shows that it is locally present at high concentrations (Fig. 4.12c).

4.5.7 Influence of depositional controls on reservoir quality

Depositional controls have two effects on reservoir quality and reservoir architecture: (1) stratigraphic controls caused by sea level rise as seen in the intra-Corallian: this caused compartmentalisation of the reservoirs into upper and lower units, (2) regional lateral controls caused by tectonism, as seen in the additional (anomalous) uppermost sand package (S3) in BL5 as well as the elevated clay content in BL5 (Figs. 4.7, 4.12 and 4.13)

Syn-depositional tectonism in the Weald Basin, with predominantly downthrown faults to the south is interpreted to have caused an increase in water depth south of the fault, as indicated by the greater prevalence of lower energy, deeper water, facies associations in BL5 compared to PW3 and PW7 (Fig. 4.8). The increase in water depth is interpreted to have had three effects: (1) potential recycling of sediments from the upthrown side (PW3 and PW7) to the downthrown side (BL5) (Fig. 4.13), (2) increase in accommodation space leading to the deposition of a thicker Corallian section in BL5 (Figs. 4.7 and 4.13) and (3) reduction in energy leading to the deposition of finer-grained, lower energy facies associations (Fig. 4.8) as well as fewer bioclasts (Fig. 4.12d). From a reservoir quality perspective, porosity decreases across the fault from an average 12% in PW7 and 13% in PW3 to 8% in BL5 (Fig. 4.12a). However, BL5 has the lowest quantity of calcite of the three wells (Fig. 4.12b) with a mean of only 9.3 % as against PW3's 38.9 % and PW7's 22.3 %. The difference in calcite quantity is interpreted to be a consequence of the reduction in energy in the depositional environment across the fault,

hence a reduction in capacity to transport bioclasts that then neomorphosed to calcite cement (Scotchman et al. 1989; Adams 1998; Worden et al. 2019).

In summary, the integration of sedimentology and sequence stratigraphy supported by wireline analysis and petrography in this study has highlighted the importance of a multi-proxy approach as well as including depositional controls in reservoir quality analysis. The results highlighted climatic influence on the supply of mature, compaction-resistant sands. Sea level rise split the reservoir into upper and lower good reservoir quality stratigraphic units. Tectonism produced two separate hydrodynamic regimes up-dip and down-dip of a fault separating the two fields thereby causing differences in supply of bioclasts and clay mineral accumulation. Tectonism consequently caused poorer reservoir quality down-dip of the fault as well as lateral separation of good and poor reservoir quality units across the fault. Integrating depositional controls in reservoir quality analysis therefore has the potential to improve and extend reservoir quality prediction on a regional scale away from well control points. This study was limited by the number of core and supporting data available for sedimentological, sequence stratigraphic, wireline and petrographic analysis hence only these two fields are involved in the study.

The study has broad implications for reservoir quality analysis in shallow marine environments particularly those that experienced syndepositional tectonism with specific regard to investigating the lateral and stratigraphic extent of good and poor reservoir quality sandstone units.

4.6 Conclusion

1. In the Palmers Wood and Bletchingley area of the Weald Basin, the majority of the Corallian sandstones were deposited as two distinct sand bodies separated by a flooding surface, represented by an intra-Corallian mud- and silt-stone section. Both upper and lower sand bodies have numerous coarsening upward cycles, characteristic of highstand conditions, where sediment supply outpaced base-level rise during normal regression conditions. The absence of paleosols, rhizocretions or terrestrial ichnofossils suggests emergence did not happen and support an interpretation of deposition under highstand conditions with sediment supply transiently outpacing eustatic sea level rise. The major evidence for a eustatic influence on deposition is the intra-Corallian fine-grained section and flooding surface which suggests a major allostratigraphic event caused by base level rise outpacing sediment supply.

2. Evidence of a tectonic influence on the Corallian sandstones include non-correlation of erosional and hiatal surfaces across a major E-W fault, non-contiguous facies associations and thickening of the Corallian sandstone across the fault.

3. Climatic conditions during weathering and transport of the Corallian sediments, from the hinterland in the north are here interpreted to have been warm and humid with abundant vegetation. These conditions were responsible for the accumulation of iron-rich, sand-dominated sediment that may have been nutrient-rich, thus encouraging the intense bioturbation typical of the Corallian clastic sediments.

4. There is not a strong relationship between facies association and reservoir quality. Depositional controls, however, influenced reservoir quality distribution and reservoir architecture. The sandstone reservoir units are compartmentalised into an upper and lower unit by eustatic controls. Tectonism caused the increase in net thickness of the sandstone units in BL5. Tectonism also caused the horizontal separation of the sandstone unit S3 from the other reservoir sections and the reservoir quality is somewhat poorer across the fault in BL5 which has a slightly higher clay content than the Palmers Wood wells, caused by tectonism.

5. Reservoir quality variations, in these shallow buried sandstones, are largely controlled by the variable abundance of calcite cement. The best reservoir quality is associated with the lowest amounts of calcite cement. Calcite cement abundance is directly linked to the proportion of primary calcareous bioclasts revealing that autogenic controls dominate reservoir quality.

Chapter 5: Reservoir Quality of Upper Jurassic Corallian Sandstones, Weald Basin, UK

Chapter five extends the effects of surface and depositional processes examined in chapter four to diagenetic effects on reservoir quality with burial. As the sandstones are buried to less than 2000 m and therefore within the eodiagenetic realm, understanding the controls on their reservoir quality will not only enhance reservoir quality prediction away from well control points but also answer important questions about the role of shallow burial eodiagenesis in conditioning sediments for burial diagenesis. The study will investigate the positive and negative controls on reservoir quality in these sandstones with specific aims to examine the relative role of depositional and diagenetic controls in eodiagenetic shallow marine bioclastic sandstone reservoir quality evolution. The study will also examined the effects of residence time in thermally-driven mineral development in these shallow buried reservoir rocks. This chapter has been published in Geosciences:

Barshep, D.V. & Worden, R.H. 2021. Reservoir Quality of Upper Jurassic Corallian Sandstones, Weald Basin, UK. *Geosciences*, **11**, 446,

http://doi.org/ https://doi.org/10.3390/geosciences11110446.

ABSTRACT

The Upper Jurassic, shallow marine Corallian sandstones of the Weald Basin, UK, are significant onshore reservoirs due to their future potential for carbon capture and storage (CCS) and hydrogen storage. In addition, studies of eogenetic sandstones can provide answers to important questions about the pivotal role of eogenesis to calcite growth, clay coat formation, and compaction as well as their relation to mesogenetic processes such as compaction and chlorite coat formation. These reservoir rocks, buried no deeper than 1700 m before uplift to a depth of 850 to 900 m at the present time, also provide an opportunity to study the pivotal role of shallow marine sandstone eodiagenesis. With little evidence of compaction, these rocks show low to moderate porosity for their relatively shallow burial depths. The Corallian sandstones of the Weald Basin are relatively poorly studied; consequently, there is a paucity of data on their reservoir quality which limits any ability to predict porosity and permeability away from wells. This study presents a potential first in the examination of diagenetic controls of reservoir quality of the Corallian sandstones, of the Weald Basin's Palmers Wood and

Bletchingley oil fields, using a combination of core analysis, sedimentary core logs, petrography, wireline analysis, SEM-EDS analysis and geochemical analysis to understand the extent of diagenetic evolution of the sandstones and its effects on reservoir quality, especially the relative influence of compactional and cementational porosity loss. The analyses show a dominant quartz arenite lithology with minor feldspars, bioclasts, Fe-ooids and extra-basinal lithic grains. It is here concluded that little compactional porosity-loss occurred with cementation being the main process that caused porosity-loss. Early calcite cement, from neomorphism of contemporaneously deposited bioclasts, represents the majority of the early cement, which subsequently prevented mechanical compaction. Calcite cement is also interpreted to have formed during burial from decarboxylation-derived CO_2 during source rock maturation. Other cements include the Fe-clay berthierine, apatite, pyrite, dolomite, siderite, quartz, illite and kaolinite. Reservoir quality in the Corallian sandstones show no significant depositional and textural controls; it was reduced by dominant calcite cementation, locally preserved by berthierine grain coats that inhibited quartz cement and enhanced by detrital grain dissolution as well as cement dissolution. Reservoir quality in the Corallian sandstones can therefore be predicted by considering abundance of calcite cement from bioclasts, organically derived CO_2 and Fe-clay coats. This study broadly emphasizes the importance of considering biogenic input in reservoir quality analysis as well as considering residence time in analyzing kinematic-controlled processes such as quartz and illite cementation. The study has major implications for understanding bioclasts-derived retardation of compactional porosity loss, the effect of residence time in kinematic-controlled mineral development and shallow marine eogenetic conditioning of minerals before mesogenesis.

Keywords: Corallian sandstones; reservoir quality; bioclastic sandstones; early carbonate cementation; shallow reservoirs; berthierine grain-coats; low temperature quartz cement

5.1 Introduction

Diagenesis involves physical, chemical and biological processes which act on texturally and compositionally unstable sediments, causing them to reach mineralogical and textural maturity and converting sediment into rock (Burley & Worden 2003a). Diagenetic processes alter the porosity and permeability of sedimentary rock (reservoir quality) as burial progresses (Wilson & Stanton 1994). Understanding the controls and processes involved in diagenetic alteration is therefore useful in predicting reservoir quality evolution (Byrnes 1994).

Under some circumstances, differences in reservoir properties, such as porosity and permeability, can be linked to variations within their depositional systems (Burley & Worden 2003a). The specific characteristics of primary depositional systems are paramount for reservoir quality in shallow reservoirs but they become relatively less important as burial proceeds and as mesogenetic processes become dominant (Bloch & McGowen 1994). It therefore follows that, for shallow-buried, slightly diagenetically-altered sandstones, understanding the dominant depositional controls (texture and composition) may be sufficient to predict reservoir quality (Bloch & McGowen 1994). Near surface (eogenetic) processes represent a continuum during the gradual adoption of a close-packed structure due to compaction and alteration of reactive detrital grains during the first 2000m of burial before the onset of deeper-burial related physicochemical adjustments that allow sedimentary rocks to achieve true textural and thermodynamic equilibrium (Worden et al. 2018c). Understanding the controls on eogenetic processes can permit prediction of reservoir quality in rocks that have not entered the mesogenetic realm. If eogenetic processes, such as early calcite growth, clay coat formation and initial compactional processes, are better understood, then this may permit enhanced prediction of reservoir quality even in more deeply buried rocks that have inevitably undergone eodiagenesis (Burley & Worden 2003a; Worden et al. 2018c) e.g. through forward modelling. This study of iron-rich and bioclastic Jurassic sandstones at a relatively shallow present-day depth of about 850 to 900 m (true vertical depth, TVD) in the Weald Basin, UK, sheds light on eogenetic processes and will provide an important reference for reservoir quality studies for the Weald area as well as similar shallow marine environments.

The onshore Mesozoic Weald Basin, in southeast England, contains many small petroleum accumulations, including the shallow (less than 1000 m) Palmers Wood and Bletchingley fields (Trueman 2003a; Andrews 2014; Pullan & Butler 2019). There are many small oil fields on the southern and western flanks of the Weald Basin with a combination of oil and gas fields on the northern flank (Trueman 2003a; Pullan & Butler 2019). Oil and gas have been produced from Palmers Wood and Bletchingley accumulations, at relatively low flow rates, from Upper Jurassic Corallian Group sandstones since 1983 (Hawkes et al. 1998; Trueman 2003a). These sandstone reservoirs represent a combination of quartz- and bioclast-rich, and iron-bearing clastic deposits (McPhee et al. ; Arkell 1933a; Sun 1992; de Wet 1998). The producing intervals have overall sandstone thickness of about 9 to 25 m (Sun 1992) but they have low production rates, so that a simple sedimentological approach (defining reservoir and non-reservoir zones by the presence or absence of sand) is insufficient to understand their reservoir quality. Several

studies reported on the tectonic evolution, regional geology and hydrocarbon potential of the basin (Sellwood et al. 1986; Hawkes et al. 1998; Hansen et al. 2002; Trueman 2003a; Hillis et al. 2008b; Pullan & Butler 2019) but there is little published on diagenesis and its effect on the reservoir quality of Corallian sandstone reservoirs.

Reservoir quality is a key risk factor in hydrocarbon exploration (Bloch 1994; Kupecz et al. 1997a; Gier et al. 2015; Worden et al. 2018c), so that it is important to understand the effects of diagenesis on reservoir quality evolution of sandstones to enable prediction of reservoir quality away from wells. This study aimed to advance the knowledgebase about the controls on reservoir quality of shallow buried reservoir rocks and the potential effects of early diagenesis on subsequent diagenesis. Furthermore, the two structures (Palmers Wood and Bletchingley) are relatively close to London and other populous parts of the south-east of the UK. Considering the proximity of these fields to areas of high demand for energy and the UK's progressive drive to carbon-neutrality, it is possible that these old petroleum fields might be re-purposed, as the energy transition progresses, for carbon capture-, compressed air- or hydrogen-storage. Understanding the controls on the distribution of storage (porosity) and injectivity (permeability) in these fields may become increasingly important as the energy transition advances.

This study incorporated conventional oil field data from Bletchingley and Palmers Wood in the northern flank of the Weald Basin. New data were produced on the diagenetic controls on reservoir quality of the Corallian sandstones in order to answer the following research questions:

1. What depositional characteristics have influenced reservoir properties in these Upper Jurassic shallow marine and eogenetically-altered sandstone?
2. What pore-filling, grain-replacive or grain-coating mineral cements are found in these sandstones?
3. How much compaction has occurred in these sandstones?
4. What processes have dominated reservoir quality in these sandstones?

5.2 Geological Background

5.2.1 Regional Geology

The Weald Basin is bound to the north by the London-Brabant platform, to the south by the Portsdown-Paris Plage ridge (Portsdown-Middleton trend) and the Hampshire-Wessex Basin

to the west (Lake & Karner 1987; Butler & Pullan 1990; Hansen et al. 2002) (Fig. 5.1). The Weald Basin is underlain by Middle Devonian to Lower Palaeozoic basement rocks which were deformed during the Carboniferous Variscan Orogeny (Hansen et al. 2002; Trueman 2003a). The Variscan orogeny (~370-290 Ma) produced east-west trending fault system. These faults underwent reactivation and became the main structural controls on rift basin formation, and the creation of accommodation space, in the Weald area (Fig. 5.1).

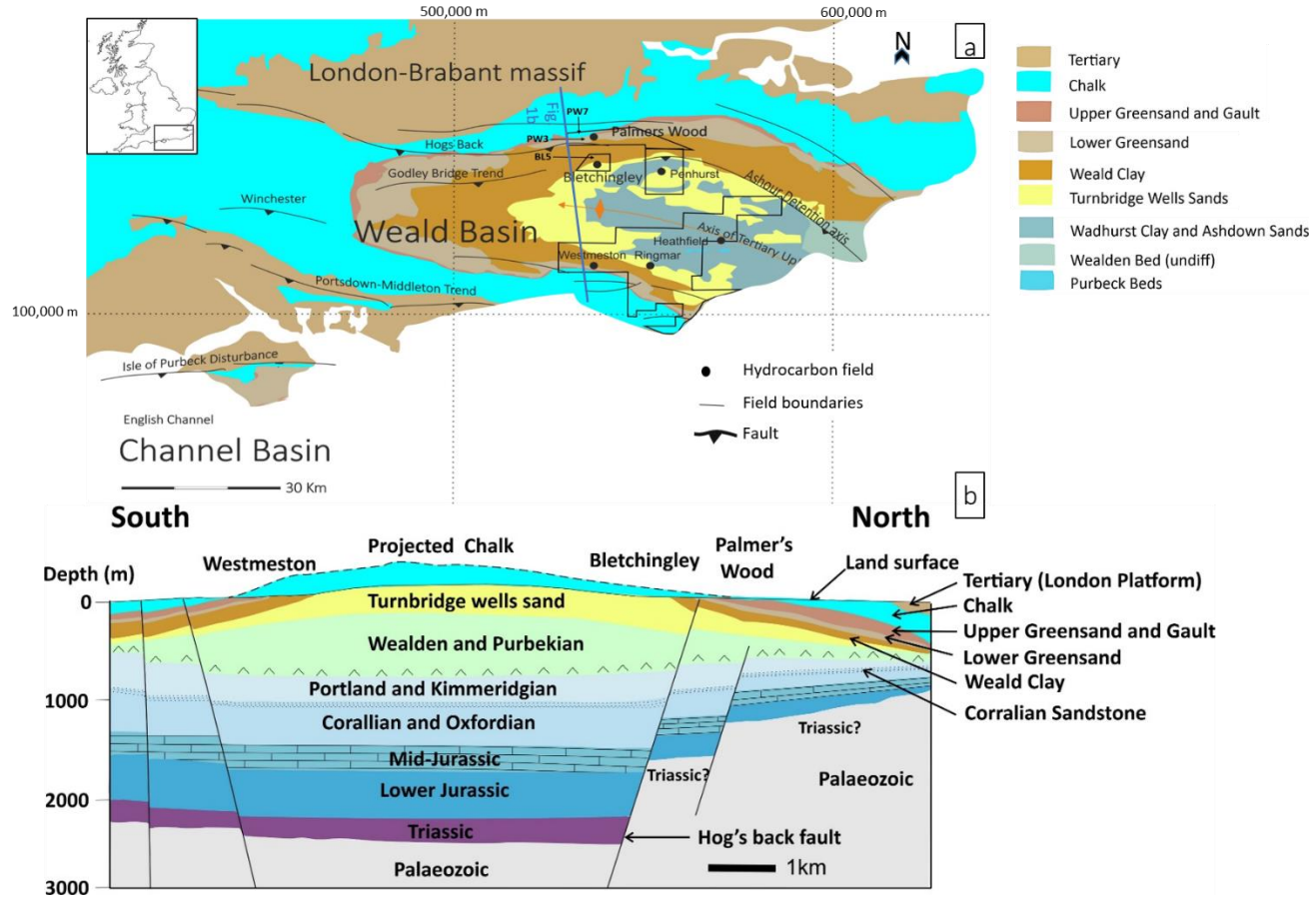

Figure 5.1:(a) Location map of the Weald Basin showing surface geology with major structural trends (b) Schematic of the subsurface through the line of section in (a) as adapted from Andrews (2014); Butler & Pullan (1990).

During the middle part of the Mesozoic, thermal subsidence, associated with block faulting, created accommodation during the Lower Jurassic Rhaetic transgression and the subsequent deposition of the Lower Jurassic White Lias, Lower Lias, Middle Lias and Upper Lias units (Fig. 5.2) (Sellwood et al. 1986; McLimans & Videtich 1989; Andrews 2014). A broad, shallow, carbonate bank developed due to tectonic uplift at the end of the early Jurassic on which Middle Jurassic Bajocian Inferior Oolite and Bathonian Great Oolite were deposited

(Fig. 5.2) (Talbot 1973; Lake & Karner 1987; Andrews 2014). Continued rifting, thermal subsidence and transgression from the Middle Jurassic (Callovian) to Lower Cretaceous caused the deposition of marine mudstones and limestones of the Oxford Clay Formation, Corallian Group, Kimmeridge Clay Formation and Portland Group (Sellwood et al. 1986; Hansen et al. 2002). The deposition of these marine mudstones and limestones was interrupted by the deposition of the coarse clastic Upper Oxfordian (Corallian Group) and Portlandian (Portland sandstone Formation) sandstones, which were reported to be sourced from the London Brabant Massif, to the north of the basin (Sellwood et al. 1986; Butler & Pullan 1990). The overlying, sabkha-related Purbeck Group was subsequently deposited at the very end of the Jurassic through to the Lower Cretaceous, as relative sea-level fell (Butler & Pullan 1990; Hansen et al. 2002; Radley 2006). This was followed by the deposition of the continental Valanginian Wealden Group clastic sediments (Radley 2006).

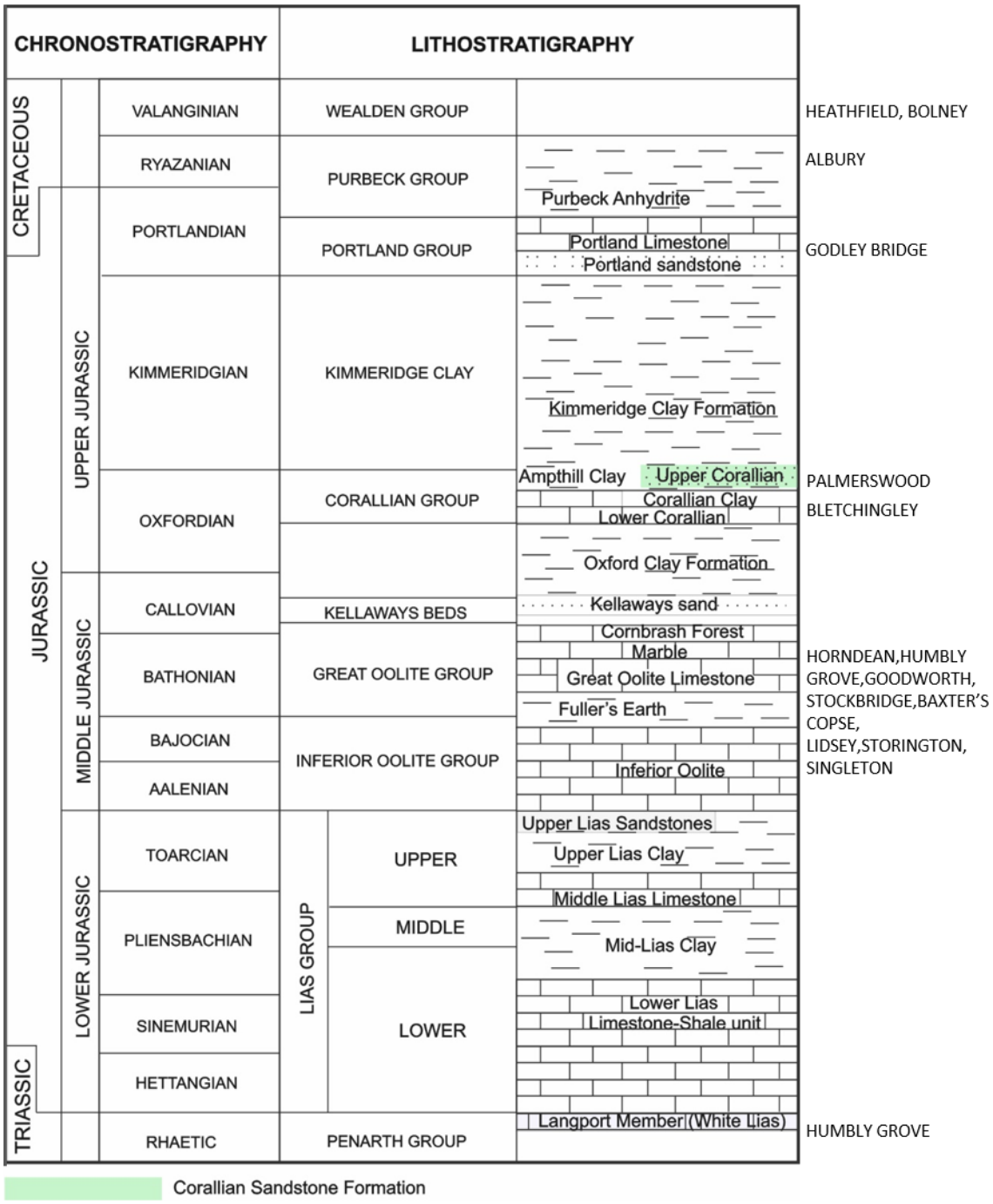

Figure 5.2: Generalised stratigraphic section for the Jurassic of the Weald Basin as adapted from Andrews (2014). Showing lithologic units as well as selected hydrocarbon fields and their reservoir sections. The Corallian sandstone Formation is highlighted in green

Cenozoic fault reactivation and basin inversion occurred in response to compressive forces from the south during the opening of the North Atlantic in the Paleogene, with a second phase in the Miocene possibly associated with the Alpine tectonism (Jones 1999a). The resulting

inversion caused a regional uplift, reported to be as much as 2134 m (7000 ft) (Hillis et al. 2008b). Basin inversion led to the formation of broad, dome-shaped, hanging-wall anticlines (with the London Basin to the north and the Hampshire-Dieppe Basin to the south), subsiding to form flanking basins in the late Paleogene-Eocene (Hansen et al. 2002). The Cenozoic inversion led to erosion and removal of sediments younger than the Valanginian Wealden Group (Sellwood et al. 1986).

5.2.2 Trap Formation and Hydrocarbon Occurrence

The Upper Jurassic to Lower Cretaceous rifting caused the development of extensional trapping geometries, trending east-west along low angle faults, which originated from earlier Variscan thrusts (Hawkes et al. 1998; Hansen et al. 2002).

Organic-rich candidate source rocks in the Weald Basin include the Liassic shales (Ebukanson & Kinghorn 1986; Butler & Pullan 1990; Hansen et al. 2002), the Oxford Clay Formation and the Kimmeridge Clay Formation (Ebukanson & Kinghorn 1986; Butler & Pullan 1990; Andrews 2014; Palci et al. 2018b). It has been suggested that the Lias and Oxford Clay reached the gas generation window in the centre of the Weald Basin while the Kimmeridge Clay may have only reached the oil generation window (Palci et al. 2018b).

Others have suggested that the Lower Jurassic source rocks reached maturity and expelled hydrocarbons in the early Cretaceous (Ebukanson & Kinghorn 1986; Butler & Pullan 1990; Hansen et al. 2002). Expulsion of hydrocarbons terminated during Cenozoic fault reactivation, inversion and cooling of source rocks (Hawkes et al. 1998; Hansen et al. 2002).

5.2.2.1 Bletchingley Field

The relatively shallow Bletchingley field was discovered in 1963, near the village of Bletchingley, when seismic surveys showed two faulted structures within existing mining leases (Trueman 2003a). The seismic survey resulted in the drilling of four wells between December 1965 and 1966; wells BL1 and BL2 on the eastern flank both tested gas from the Upper Jurassic Corallian limestone with a maximum flow rate of 9.65 MMSCF/day (Trueman 2003a). Gas in place was estimated to be between 1 to 6 BCF (Trueman 2003a). Wells BL5 and BL6 were drilled in 2008 and the Corallian sandstone, the subject of this paper, reportedly flowed at about 250 b/d in BL5 at a true vertical depth of about 850 m. Well BL5 was drilled at a low angle so that measured depths (m MD) are significantly greater than true vertical depths

(m TVD). In this study, logs and core sample from BL5 have depths reported in terms of the measured depths (m MD).

5.2.2.2 Palmers Wood Field

Similar to Bletchingley, the relatively shallow Palmers Wood field is also a seismically-defined prospect located on the northern flank of the Weald Basin (Trueman 2003a). In 1983, the first well was drilled at Rook's Nest farm and tested oil at unstable rates of 540 b/d from a 9.1 m (30 ft) Corallian sandstone section (Trueman 2003a), at a true vertical depth of about 900 m. Further testing, in new appraisal wells, from 1984 to the 1990s tested oil (Trueman 2003a). Average porosity is about 17 % with mean permeability ranging from 5 to 7 mD, explaining the low production rates. The stock tank oil initially in place (STOIIP) was initially estimated to be 11.73 MMSTB (Trueman 2003a).

5.3 Materials and Methods

5.3.1 Sedimentary Core Logging

The sedimentary cores were originally measured in feet, as all well depths (logs and core) were recorded in feet, but the depths have here been converted to metres. High resolution sedimentary core logging of three wells: Bletchingley 5 (BL5), Palmers Wood 3 (PW3) and Palmers Wood 7 (PW7), was carried out at the British Geological Survey (BGS) core store in Keyworth, Nottinghamshire. The wells were logged on a scale of 1:24, recording grain size, lithology, sedimentary structures, bioclasts, ichnofabrics, cementation, fractures, hydrocarbon stains and well deviation. About 17 m of core was available from PW3, 17 m of core was available from PW7 and nearly 20 m of core was available from BL5.

Ichnofabrics and depositional environments were determined using methods outlined by Hampson & Storms (2003) and Pemberton et al. (2012b). Sedimentary logs have been summarised and digitised to a scale of 1:240 and related to wireline and routine core analysis data.

5.3.2 Wireline Analysis

Wireline logs used in this study include neutron logs, density logs and gamma ray logs. Gamma ray logs were used to determine shale proportions (Vshale) using the formula:

$$\mathrm{Vshale} = \frac{\mathrm{GR_{meas}} - \mathrm{GR_{min}}}{\mathrm{GR_{max}} - \mathrm{GR_{min}}}$$

(Equation 5.1)

Where GR_{meas} is the measured gamma ray value for the depth of interest, GR_{max} is the maximum gamma ray log value for the rock section of interest and the minimum gamma ray value for the rock section of interest is denoted by GR_{min}.

Wireline neutron-density cross-over plots were used to define pay and non-pay zones as is conventional in petrophysical analysis (Rider 1986). Core-to-log depth shifts were made to match density log porosity to core analysis porosity and Vshale to mudstones identified during core description.

5.3.3 Petrographic Analysis

Petrographic analysis was carried out to determine mineralogy, modal composition, textural relationships, pore space morphology, and types of cements present, as well as the relative timing of diagenetic events. In this case, 51 polished sections were prepared from plugs used for core analysis from PW7, PW3 and BL5, in the standard manner for water-sensitive plugs. Polished thin sections were used for both optical microscopic examination and SEM analysis. The polished sections were all impregnated with blue-dyed epoxy resin to aid in the characterisation of pores. Light microscopy was undertaken using an Olympus BX51 microscope. In this case, 48 samples were point counted to determine modal composition using an Olympus BX53M microscope fitted with a Conwy Valley systems Petrog stage and software. For point counting, appropriate grid spacing was chosen to enable representative sampling of 300 compositional points with a X10 magnification objective. Attention was paid to cement types, cement stratigraphy and replacive cements to help reveal the order of diagenetic events (i.e., paragenetic sequence) as well as enable quantification of compactional and cementation porosity loss as described by Houseknecht (1987). A further 250 points were analysed with a X5 objective to measure grain size and sorting.

Backscattered Scanning Electron Microscopy (BSEM) was carried out using a Hitachi TM3000 table-top SEM. This was undertaken to ascertain mineralogy, mineral/cement growth relationships and textural relationships.

Automated mineralogy data were acquired using SEM-EDS technology developed by FEI (Worden et al. 2018b); SEM-EDS is a scanning electron microscope (SEM) equipped with

high-speed Energy Dispersive X-Ray Spectroscopy detectors (EDS) (Armitage et al. 2011). SEM-EDS identifies minerals using Species Identification Protocols (SIPs) which represents an extensive mineral chemical database archived in a library (Pirrie et al. 2004; Armitage et al. 2010) to produce a quantitative evaluation of mineral proportions. SEM-EDS analysis produces quantitative mineral proportions, grain and pore space morphology and distribution to a minimum resolution of about 1 to 2 μm (i.e., equal to the diameter of the smallest beam-sample interaction volume). SEM-EDS analyses were undertaken with a user-defined resolution depending on the level of detail required and analysis time. In this study, SEM-EDS analyses were undertaken at the University of Liverpool, using a tungsten-filament, operating at 15 kV, equipped with two Bruker EDS detectors (Wooldridge et al. 2018). A minimum spacing of 2 μm was used for higher resolution and 20 μm spacing resolution was used where average mineralogy was required across a whole polished section.

X-ray diffraction (XRD) analyses were undertaken at the University of Liverpool's Diagenesis Research Group lab. The analysis was carried out using randomly oriented powders with a PANalytical X'Pert Pro MPD X-ray diffractometer (Malvern PANalytical, UK). Minerals were quantified by the relative intensity ratio (RIR) (Chung 1974) method using the PANalytical HighScore Plus software. XRD analysis was carried out to determine bulk rock mineralogy with specific interest on identifying berthierine. Presence of berthierine was determined by heating samples to temperature from ambient to 300 °C, 400 °C and 550 °C.

5.3.4 Routine Core Analysis

Porosity and permeability were measured by industry core laboratories, from one-and-a-half-inch diameter core plugs, cleaned in hot refluxing solvents to remove hydrocarbons and residual brines. Helium porosity was determined using a Boyle's Law porosimeter. The porosity of six additional core plugs from PW3 and PW7 was measured at the rock deformation laboratory University of Liverpool using a Quantachrome Pycnometer. Permeability was measured using a nitrogen permeameter, with samples mounted in a "Hassler" type core holder. Permeability was measured using a steady state flow of nitrogen gas through core plugs; flow rate, temperature and differential pressure were recorded and used in conjunction with core dimensions to calculate permeability from Darcy's equation.

5.3.5 Burial History Modelling

Burial history modelling was carried out with BasinMod software, courtesy of Platte River Associates. The stratigraphic data are from well completion reports for BL5, where depths for modelling are reported as true vertical depths subsea (TVDss) in metres and formation tops defined from cuttings, measurement while drilling (MWD) gamma ray and Rate of Penetration (ROP) data. The TVDss were converted to true vertical depths (TVD) in metres to account for surface elevation above mean sea level before burial analysis was carried out. The stratigraphic sections eroded during the Aptian to Turonian (Cenozoic) inversion was modelled using the Dartford area north of the Weald Basin as Upper Cretaceous (Chalk) and Cenozoic deposits above the Weald Clay have been eroded, hence its absence in the vicinity of the two fields in question. The ages of the various stratigraphic intervals were derived from the British Geological Survey's (BGS) lexicon of named rock units (The British Geological Survey 2020) and the age for erosion inferred by calculating the duration of erosion from the deposit thicknesses and a maximum erosion rate of 14.7 m/Ma. The erosion rate was deduced by dividing the total eroded thicknesses by the number of years since erosion started (55Ma). Bottom-hole temperatures used here were from BL5 well temperature profile as provided in the well report.

5.4 Results

5.4.1 Sedimentary Core Logs

The Corallian Group sandstones are dominated by light grey to brown sandstone, siltstone and minor dark brown to black mudstone (Fig. 5.3). The results from core logging are summarised in Fig. 5.4 and Table 5.1. The sandstones are generally well-sorted (Fig. 5.3a, 5. 3b) with many poorly-sorted argillaceous intervals (Fig. 5.3c and 5. 3d).

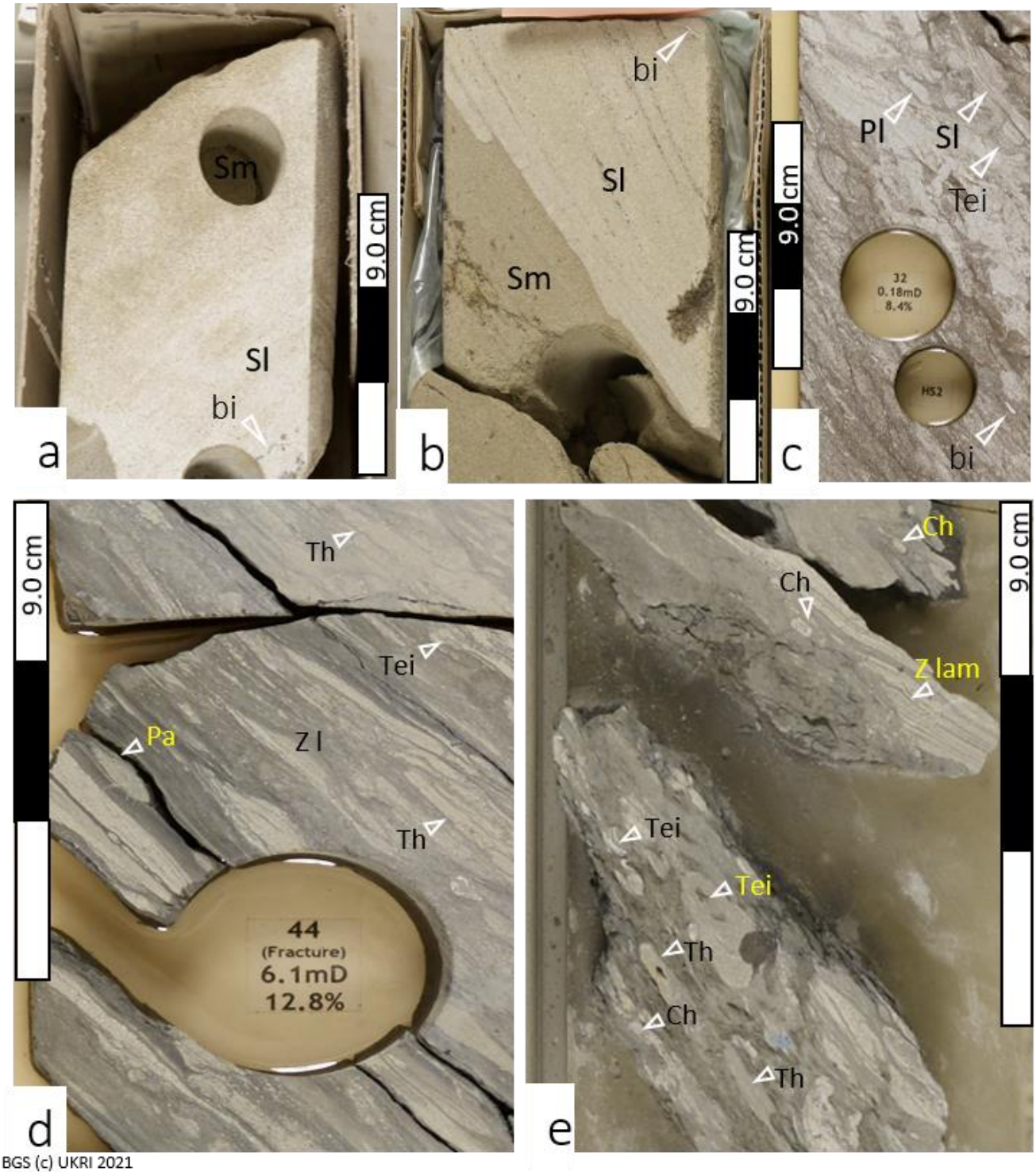

Figure 5.3: Core photographs of facies associations for the Corallian sandstones. All depths are measured depths (m MD) from core, uncorrected for true vertical depth. (a) PW3 (1090.6–1090.7 m MD) showing a foreshore sandstone. (b) is an upper shoreface sandstone from PW7 (1135.2–1135.4 m MD) (c) BL5 (2195.9–2196.1 m MD) is a proximal lower shoreface

sandstone. (d) BL5 (2199.4–2199.47 m MD) is a distal lower shoreface sandstone. (e) PW3 (1096.8–1096.9 m MD) shows bioturbated dark mud of the offshore shelf facies association. The cores show an alternation in hydrocarbon stains (brown coloration) in strongly and weakly cemented zones. The core also show that cementation is not closely linked to facies association. Sl: laminated sandstone, Sm: massive sandstone, Zlam: laminated siltstone, Zl: lenticular bedded siltstone, bi: bivalve shell, Pa*: Palaeophycus*, Tei:*Teichichnus*, Th: *Thalasinoides*, Ch: *Chondrites*, Pl: *Planolites*.

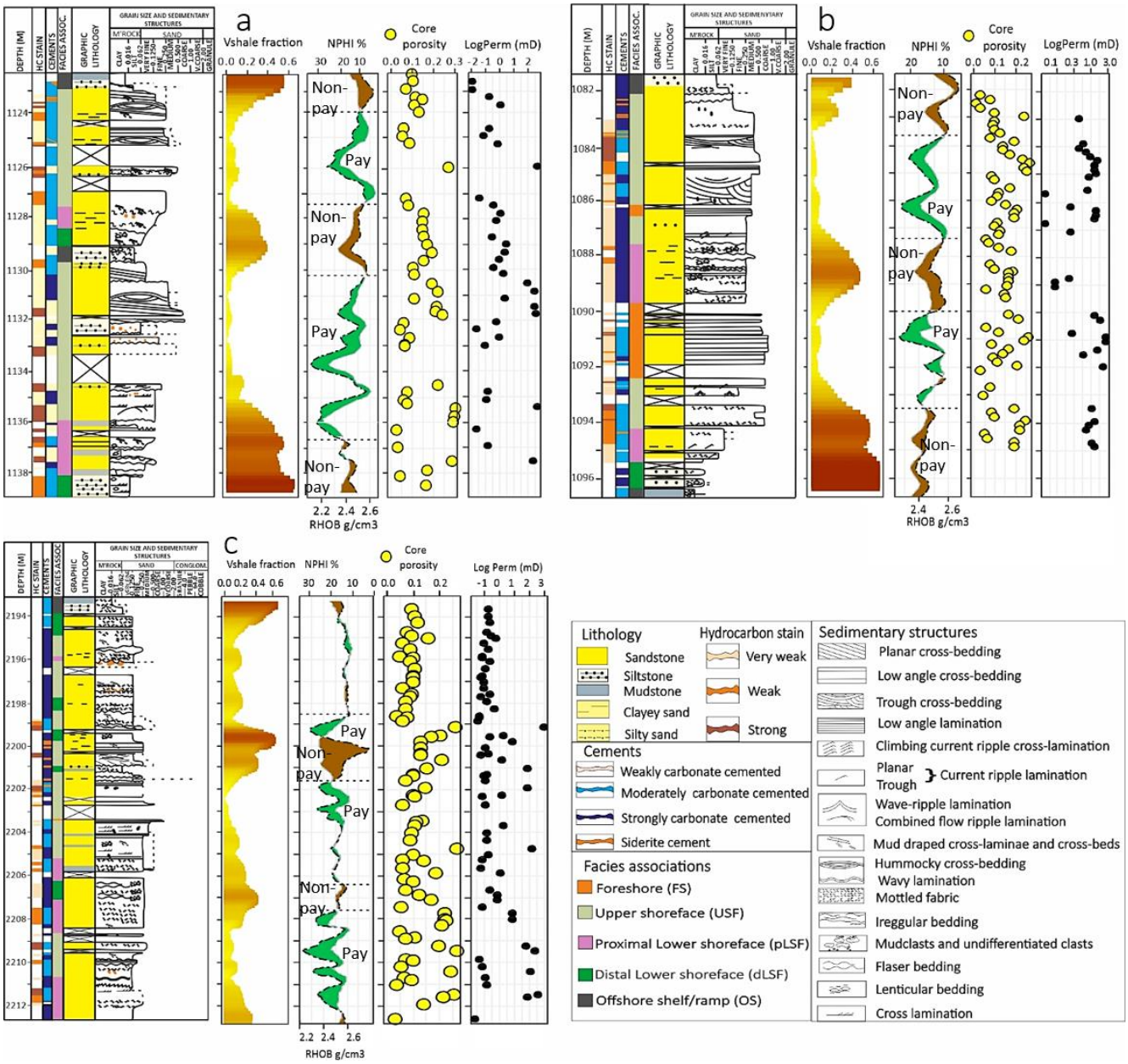

Figure 5.4: Shows sedimentary log, Vshale log, neutron (NPHI) and density (RHOB) cross-over plot, core analysis porosity log and core permeability log for wells, (a) PW7, (b) PW3, and (c) BL5. Sedimentary logs show short-range heterogeneity in sedimentary structures and intensity of cementation. They also show variation in hydrocarbon stains with depth. The wireline logs (Vshale, NPHI and RHOB) track the variation in shale content from the sedimentary logs with the core porosity and permeability logs showing the best reservoir quality sections in the sand-rich portions of the logs. Even though the logs show the highest porosity and permeability in the sandier zones. They also have low porosity and permeability in the sandier zones suggesting that lithology is not the dominant control on reservoir quality. The intervals with high calcite cement and clay content show lower porosity and permeability giving an initial indication of possible reservoir quality controls.

Table 5:1: Facies association for the Corallian sandstones.

Facies association	**Lithology and Sedimentary Structures**	**Bioturbation**
1. Foreshore (FSFA)	Fine to medium-grained low angle planar-parallel laminated sandstone. Commonly highly cemented. Sedimentary structures indicate deposition under high energy shallow water conditions.	Mostly absent. Rare *Macaronichnus* if present.
2. Upper shoreface (USFA)	Consists of upper-fine to medium-grained sandstone making up low angle cross beds, trough and tabular cross-beds with minor planar lamination and hummocky cross-stratification. Cementation is variable. Sedimentary structures indicate high energy deposition with deeper water depths than the foreshore facies association.	Sparse to moderate (*Skolithos, Ophiomorpha, Cylindrichnus, Planolites some Anchonichnus and Macaronichnus*).
3. Proximal lower shoreface (pLSFA)	Very-fine to fine-grained amalgamated sandstone beds comprised of current ripple lamination, wave ripple cross-lamination with some mud-drapes. Cementation is variable. Sedimentary structures indicate moderate energy conditions.	Moderate to intense (Arenicolites, *Anconichnus, Palaeophycus, Rhizocorallium, Ophiomorpha* some *Teichichnus rectus, Cyclindrichnus, Thalasinoides and Chondrites*).

4. Distal lower shoreface (dLSFA)	Comprised of clayey siltstone and sandstone with some fine-grained and minor medium-grained sand. Beds are non-amalgamated with flaser bedding, minor wavy lamination and wave ripple cross-lamination. Cementation is variable. Sedimentary structures indicate low energy conditions with sediments disturbed by waning storm currents.	Moderate to intense (*Chondrites, Teichichnus rectus, Rosellia, Planolites, Palaeophycus, Rhizocorallium, Terebellina, Ophiomorpha, Arenicolites* and *Thalasinoides*).
5. Offshore shelf/ramp (OSFA)	Consists of mudstone, silty mudstone, siltstone with some beds of very fine-to upper fine-grained sandstone. Current ripple lamination, wave ripple lamination, sand-mud heterolithics beds. Cementation is variable. Sedimentary structures indicate low energy conditions with deposition mainly from suspension and disturbed by waning storm currents.	Intense (*Cylindrichnus, Chondrites, Paleophycus, Terebellina, Planolites, Teichichnus zig-zag, Thalasinoides, Teichichnus rectus* some *Rhizocorallium*).

The sandstones have a variety of sedimentary structures which underscore the changing hydrodynamic conditions during deposition (Fig. 5.4). These sedimentary structures include planar cross-stratification, low angle cross-stratification, trough cross-stratification, low angle lamination, mud drapes, massive bedding, and hummocky cross-stratification, lenticular bedding, flaser bedding, cross lamination, current ripple lamination, wave ripple lamination and climbing current ripple lamination (Fig. 5.4).

The core is locally bioturbated. Bioturbation is most evident in argillaceous intervals (Fig. 5.3d, e) but it also homogenises sandy and clay-rich intervals (Fig. 5.3d). Ichnofabrics present include *Thalasinoides, Teichichnus, Planolites* and *Chondrites* (Fig. 5.3). Others include *Rhizocorallium, Diplocraterion, Rosellia, Palaeophucus, Skolithos* and *Ophiomorpha* (Figs. 4.4 to 4.7).

Centimetre-scale thin beds are common in the Corallian sandstones. From lithology, sedimentary structures and bioturbation, twelve (12) discrete facies have been identified on the basis of lithology, sedimentary structures and bioturbation. The facies are then group into five facies associations, based on the classification by Hampson & Storms (2003) and listed below. In order of interpreted reducing depositional energy, the facies associations described in Table 5.1 are: (1) foreshore facies association (FSFA), (2) upper shoreface facies association (USFA), (3) proximal lower shoreface facies association (pLSFA), (4) distal lower shoreface facies association (dLSFA), (5) offshore/ ramp facies association (OSFA).

The core is locally hydrocarbon stained. Sandstones typically react with hydrochloric acid indicating the occurrence of calcite, present as both recognizable bioclasts and in cemented intervals. Calcite cementation is of variable intensity, hydrocarbon staining is most intense where calcite cement seems to be least abundant (Figs. 5.3 and 5.4) and weak or no hydrocarbons staining occurs in intensely cemented areas (Fig. 5.4a PW3 1135.0 m MD and Fig. 5.4c BL5 2195.0–2199.0 m MD).

5.4.2 Wireline Analysis

The Vshale log (derived using Equation (5.1)) reveals the presence of radioactive clay mineral zones as well as the presence of non-radioactive, sand-dominated reservoir sections in the Corallian sandstones (Fig. 5.4). The neutron-density cross-over plot (Rider 1986) typically is assumed to differentiate pay from the non-pay intervals (Fig. 5.4). There is good agreement between the Vshale logs and the neutron-density cross-over diagram. However, not all the net-sand intervals show the wide separation in neutron-density cross-over typical of pay zones (e.g., BL5, Fig. 5.4c, 2204.0–2206.0 m MD, 2194.0–2197.0 m MD). This suggests that the presence of sand is not the only determinant of pay and non-pay zones.

5.4.3 Routine Core Analysis Porosity and Permeability

Core porosity and permeability seem to show a good relationship with each other (Figs. 5.4a, 5.4b, 5.4c and 5.5a). The whole of the cored section, including sandstones and much finer-grained lithologies from BL5, has a porosity range of 2.7 to 26.6% with a mode of 10% and with values skewed towards the lower porosity range (Fig. 5.5a). Core from BL5 has a permeability range of 0.02 to 887 mD with a mode of 0.08 mD (Fig. 5.5c). Core from PW3 has a porosity range of 0.8 to 23.1% with bimodal porosity with modes at 9.4% and 18.5% (Fig. 5.5b). PW3 has a permeability range of 0.01 to 508 mD and a mode 0.95 mD (Fig. 5.5c). Core from PW7 has a porosity range of 2.6 to 30% with a mode of 10.5% (Fig. 5.5b) and a permeability range of 0.01 to 401 mD (Fig. 5.5c). PW7 has bimodal permeability with modes at 0.1 mD and 4 mD (Fig. 5.5c).

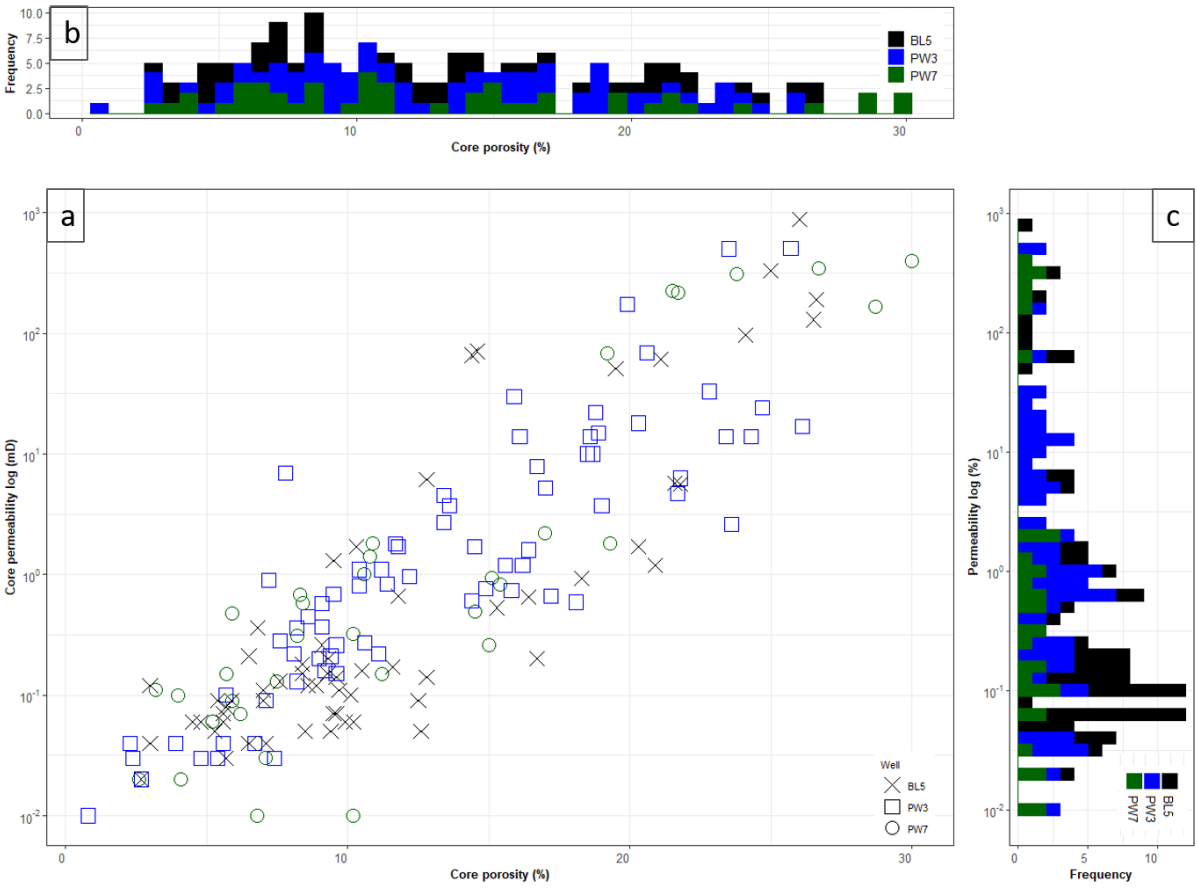

Figure 5.5: Show a scatter plot with porosity vs. permeability on a scatter plot. Margins of the scatter plot shows histograms of porosity (Fig. 5.5b: top) and permeability (Fig. 5.5c: right). The scatter plots show good porosity and permeability relationship with permeability spread locally over two orders of magnitude suggesting other controls on permeability apart from porosity.

The highest porosity intervals (up to 30% core analysis porosity) are in sandstone intervals (e.g., Fig. 5.4a PW7 1126.0 m MD, Fig. 5.4b PW3 1084.5 m MD and Fig. 5.4c BL5 2204.6 m MD) but relatively high porosity (up to 18% core porosity) also occurs in argillaceous intervals (Fig. 5.4c BL5 2205.8 m MD). The highest permeability sections are all in sandstone intervals (Fig. 5.4a PW7 1125.6 m MD, Fig. 5.4b PW3 1084.3 m MD and, Fig. 5.4c BL5 2204.6 m MD), which also corresponds to the pay zones in the neutron-density crossover plots. There are also low porosity and low permeability sections in the sandstone intervals (Fig. 5.4a PW7 1125.0 m MD Fig. 5.4a PW7 1135.0 m MD, Fig. 5.4c 2193.0–2197.0 m MD) suggesting that lithology is not the only control on sandstone porosity and permeability. In addition, permeability varies

over two orders of magnitude for a given porosity (Fig. 5.5a) suggesting that permeability is affected by factors other than porosity.

5.4.4 Petrography

5.4.4.1 Detrital Composition and Fabric

The Corallian sandstones are composed of moderately- to moderately well-sorted quartz arenites with dominant quartz (Q) grains and minor feldspar (F) and lithic (L) grains. The proportion of quartz to feldspars and lithic grains is in the range of 83.2 to 99.5 %, with an average composition of $Q_{94}F_3L_3$ (Fig. 5.6).

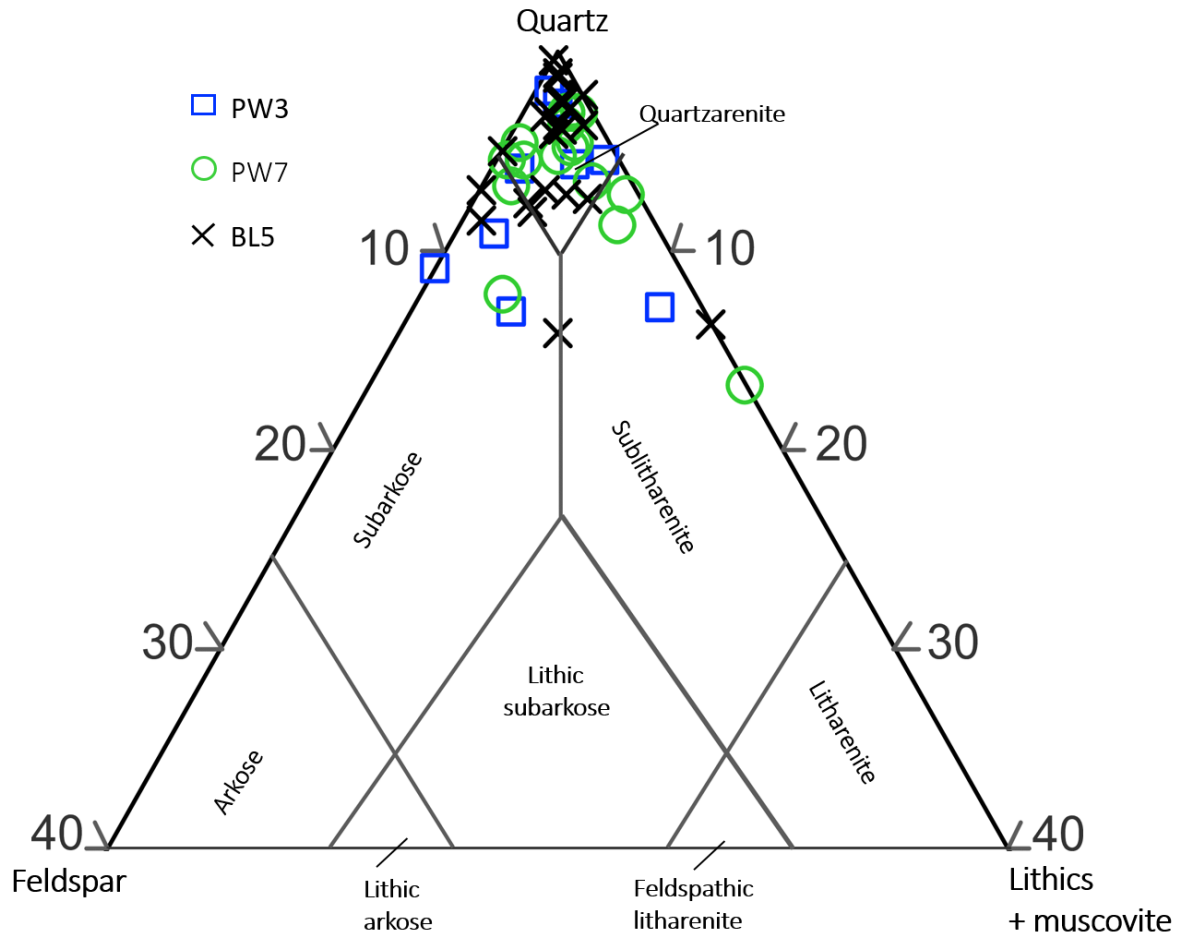

Figure 5.6: Modal composition for the Corallian sandstones, after McBride (1963) showing predominantly quartz arenite lithology.

Point count grain size analysis revealed fine- to medium-grained, subrounded to rounded sand grains (Figs. 5.7, 5.8, 5.9 and 5.10), with grains either separated from each other in a loosely

compacted fabric (Figs. 5.7a and 5.11b), or with pores filled with cement (Figs. 5.7b, 5.8a, 5.d and 5.11a). Close-packed framework grain structures are absent (Fig. 5.10a) and there is no evidence of stylolites, suggesting that advanced compaction has occurred.

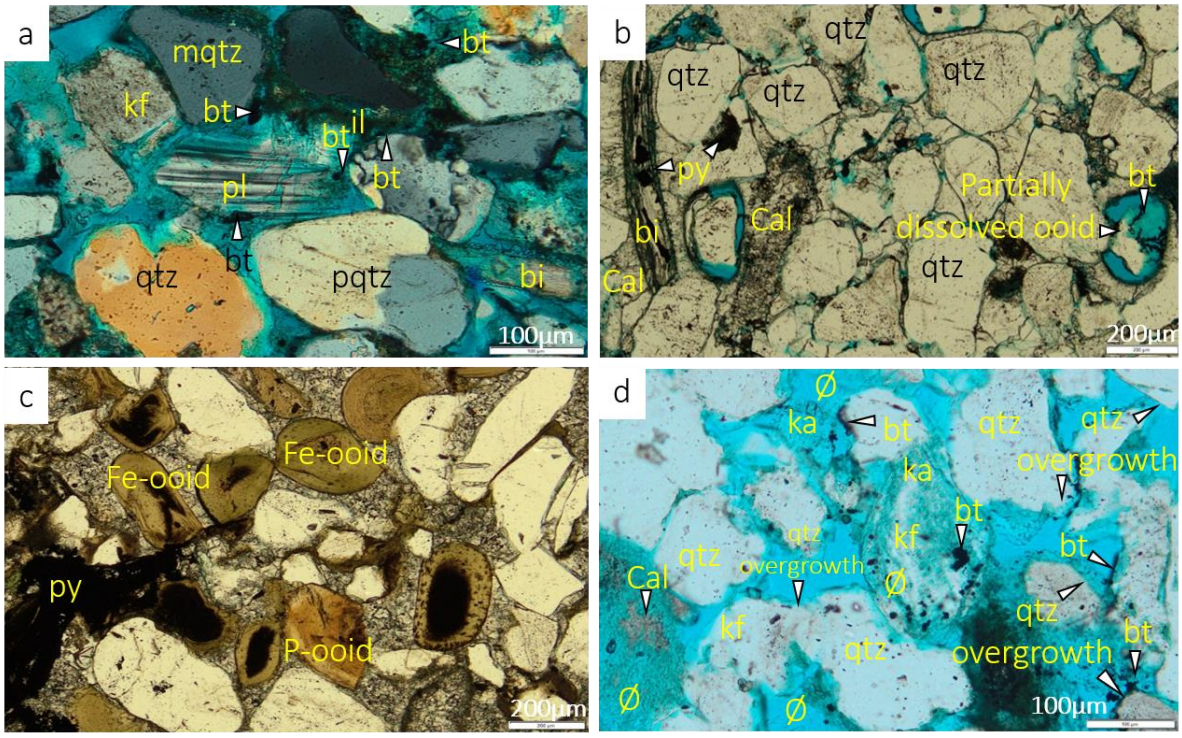

Figure 5.7: Photomicrographs showing framework grains, minor grains, cement types and porosity for the Corallian sandstones. (a) BL5 (2211.63 m MD) is a cross-polarised photomicrograph showing a dissolved plagioclase feldspar (centre-left), polycrystalline quartz, monocrystalline quartz and bivalve shell in an open-framework grain texture. (b) PW3 (1091.4 m MD): shows a highly cemented rock with bivalve shells replaced by pyrite as well as neomorphosed into calcite cement. The circular pores at the centre-right and centre-left are typical of dissolved ooids. (c) BL5 (2199.9 m MD): shows a highly cemented sandstone with Fe-ooids, phosphate ooids and framework quartz cemented by pyrite and calcite cement. Some of the Fe-ooids-e.g., top-left show signs of abrasion suggesting mechanical breakdown from transport. (d) BL5 (2199.09 m MD): is a high porosity sandstone (QEMSCAN porosity 20.76%) showing extensive grain dissolution with intergranular porosity between grains as well as moldic and microporosity from dissolved grains. The photomicrograph also shows

dissolved calcite cement (bottom-left). The feldspar grains have been intensely dissolved and altered to kaolinite with bitumen present within the altered feldspar grains (centre and bottom-right). Bitumen also is also shown lining quartz overgrowths (bottom-left) suggesting that hydrocarbon charge post-dated quartz cementation. Inclusions of bitumen in the micropores as well as at the edge of kaolinite at the top-left suggest some contemporaneous hydrocarbon charge and kaolinite precipitation. Definition of abbreviations used on the images: plagioclase feldspar (pl), k-feldspar (kf), polycrystalline quartz (pqtz), monocrystalline quartz (mqtz), quartzite (qte), iron ooid (Fe-ooid), phosphate ooid (P-ooid) bivalve shell (bi), bitumen (bt), echinoderm (ech), foraminifera (fm), pyrite (py).

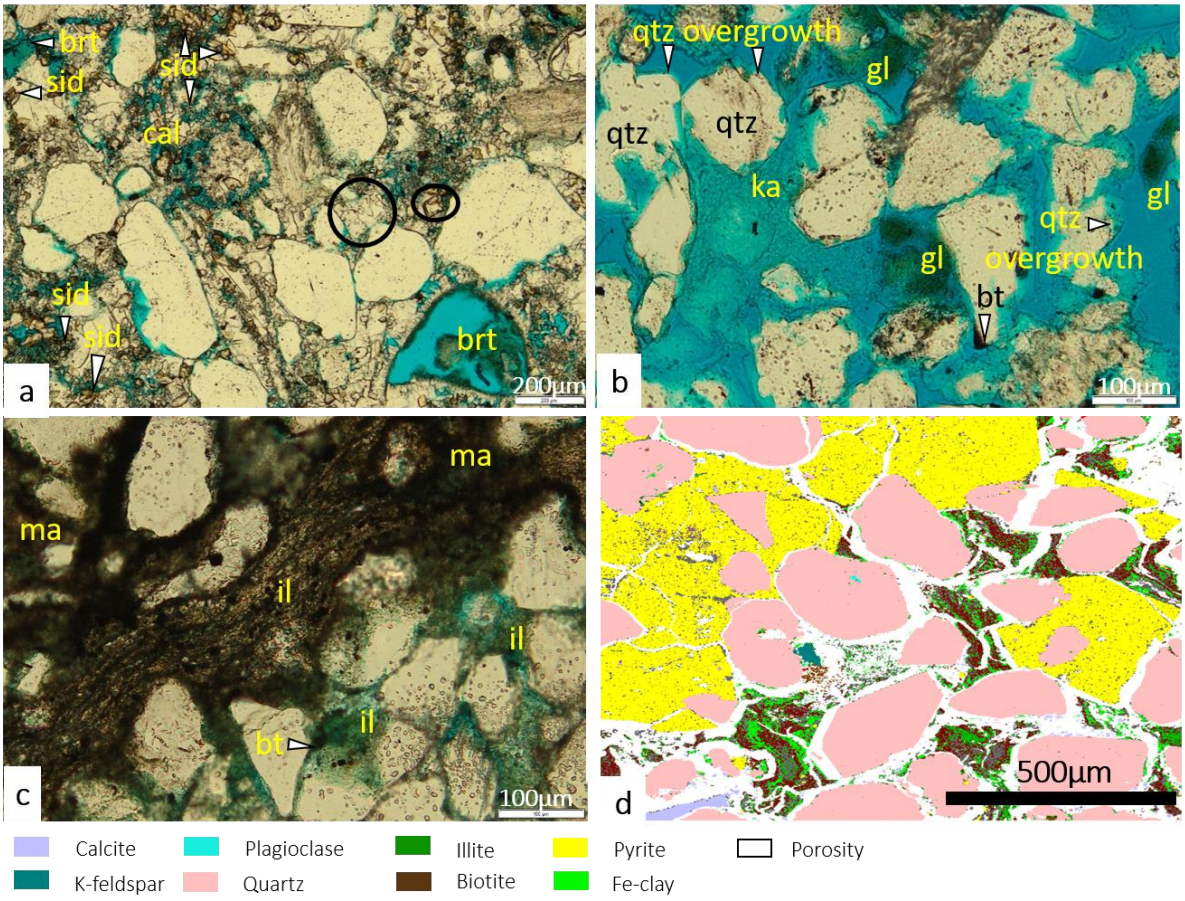

Figure 5.8: (a) is a photomicrograph from PW7 (1130.05 m MD) showing calcite cement, siderite filling moldic pores from Fe-ooid dissolution (bottom-left), berthierine replacing an Fe-ooid (bottom-right) and pore-filling dolomite (circled in black). (b) PW7 (1136.52 m MD): is a high intergranular porosity sample with authigenic illite and kaolinite in pore spaces. Quartz overgrowths project from grain surfaces into pore spaces thereby reducing porosity. (c)

BL5 (2206.8 m MD): muscovite replaced by illite with pore-filling illite at the bottom centre. (d) PW7 (1123.19 m MD): is an SEM-EDS image with pore-filling pyrite and Fe-clay in a biotite rich matrix. The biotite and Fe-clay occur together which might suggest a genetic relationship. Definition of abbreviations used on the images: quartz grain (qtz), glauconite (gl), calcite cement (cal), siderite (sid), berthierine (brt), illite (il), kaolinite (ka), glauconite (gl), matrix (ma).

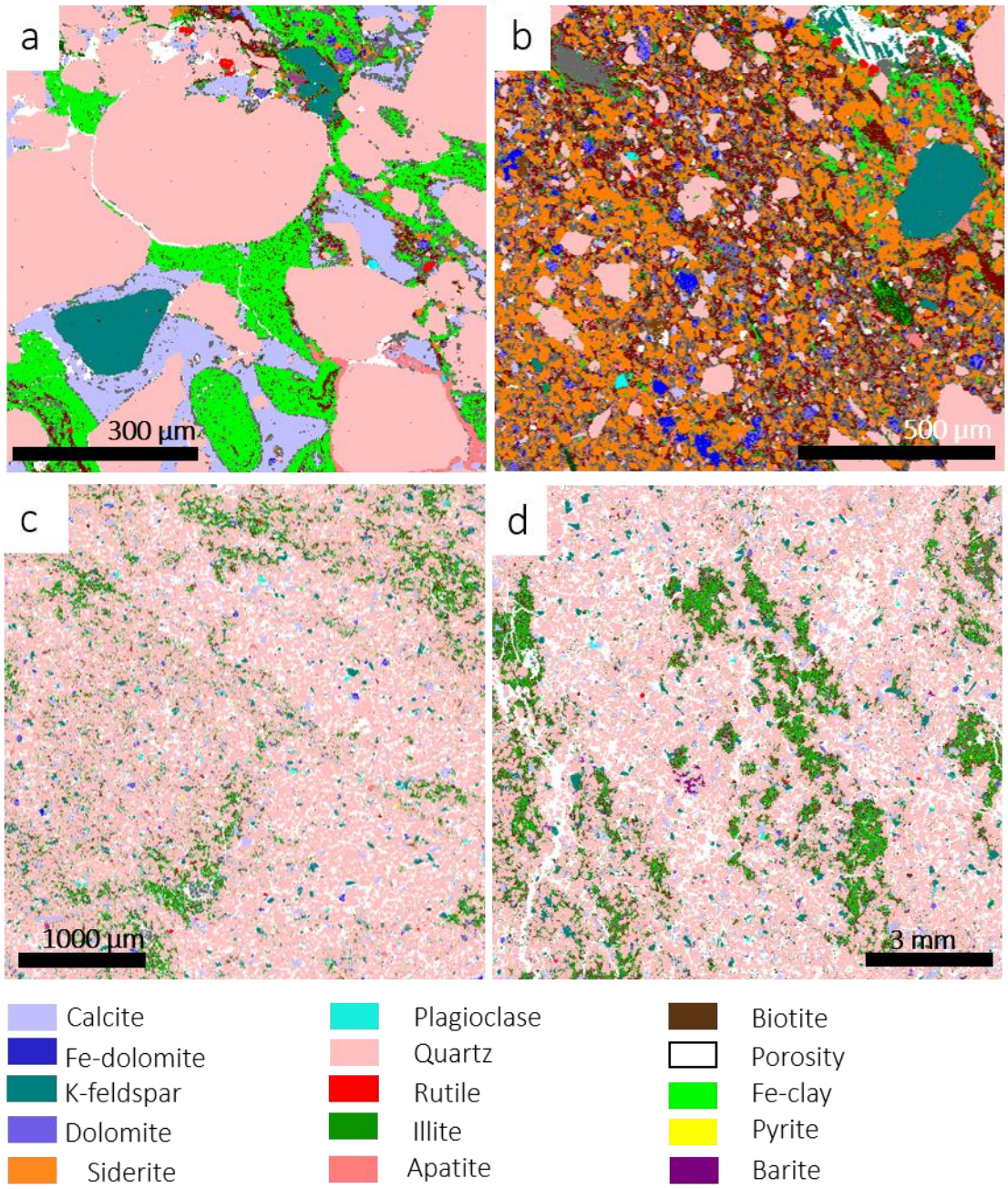

Figure 5.9: (a) BL5 (2199.9 m MD) at 2 µm resolution: SEM-EDS porosity (1.67%) shows dissolved K-feldspar with the former grain boundaries outlined where calcite cement has filled the dissolved grain portion (bottom-left). Pore-filling apatite is seen at the bottom-right lining a quartz grain. (b) Same sample as Fig. 5.9a, non-bioturbated upper shoreface sandstones. Siderite matrix occupies most of the image truncated by Fe-dolomite and detrital biotite. The top-right shows moldic porosity from a dissolved K-feldspar grain. (c) BL5 (2208.0 m MD): SEM-EDS porosity 19.7%, core porosity 21.6, permeability 5.7 mD, sandstone sampled from

a zone homogenised by bioturbation. (d) PW7 (1135.7 m MD) at 20 µm resolution: core porosity 29.6% showing microfractures.

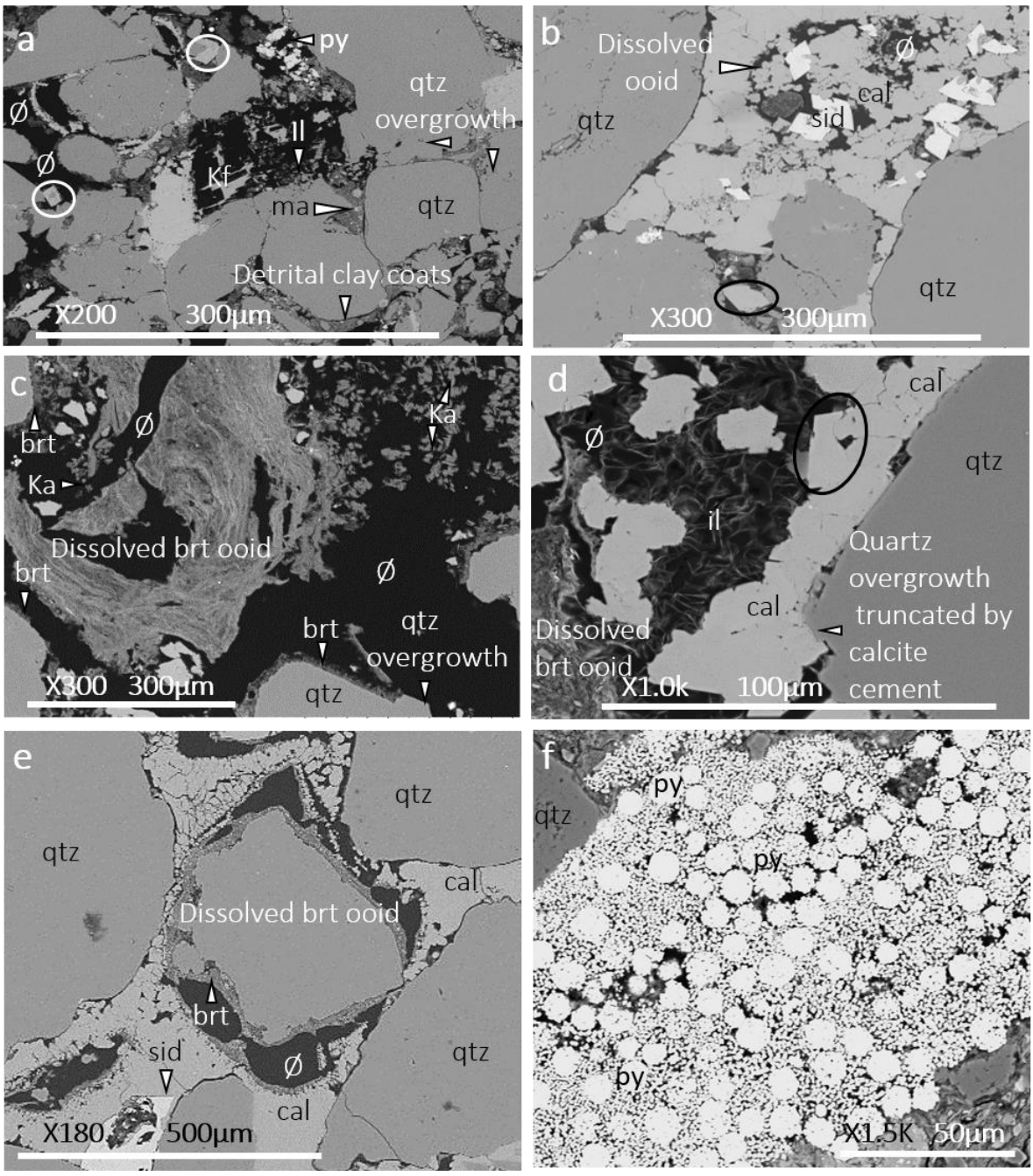

Figure 5.10: (a) BL5 (2211.6 m MD): altered K-feldspar (centre) and dissolved Fe-ooid (top-left) with some compaction to the top-left. Grain contacts show close-packing texture at the centre-right adjacent to detrital clays. (b) PW3 (1091.4 m MD): shows where calcite and

siderite have replaced a dissolved ooid (top) with the relic of the ooid still visible at the top-right and bottom-left corners of the dissolved grain outline. (c) PW3 (1085.1 m MD): relics of a Fe-ooid can be seen in the middle of the photomicrograph while about 30 µm thick berthierine coats quartz grains to the centre-right, bottom and bottom-left. Kaolinite filled intergranular pore space to the top-right. (d) PW3 (1085.1 m MD): pore filling illite can be seen in the centre of the photomicrograph with quartz overgrowths overlying a detrital quartz grain. (e) BL5 (2202.2 m MD): dissolved Fe-ooid with relic of cortice forming grain coat. (f) PW3 (1098.3 m MD): pore-filling framboidal pyrite aggregates. Definition of abbreviations used on the images: quartz grain (qtz), K-feldspar grain (kf), berthierine (brt), matrix (ma), calcite (cal), siderite (sid), kaolinite (Ka), illite (il), pyrite (py), porosity (Ø).

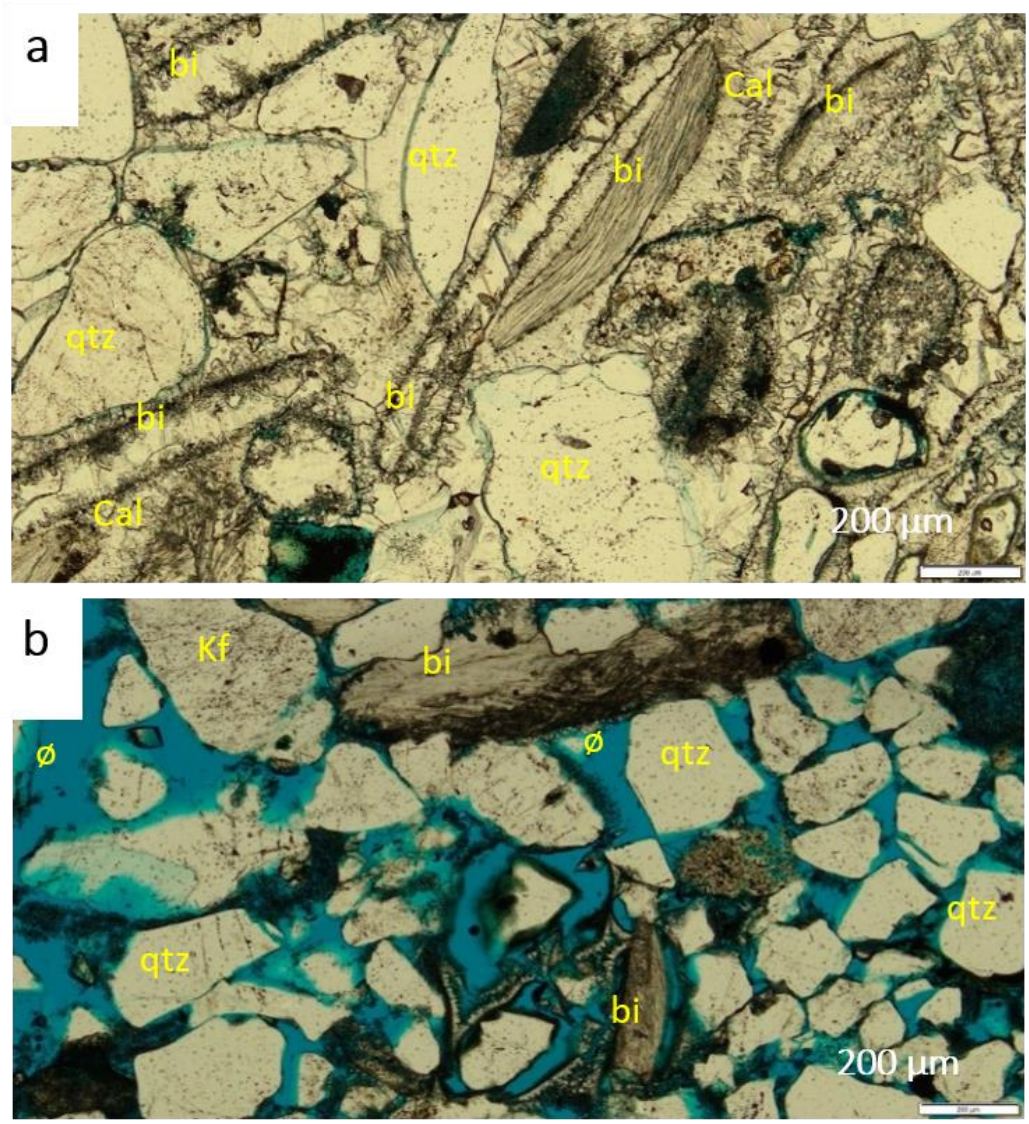

Figure 5.11: (a) PW7 (1130.0 m MD) light optics showing intense neomorphism of bivalve shells to calcite. The bivalve shells are not distinguishable from calcite cement and are only identified by the micrite envelopes outlining them in the cement (b) PW7 (1125.9 m MD)-in contrast to (a) shows fewer bivalve shells with less neomorphism and less calcite cementation Calcite cement (Cal), quartz (qtz), K-feldspar (Kf), bivalve (bi), pore space (ø).

There is 13.3 to 54.6% monocrystalline quartz (average 36.1%) and about 0.7 to 16.4% polycrystalline quartz (average 9.0%) (Table 5.A1). Quartz is texturally mature with sub-rounded to rounded grains (Figs. 5.7, 5.8, 5.9 and 5.10). Quartz is most abundant in the proximal upper shoreface facies association but shows no clear relationship from the foreshore to the offshore facies associations (Fig. 5.12k).

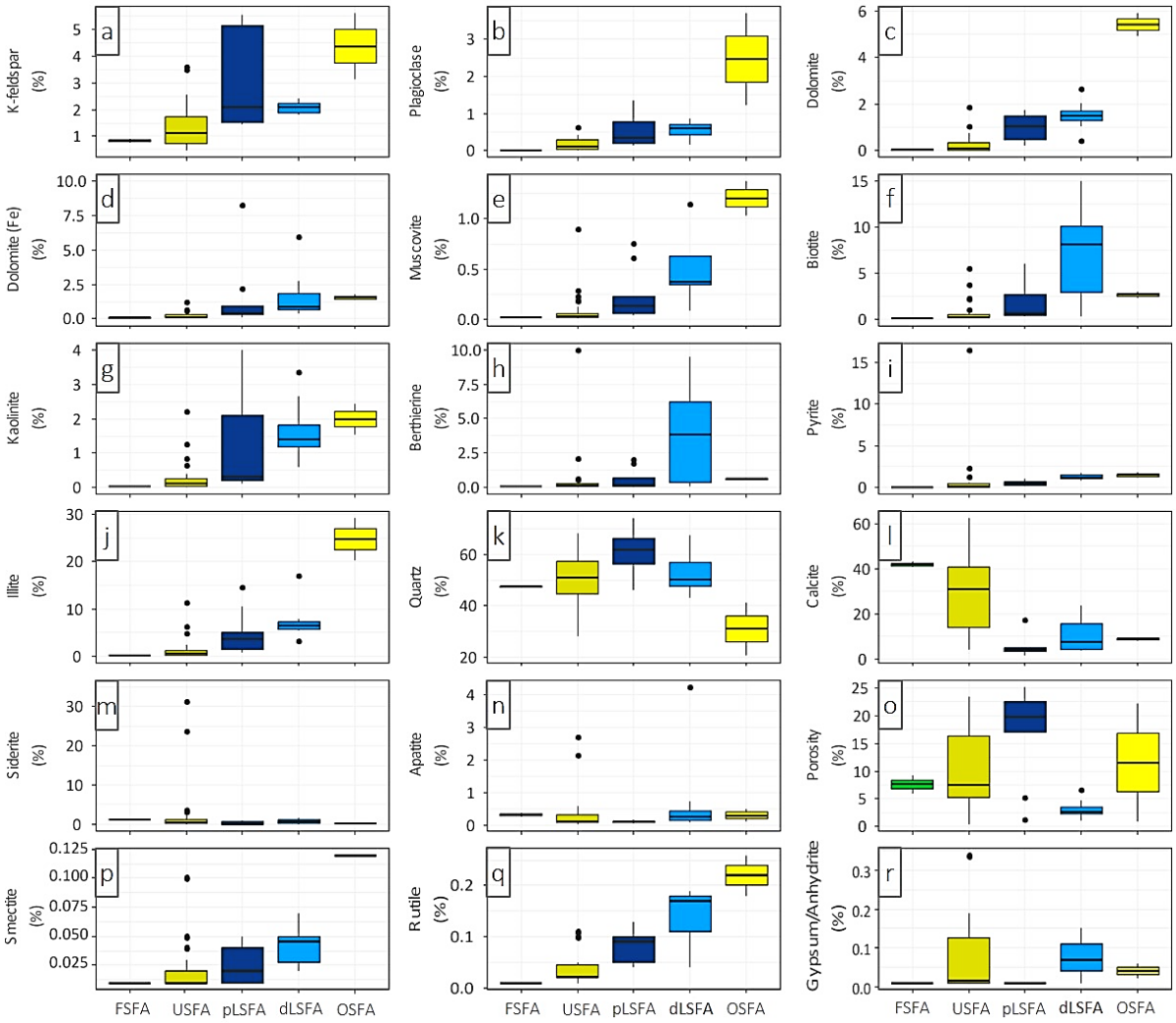

Figure 5.12: Boxplots relating SEM-EDS mineralogy to facies association. K-feldspar, plagioclase feldspar, dolomite, Fe-dolomite, muscovite, biotite, kaolinite, berthierine, pyrite and illite (a–j) increase basinward. Quartz (k), siderite (m), apatite (n), porosity (o) and gypsum/anhydrite (r) do not show a clear relationship with facies association. Smectite (p) and rutile (q) show an increase basinward from foreshore to offshore facies association. In contrast, calcite (l) shows a decrease basinward.

The feldspars are mainly K-feldspar, which comprises trace to 4.0% of the total rock with an average of 1.0%. Plagioclase feldspar comprises trace to 1.7%, with an average of 0.2% (Table 5.A1). The feldspars occur in various stages of dissolution (Figs. 5.7a, 5.9a, 5.9b and 5.10a) with dissolved grains resulting in secondary porosity. Both feldspar types increase in

proportion from the foreshore to offshore depositional environment (Figs. 5.12a and 5.12b) possibly suggesting primary depositional controls on their abundance.

Lithic grains in these sandstones are composed of extrabasinal mudstones, quartzite, sandstone and chert. In the QFL analysis, bioclasts, Fe-ooids and muscovite are considered as lithic grains and have here been added to the lithics (Fig. 5.6). Bioclasts are dominated by bivalves with minor echinoids, foraminifera and ostracods; bioclasts collectively represent about 0 to 4.0% with an average of 0.8%. Fe-ooids, described later, make up between about 0 to 2.7% with an average of 0.12%. Trace amounts of chlorite are present in the Corallian sandstones (Fig. 5.13); however, it is not certain if chlorite is authigenic or detrital as chlorite is not evident as a cement or pore filling phase in optical petrographic analyses.

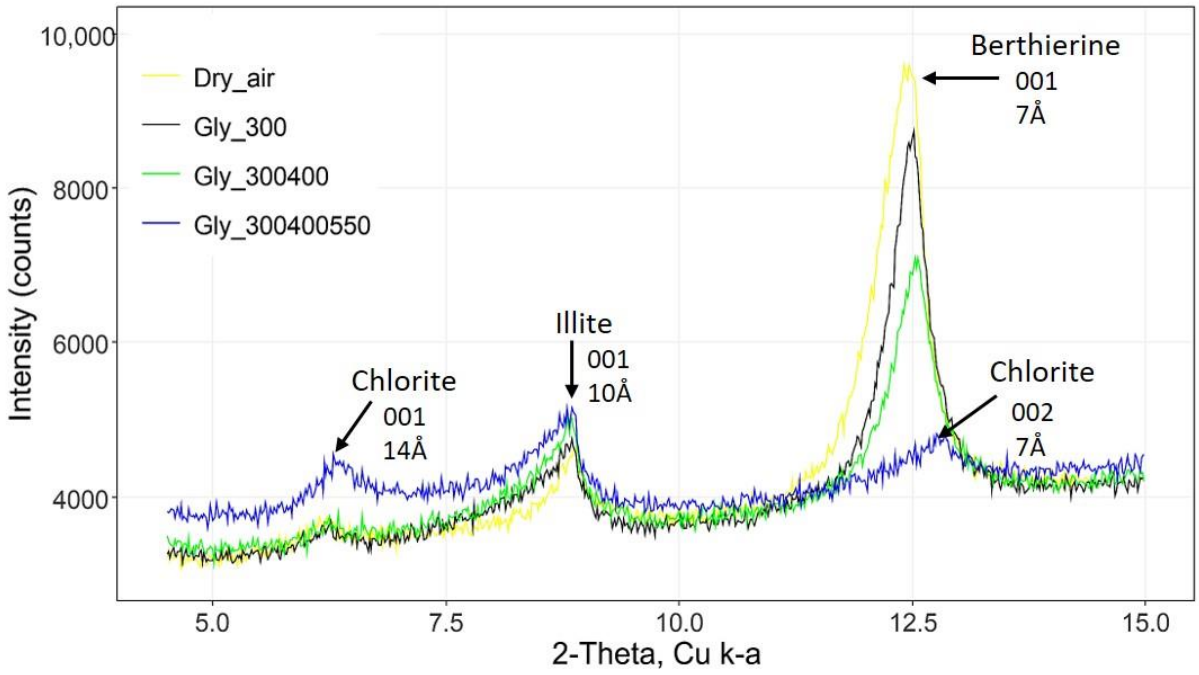

Figure 5.13: Various XRD traces from an Fe-rich clay-bearing sample from BL5 (2200.9 m MD) following various pre-analysis treatments: air-drying, glycolation followed by heating to 300 ˚C, 400 ˚C and 550 ˚C to investigate Fe-clay types. The X-ray peaks show mineralogy with the separation showing reduction in peak intensity for Fe-clay, diagnostic of berthierine.

Fe-ooids have brown to olive-green cortices surrounding a nucleus composed of either quartz or heavy minerals (Fig. 5.7c). Optical microscopy and SEM-EDS images reveal the presence of Fe-rich clay; XRD analysis confirmed the presence of berthierine (Fig. 5.13).

Fe-ooids have a floating grain fabric where they are separated from other grains by pores or cement; cement growth locally truncates their grain boundaries, proving their detrital origin (Figs. 5.7c, 5.9a and 5.10c). Fe-ooids increase in quantity from the foreshore to the proximal lower shoreface but there are none in the distal lower shoreface and offshore (Fig. 5.14f).

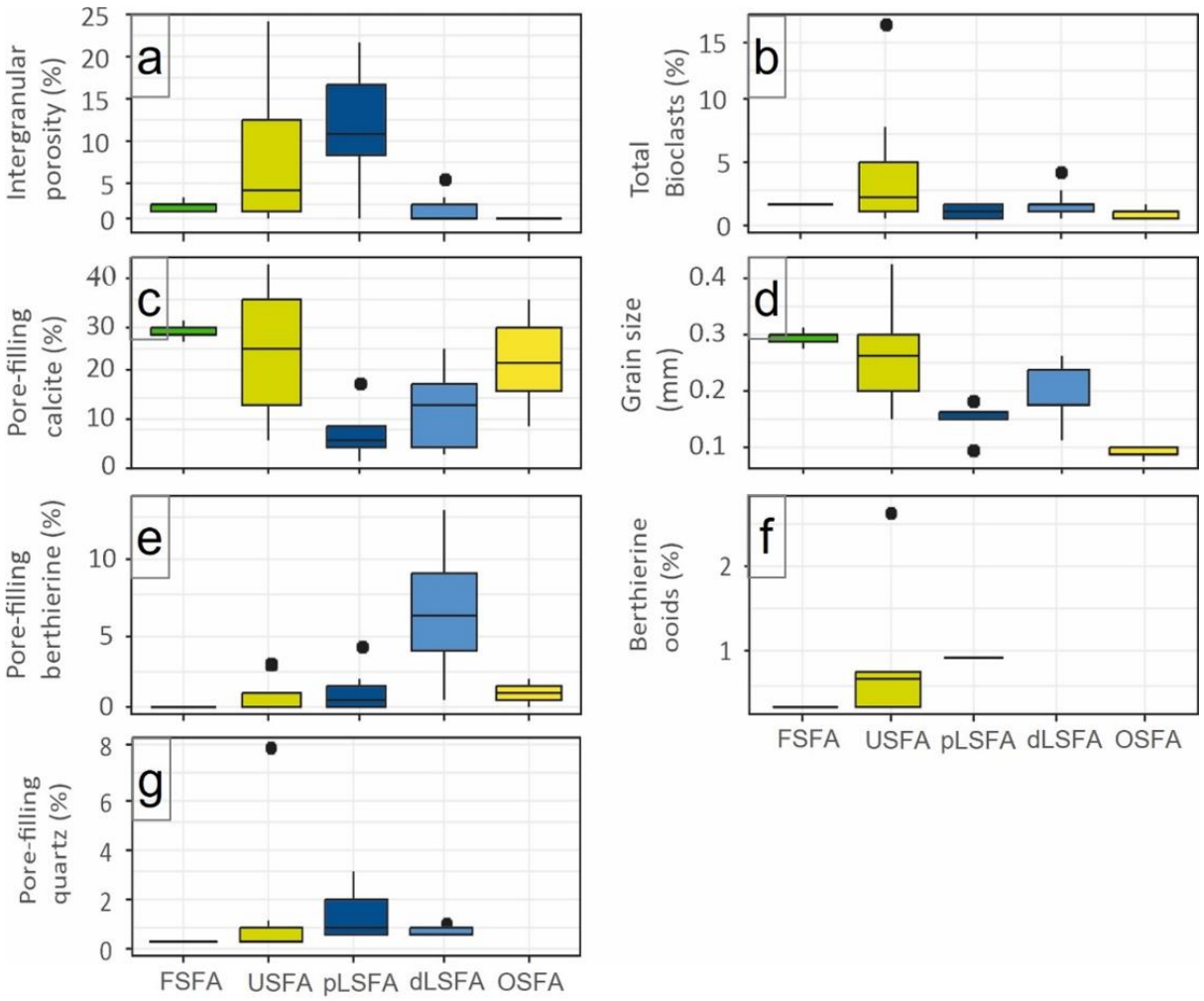

FSFA: Foreshore facies association; USFA: Upper shoreface facies association; pLSFA: Proxima lower shoreface facies association; dLSFA: Distal lower shoreface facies association; OSFA: offshore facies association

Figure 5.14: Boxplots relating point count data to facies associations: (a) intergranular porosity, (b) bioclasts, (c) pore-filling calcite, (d) grain size, (e) pore-filling berthierine, and (f) Fe-ooids. Intergranular porosity and pore-filling calcite show an inverse relationship while bioclasts and grain size show a good relationship with both reducing basinward from foreshore to offshore facies association. Pore-filling berthierine show an increasing trend from the foreshore to the proximal lower shoreface (e) similar to Fe-ooids (f) suggesting a genetic relationship.

However, the absence of Fe-ooids in the distal lower shoreface and offshore facies association suggests other sources of authigenic berthierine apart from reprecipitation of Fe-ooids.

Bioclasts are dominated by bivalves (Figs. 5.7b, 5.8a and 5.11a) and show evidence of intense bioerosion by micritisation (Fig. 5.11a). Bioclast concentration is highest in the upper shoreface facies association and is lowest in the offshore facies association (Fig. 5.14b); the variable degree of bioclast neomorphism makes interpretation of point count abundance difficult. If all calcite was derived from bioclasts, then total calcite from SEM-EDS analysis may be used as a proxy for total initial quantity of bioclasts; in this case offshore sediment had the lowest quantity of bioclasts (Fig. 5.12l).

The mineralogy of fine-grained sediment was resolved using SEM-EDS data (Figs. 5.8d and 5.9c). Fine-grained sediments are mostly composed of illite, kaolinite, muscovite, biotite, minor quantities of pyrite, quartz, K-feldspar and plagioclase, as well as trace quantities of smectite (Figs. 5.7d, 5.9b and 5.9c). SEM-EDS data show that biotite (Fig. 5.12f), muscovite (Fig. 5.12e), kaolinite (Fig. 5.12g), pyrite (Fig. 5.12i), illite (Fig. 5.12j), and smectite (Fig. 5.12p) all increase in proportion from foreshore to offshore environments.

Heavy minerals are dominated by apatite, which makes up about 0 to 1.0% (average 0.1%) of total rock volume. Other heavy minerals include zircon, rutile and iron oxide, which occur in minor quantities (<1%). Apatite occurs as fine grains visible in SEM-EDS (Fig. 5.9a and 5.9c) and does not show a relationship with facies associations (Fig. 5.12n).

5.4.4.2 Diagenetic Minerals and Cements

The most common cements in these Corallian sandstones are, in order of abundance, calcite (Figures 5.7b,5.7c, 5.12l and 5.14c), illite (Figures 5.10d and 5.7c), siderite (Figures 5.7a and 5.12m), berthierine (Figures 5.7d and 5.14e), pyrite (Fig. 5.7c and 5.7d), dolomite (Fig. 5.12c), Fe-dolomite (Fig. 5.12d), quartz (Figures 5.10c, 5.10d and 5.14g), kaolinite (Figures 5.7b, 5.7d and 5.10c), and apatite (Fig. 5.9a).

Calcite cement occurs as acicular and isopachous cements lining bivalve shells (Fig. 5.7b) and poikilotopic crystals (Fig. 5.11a) that fill pore spaces. Calcite represents the dominant cement by volume in the Corallian sandstones, locally constituting more than 40% of rock volume (Fig. 5.14c). Pore-filling calcite constitutes about 1.6% in high porosity samples and up to 42.0% in samples with the lowest porosity (Table 5.A1). A significant proportion, up to 23.7%, of calcite cement is replacive (Fig. 5.10b) (Table 5.A1). Some calcite cement shows evidence of

neomorphism of bivalve shells (Fig. 5.11a), identifiable by the presence of earlier micrite envelopes.

Dolomite occurs as rhombic crystals (Figs. 5.7a and 5.10a). Dolomite occurs in samples with evidence of calcite cement and grain dissolution (Figs. 5.7a, 5.9a and 5.10a, 5.10b and 5.10d) and is also common in proximity to iron-rich minerals, e.g., siderite (Fig. 5.9b). SEM-EDS analysis shows that non-ferroan dolomite constitutes up to 6%, with an average of 0.7%, while ferroan dolomite constitutes up to 13%, with an average of 1.0% (Fig. 5.12c and 5.12d respectively).

Siderite occurs as yellow-brown rhombohedra under plain polarised light (Fig. 5.7a). Siderite is heterogeneously distributed. It is pervasive in areas with calcite cement (Fig. 5.7a) and occurs filling moldic pores from detrital grain dissolution (Figs. 5.7a and 5.10b). Siderite is present up to 4.3% as pore-filling siderite, with an average value of 1.9% (Table 5.A1). Grain replacive siderite locally constitutes up to 15.4% with a mean value of 0.49% (Table 5.A1).

Berthierine occurs as pore-filling (Fig. 5.9a), grain replacive (Figs. 5.7b and 5.7d) and grain coating cement (Fig. 5.10c). Berthierine grain coats form discontinuous rims around detrital grains and range from trace to 2.6% with an average of 0.2% of total rock volume (Table 5.A1). Grain-coating berthierine has locally inhibited the growth of quartz cement (Fig. 5.10c). Pore-filling berthierine occurs next to iron-rich minerals, for example, in Figure 5.8d, berthierine occurs adjacent to biotite-rich matrix and pyrite cement. Partly dissolved Fe-ooids, with their initial concentric laminae, contain replacive structureless berthierine (Figs. 5.8a and 5.9a). Berthierine (Fig. 5.12h) and biotite (Fig. 5.12f) show an increase from foreshore to the distal lower shoreface, where they have the highest quantity, and then a reduction in quantity in the offshore, suggesting a genetic relationship between biotite and berthierine.

Illite is present as a porous, fiber-like mass of irregular crystals that fill pore spaces (Fig. 5.10d). Rare grain-replacive illite is present (Fig. 5.7c) where illite has grown in place of detrital muscovite. Pore-filling illite has an average of 2.7%; replacive illite represents an average of 0.2% (Table 5.A1).

Pyrite occurs in three main forms. Pore-filling pyrite surrounds detrital quartz and other grains (Fig. 5.8d) and has equant outlines where it has grown into open pores (Fig. 5.8d). Aggregates of framboidal pyrite (Fig. 5.10d), and bioclast-replacive pyrite (Fig. 5.7b) are also present in these sandstones. Pore-filling pyrite represents an average of 1.3% of total rock volume with a range between trace to a maximum of 14.8% of total rock volume (Table 5.A1).

Apatite seems to be present as a cement as well as a detrital grain as it occurs as an unusual grain-coating phase (Fig. 5.9a) but it only represents 0.1% of the sandstones, on average.

Incipient syntaxial quartz overgrowths have formed relatively early as they are surrounded by calcite cement (Fig. 5.10d). Quartz cement is present as small (11 to 20 μm) euhedral outgrowths on detrital quartz grains (Fig. 5.10c). Fluid inclusions seem to be absent in the quartz cements (Figs. 5.7c and 5.7d). Authigenic quartz ranges from trace quantities to 7.9% with an average of 0.6% (Table 5.A1). Quartz cement does not have rounded edges suggesting that it is not recycled from a previously deeply buried sandstone; quartz cement has grown in situ. For example, Figure 5.8b displays perfectly euhedral multiple quartz outgrowths on a single grain that would not have survived weathering, erosion, transport, and deposition. Locally, quartz cement growth seems to have been inhibited by berthierine grain coats (Fig. 5.10c). Quartz cement is more common in the cleaner, higher porosity sandstones that have less calcite cement (Figs. 5.7d, 5.8b and 5.10d). Quartz cement increases from the foreshore facies association to the proximal lower shoreface facies association (Fig. 5.14g).

Kaolinite occurs in the Corallian sandstones as discrete booklets and is visible where calcite cement is absent (Figs. 5.8b, 5.7d and 5.10c). Pore-filling kaolinite ranges from trace to 3.3% (Fig. 5.10c); replacive kaolinite (typically after K-feldspar) ranges from trace to 1.3% (Fig. 5.7d), (Table 5.A1).

5.4.4.3 Modal Porosity

Point count porosity ranges from trace to 28.2%. The main porosity type is intergranular porosity, which constitutes up to 23.0% of total rock volume, followed by moldic porosity which makes up to about 14.0% of total rock volume. Intergranular porosity tends to be lowest in samples with the greatest quantity of authigenic cements (Fig. 5.11a). Moldic porosity occurs due to the dissolution of detrital grains such as Fe-ooids (Fig. 5.8a and 5.7b) and feldspars (Figs. 5.7a and 5.9b). Other porosity types include cement dissolution porosity (Fig. 5.7d), intercrystalline porosity (Fig. 5.10b), matrix porosity (Fig. 5.8c) and fracture porosity (Fig. 5.9d).

5.4.5 Burial and Thermal History Modelling

Burial curves show that the base of the Corallian sandstones (which is also the top of the Ampthill Clay Formation) was buried to a maximum depth of ~1700 m TVD before uplift to the present depth of ~840 m TVD.

Compactional porosity-loss was modelled as a function of depth and clay fraction following Ramm et al. (1997b) with core analysis porosity data added from BL5, PW3 and PW7 (Fig. 5.15b). The core porosity values were also projected to maximum burial, as modelled in Figure 5.15a. At the current depths, porosity is low compared to the modelled compaction curves (Fig. 5.15b). If we assume that the sandstones had approximately 20% clay, then the best reservoir quality sandstones accord to rocks buried approximately 1000m deeper than they are at the present time, if we assume that compaction was the dominant porosity-loss mechanism in the best reservoir quality sandstones. However, most of the core porosity cannot be accounted for by compactional processes, alone, implying that cement growth had a major impact on porosity. Overall, Figure 5.15b suggests that the porosity values at current depths are not just the result of compactional porosity-loss at maximum burial.

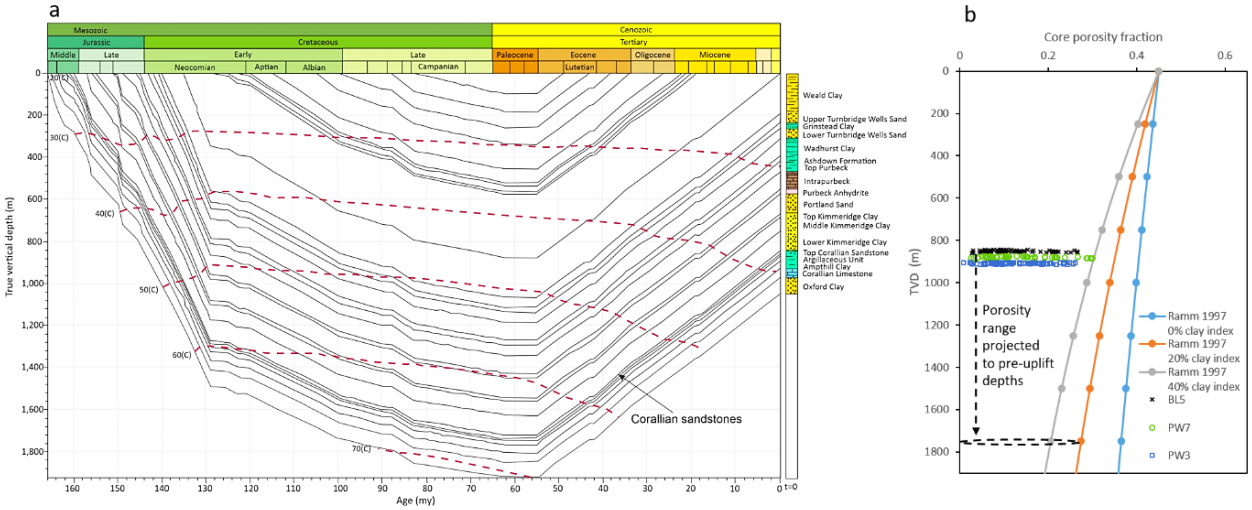

Figure 5.15: (a) Burial curve for the Weald area around Bletchingley-5 showing burial to the base of well BL5 in the Oxford Clay up to ~1920 m. The curve also shows uplift from 55 Ma to current depths. (b) Shows modelled compactional porosity-loss curves at different clay content after Ramm et al. (1997b) and core porosity fractions from BL5, PW7 and PW3. Porosity loss in the Corallian sandstones did not follow the expected trend for mechanical compaction.

The burial model (Fig. 5.15a) shows that the Corallian sandstones underwent initially rapid burial and heating and reached 60 °C at 124 Ma (when at 1310.0 m TVD). The rate of burial and heating then slowed and they reached a maximum depth of about 1700 m and a temperature of about 66 °C between 65 Ma to 55 Ma. Subsequently, uplift led to the Corallian sandstones being cooled to the present-day depth of 800 to 900 m TVD and a temperature of between 35

and 40 °C. The burial and thermal model (Fig. 5.15a) seems to be supported by the analysis of porosity and compactional porosity-loss (Fig. 5.15b).

There are two possible petroleum source rocks in the modelled section: the Oxford Clay and the Kimmeridge Clay Formations. The top of the Oxford Clay Formation was buried to ~1859 m TVD (Fig. 5.15a). The younger Kimmeridge Clay Formation was buried to ~1707 m TVD (Fig. 5.15a). In this well, neither source rock reached thermal maturity sufficient for oil generation but note that the deeper (and thus hotter) Lower Jurassic Liassic source rock was not included in the model as it was not penetrated by the well.

5.5 Discussion

5.5.1 Timing of Diagenetic Events

Diagenesis in the Corallian sandstones occurred only in the eogenetic realm as the Corallian sandstones have only reached about 60 °C (Figs. 5.15 and 5.16) with the boundary between eo- and meso-diagenesis defined as being about 60 to 70 °C coinciding with the depth range where microbial processes cease, mechanical compaction is retarded and chemical processes become dominant (Worden et al. 2018c). The timing of diagenetic events is summarised in Fig. 5.16. It is here interpreted that the first event was feldspar dissolution (Fig. 5.7a and 5.7b) which may have begun during weathering and sediment transport as well as continuing after burial (Emery et al. 1990; Glasmann 1992). Shell bioerosion (Fig. 5.7b) is interpreted to have occurred early, under open marine photic conditions which are needed for the vital activities of microscopic boring algae (Adams & Mackenzie 1998; Scholle & Ulmer-Scholle 2003). Locally intense bioturbation (Fig. 5.3e) occurred soon after burial, when animals were either seeking shelter or food (Pemberton et al. 2012b); it is likely that bioturbation led to any remaining organic matter associated with the bioclasts being destroyed. The initial stages of compaction seems to have occurred next (Figs. 5.7b and 5.10a). There was locally abundant growth of framboidal pyrite soon after deposition (Fig. 5.10f) that also probably occurred during the initial stages of burial (Goldhaber 2003). Framboidal pyrite was followed by the development of apatite, berthierine and calcite cement. Apatite occurs as a relatively unusual grain-coating phase (Fig. 5.9a). Berthierine occurs as a grain-coating and pore-filling cement phase (Fig. 5.10c and 5.10d). Poikilitopic calcite (calcite-2; Figs. 5.7b and 5.11a) overlies an earlier generation of acicular calcite cement (calcite-1; Fig. 5.7b); the latter possibly formed on or near the sediment surface. Poikilotopic calcite, the most important of all the pore-filling

cements in the Corallian sandstones, locally filled most pore spaces with intergranular volumes of up to about 43%, confirming that such cement formed before significant compaction had occurred (Rahman & Worden 2016a).

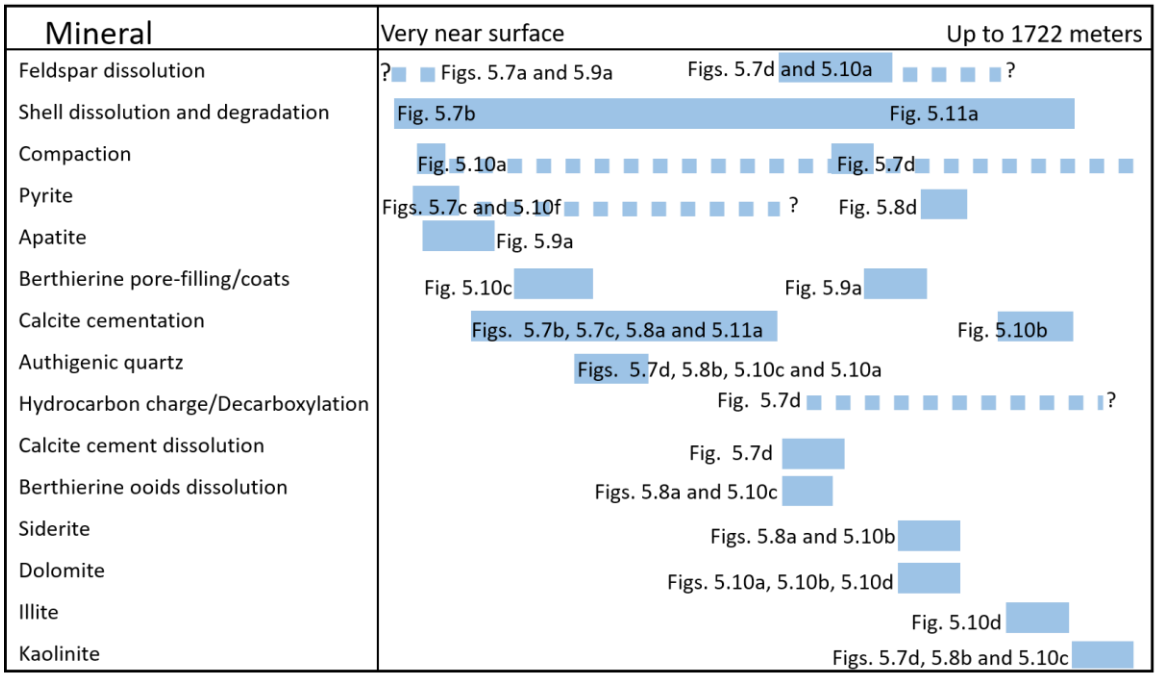

Figure 5.16: Paragenetic sequence for the Corallian sandstones showing the sequence of diagenetic events. The sequence shows eogenetic events as the rocks have not been buried to more than about 1722 m and not exceeded about 60 °C (Fig. 5.15a). The source of the evidence behind each interpreted step in the paragenetic sequence is listed in the figure. Evidence for the paragenetic sequence include K-feldspar dissolution (Figs. 5.7a, 5.7d, 5.9a and 5.10a), shell dissolution and shell degradation (Figs. 5.7b and 5.11a), compaction (Fig. 5.10a), pyrite (Figs. 5.7b, 5.8d and 5.10f), apatite (Fig. 5.9a), berthierine pore-filling/coats (Figs. 5.9a and 5.10c), calcite cementation (Figs. 5.7b, 5.7c, 5.8a and 5.11a), quartz overgrowth (Figs. 5.10c and 5.10d), hydrocarbon charge (Fig. 5.7d), calcite dissolution (Fig. 5.7d), Fe-ooids dissolution Figs. 5.8a and 5.10c), siderite (Figs. 5.8a and 5.10b), dolomite (Figs. 5.10a, 5.10b and 5.10d), illite (Fig. 5.10d), kaolinite (Figs. 5.7d, 5.8b and 5.10c).

Subsequent diagenetic processes included quartz overgrowth formation (Figs. 5.7d, 5.8b, 5.10a and 5.10c). Partial dissolution of Fe-ooids (Figs. 5.8a and 5.10c) and feldspars (Fig. 5.7a) occurred, possibly after quartz growth as quartz was preceded by berthierine coat formation (Fig. 5.10c). Quartz growth and Fe-ooid dissolution were followed by hydrocarbon charge as

shown by the presence of bitumen staining on quartz cement (Fig. 5.7d) and on the internal dissolution surfaces of ooids (Fig. 5.7b).

These events were followed by minor quantities of siderite and dolomite cement, replacive calcite (labelled calcite-3), and illite and kaolinite. The timing of siderite and dolomite cannot be differentiated (Fig. 5.10b) but they occurred after Fe-ooid dissolution (Fig. 5.10b). Replacive calcite-3 developed after siderite and dolomite (Fig. 5.10b) but at about the same time as pore-filling illite (Fig. 5.10d). Kaolinite seems to have been a late-stage diagenetic mineral that grew at the expense of detrital feldspars (Fig. 5.10c).

Compaction occurred during burial, but these sandstones are typically cementation-dominated rather than compaction-dominated (Fig. 5.17); this was caused by the extensive development of locally-dominant poikilotopic calcite (Fig. 5.11a) and other pore-filling minerals (Fig. 5.7a). The least calcite-cemented sandstones display long grain to grain contacts evidencing the occurrence of compaction (Fig. 5.7d).

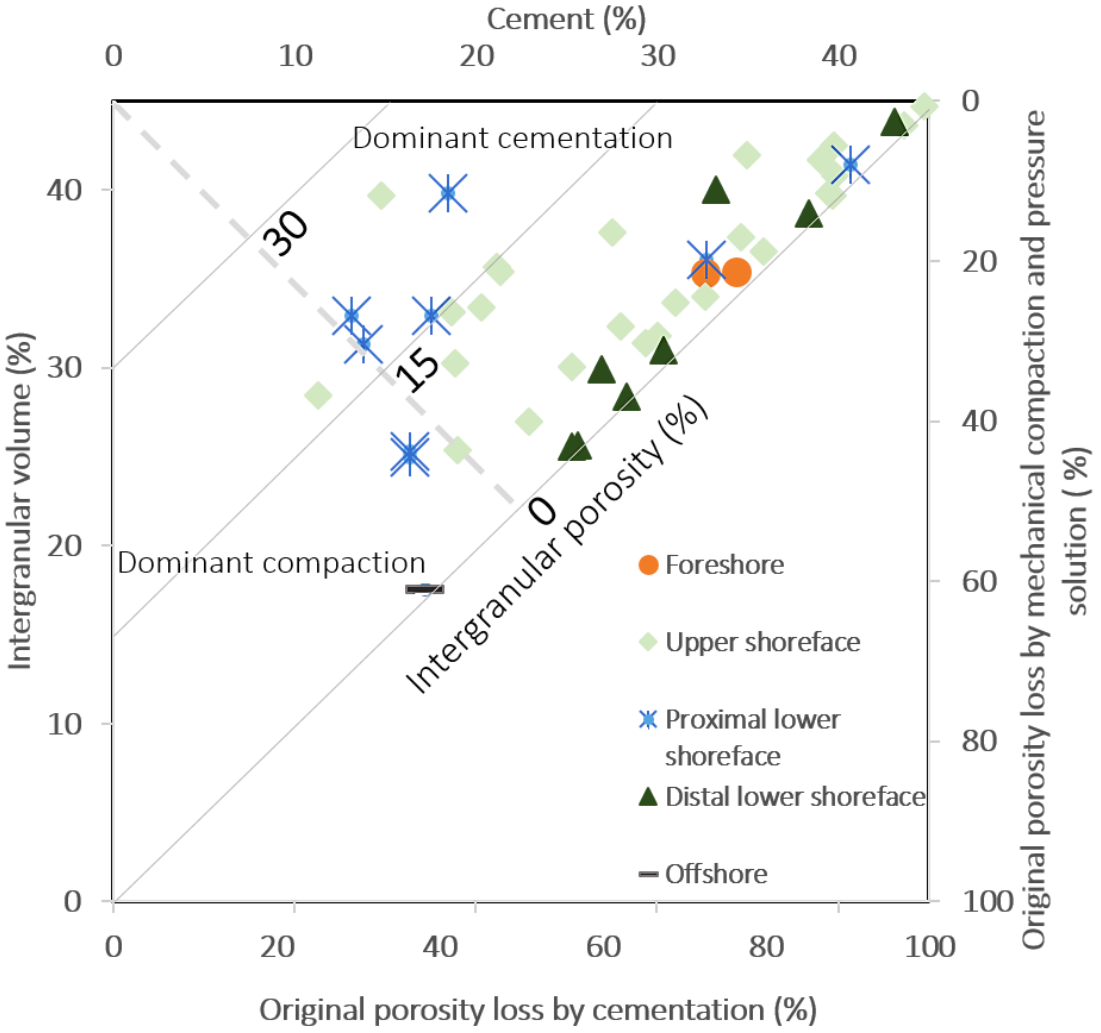

Figure 5.17: Intergranular volume (%) versus cement (%) diagram after the method developed by Houseknecht (1987) showing the role of cementation and compaction in initial porosity-loss. The quadrant to the top-centre shows samples with predominant porosity-loss by cementation while the quadrant to the centre-left shows samples with dominant porosity-loss by mechanical compaction. The distal lower shoreface and offshore facies associations have the highest initial porosity-loss as they plot mostly between 0-7% intergranular porosity.

The dissolution of calcite cement (Fig. 5.7d), Fe-ooids (Figures 5.7b and 5.8a) and feldspars (Fig. 5.7a and 5.7d), towards the end of the succession of events, led to the creation of secondary porosity. Based on XRD data, chlorite is present in trace quantities (Fig. 5.13) but it is not apparent in optical images, therefore it is not certain if it had detrital or authigenic

origins. Chlorite is not present in sufficient quantity to influence reservoir quality or to ascertain its diagenetic relationships.

5.5.2 Sources of Mineral Cements

5.5.2.1 Pyrite

Pyrite formed early and precipitated throughout burial in the Corallian sandstones (Figs. 5.8d and 5.10f). In addition, pyrite partly replaced bioclasts (Fig. 5.7b) suggesting early sulfide mineral formation, before neomorphism of bivalves to calcite cement. Pyrite-filled pores (Fig. 5.10f) formed adjacent to detrital grains and completely occluded pore spaces suggests that early diagenetic growth continued during subsequent burial. Framboidal pyrite is characteristic of early diagenesis while the coarser morphologies of pyrite, e.g., Figure 5.8d, typically represent later diagenesis (Burley & Worden 2003a; Goldhaber 2003). Pyrite in marine sediments requires organic-rich, anoxic, reducing conditions to convert marine aqueous sulphate to sulfide and ferric iron to ferrous iron (Berner 1964; Goldhaber 2003). The iron in pyrite in the Corallian sandstones may have been supplied by depositional biotite, Fe-ooids, and detrital or seabed-related glauconite (Figs. 5.8b and 5.8d). The Corallian sandstones were deposited in sulphate-rich sea water and the decomposition of organic matter potentially consumed oxygen and reduced the redox potential (Eh) producing sulfide and ferrous iron (Tucker 1981). In the absence of carbonates, sulfide and ferrous iron combine to form iron sulfide.

5.5.2.2 Apatite

Apatite requires a source for phosphorus; apart from heavy mineral deposits, apatite is commonly associated with sediments that experienced much biological activity. Detrital apatite may be derived from bone and teeth fragments (Pettijohn et al. 1973; Tucker 1981; Macquaker et al. 1996). Apatite can also be enriched in coprolites (Tucker 1981) and can occur at a trace concentration in bioclasts (Tucker 1981; Ruttenberg & Berner 1993). It is likely that much of the diagenetic apatite found in the Corallian sandstones is recrystallised detrital apatite derived from bone fragments (Pettijohn et al. 1973).

5.5.2.3 Berthierine

Berthierine is here interpreted to have formed under reducing conditions during shallow burial (Bhattacharyya 1983; Fritz & Toth 1997; Williams 2003; Fu et al. 2015). Grain-coating and

pore-filling berthierine developed after dissolution of Fe-ooids which suggests that Fe-ooids may have sourced diagenetic berthierine (Figs. 5.8a and 5.10c).

Berthierine forms as a result of reduction of iron at low Eh conditions (Bhattacharyya 1983; Fritz & Toth 1997; Fu et al. 2015); these conditions commonly occur in nutrient-rich coastal waters (Worden & Morad 2003b). The presence of detrital Fe-rich biotite (Fig. 5.9b) and Fe-ooids in these sediments (Fig. 5.7c) indicates that the primary sediment was enriched in iron. The presence of diagenetic siderite (see later and Fig. 5.9b) and pyrite (Figs. 5.8d and 5.10f), as well as berthierine, confirms that Fe-diagenesis was an important aspect of the evolution of these rocks. The specific dominant Fe-phase was influenced by the supply of sulfide and bicarbonate, both probably from organic sources (Macquaker et al. 1996; Worden et al. 2020b). Berthierine grows in sulfide- and bicarbonate-limited pore waters, influenced by a suite of bacterial processes (Aagaard et al. 2000). The degradation of Fe-ooids led to the formation of thin berthierine coats (Fig. 5.10) and pore-filling berthierine (Fig. 5.7a) similar to berthierine in the Wealden sandstones of the Paris Basin (Virolle et al. 2021).

Another possible source of berthierine is detrital biotite (Fig. 5.7d). Authigenic berthierine tends to be physically close to detrital biotite-rich matrix (Figs. 5.8d and 5.9a). There is a significant correspondence between biotite and berthierine enrichment patterns as a function of facies association (Fig. 5.12f, h). Biotite can be a source of the main ingredients for berthierine; however, the latter has a higher Al/Si ratio than the former suggesting either that (i) silica was exported to other parts of the Corallian sandstone (e.g., as quartz cement) or (ii) Al was imported from other parts of the Corallian sandstone (e.g., from alumino-silicate mineral breakdown).

5.5.2.4 Calcite

Early calcite cement is here interpreted to have formed from neomorphism of bivalve tests, starting soon after deposition and continuing during burial. Petrographic evidence shows bivalve shells with various degrees of neomorphism (Figs. 5.7b, 5.8a and 5.11a) to calcite (Scotchman et al. 1989; Adams 1998; Worden et al. 2019). Neomorphism of aragonitic bivalve shells is emphasised in Figure 5.11a where pervasive calcite cement cannot be distinguished from bivalve shells except where micrite envelops outline the boundary of bivalve shells which neomorphosed into calcite. In contrast, Figure 5.11b shows a porous rock, with unaltered bivalve shells and very little calcite cement as the shells have only been slightly micritised, with no significant neomorphism (Fig. 5.11b), leading to a low calcite cement volume.

Calcite-1 forms acicular rims on bivalve shells (Figs. 5.7b and 5.11a) and does not significantly project into pore space, indicating early formation. Acicular rims are surrounded by poikilotopic calcite (calcite-2) which pervasively fills pore spaces indicating development of calcite as neomorphism progressed (Fig. 5.11a).

Secondary calcite (calcite-3) is here interpreted to have formed after local dissolution of detrital or eogenetic calcite following addition of CO_2-rich waters during burial, possibly by source rock decarboxylation. There is evidence for dissolution of calcite cement (Fig. 5.7d), Fe-ooids (Figs. 5.8a, 5.10c and 5.10e) and feldspars (Figs. 5.7a, 5.7d, 5.9a and 5.9b). There is evidence of calcite development following grain dissolution (Figs. 5.9a and 5.10b). The development of calcite-3 after dissolution is here interpreted to occur due to reduction in the partial pressure of CO_2 (PCO_2) during grain and cement dissolution causing a reduction in acidic conditions and a return to more neutral conditions suitable for calcite development.

5.5.2.5 Quartz

Typically, quartz cementation is a kinetically-driven process whose rate depends on a silica source, mass transfer to the site of cementation and, finally, cement precipitation (Worden et al. 1998). Quartz cement requires a silica source, a mode of transport and a site for deposition or crystallisation; these depend on detrital mineralogy, temperature, grain size and degree of grain coat coverage (Walderhaug 2000). Silica for quartz cementation is here interpreted to be sourced from feldspar dissolution (Figs. 5.7a, 5.7d, 5.9a and 5.9b) (Emery et al. 1990; Bjørkum et al. 1998a; Worden & Morad 2000) as well as the alteration of other detrital alumino-silicates such as Fe-ooids (Fig. 5.10c and 5.10e), of biotite (Fig. 5.9a) and muscovite (Fig. 5.8c).

The low temperature (<60 °C), shallow depth (Fig. 5.15) of the quartz cement in the Corallian sandstones is significant as it shows that incipient quartz cementation occurs at shallow depths, similar to Lower Cretaceous Wealden sands in the Paris Basin (Virolle et al. 2021). This is noteworthy as it shows that quartz cement does not only develop at temperatures greater than 80 °C as has been widely reported in literature (Walderhaug 1994a, 2000; Worden & Morad 2000; Worden et al. 2018a). Furthermore, this low temperature quartz cement was locally inhibited by berthierine coats (Fig. 5.10c). Inhibition of quartz cement is commonly linked to chlorite grain coats with berthierine serving as a possible precursor mineral for chlorite (Aagaard et al. 2000; Worden & Morad 2003b). The inhibition of quartz overgrowth here proves that the preservation of reservoir quality by grain-coats starts during eodiagenesis with berthierine coats. Berthierine coats are therefore potentially important in shallow reservoirs

where chlorite coats have not developed. As has been recently shown for shallow buried sandstones in NW France (Virolle et al. 2021), berthierine coats can therefore preserve reservoir quality by inhibiting quartz cement at temperatures much lower than 70 °C.

5.5.2.6 Siderite

The precipitation of siderite is interpreted to be a late-stage event, as seen in Figure 5.10b, where siderite precipitated in moldic pore. Siderite was probably derived from iron supplied by alumino-silicates (e.g., berthierine in Fe-ooids, Figure 5.7a, or biotite) and carbonates. This is similar to models of siderite origin published by Macquaker et al. (1996), Gehring (1990).

5.5.2.7 Dolomite

Dolomite is here interpreted to have developed following the dissolution of calcite cement and biotite or Fe-ooids. Dolomite rhombohedra locally occur close to dissolved Fe-ooids (Figs. 5.8a, 5.10a and 5.10d). As magnesium and iron ions are present in berthierine (Bhattacharyya 1983), alteration of berthierine in ooids releases Fe^{2+} and Mg^{2+} to combine with carbonate ions to produce dolomite (Fu et al. 2015). In addition, dolomite and Fe-dolomite show a similar pattern, by facies association, to biotite (Fig. 5.12c, 5.12d, and 5.12f) which suggests a genetic relationship where iron and magnesium released from biotite alteration can also combine with carbonate ions to produce dolomite.

5.5.2.8 Illite

Illite cement is here interpreted to develop from the alteration of phyllosilicate minerals such as muscovite (Fig. 5.8c) and K-feldspar (Fig. 5.10a) (Ehrenberg & Nadeau 1989). Illite is also interpreted to result from the dissolution of feldspars (Fig. 5.7a) (Scotchman et al. 1989).

5.5.2.9 Kaolinite

Similar to illite, kaolinite is interpreted to have precipitated following alumino-silicate mineral breakdown, e.g., Emery et al. (1990); Orem & Finkelman (2003). Meteoric water flushing has widely been discussed as causing the growth of kaolinite in shallow sandstones (Emery et al. 1990; Glasmann 1992), with the leaching of feldspars and mica occurring at depths as shallow as 10 to 20 m (Bjørlykke 1998). As kaolinite is mostly in pore spaces close to dissolved silicates (Fig. 5.10c), it is interpreted to have formed as a result of dissolution of K-feldspar (Scotchman et al. 1989) (Figs. 5.7d, 5.9a and 5.9b) in iron-deficient acidic pore-fluids after CO_2 flux, possibly from source rocks.

5.5.3 Role of Compaction and Cementation on Porosity

Detrital mineralogy in the Corallian sandstones is dominated by quartz (Fig. 5.6). Quartz-rich sandstones undergo less compaction than ductile-rich sandstones (Houseknecht 1984, 1987). As the modelled burial curves in Figure 5.15b illustrate, porosity-loss did not follow the expected trend for mechanical compaction. The deviation from the modelled trend suggests that mechanical compaction is not the dominant control on porosity evolution.

The degree of compactional and cementational porosity-loss was quantified using point count data using the approach described by Houseknecht (1987) employing an assumed initial porosity of 45% (Fig. 5.17). The Houseknecht plot shows that cementation is the dominant control on reservoir quality for the Corallian sandstones. All but three samples plot in the quadrant for porosity-loss being dominated by cementation. The three samples that lie in the field of dominant compactional porosity-loss either have a relatively low cement content (i.e., BL5-2209.46 m MD, cement content of 11.34%; BL5-2208.0 m MD, cement content of 16.35%; BL5-2211.6 m MD, cement content of 16.36%) or have a high matrix clay content (PW3-1098.3 m MD, 61% clay).

5.5.4 Controls on Diagenesis and Reservoir Quality

The Corallian sandstones do not have a simple relationship between depositional facies and reservoir quality. For example, there is no clear relationship between reservoir quality and either grain size or sorting (Fig. 5.18a). In addition, there is no apparent relationship between facies association and reservoir quality (Fig. 5.18b). The best reservoir quality samples, i.e., those that plot in the top-right corner of Figure 5.18c, tend to have little calcite or clay minerals. The worst reservoir quality samples have high calcite and/or clay contents (Fig. 5.18c). This shows that there is a strong diagenetic and cement-related control on reservoir quality. Samples with moderate to high porosity, low calcite but high clay content, have lower permeability, by up to an order of magnitude or more, than samples in their porosity range (Figs. 5.5 and 5.18c). This indicates that permeability is strongly affected by clay mineral content, even in high porosity samples.

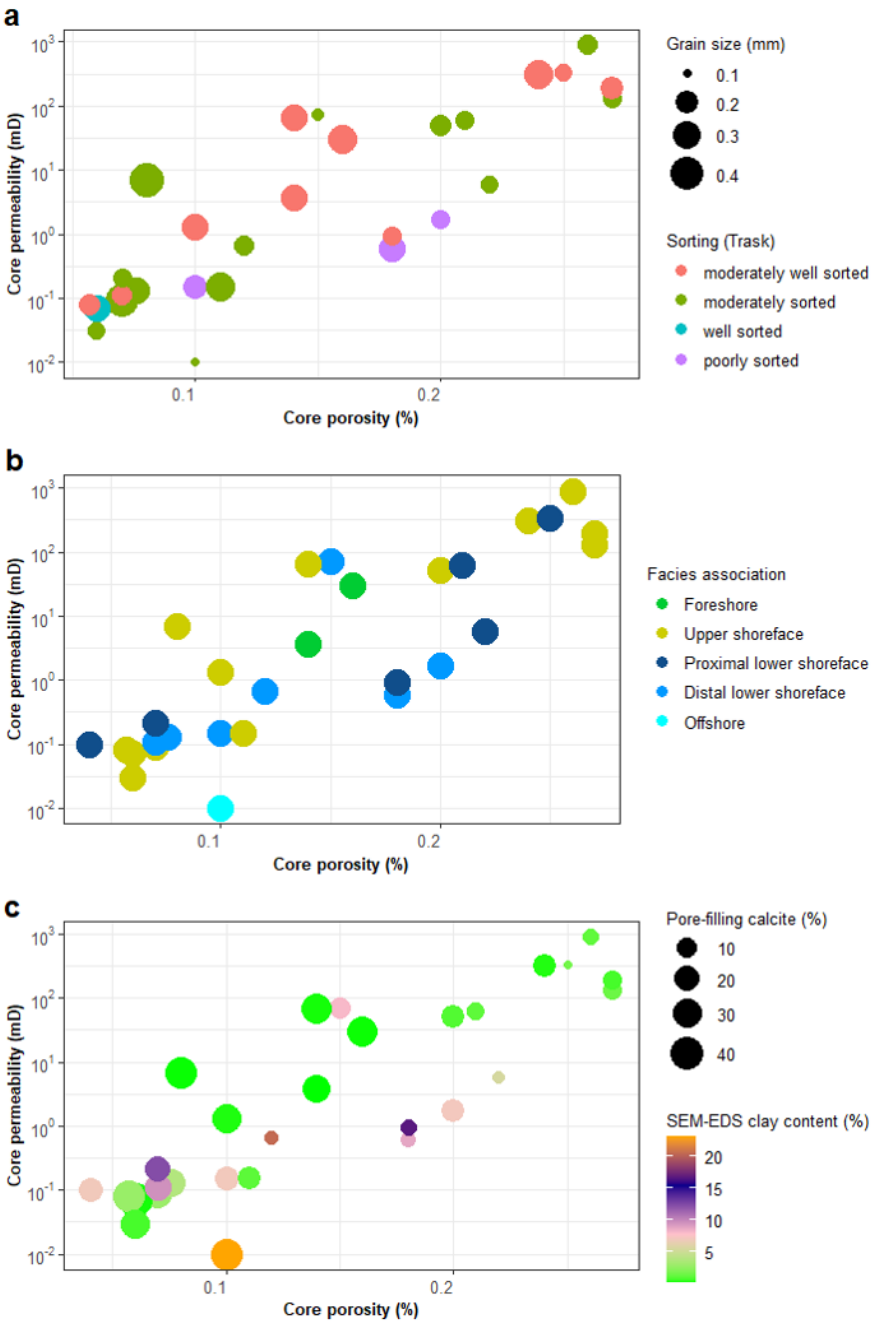

Figure 5.18: Assessment of the controls on core porosity and permeability for all three wells: (a) No clear pattern between grain size and sorting with porosity and permeability (b) No clear relationship between porosity and permeability with facies associations as the best reservoir quality is in the upper shoreface and proximal lower shoreface facies associations which also have samples with low porosity and permeability. (c) The best reservoir quality zones have low calcite content and clay content. Samples with low calcite content and high clay content have a lower permeability range than samples in their porosity range.

Reservoir quality was partly preserved by berthierine grain coats which inhibited the development of quartz cement (Fig. 5.10c). Porosity was significantly enhanced by grain dissolution and the creation of secondary porosity (Figs. 5.7a, 5.7b, 5.8a, 5.10c, 5.10d and 5.10e). However, reservoir quality was minimally affected by grain replacive cementation which filled secondary pores created by dissolved grains without enhancing or destroying porosity (Fig. 5.10b).

5.5.5 Reservoir Quality Model

A reservoir quality evolutionary path, showing the effects of calcite and clay minerals, is illustrated in Figure 5.19 illustrating the controls on reservoir quality using SEM-EDS images for selected points. The lines connecting the SEM-EDS images show the reservoir quality evolutionary path for various sandstone types. Pattern 1 shows the evolutionary path of clean sandstones and illustrates how an increase in overall clay mineral content and calcite destroyed reservoir quality. Pattern 2 shows the effect of dissolution of cements and grains on reservoir quality, whereby there is an increase of porosity and permeability. Pattern 2 has a higher permeability range than sediments on pattern 1, possibly because of extensive creation and connection of pores from dissolution at the current shallow depths without significant compensative pore size reduction from compaction. Pattern 3 shows how clays disproportionally decrease permeability in calcite-poor samples indicating that calcite-poor sandstones will not have high permeability if they are clay-rich due to occlusion of pore throats by clays in high porosity samples.

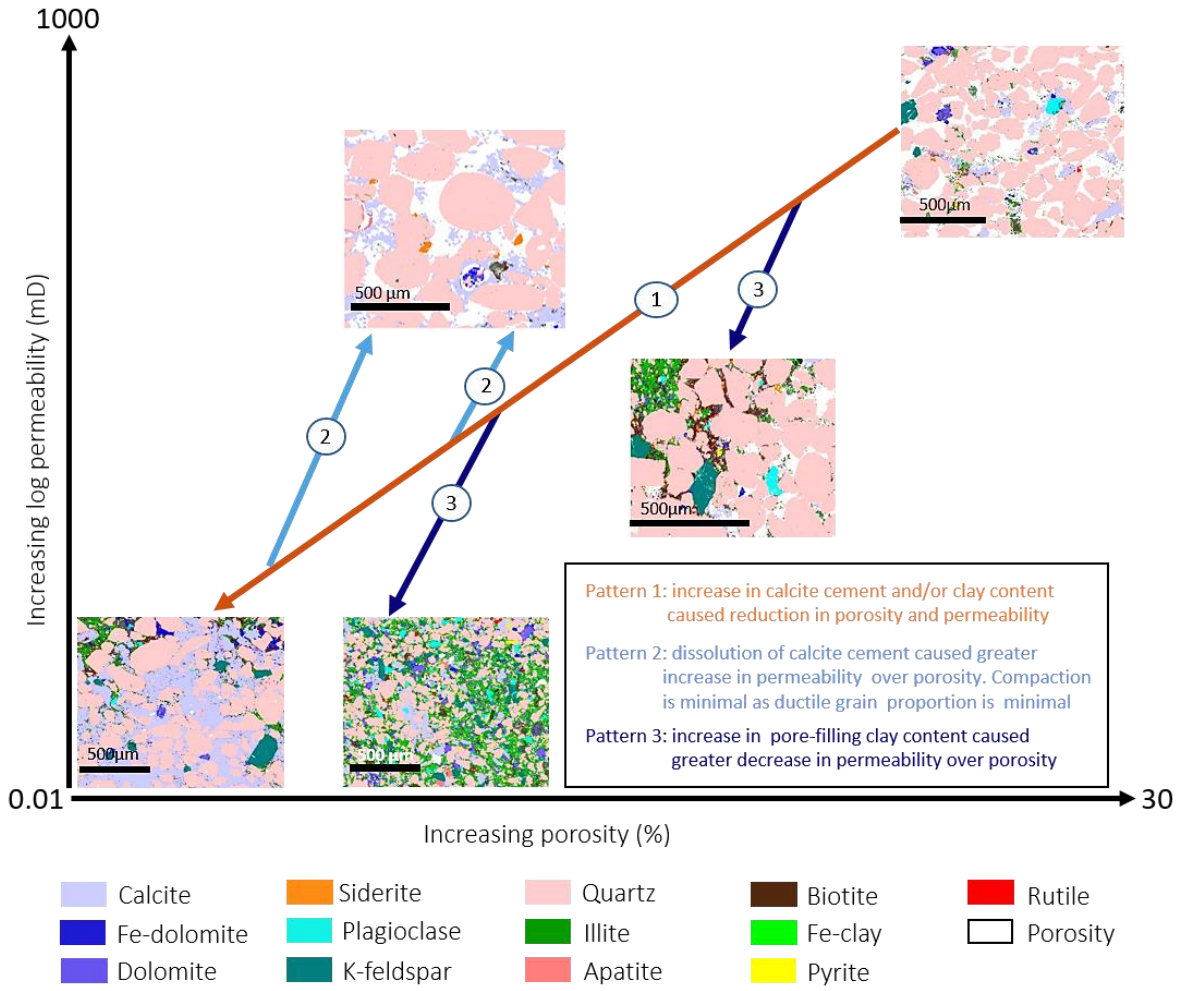

Figure 5.19: A model for reservoir quality evolution of the Corallian sandstones with SEM-EDS images of selected samples from points in Figure 5.18c. The arrows are a schematic for reservoir quality evolution patterns from a clean sand-rich. (1) Corallian sandstones to an argillaceous calcite cemented sandstone. (2) The effect of calcite cement dissolution and grain dissolution while. (3) The effects of clay under different porosity levels. The model emphasises the dominant influence of calcite cement on mechanical compaction, porosity and permeability loss as well as clay minerals in permeability reduction.

Corallian sandstones rich in bioclast-derived calcite presumably were deposited in shallow, limpid ocean waters with a great abundance of biological activity. The addition of a quartz-dominated sand to a site of active bioclast accumulation led to compromised reservoir quality in the subsurface due to the propensity for such bioclast-quartz sand hybrids to become calcite cemented (Bryant et al. 1988; Sun 1992; Worden et al. 2019). Conversely, sandstones rich in

matrix clay, presumably in turbid ocean waters, near to the site where rivers fed sediment into the ocean, have far fewer bioclasts and thus much less calcite cement (Bryant et al. 1988). However, these clay-rich Corallian sandstones have their subsurface reservoir quality strongly affected by the presence of the same clay minerals that inhibited bioclast development at the site of deposition.

In summary, despite the shallow burial depth of these sandstones, depositional characteristics have not influence their reservoir quality. Very little compaction has occurred in these sandstones as compactional porosity-loss was retarded by calcite cement within a quartz-rich rock hence cementation was the main cause of porosity-loss. The cementational porosity-loss is dominated by calcite cement with minor dolomite, siderite, berthierine, pyrite, illite, kaolinite, apatite, and quartz cement. This chapter presents a first comprehensive analysis on the reservoir quality of the Corallian sandstones in the Palmers Wood and Bletchingley area. It also highlights the effect of bioclast-derived calcite cement in reversing depositional controls on reservoir quality in eogenetic sandstones. This study shows that quartz cement and illite formed at lower temperatures of less than 70°C in contrast to the widely accepted higher temperature ranges expected for their development. Thus this chapter adds to the discussion on the effect of residence time on diagenetic reactions and emphasizes the influence of residence time rather than temperature alone on thermally-driven mineral development e.g. quartz cement and illite cement during eodiagenesis. Another notable result from this research is that reservoir quality preservation by grain coats occurs with eodiagenetic berthierine grain coats formed at shallow temperatures. This indicates that porosity preservation by grain coats is not exclusive to chlorite grain coats and also begins during eodiagenesis. The occurrence of berthierine grain coats also answers important reservoir quality questions regarding the origin of mesodiagenetic chlorite grain coats as berthierine is a chlorite precursor mineral.

Limitations of this study include the absence of fluid inclusions or vitrinite reflectance data to constrain temperature during burial analysis. The study has broad implications for understanding the effect of bioclast-rich sandstones on compactional porosity loss, the potential for eodiagenetic quartz cementation as well as the role of berthierine in porosity preservation in Fe-rich shallow marine eodiagenetic reservoirs. The results of this research can be applied in other shallow-buried shallow marine rocks and have broader implications for understanding mesodiagenetic processes such as reservoir quality preservation by chlorite grain coats.

5.6 Conclusions

1. The Corallian sandstones have moderate to poor reservoir quality. The diagenetic processes that modified these sandstones include the growth of various cements (in approximate order of abundance: calcite, siderite, dolomite, Fe-dolomite, quartz, pyrite, apatite, berthierine, kaolinite and illite) as well as minor compaction. Reservoir quality was also influenced by dissolution of Fe-ooids, K-feldspar, plagioclase feldspar and calcite cement.
2. Reservoir quality does not seem to have strong depositional controls. Corallian sandstones are cementation-dominated, as opposed to compaction-dominated, calcite is the dominant cement and the main control on reservoir quality. Calcite cement was derived from detrital bioclasts co-deposited with the sand grains.
3. Kaolinite and illite occur as pore-filling clays while berthierine occurs as pore-filling, grain replacive and grain coating clay.
4. Quartz cement has a low temperature, early diagenetic origin but is volumetrically minor, at least, in part, due to its inhibition by berthierine grain coats. Berthierine clay coats locally preserved reservoir quality by preventing quartz overgrowths.
5. Clay minerals (kaolinite and illite) locally reduced reservoir quality, especially decreasing permeability for only a small decrease in porosity.
6. Secondary porosity, following dissolution of calcite cement and detrital feldspars and Fe-ooids, locally increased porosity and permeability.
7. The best reservoir quality in Corallian sandstones is found in the cleanest, most clay-free sandstones with the least amount of calcite cement. Detrital bioclast content is the over-riding control on reservoir quality in these sandstones.

Appendix 5.A

Table 5.A1. Point count data for the Corallian sandstones.

Well	Depth (m)	Grain Size (mm)	Sorting (Trask)	%Quartz Monocrystalline	%Quartz Polycrystalline	%Quartz Pore-Filling	%Extrabasinal-Chert	%Extrabasinal-Quartzite	%Extrabasinal-Sandstone	%Intergranular Porosity	%Cement Dissolution Porosity	%Partial Grain Dissolution, Bioclasts	%Partial Grain Dissolution, Others	%Fracture porosity
PW3	1082.34	0.4	1.4	22.0	9.0	0.0	0.3	0.3	0.0	0.0	0.0	0.0	0.0	0.0
PW3	1085.09	0.4	1.4	33.4	12.8	0.0	0.0	1.0	0.0	2.6	0.0	0.7	1.3	0.0
PW3	1087.53	0.2	1.3	35.4	9.7	0.0	0.0	0.0	0.0	1.3	0.0	0.0	0.3	0.0
PW3	1088.29	0.2	1.2	27.1	4.7	0.0	0.0	0.0	0.0	0.6	0.0	0.0	0.0	0.0
PW3	1088.52	0.3	1.0	29.3	4.0	0.0	0.0	0.0	0.0	3.0	0.0	0.0	0.0	0.0

PW3	1091.40	0.3	1.2	38.8	11.7	0.0	0.0	0.7	0.0	1.0	0.0	0.6	4.0	0.0
PW3	1091.49	0.3	1.2	38.5	14.8	0.3	0.0	0.0	0.0	2.7	0.0	0.7	1.3	0.0
PW3	1093.99	0.2	1.2	34.5	12.8	0.0	0.3	0.0	0.0	0.7	1.0	0.3	2.2	0.0
PW3	1098.26	0.1	1.2	13.3	0.7	0.0	0.0	0.0	0.0	0.3	0.0	0.0	0.0	0.0
PW7	1122.50	0.1	1.2	21.3	2.3	0.0	0.0	0.0	0.0	0.0	0.0	0.0	0.0	0.0
PW7	1123.19	0.3	1.2	32.8	11.7	0.0	0.0	1.0	0.0	6.7	0.3	0.0	0.9	0.0
PW7	1123.28	0.3	1.2	25.4	6.7	0.0	0.0	0.6	0.0	4.0	0.0	0.0	0.0	0.0
PW7	1124.03	0.3	1.2	35.9	15.1	0.0	0.0	0.3	0.0	4.7	0.0	0.0	2.7	0.0
PW7	1124.94	0.3	1.2	35.5	12.4	0.0	0.0	0.0	0.3	0.7	0.3	0.0	3.3	0.0
PW7	1126.04	0.3	1.4	32.9	16.4	0.0	0.0	0.0	0.0	23.9	1.0	0.0	0.3	0.0
PW7	1130.05	0.4	1.2	18.1	6.3	0.0	0.0	0.0	0.0	0.3	0.0	0.3	1.6	0.0
PW7	1131.57	0.3	1.2	33.5	15.4	0.3	0.0	0.0	0.0	10.1	0.0	0.0	0.6	0.0
PW7	1131.72	0.3	1.2	28.5	11.1	0.0	0.0	0.0	0.0	11.4	0.0	0.0	3.8	0.0
PW7	1132.88	0.3	1.1	33.1	13.4	0.0	0.0	0.3	0.0	2.7	0.0	0.3	0.3	0.0
PW7	1133.02	0.3	1.1	33.1	8.0	0.0	0.3	0.3	0.0	0.0	0.0	0.0	1.7	0.0
PW7	1134.62	0.2	1.2	36.4	8.3	0.0	0.0	0.3	0.0	6.4	0.0	0.3	0.6	0.0
PW7	1135.23	0.2	1.2	38.4	14.7	0.0	0.0	1.6	0.0	2.0	0.0	0.3	0.3	0.0
PW7	1135.68	0.2	1.2	37.4	7.3	0.3	0.0	0.3	0.0	14.0	0.0	0.0	0.3	0.0
PW7	1136.52	0.1	1.3	51.6	7.7	2.9	0.0	0.0	0.0	19.4	0.3	0.0	0.0	0.0
PW7	1137.36	0.1	1.2	46.9	5.0	1.0	0.0	0.0	0.0	21.4	0.0	0.3	0.0	0.0
BL5	2194.68	0.3	1.8	41.7	11.4	0.7	0.0	0.0	0.3	0.3	0.0	0.0	0.0	0.0
BL5	2195.20	0.2	1.3	38.5	6.3	1.3	0.0	0.0	0.0	0.0	0.0	0.0	0.0	0.3
BL5	2197.91	0.2	1.2	28.7	7.3	0.7	0.0	0.0	0.0	0.3	0.0	0.0	0.0	0.0
BL5	2198.83	0.2	1.3	39.1	6.7	0.0	0.0	0.3	0.0	0.6	0.0	0.0	0.0	0.0
BL5	2199.09	0.2	1.3	43.9	10.0	7.9	0.0	0.0	0.0	14.5	0.0	0.0	1.5	0.3
BL5	2199.47	0.2	1.4	41.8	8.0	0.6	0.0	0.0	0.0	5.7	1.0	0.0	0.3	0.0
BL5	2199.92	0.3	1.2	18.4	8.0	0.3	0.0	0.6	0.0	0.0	0.0	0.0	0.0	0.3
BL5	2200.99	0.1	1.5	27.1	3.3	0.0	0.0	0.0	0.0	0.0	0.0	0.0	0.0	0.0
BL5	2201.88	0.3	1.2	31.3	10.7	0.0	0.0	0.0	0.0	2.0	0.7	0.0	0.7	0.0
BL5	2202.21	0.3	1.2	37.1	9.3	0.3	0.0	0.7	0.0	1.0	1.6	0.0	3.0	0.0
BL5	2204.69	0.2	1.3	51.5	7.0	0.7	0.0	0.0	0.0	14.5	0.0	0.0	1.3	0.0
BL5	2205.84	0.2	1.2	39.0	6.7	1.0	0.0	0.0	0.0	3.3	0.0	0.0	0.9	0.3
BL5	2206.60	0.2	1.3	32.8	3.3	0.7	0.0	0.0	0.0	0.7	0.0	0.0	0.3	0.0
BL5	2206.87	0.2	1.5	33.0	7.0	1.3	0.3	0.0	0.0	0.0	0.0	0.0	0.3	0.0
BL5	2207.15	0.2	1.5	39.9	9.0	0.0	0.0	0.0	0.0	0.3	0.0	0.3	0.3	0.0
BL5	2208.00	0.2	1.2	47.1	5.7	0.7	0.0	1.0	0.0	8.9	0.0	0.0	0.9	0.0
BL5	2208.86	0.2	1.2	35.9	4.7	0.0	0.0	0.3	0.0	0.7	0.0	0.3	3.4	0.0
BL5	2209.24	0.2	1.3	53.3	6.7	0.3	0.0	0.3	0.0	13.1	0.0	0.0	1.3	0.0
BL5	2209.46	0.2	1.2	52.2	12.3	0.0	0.0	0.0	0.0	17.1	0.0	0.0	0.0	0.0
BL5	2210.41	0.2	1.3	34.8	10.0	0.0	0.0	0.3	0.0	3.0	1.3	0.0	0.9	0.0
BL5	2211.45	0.2	1.2	54.6	7.3	3.0	0.0	0.0	0.0	16.8	0.7	0.0	0.0	0.3
BL5	2211.57	0.2	1.4	46.2	15.8	0.6	0.0	0.0	0.0	8.0	0.6	0.0	5.3	0.0
BL5	2211.63	0.2	1.2	50.2	10.7	2.0	0.0	0.6	0.0	14.4	1.0	0.0	1.6	0.0
	Mean	0.22	1.27	36.07	8.95	0.56	0.03	0.23	0.01	5.52	0.21	0.09	0.99	0.03

Well	**Depth (m)**	**%Grain Moldic Porosity**	**%Intercrystalline Porosity**	**%Intragranular Porosity**	**%Matrix/ Microporosity**	**%K-Feldspar**	**%Plagioclase Feldspar**	**%Bioclast**	**%Carbonate Grains, (Pelloids, Pisoids, ooids)**	**%Pore-Filling Calcite**	**%Replacive Calcite**	**%Pore-Filling Dolomite**	**%Replacive Dolomite**	**%Pore-Filling Siderite**
PW3	1082.3	0.0	0.0	0.0	0.3	0.7	0.0	3.0	0.0	32.8	21.3	0.3	0.0	4.3
PW3	1085.1	0.3	1.3	0.0	0.0	0.3	0.0	0.7	0.0	37.4	5.0	0.0	0.0	0.3
PW3	1087.5	4.0	0.0	0.0	0.0	1.0	0.0	1.7	0.0	31.1	12.7	0.0	0.0	1.3
PW3	1088.3	0.0	0.0	0.0	2.4	2.6	0.0	0.6	0.0	16.4	1.5	0.0	0.0	2.7
PW3	1088.5	0.0	0.0	0.0	0.0	3.0	0.3	1.7	0.0	5.0	0.7	0.3	0.0	1.0
PW3	1091.4	4.3	0.3	0.0	0.0	0.7	0.0	0.0	0.0	31.4	2.9	0.7	0.0	2.0
PW3	1091.5	0.9	0.0	0.0	0.0	0.7	0.0	0.0	0.0	25.8	6.9	0.3	0.0	4.0
PW3	1094.0	1.7	0.0	0.0	0.0	1.6	0.7	0.3	0.0	26.7	13.0	0.0	0.3	0.0
PW3	1098.3	0.0	0.0	0.0	2.0	1.0	0.7	0.0	0.0	9.0	2.7	3.3	0.3	0.0
PW7	1122.5	0.0	0.0	0.0	0.0	1.3	1.0	1.0	0.0	35.8	1.0	4.7	0.0	1.7
PW7	1123.2	0.9	0.0	0.0	0.0	0.7	0.0	0.0	0.0	15.1	7.6	0.0	0.3	0.3
PW7	1123.3	1.3	0.0	0.0	0.0	0.3	0.3	1.0	0.0	12.6	5.0	0.0	0.0	8.3
PW7	1124.0	5.2	1.3	0.6	2.0	0.0	0.3	1.0	0.0	22.4	4.9	0.7	0.0	0.3
PW7	1124.9	1.6	0.3	0.3	0.0	0.3	0.3	0.3	0.0	39.5	3.6	0.0	0.3	0.0
PW7	1126.0	0.3	1.3	1.4	0.0	0.3	0.3	0.9	0.0	13.3	5.8	0.9	0.3	0.0
PW7	1130.0	3.3	0.0	0.0	0.0	0.0	0.0	4.6	0.0	39.2	23.7	0.0	0.0	0.3
PW7	1131.6	2.6	0.0	0.0	0.0	0.3	0.0	3.4	0.0	20.4	5.6	0.3	0.0	4.3
PW7	1131.7	9.2	0.0	0.0	0.0	0.7	0.0	2.3	0.0	14.3	10.2	0.6	0.6	2.0
PW7	1132.9	2.6	0.0	0.0	0.0	1.6	0.3	0.0	0.0	37.4	5.6	0.0	0.0	2.3

PW7	1133.0	1.3	0.0	0.0	0.0	0.7	0.0	0.7	0.0	42.7	9.0	0.0	0.0	0.3
PW7	1134.6	3.0	0.0	0.0	1.0	2.3	0.3	0.3	0.0	5.3	0.6	0.7	0.0	2.0
PW7	1135.2	1.6	0.0	0.0	0.0	1.0	0.0	0.0	0.0	28.8	10.6	0.0	0.0	0.3
PW7	1135.7	2.0	0.0	0.0	0.0	1.0	1.0	0.3	0.0	5.6	1.3	0.0	0.0	0.7
PW7	1136.5	4.1	0.0	0.0	0.0	1.3	0.3	1.7	0.0	3.7	0.3	0.3	0.0	0.0
PW7	1137.4	2.0	0.0	0.0	0.0	1.0	1.7	0.3	0.0	5.3	0.3	1.0	0.0	0.0
BL5	2194.7	0.0	0.0	0.0	1.0	2.7	0.3	1.3	0.0	24.9	0.0	7.1	0.0	0.3
BL5	2195.2	0.0	0.0	0.0	0.6	2.0	0.3	0.0	0.3	37.8	0.0	1.0	0.0	1.3
BL5	2197.9	0.0	0.0	0.0	1.3	2.0	0.0	1.0	0.3	22.4	0.0	17.7	0.0	2.0
BL5	2198.8	0.6	0.0	0.0	0.0	1.3	0.3	1.6	0.0	30.1	11.9	2.1	0.0	0.6
BL5	2199.1	3.6	0.0	0.0	0.0	4.0	0.0	0.0	0.0	6.4	0.0	1.0	0.0	0.3
BL5	2199.5	1.0	0.0	0.0	1.0	1.0	0.0	0.3	0.0	14.3	0.3	2.3	0.0	0.7
BL5	2199.9	0.0	0.0	0.0	0.0	0.0	0.0	0.6	0.0	12.7	0.3	0.3	0.0	41.2
BL5	2201.0	0.0	0.0	0.0	0.3	0.7	0.0	0.6	0.0	12.0	0.3	2.3	0.0	1.0
BL5	2201.9	1.3	0.0	0.0	0.0	0.3	0.0	1.3	0.0	34.0	14.8	0.0	0.0	0.3
BL5	2202.2	1.6	0.0	0.0	0.0	0.0	0.0	0.3	0.0	28.4	10.9	1.0	0.3	1.0
BL5	2204.7	2.9	0.6	0.0	0.0	1.0	0.3	0.6	0.0	9.3	0.9	1.0	0.0	1.0
BL5	2205.8	1.3	0.0	0.0	2.0	2.0	0.0	0.7	0.0	6.3	0.0	0.7	0.0	0.7
BL5	2206.6	0.0	0.0	0.0	1.6	2.7	0.3	0.0	0.3	19.1	3.3	8.3	0.0	1.7
BL5	2206.9	0.0	0.0	0.0	2.4	3.0	0.3	1.3	0.0	3.4	0.7	0.0	0.3	0.3
BL5	2207.1	0.0	0.0	0.0	1.0	1.0	0.3	2.3	0.0	4.6	1.0	2.0	0.0	0.0
BL5	2208.0	3.9	0.0	0.0	1.0	1.0	0.0	0.0	0.0	3.0	0.0	0.3	0.0	0.7
BL5	2208.9	0.6	0.0	0.0	0.3	0.7	0.0	0.6	0.3	37.8	8.2	0.3	0.6	0.7
BL5	2209.2	1.9	0.0	0.3	0.0	0.3	0.0	0.0	0.0	15.1	0.9	0.0	0.0	0.0
BL5	2209.5	3.6	0.0	0.0	0.3	0.6	0.0	1.3	0.0	8.3	0.9	0.7	0.0	0.0
BL5	2210.4	1.3	0.0	0.0	1.0	0.0	0.3	0.0	0.7	24.8	13.9	0.3	0.0	0.3
BL5	2211.4	3.6	0.0	0.0	0.3	0.7	0.0	0.9	0.0	1.6	0.3	1.3	0.0	0.3
BL5	2211.6	1.9	0.0	0.3	2.0	0.0	0.3	0.0	0.0	8.7	0.3	2.7	0.0	0.7
BL5	2211.6	2.3	0.0	0.0	0.7	0.3	0.3	0.3	0.0	7.3	0.0	0.3	0.0	0.0
	Mean	1.75	0.11	0.06	0.51	1.08	0.22	0.85	0.04	19.37	4.82	1.39	0.07	1.95

Well	**Depth (m)**	**%Replacive Siderite**	**%Pore-filling Illite**	**%Replacive Illite**	**%Muscovite**	**%Biotite**	**%Pore-filling Kaolinite**	**%Replacive Kaolinite**	**%Berthierine Replacive**	**%Berthierine Ooids**	**%Berthierine Replacing Berthierine Ooid**	**%Pore-Filling Berthierine**	**%Replacive Berthierine**	**%Glauconite**
PW3	1082.3	0.7	0.3	0.0	0.0	0.0	0.0	0.0	0.0	0.3	0.0	0.0	0.0	0.0
PW3	1085.1	0.0	0.0	0.0	0.0	0.3	0.0	0.0	0.0	0.6	0.0	1.0	0.0	0.0
PW3	1087.5	0.9	0.0	0.0	0.0	0.0	0.0	0.0	0.0	0.0	0.0	0.0	0.0	0.0
PW3	1088.3	0.0	1.3	0.3	0.0	0.0	0.0	0.0	0.0	0.0	0.0	6.3	0.0	0.0
PW3	1088.5	0.0	5.7	0.3	0.0	0.0	0.0	0.0	0.0	0.0	0.0	13.3	0.0	0.0
PW3	1091.4	0.3	0.0	0.0	0.0	0.0	0.0	0.0	0.0	0.0	0.0	0.3	0.0	0.0
PW3	1091.5	0.0	0.0	0.0	0.0	0.0	0.0	0.0	0.0	0.3	0.6	0.9	0.6	0.0
PW3	1094.0	0.0	0.7	0.3	0.0	0.0	0.0	0.0	0.0	0.0	0.0	0.3	0.0	0.3
PW3	1098.3	0.0	0.0	0.0	0.0	0.3	0.0	0.0	0.0	0.0	0.0	0.3	0.0	0.3
PW7	1122.5	0.0	0.3	0.0	0.0	0.3	0.0	0.0	0.0	0.0	0.0	2.0	0.0	0.7
PW7	1123.2	0.0	0.0	0.0	0.0	0.0	0.0	0.0	0.3	0.0	0.7	3.8	1.0	0.0
PW7	1123.3	15.4	0.0	0.0	0.0	0.0	0.0	0.0	0.0	0.0	0.0	0.0	0.0	0.0
PW7	1124.0	0.0	0.0	0.0	0.0	0.0	0.0	0.0	0.0	0.0	0.3	1.9	0.3	0.0
PW7	1124.9	0.0	0.0	0.3	0.0	0.0	0.0	0.0	0.0	0.0	0.0	0.3	0.0	0.0
PW7	1126.0	0.0	0.0	0.0	0.0	0.0	0.0	0.0	0.0	0.0	0.0	0.3	0.0	0.0
PW7	1130.0	0.9	0.0	0.0	0.0	0.0	0.0	0.0	0.0	0.3	0.3	0.0	0.3	0.0
PW7	1131.6	0.3	0.7	0.0	0.0	0.0	0.0	0.0	0.0	0.0	0.6	0.9	0.6	0.0
PW7	1131.7	2.3	0.0	0.0	0.0	0.0	0.0	0.0	0.0	0.7	0.0	1.6	0.0	0.0
PW7	1132.9	0.0	0.0	0.0	0.0	0.0	0.0	0.0	0.0	0.0	0.0	0.0	0.0	0.0
PW7	1133.0	0.3	0.3	0.6	0.0	0.0	0.0	0.0	0.0	0.0	0.0	0.0	0.0	0.0
PW7	1134.6	0.0	7.3	1.0	0.0	0.3	0.3	0.7	0.0	0.0	0.0	1.0	0.0	0.3
PW7	1135.2	0.0	0.0	0.0	0.0	0.0	0.0	0.0	0.0	0.0	0.0	0.0	0.0	0.0
PW7	1135.7	0.0	10.0	0.0	0.0	0.0	0.7	0.0	0.0	0.0	0.0	0.0	0.0	0.0
PW7	1136.5	0.0	4.6	0.0	0.0	0.0	0.0	0.0	0.0	0.0	0.0	0.3	0.0	0.0
PW7	1137.4	0.0	4.5	0.0	0.0	0.0	3.3	1.3	0.0	0.0	0.0	0.6	0.0	0.7
BL5	2194.7	0.0	2.3	0.0	0.0	0.0	0.0	0.0	0.0	0.0	0.0	0.7	0.0	0.0
BL5	2195.2	0.0	1.0	0.3	0.0	0.0	0.0	0.3	0.0	0.0	0.0	0.0	0.0	0.0
BL5	2197.9	0.0	0.3	0.0	0.0	0.0	0.0	0.0	0.0	0.0	0.0	0.0	0.0	0.0
BL5	2198.8	0.0	0.7	1.3	0.0	0.0	0.0	0.0	0.0	0.0	0.0	0.7	0.0	0.3
BL5	2199.1	0.0	0.7	0.0	0.0	0.0	0.3	0.0	0.0	0.0	0.0	2.5	0.0	0.7
BL5	2199.5	0.0	6.3	0.0	0.3	0.3	0.0	0.0	0.0	0.0	0.0	4.0	0.0	0.0
BL5	2199.9	0.0	1.3	0.0	0.3	3.3	0.0	0.0	0.0	2.7	0.0	3.6	0.0	0.0
BL5	2201.0	0.0	0.3	0.0	0.0	0.3	0.0	0.0	0.7	0.0	0.0	11.3	0.7	0.3

BL5	2201.9	0.6	0.0	0.0	0.0	0.0	0.0	0.0	0.0	0.0	0.3	0.3	0.3	0.0
BL5	2202.2	0.7	0.0	0.3	0.0	0.3	0.0	0.0	0.7	0.0	0.7	0.0	1.4	0.0
BL5	2204.7	0.0	2.0	0.7	0.0	0.0	0.0	0.0	0.0	0.0	0.0	3.6	0.0	0.0
BL5	2205.8	0.0	22.0	0.3	0.7	5.0	0.0	0.3	0.0	0.0	0.0	1.3	0.0	0.0
BL5	2206.6	0.0	11.7	0.3	0.3	0.3	0.0	0.0	0.0	0.0	0.0	1.3	0.0	0.3
BL5	2206.9	0.0	12.0	1.0	1.7	3.3	1.0	0.0	0.0	0.0	0.0	3.7	0.0	0.0
BL5	2207.1	0.0	10.3	0.3	0.3	0.3	0.0	0.0	0.0	0.0	0.0	7.0	0.0	0.0
BL5	2208.0	0.0	10.0	0.6	0.0	0.0	0.0	0.0	0.0	0.0	0.0	0.6	0.0	0.0
BL5	2208.9	0.0	1.3	1.3	0.0	0.0	0.0	0.0	0.0	0.0	1.3	0.3	1.3	0.0
BL5	2209.2	0.0	3.9	0.0	0.0	0.0	0.0	0.3	0.0	0.0	0.0	1.0	0.0	0.3
BL5	2209.5	0.0	1.0	0.0	0.0	0.0	0.0	0.0	0.0	0.0	0.0	1.0	0.0	0.0
BL5	2210.4	1.0	0.3	0.7	0.0	0.0	0.3	0.0	0.0	0.0	0.0	0.0	0.0	0.0
BL5	2211.4	0.0	2.3	0.0	0.0	0.0	0.0	0.0	0.3	0.0	0.0	1.0	0.3	0.0
BL5	2211.6	0.0	2.0	0.0	0.0	0.0	0.3	0.0	0.0	0.0	0.0	0.3	0.0	0.0
BL5	2211.6	0.0	1.7	0.0	0.0	0.0	0.3	0.0	0.0	0.0	0.0	2.3	0.0	0.0
	Mean	0.49	2.70	0.21	0.08	0.30	0.14	0.06	0.04	0.10	0.1	1.7	0.1	0.1
Well	**Depth (m)**	**%Pore-Filling Pyrite**	**%Replacive Pyrite**	**%Apatite Pore-Filling**	**%Apatite Detrital**	**%Others Pore-Filling**	**%Organic Material**	**%Extrabasinal-Mudstone**	**%Matrix**	**%Pore-Filling Cements**	**IGV(PMc)**		**CEPL (Houseknecht)**	**COPL**
PW3	1082.3	1.0	0.0	1.0	0.3	0.0	0.0	0.0	2.0	39.7	39.7		94.5	5.5
PW3	1085.1	0.0	0.0	0.0	0.3	0.0	0.3	0.0	0.3	39.1	41.7		93.0	0.8
PW3	1087.5	0.3	0.0	0.0	0.0	0.0	0.0	0.0	0.3	32.7	34.0		77.8	19.1
PW3	1088.3	0.7	0.0	2.3	0.3	0.3	0.3	0.0	29.4	30.4	31.0		72.3	26.3
PW3	1088.5	1.3	0.0	0.3	0.0	0.0	0.0	0.0	30.7	26.9	29.9		64.1	28.7
PW3	1091.4	0.0	0.0	0.0	0.3	0.0	0.0	0.0	0.0	34.4	35.4		81.8	15.8
PW3	1091.5	0.7	0.0	0.0	0.0	0.6	0.0	0.0	0.0	32.6	35.3		77.7	15.9
PW3	1094.0	0.3	0.0	0.0	0.0	2.0	0.0	0.0	0.0	30.1	31.8		71.5	24.4
PW3	1098.3	3.3	0.0	0.0	0.0	1.3	0.0	0.0	61.1	17.2	17.5		41.0	58.2
PW7	1122.5	2.3	0.0	0.0	0.0	0.3	0.0	0.0	23.9	47.1	47.1		112.1	−12.1
PW7	1123.2	14.8	1.0	0.0	0.0	1.0	0.0	0.0	0.0	34.9	42.0		83.2	0.1
PW7	1123.3	2.0	1.0	0.0	0.0	0.0	0.0	0.0	16.0	22.9	27.0		54.6	35.8
PW7	1124.0	0.0	0.0	0.0	0.0	0.0	0.0	0.0	0.0	25.3	30.1		60.3	28.5
PW7	1124.9	0.0	0.0	0.0	0.0	0.0	0.0	0.3	0.0	39.8	40.8		94.9	2.7
PW7	1126.0	0.3	0.0	0.0	0.0	0.0	0.0	0.0	0.0	14.8	39.7		35.2	5.5
PW7	1130.0	0.0	0.0	0.0	0.0	0.0	0.0	0.0	0.7	39.5	39.8		94.0	5.2
PW7	1131.6	0.3	0.0	0.0	0.0	0.3	0.0	0.0	0.0	27.6	37.6		65.6	10.4
PW7	1131.7	0.0	0.3	0.0	0.0	0.0	0.3	0.0	0.0	18.9	30.2		44.9	28.0
PW7	1132.9	0.0	0.0	0.0	0.0	0.0	0.0	0.0	0.0	39.8	42.5		94.7	−1.1
PW7	1133.0	0.3	0.0	0.0	0.3	0.0	0.0	0.0	0.0	43.6	43.6		103.9	−3.9
PW7	1134.6	1.0	0.0	0.0	0.0	1.3	0.0	0.0	18.8	19.0	25.4		45.2	39.5
PW7	1135.2	0.3	0.0	0.0	0.0	0.0	0.0	0.0	0.0	29.4	31.4		70.0	25.3
PW7	1135.7	1.7	0.0	0.0	0.0	2.3	0.0	0.0	13.7	21.3	35.4		50.8	15.8
PW7	1136.5	1.0	0.0	0.0	0.0	0.0	0.3	0.0	0.0	13.2	32.9		31.4	21.7
PW7	1137.4	2.0	0.0	0.0	0.0	0.7	0.0	0.0	0.7	18.5	39.8		43.9	5.2
BL5	2194.7	2.0	0.0	0.3	0.3	0.0	0.0	0.0	2.3	38.3	38.6		91.3	8.0
BL5	2195.2	1.3	0.0	0.0	0.0	0.0	1.0	0.0	6.3	44.7	44.7		106.5	−6.5
BL5	2197.9	2.7	0.0	0.0	0.0	0.0	0.0	0.0	13.3	45.8	46.1		109.0	−9.8
BL5	2198.8	1.7	0.0	0.0	0.0	0.0	0.0	0.0	0.0	35.9	36.5		85.5	13.1
BL5	2199.1	1.7	0.0	0.0	0.0	0.0	0.3	0.0	0.3	21.2	35.6		50.4	15.1
BL5	2199.5	4.3	0.0	0.0	0.0	0.7	0.0	0.0	5.7	33.3	40.0		79.2	4.8
BL5	2199.9	1.0	0.0	1.0	0.0	1.7	0.0	0.0	2.3	63.1	63.1		150.3	−50.3
BL5	2201.0	0.7	0.0	0.0	0.0	0.7	0.0	0.0	38.1	28.4	28.4		67.5	32.5
BL5	2201.9	0.0	0.3	0.0	1.0	0.0	0.0	0.0	0.0	34.6	37.3		82.5	11.1
BL5	2202.2	0.0	0.0	0.0	0.0	0.3	0.0	0.0	0.3	31.0	33.6		73.9	19.9
BL5	2204.7	1.0	0.0	0.0	0.0	0.0	0.0	0.0	0.0	18.7	33.1		44.5	21.1
BL5	2205.8	0.7	0.0	0.0	0.0	0.0	0.0	0.0	4.7	32.7	36.0		77.9	14.2
BL5	2206.6	0.3	0.3	0.0	0.0	0.0	0.0	0.0	10.0	43.1	43.8		102.7	−4.4
BL5	2206.9	3.6	0.0	0.0	0.0	0.3	0.0	0.0	19.7	25.6	25.6		61.0	39.0
BL5	2207.1	1.3	1.3	0.0	0.7	0.0	0.0	0.0	16.4	25.3	25.6		60.2	39.0
BL5	2208.0	1.0	0.0	0.0	0.0	0.0	0.0	0.0	13.4	16.3	25.3		38.9	39.8
BL5	2208.9	0.3	0.0	0.0	0.0	0.0	0.0	0.0	0.0	40.7	41.4		96.9	1.4
BL5	2209.2	0.0	0.0	0.0	0.0	0.0	0.0	0.0	1.0	20.3	33.4		48.3	20.6
BL5	2209.5	0.0	0.0	0.0	0.0	0.0	0.3	0.0	0.3	11.3	28.4		27.0	32.3
BL5	2210.4	1.0	0.0	0.0	0.0	1.0	0.0	0.0	2.7	28.0	32.3		66.7	23.0
BL5	2211.4	1.3	0.3	0.0	0.0	1.3	1.6	0.0	0.0	13.8	31.3		32.8	25.5
BL5	2211.6	0.0	0.0	0.0	0.0	0.3	0.7	0.0	2.9	16.4	25.0		39.0	40.5
BL5	2211.6	0.7	0.0	0.0	0.0	1.3	1.6	0.0	0.0	17.6	32.9		41.8	21.6
	Mean	1.3	0.1	0.1	0.1	0.4	0.1	0.0	7.0	29.7	35.4		70.7	15.7

Chapter 6: Synthesis, discussion and conclusions

The porosity and permeability evolution of sandstones depends on factors including source-area mineralogy (provenance), transport and hydrodynamic processes that serve to split different minerals via grain size separation processes, depositional environment, diagenesis via effective stress history, burial history, thermal history, hydrocarbon charge and structural deformation (Worden et al. 2018d). Although the effects of the above-listed factors occur in deeply buried reservoirs, the influences may be irregular or reversed during burial (Wilson & Stanton 1994). Understanding the inter-relations between these factors will not only identify the dominant controls on reservoir quality but also allow reservoir quality prediction away from wells.

The shallow marine sandstones investigated in this study are from the Weald Basin and have relatively low porosity for their burial depths of less than 900m (Fig. 5.15). They have a detrital mineral assemblage massively dominated by quartz, but also with feldspars, iron ooids and local enrichments of bioclasts (Figs. 5.7). They also show minor but abnormal quartz cementation for their shallow depths, and authigenic quartz inhibition by berthierine grain coats (Figs. 5.10c and 5.10d). These coarse siliciclastic rocks were deposited during a period of active tectonism and sea level rise (Fig. 4.1c). These rocks are also in the eogenetic regime approaching the boundary with mesogenetic processes hence can provide useful insight into pre-mesogenetic sediment conditioning (Worden et al. 2018d).

To understand the controls on reservoir quality for these rocks, this study investigated the fundamental controls on reservoir quality starting from provenance analysis and depositional controls on the siliciclastic sediments (Dickinson 1985), through climatic controls as expressed in rock mineralogy and weathering characteristics (Ruffell & Rawson 1994). The study further analysed the depositional controls on facies distribution (Hampson & Storms 2003) and sediment mineralogical distribution (McBride 1963; Odom et al. 1976). The study further investigated the evidence of depositional controls viz. tectonism, eustasy and climate on sediment supply, reservoir architecture and reservoir quality distribution. Finally, the study has highlighted the main controls and effects of shallow burial diagenetic evolution on reservoir quality. The following sections will answer some of the key questions posed in the introduction to this thesis.

6.1 Discussion and response to key questions

6.1.1 What is the provenance of the Corallian sandstones?

Point count analysis indicate that the Corallian sandstones are derived from a quartzose recycled orogen (Fig. 3.8b) typically where stratified rocks are deformed, uplifted and eroded (Dickinson & Suczek 1979; Dickinson 1985). Detrital mineralogy in the Corallian sandstones is dominated by medium-grained monocrystalline quartz grains (Table 3.1, Fig. 3.6a and 3.8b) which indicates an original plutonic igneous or metamorphic source-area (Pettijohn et al. 1973). Polycrystalline quartz constitutes up to 16% (average 10.04%) and with quartzites, constitute the dominant lithic grains (Fig. 3.8c and Table 3.1) to indicate metamorphic provenance (Blatt 1967; Pettijohn et al. 1973; Basu et al. 1975). Lithic grains of sedimentary origin e.g. extrabasinal mudstone are also present (Table 3.1) which suggests reworking of both sedimentary and metamorphic rocks (Dickinson & Suczek 1979). The Corallian sandstones are therefore most likely sourced from a metasedimenary source-area.

Geochemical analysis using Ti-Al atomic fractions (Andersson & Worden 2004) indicate a mixed mafic-felsic (intermediate) provenance for the Corallian sandstones (Fig. 3.4a) which have been enriched in quartz by hydrological sorting (Fig. 3.4b). The samples were conditioned for hydrological sorting by intense weathering indicated by the elevated Al to K content in Figure 3.4c. Textural indicators including rounding and grain sorting as well as the high maturity of the sandstones suggest significant transport hence substantial weathering and hydrologic sorting during transport (Figs. 5.7c, 5.9a and Table 5.2). Fe-Al cross plot of the Corallian samples indicate a significant Fe input from the source area as evidence in the occurrence of detrital biotite (Fig. 3.6c and 3.6d). Fe was enriched by sedimentological processes such as weathering of Fe-rich source-area as shown by vast sample points plotting off the basalt and granite lines in Figure 3.4d and presence of Fe-ooids which indicates transport over Fe-rich pathways (Fig. 3.7b).

The high iron content, dominance of kaolinite over smectite and evaporites (Fig. 3.6, Table 5.A1), presence of coarse siliciclastic grains (Figs. 3.6 and 3.9a) and embayment in quartz grains indicate a humid hinterland climate with high rainfall rates conducive for acidic chemical oxidation and fluvial transport of medium-grained sands (Cleary & Conolly 1971; Potter 1978; McKinley et al. 2003b; Worden & Morad 2003a).

The main provenance implications for the reservoir quality of the Corallian sandstones include the supply of significant quantities of brittle monocrystalline and polycrystalline quartz which were enriched by hydrologic sorting thereby enhancing resistance to mechanical compaction. Another important implication is the supply of significant quantities of iron which have implications for the development of important reservoir quality preserving minerals such as berthierine and chlorite (Aagaard et al. 2000; Worden & Morad 2000; Worden & Morad 2003b; Worden et al. 2020b; Barshep & Worden 2021).

6.1.2 What are the controls on sediment transport, deposition and redistribution in the Weald Basin?

The predominantly medium-grained Corallian sandstones of the Weald Basin were deposited in a tectonically active phase (Butler & Pullan 1990; Hawkes et al. 1998; Hansen et al. 2002), during a period of general sea level rise (Hallam 1975; Hardenbol et al. 1998; Haq 2017). The occurrence of detrital kaolinite (Fig. 4.11b and d), Fe-ooids and medium-grained mature sands indicates significant rainfall that promoted fluvial discharge and sediment transport to the basin, as well as caused source-area weathering (Fig. 3.4c), (Ruffell & Rawson 1994; Leeder et al. 1998). This is because significant rainfall will produce a verdant source-area capable of significant fluvial recharge, transport of medium grained siliciclastics and decay of organic matter which will produce acidic conditions required for intense chemical weathering to form kaolinite (Burley & Worden 2003a; McKinley et al. 2003a). Upper Jurassic tectonism in the Weald area was accompanied by the relatively stable London Platform (Chadwick 1985b; Hawkes et al. 1998) thereby creating a gradient for fluvial sediment transport. The occurrence of coarsening upward cycles (Figs. 4.5-4.7) during transgression indicates that sediment supply outpaced sea level rise which is typical of tectonically-driven sediment transport (de Wet 1998). This is because tectonically-driven subsidence increases accommodation space, increases source to sink gradient and accelerates coarse siliciclastic sediment supply (Walker & James 1992). An example of increased gradient and sediment supply is the thicker Corallian section downdip of the fault separating BL5 from the Palmers Wood wells (Figs. 4.7, 4.8) e.g. Childs et al. (2003). Other evidence of fault-controlled sediment accumulation include anomalous, as well as short-range, juxtaposition of facies associations (Sun 1992; de Wet 1998; Cecil 2013; Castro et al. 2019) as observed in the juxtaposition of upper shoreface and distal lower shoreface sands in sandstone packages S3 (Fig. 4.8).

The sediment distribution in the basin is controlled by accommodation and redistributed by wave and storm activity as well as tectonism. Evidence of storm activity include the presence of massive beds as well as erosional discontinuities (Figs. 4.2, 4.4, 4.5 and 4.6), typical of high energy deposition following storms. Other evidence of high energy wave deposition include lenticular bedding, trough cross-stratification, planar cross-stratification and wave ripple lamination (Figs 4.4, 4.5 and 4.6).

Sediment redistribution within the basin occurred across Palmers Wood and Bletchingley. The Palmers Wood wells have coarser grain sizes (Fig. 3.9a), more bioclasts (Fig. 4.12d) as well as more sedimentary structures typical of high energy deposition such as massive bedding and trough-cross bedding (Fig. 4.4-4.6). The Bletchingley area has finer-grained fractions (Fig. 3.9a), more monocrystalline quartz (Fig. 3.9b), more feldspars (Figs. 3.10b and 3.10c), more zircon (Fig. 3.10d) and rutile (Fig. 3.10e), less bioclasts (Fig. 4.12d) and more sedimentary structures typical of low energy deposition such as bioturbation, flaser bedding and mud drapes (Figs. 4.4-4.6). These differences emphasise hydrodynamic controls on sediment redistribution in the Basin. It also emphasises the effect of fault displacement which caused greater water depths in the Bletchingley area compared to Palmers Wood (Fig. 4.14) hence deposition of finer-grained, more feldspathic recycled sediments from the higher energy Palmers Wood area.

Sea level rise played a relatively minor role in deposition as seen in the regionally correlated argillaceous intra-Corallian (Figs. 4.7, 4.8). The intra-Corallian is of regional extent and was described as lithofacies unit 4 by Sun (1992) and correlated in the Palmers Wood, Bletchingley and Collendean Farm 1 in the Weald Basin, as well as in the Wessex Basin (Sun 1989). The deposition of the regionally correlated fine-grained argillaceous intra-Corallian is indicative of sea level rise temporarily outpacing coarse siliciclastic sediment supply.

6.1.3 What were the consequences of syn-sedimentary tectonism on reservoir architecture and reservoir properties (especially porosity)?

The main effect of syn-tectonism within the Weald Basin was the reduction in energy across the fault separating BL5 from PW3 and PW7. Downdip fault displacement in the Bletchingley area caused an increase in local water depth (Fig. 4.13) with consequent deposition of lower energy facies associations in the Bletchingley area (Fig. 4.8). Intermittent fault movement at the top of the Corallian section, evident in BL5 (upper sand package S3) caused irregular deposition of distal lower shoreface and proximal lower shoreface sands facies associations

within Upper shoreface sands (Fig. 4.9). Unlike other facies associations in the Bletchingley area, S3 does not correlate with any of the sand bodies in the Palmers Wood area (Fig. 4.8). S3 also has intense calcite cementation (Fig. 4.6) and hence lower porosity (Fig. 4.8) and hydrocarbon charge effectively illustrating how tectonism has caused diagenetic reservoir compartmentalisation.

The lower energy sediments deposited downdip of the fault have lower porosity (Fig. 4.13a), finer grain sizes (Fig. 3.9a), fewer bioclasts (Fig. 4.13d), less calcite cement (Fig. 4.13b) and a greater quantity of clay minerals (Fig. 4.13c). The finer grain size, lower calcite and higher clay mineral contents are due to hydrodynamic controls where lower density sediments were deposited under lower energy conditions deeper water conditions (Tucker 1981; Walker & James 1992). The less abundant bioclasts correspondingly neomorphosed to less abundant calcite (Scholle & Ulmer-Scholle 2003; Worden et al. 2019) in the Bletchingley area. Higher clay content on the downthrown side caused lower porosity in the Bletchingley area (Figs. 4.12a and 4.12c). Syn-tectonic sedimentation therefore led to lower porosity on the downthrown fault area of the Corallian sandstones reservoir.

6.1.4 What controls reservoir quality in these sandstones

As a general rule, porosity and permeability in sandstones typically decrease with burial (Gluyas & Cade 1997; Ramm et al. 1997b) as well as age (Ehrenberg et al. 2009). However other factors, such as primary mineralogy, uplift, pore-fluid chemistry, temperature and hydrocarbon charge, can interlink in any number of ways to influence reservoir quality (Taylor et al. 2010) (Figs.5.19). It is therefore critical for reservoir quality prediction to assess how these factors combine to modify sandstones. The Corallian sandstones do not show significant evidence of porosity-loss by compaction (Figs. 5.15b and 5.17). The predominantly quartzose lithology of the Corallian sandstones (Figs. 3.6, 3.7,4.9,4.11, 5.6 and 5.9), means that they are able to resist mechanical compaction during burial compared to sandstones rich in ductile grains (Houseknecht 1984, 1987; Chuhan et al. 2002). The absence of compactional porosity-loss is emphasised by the open-framework grain structure in the sandstones where detrital grain show face-to edge contacts with no evidence of pressure solution (Figs. 3.6a, 3.6b, 4.10a, 5.11). The absence of chemical compaction in these sandstones is expected as they have been buried to much less than 2000m (Gluyas & Cade 1997; Bjorlykke et al. 2009) (Fig. 5.15). The modelled compactional porosity-depth curve after (Ramm et al. 1997b) shows the porosity-

loss for these sandstones, at their current and maximum buried depth, exceeds the expected loss by compaction alone (Fig. 5.15b). The modelled compaction versus cementation porosity-loss plot after Houseknecht (1987) (Fig. 5.17) shows that cementation is a dominant control on porosity-loss in these sandstones.

The Corallian sandstones do not seem to show strong depositional controls on reservoir quality (Figs. 4.12 and 5.17). The muted depositional controls on porosity can be seen in Figure 4.12a where density porosity is lower in BL5 but does not show any definite patterns by facies association when compared to PW3 and PW7 (Fig. 4.12a). Cross-plots of porosity and permeability also do not show a unique relationship for high and low reservoir quality by grain size, sorting or facies association (Fig. 5.18a and 5.18b). The cross-plots, however, show a relationship between pore-filling calcite and clay with reservoir quality with the best reservoir quality in the calcite-poor, clay-poor samples and the worst reservoir quality in the calcite-rich, clay-rich samples (Fig. 5.18c). Moderate porosity samples with high clay content show lower permeability for their porosity range (Fig. 5.19) indicating that clay mineral content plays a significant role in permeability-loss.

The hydrodynamic enrichment and supply of quartz-rich sand from the mixed mafic-felsic source-area caused limited compaction during early burial. The development of early calcite cement, derived from contemporaneously deposited bioclasts, reinforced the mechanical resistance of the quartzose sandstone and inhibited mechanical compaction through burial (Figs. 4.9, 5.7c and 6.1). Calcite neomorphism and cementation, even in the ductile-rich argillaceous sections (Fig. 4.11a and 4.11b), inhibited mechanical compaction (Worden et al. 2018c) , reduced porosity and, in the case of the intra-Corallian, formed a horizontal baffle to vertical fluid flow (Fig 4.7).

Calcite cementation is volumetrically dominant in the Corallian sandstones (Table 5.A1) and is the main cause of reservoir quality destruction. Other cements that filled pore spaces include quartz, pyrite, siderite, apatite, berthierine, dolomite, illite and kaolinite (Table 5.A1)

Reservoir quality was improved by dissolution of unstable grains (Surdam & Crossey 1985; Emery et al. 1990), e.g., feldspars and Fe-ooids (Figs. 4.9a, 4.9d, 5.7a, 5.7b, 5.7d, 5.9b and 5.10c). Dissolution of feldspars and ooids occurred under acidic conditions (Emery et al. 1990; Fritz & Toth 1997), when the minerals' constituent elements were undersaturated in pore

waters. Dissolution of calcite cement also enhanced reservoir quality and, together with berthierine and feldspar dissolution, makes up about 3% of total rock volume (Table 5.A1).

Reservoir quality was preserved by grain replacive cements as well as berthierine grain coats. The grain replacive cements include calcite which replaced dissolved grains such as bioclasts (Fig. 4.10) as well as feldspars (Fig. 5.9a), dolomite (5.10a), siderite (Fig. 5.10b), kaolinite (Fig. 5.7c), pyrite (Fig. 5.7b) and berthierine (Figs. 4.10c and 5.8a). Reservoir quality preservation by berthierine coats on detrital quartz (Figs. 5.10c) is significant as berthierine is a precursor mineral for chlorite whose grain coats preserve porosity during burial diagenesis (Worden et al. 2020b).

6.1.5 What are the key aspects of diagenesis to consider in assessment and prediction of reservoir quality in shallow buried, shallow marine siliciclastic rocks?

Shallow marine environments are prone to terrestrial and marine influences which affect the characteristics of sediments that are deposited within them. As sandstone compositions are linked to provenance, sediment weathering, transport and deposition processes, as well as the type of basin (Dickinson 1985), important aspects to consider in the analysis of shallow marine siliciclastic rocks include provenance, weathering and transport regimes, depositional environment as well as depositional controls.

6.1.5.1 Provenance, weathering and transport

Given that provenance, weathering and transport characteristics controls the primary composition of sediments which in turn affects how the sediments will behave during burial (Ingersoll 1990). The relatively low proportion of ductile grains in the Corallian sandstones (Fig. 5.6) and the predominant hydrologically enriched quartzose lithology, has inhibited mechanical compaction (Figs. 5.7, 5.15b, 5.17). The quartzose lithology also provides abundant nucleating surfaces for early quartz cementation which promotes rigid rock composition and inhibits mechanical compaction (Bjørlykke 2014) (Fig. 5.7d). The presence of detrital kaolinite, Fe-minerals and sediment maturity in the sandstones points to intense weathering conditions in the hinterland to produce mature sediments (Hallam 1975; Ruffell & Rawson 1994). This indicates hinterland weathering as a key factor to consider in analysis of shallow marine sandstones. The high iron content indicates intense chemical weathering of iron-rich hinterland under humid conditions necessary for weathering ferricrete and supplying iron to the basin (Macquaker et al. 1996). It also indicates sediments were sourced over areas

of sedimentological Fe-enrichment e.g. Fe-ooid formation (Fig. 3.7b). High iron content was conducive for the deposition of berthierine coats which preserved porosity. Intense weathering also affects unstable minerals such as feldspars whose instability and dissolution during transport can released silica for shallow quartz cementation (Emery et al. 1990) (Fig. 5.10c).

6.1.5.2 Depositional environment

Shallow reservoirs frequently have strong controls on reservoir quality exerted by provenance and depositional conditions (Bloch & McGowen 1994). However these controls have been reversed by syn-depositional bioclasts in the Corallian sandstones (Fig. 4.10, 5.15b). Shallow-buried sandstone reservoirs are potentially good reservoirs, as they typically have minimal mechanical compaction and less burial diagenetic chemical compaction than sandstones buried deeper than 2000 m (Gluyas & Cade 1997). However the occurrence of micritised bioclasts (Fig. 5.11) indicates deposition under aerobic, nutrient –rich, photic conditions suitable for marine biodiversity (Scholle & Ulmer-Scholle 2003). The bioclastic remains of living organisms in these reservoirs caused significant calcite cementation to reverse the expected high reservoir quality (Fig. 5.15). Intense bioturbation has here also caused homogenisation of sand and clay beds (Fig. 5.3) thereby reducing reservoir quality e.g. Needham et al. (2005). Coarse siliciclastic supply to this part of the Weald Basin hindered development of Corallian limestones and mudstones, instead, neomorphism of bioclasts formed cements in the Corallian sandstones (de Wet 1998). The reservoir quality in these shallow buried sand-rich reservoirs have predominantly been affected by biogenic factors within the depositional environment hence emphasising the importance of biological activity on reservoir quality analysis of shallow marine environments.

6.1.5.3 Depositional controls

As observed in this study, sedimentology (presence or absence of reservoir rock) alone is not sufficient for assessing and predicting reservoir quality. An analysis of depositional controls on quartz-rich sands in shallow marine settings can provide useful insight into sediment distribution, reservoir architecture, reservoir quality and reservoir quality distribution. The effect of depositional controls is emphasised in the tectonically-driven sediment supply to the Weald Basin, as well as sediment redistribution in the basin. Tectonism also influenced the distribution of bioclasts and clays and caused the lateral variation in reservoir quality between PW3, PW7 and BL5 (Fig. 4.12a, 4.12c, 4.12d). Eustatic controls caused the deposition of the intra-Corallian section which demarcated the Corallian sandstone into upper and lower units

(Fig.4.7). This is an important consideration in shallow marine reservoirs deposited during highstand conditions as it has implications for vertical connectivity and reservoir production.

6.2 Conclusions

- The Corallian sandstones were sourced from an intermediate hinterland with significant iron sources. The hinterland is typical of a quartzose recycled orogen composed of uplifted and eroded metasedimentary rocks. Physical and chemical weathering in a warm, humid, vegetated hinterland supplied mature sediments and significant iron which formed iron-rich minerals in the Weald Basin. Fe was also enriched in the hinterland by sedimentological processes which also weathered and supplied iron to the Weald Basin.

- Sediment transport to the Weald Basin was predominantly driven by tectonic activity which created a gradient from the source-area to the Basin as well as created a gradient for sediment redistribution within the basin. Tectonic activity also created depth differences within the basin which caused redistribution of fine and coarse sediment. Climate-controlled rainfall and fluvial transport were important to sediment transport over the gradient created by tectonism. There was a strong hydrodynamic control on sediment redistribution in the basin where wave and storm activity deposited coarser-grained sediments in the Palmers Wood area and relatively finer-grained sediments in the Bletchingley area.

- Syn-sedimentary tectonism caused two hydrodynamic regimes in the Corallian sandstones leading to more bioclasts and consequent elevated calcite cementation in the up-dip Palmers Wood area and fewer bioclasts and elevated clay content in the down-dip Bletchingley area. Syn-depositional tectonism caused lateral compartmentalisation of the Corallian reservoir with a low reservoir quality non-correlated reservoir unit at the top of BL5.

- When sediment supply was outpaced by tectonic activity, the low porosity argillaceous intra-Corallian unit was deposited and compartmentalised the Corallian sandstone reservoirs into an upper and lower unit.

- The predominant control on reservoir quality in these sandstones is early calcite cementation. Early calcite cementation reinforced the rigid fabric of the sandstones and hindered porosity-loss from mechanical compaction but caused significant porosity loss from cementation. Other causes of reservoir quality loss include detrital clays, authigenic berthierine, siderite, illite, dolomite, pyrite, quartz, kaolinite and apatite. Reservoir quality

was enhanced by grain and cement dissolution and preserved by early quartz cement inhibiting berthierine grain coats.

- This study has shown that provenance and sedimentology may not be adequate to predict reservoir quality in shallow-buried sandstones. Important aspects to consider in reservoir quality assessment and prediction in shallow-buried shallow-marine siliciclastic rocks include biogenic activity e.g. bioturbation and bioclasts content as well as iron mineral input from the hinterland. Due to the variety and transient nature of sedimentary processes in shallow marine environments, assessment of depositional controls can significantly improve basin-scale prediction of reservoir quality. It is also important to consider the factors which might cause early quartz cementation as well as inhibition of early quartz cements as this study has demonstrated that quartz cementation can occur at shallow depths. Authigenic quartz inhibition can also occur at shallow depths by the chlorite-precursor mineral berthierine.

6.3 Limitations of work

The results of this study have to be seen in light of some limitations which should be borne in mind. These limitations include the lack of previous studies on reservoir quality of the Corallian sandstones in the Palmers Wood and Bletchingley area. There are studies covering the tectonic evolution, regional geology and hydrocarbon potential of the basin (Sellwood et al. 1986; Hawkes et al. 1998; Hansen et al. 2002; Trueman 2003a; Hillis et al. 2008b; Pullan & Butler 2019) but no published work is available on the reservoir quality of the Corallian sandstones in the study locations. This limited the background studies during the planning stages of this research and also limits the available material to compare the results of this study.

The absence of Upper Oxfordian exposures in the source-area also limited the ability to directly compare results from provenance analysis with the Upper Oxfordian source-area geology.

The absence of post-Cretaceous deposits which have been eroded away from the study location (Butler & Pullan 1990; Hawkes et al. 1998) will also limit the accuracy of burial history modelling. The absence of fluid inclusions, as well as vitrinite reflectance data also limited the ability to establish thermal controls during burial modelling

6.4 Implications of work

This study is the first comprehensive study of the diagenetic controls on reservoir quality of the Corallian sandstones in the Palmers Wood and Bletchingley area. In addition to the controls on reservoir quality already discussed, this study highlights the occurrence of eogenetic quartz overgrowths at about 60°C which are generally considered to occur during mesogenesis at temperatures above 70°C (Worden & Morad 2000; Burley & Worden 2003a; Sheldon et al. 2003). The occurrence of eodiagenetic quartz at also emphasises that reactions such as quartz cementation can occur at shallow temperatures thereby adding to the literature on the relative influence of residence time on thermally-driven diagenetic reactions such as quartz cementation. As early quartz cementation reinforces sediments and hinders mechanical compaction, this has implications for studying mechanical compaction in shallow marine sandstones. The occurrence of berthierine grain coats which has here hindered quartz overgrowths significantly adds to the literature about the origins of chlorite grain coats and also shows that reservoir quality preservation begins during eogenesis before the formation of mesogenetic chlorite grain coats.

The inclusion of sedimentological and stratigraphic controls on reservoir quality distribution in chapter four is not routine in reservoir quality studies. The identification of sedimentological controls in bioclast distribution and consequent calcite cementation with resultant differences in reservoir quality across the two fields emphasises the need for integrating sedimentological studies in reservoir quality prediction. In addition, stratigraphic controls are identified in this study as controls for lateral and stratigraphic compartmentalisation of high and low reservoir quality units thereby underscoring the need for detailed stratigraphic studies in reservoir quality analysis.

This study therefore has wider implications for reservoir quality studies in eodiagenetic, bioclast-rich shallow marine environments. It also has applications for studies on the origins of mesogenetic reservoir quality preservation through chlorite coats as well as mesodiagenetic reservoir quality destruction through quartz cementation.

6.5 Suggestions for future work

1. Generations of calcite cement were closely associated which prevented their physical separation for stable isotope analysis. A laser extraction system or micro-beam system

could be used to extract these generations of calcite cement. Secondary Ion Mass Spectroscopic (SIMS) analysis could be carried out on the generations of cement to determine their isotopic, elemental or molecular composition of the calcite phases (Bice et al. 2005; Sano et al. 2005; Drake et al. 2013).

2. Vitrinite reflectance analysis could carried out on the Oxford Clay Formation and the Kimmeridge Clay Formations below and above the Corallian Group respectively to determine their maturity and potential for CO_2 expulsion (Senftle & Landis 1991; Cardott 2012; Bullock et al. 2019). Alternatively, apatite fission track analysis could be carried out from the sandstones in the wells to confirm the burial history (Japsen et al. 2015; Villagómez Díaz et al. 2021).
3. Suitable-sized fluid inclusions are not present in this sandstones for fluid inclusion analysis to constrain the timing and temperature of diagenetic events as well as composition of pore fluids (Goldstein & Reynolds 1994). Nearby wells could be explored for suitable-sized fluid inclusions to provide more data for calibration of timing, temperature and pore-fluid chemistry of diagenetic events.
4. Develop links between petrographic/petrophysical properties and geomechanical properties from wells with a comprehensive suite of logs (namely shear sonic longs (DTS) by using lab measurements - All for the purpose of gas storage feasibility assessment (Worden et al. 2020d) .
5. Undertake benchtop XRF analysis to get a fuller suite of elements including Na and Mg, to improve the geochemical story derived from handheld XRF analysis (Middleton 1960; Nesbitt & Young 1982).
6. A dedicated heavy mineral study could be carried out to firm up the provenance story
7. Work could be extended into the Corallian limestones in both the Palmers Wood and Bletchingley fields to study their deposition, potential role of any clastic sediments, provenance and water depth.
8. A comparison of the Corallian of the Weald Basin to other mixed reservoir systems e.g. the Middle Triassic of Tunisia; and the Shuaiba Limestones of Saudi Arabia.

References

Aagaard, P., Jahren, J., Harstad, A., Nilsen, O. & Ramm, M. 2000. Formation of grain-coating chlorite in sandstones. Laboratory synthesized vs. natural occurrences. *Clay minerals*, **35**, 261-269.

Aase, N.E. & Walderhaug, O. 2005. The effect of hydrocarbons on quartz cementation: diagenesis in the Upper Jurassic sandstones of the Miller Field, North Sea, revisited. *Petroleum Geoscience*, **11**, 215-223.

Aase, N.E., Bjørkum, P.A. & Nadeau, P.H. 1996. The effect of grain-coating microquartz on preservation of reservoir porosity. *Aapg Bulletin*, **80**, 1654-1673.

Adams, A. 1998. *Carbonate sediments and rocks under the microscope: a colour atlas*. Manson Publishing Ltd., London.

Adams, A. & Mackenzie, W.S. 1998. *Carbonate sediments and rocks under the microscope: a colour atlas*. Manson Publishing Ltd., London.

Ajdukiewicz, J. & Lander, R. 2010. Sandstone reservoir quality prediction: The state of the art. *Aapg Bulletin - AAPG BULL*, **94**, 1083-1091, http://doi.org/10.1306/intro060110.

Ajdukiewicz, J.M. & Larese, R.E. 2012. How clay grain coats inhibit quartz cement and preserve porosity in deeply buried sandstones: Observations and experiments. *American Association of Petroleum Geologists Bulletin*, **96**, 2091-2119.

Alcalde, J., Heinemann, N., James, A., Bond, C.E., Ghanbari, S., Mackay, E.J., Haszeldine, R.S., Faulkner, D.R., *et al.* 2021. A criteria-driven approach to the CO2 storage site selection of East Mey for the acorn project in the North Sea. *Marine and Petroleum Geology*, **133**, http://doi.org/10.1016/j.marpetgeo.2021.105309.

Allen, P. 1975. Wealden of the Weald: a new model. *Proceedings of the Geologists' Association*, **86**, 389-437, http://doi.org/https://doi.org/10.1016/S0016-7878(75)80057-5.

Allen, P.A. & Underhill, J.R. 1989. Swaley cross-stratification produced by unidirectional flows, Bencliff Grit (Upper Jurassic), Dorset, UK. *Journal of the Geological Society*, **146**, 241-252, http://doi.org/10.1144/gsjgs.146.2.0241.

Andersson, P. & Worden, R. 2004. Mudstones of the Tanqua Basin, South Africa: An analysis of lateral and stratigraphic variations within mudstones, and a comparison of mudstones within and between turbidite fans. *Sedimentology*, **51**, 479-502, http://doi.org/10.1111/j.1365-3091.2004.00633.x.

Andrews, I. 2014. The Jurassic shales of the Weald Basin: geology and shale oil and shale gas resource estimation. *In*: DECC (ed.). British Geological Survey, London UK, 1-79.

Andrieu, S., Brigaud, B., Barbarand, J., Lasseur, E. & Saucède, T. 2016. Disentangling the control of tectonics, eustasy, trophic conditions and climate on shallow-marine carbonate production during the Aalenian–Oxfordian interval: From the western France platform to the western Tethyan domain. *Sedimentary Geology*, **345**, http://doi.org/10.1016/j.sedgeo.2016.09.005.

Arkell, W. 1933a. *The Jurassic System in Great Britain. Oxford*. Clarendon press, Oxford.

Arkell, W.J. 1933b. *The Jurassic System in Great Britain*. Clarendon Press, Oxford.

Armitage, P.J., Worden, R.H., Faulkner, D.R., Butcher, A.R. & Espie, A.A. 2016. Permeability of the Mercia Mudstone: suitability as caprock to carbon capture and storage sites. *Geofluids*, **16**, 26-42.

Armitage, P.J., Worden, R.H., Faulkner, D.R., Aplin, A.C., Butcher, A.R. & Iliffe, J. 2010. Diagenetic and sedimentary controls on porosity in Lower Carboniferous fine-grained lithologies, Krechba field, Algeria: A petrological study of a caprock to a carbon capture site. *Marine and Petroleum Geology*, **27**, 1395-1410, http://doi.org/10.1016/j.marpetgeo.2010.03.018.

Armitage, P.J., Faulkner, D.R., Worden, R.H., Aplin, A.C., Butcher, A.R. & Iliffe, J. 2011. Experimental measurement of, and controls on, permeability and permeability anisotropy of caprocks from the CO2 storage project at the Krechba Field, Algeria. *Journal of Geophysical Research: Solid Earth*, **116**.

Barclay, S.A. & Worden, R.H. 2000. Effects of reservoir wettability on quartz cementation in oil fields. *Quartz cementation in sandstones*, **29**, 103-117.

Baron, M. & Parnell, J. 2007. Relationships between stylolites and cementation in sandstone reservoirs: Examples from the North Sea, UK and East Greenland. *Sedimentary Geology*, **194**, 17-35.

Barshep, D.V. & Worden, R.H. 2021. Reservoir Quality of Upper Jurassic Corallian Sandstones, Weald Basin, UK. *Geosciences*, **11**, 446, http://doi.org/ https://doi.org/10.3390/geosciences11110446.

Barshep, D.V. & Worden, R.H. 2022. Reservoir quality and sedimentology in shallow marine sandstones: Interplay between sand accumulation and carbonate and clay minerals. *Marine*

and Petroleum Geology, **135**, 105398, http://doi.org/https://doi.org/10.1016/j.marpetgeo.2021.105398.

Basu, A., Young, S.W., Suttner, L.J., James, W.C. & Mack, G.H. 1975. Re-evaluation of the use of undulatory extinction and polycrystallinity in detrital quartz for provenance interpretation. *Journal of Sedimentary Research*, **45**, 873-882, http://doi.org/10.1306/212f6e6f-2b24-11d7-8648000102c1865d.

Beckmann, H. 1976. Geological prospecting of petroleum. Wiley : distributed by Halsted Press, New York :.

Berner, R.A. 1964. Stability fields of iron minerals in anaerobic marine sediments. *The Journal of Geology*, **72**, 826-834.

Bhattacharjee, C. & Mondal, S.K. 2021. Geochemistry of Fe-Ti oxide and sulfide minerals in gabbroic rocks and magnetitite of the Archean Mayurbhanj mafic complex (eastern India): Magma fractionation, thermometry and oxygen fugacity of re-equilibration, and implications for Ni-Cu mineralization. *Ore Geology Reviews*, **131**, 104005, http://doi.org/https://doi.org/10.1016/j.oregeorev.2021.104005.

Bhattacharyya, D.P. 1983. Origin of berthierine in ironstones. *Clays and Clay Minerals*, **31**, 173-182.

Bice, K.L., Layne, G.D. & Dahl, K. 2005. Application of secondary ion mass spectrometry to the determination of Mg/Ca in rare, delicate, or altered planktonic foraminifera: Examples from the Holocene, Paleogene, and Cretaceous. *Geochemistry, Geophysics, Geosystems*, **6**, http://doi.org/https://doi.org/10.1029/2005GC000974.

Bjorkum, P.A. & Gjelsvik, N. 1988. An isochemical model for formation of authigenic kaolinite, K-feldspar and illite in sediments. *Journal of Sedimentary Research*, **58**, 506-511, http://doi.org/10.1306/212f8dd2-2b24-11d7-8648000102c1865d.

Bjørkum, P.A., Oelkers, E., Nadeau, P.H., Walderhaug, O. & Murphy, W.M. 1998a. Porosity Prediction in Quartzose Sandstones as a Function of Time, Temperature, Depth, Stylolite Frequency, and Hydrocarbon Saturation. *Aapg Bulletin*, **82**, 637-647.

Bjørkum, P.A., Oelkers, E.H., Nadeau, P.H., Walderhaug, O. & Murphy, W.M. 1998b. Porosity prediction in quartzose sandstones as a function of time, temperature, depth, stylolite frequency, and hydrocarbon saturation. *Aapg Bulletin*, **82**, 637-648.

Bjorlykke, K., Jahren, J., Mondol, N.H., Marcussen, O., Croize, D., Peltonen, C. & Thyberg, B. 2009. Sediment compaction and rock properties. *Search and Discovery Article*, **50192**.

Bjørlykke, K. 1998. Clay mineral diagenesis in sedimentary basins — a key to the prediction of rock properties. Examples from the North Sea Basin. *Clay minerals*, **33**, 15-34, http://doi.org/10.1180/000985598545390.

Bjørlykke, K. 2014. Relationships between depositional environments, burial history and rock properties. Some principal aspects of diagenetic process in sedimentary basins. *Sedimentary Geology*, **301**, 1-14, http://doi.org/https://doi.org/10.1016/j.sedgeo.2013.12.002.

Bjørlykke, K., ElvekhØI, B.A. & Malm, A. 1979. Diagenesis in Mesozoic sandstones from Spitsbergen and the North Sea—a comparison. *Geologische Rundschau*, **68**, 1152-1171.

Blatt, H. 1967. Original characteristics of clastic quartz grains. *Journal of Sedimentary Research*, **37**, 401-424, http://doi.org/10.1306/74d716e0-2b21-11d7-8648000102c1865d.

Bloch, S. 1994. Importance of Reservoir Quality Prediction in Exploration. *In*: Michael, W.D. (ed) *Reservoir Quality Assessment and Prediction in Clastic Rocks*. SEPM Society for Sedimentary Geology, Tulsa, Oklahoma, **30**, 5-9.

Bloch, S. & McGowen, J. 1994. Influence of depositional environment on reservoir quality prediction. *In*: Wilson, M.D. (ed) *Reservoir Quality Assessment and Prediction in Clastic Rocks*. SEPM, Short Course, Tulsa, Oklahoma, **30**, 41-57.

Bloch, S., Lander, R.H. & Bonnell, L. 2002. Anomalously high porosity and permeability in deeply buried sandstone reservoirs: Origin and predictability. *American Association of Petroleum Geologists Bulletin*, **86**, 301-328.

Boggs, J., Sam. 2009a. Provenance of siliciclastic sedimentary rocks. *In*: Boggs, J.S. (ed) *Petrology of Sedimentary Rocks*. Cambridge University Press, Cambridge, 220-267.

Boggs, S. 2009b. *Petrology of sedimentary rocks. [electronic book]*. Cambridge : Cambridge University Press, c2009.

2nd ed.

Brand, N.W. & Brand, C.J. 2014. Performance comparison of portable XRF instruments. *Geochemistry: Exploration, Environment, Analysis*, **14**, 125.

Brookfield, M. 1973. Palaeogeography of the upper Oxfordian and Lower Kimmeridgian (Jurassic) in Britain. *Palaeogeography, Palaeoclimatology, Palaeoecology*, **14**, 137-167, http://doi.org/https://doi.org/10.1016/0031-0182(73)90009-6.

Bryant, l.D., Kantorowicz, J.D. & Love, C.F. 1988. The origin and recognition of laterally continuous carbonate-cemented horizons in the Upper Lias Sands of southern England. *Marine and Petroleum Geology*, **5**, 108-133, http://doi.org/https://doi.org/10.1016/0264-8172(88)90018-9.

Budd, D.A., Hammes, U. & Ward, W.B. 2000. Cathodoluminescence in Calcite Cements: New Insights on Pb and Zn Sensitizing, Mn Activation, and Fe Quenching at Low Trace-Element Concentrations. *Journal of Sedimentary Research*, **70**, 217-226.

Bullock, L., Parnell, J., Muirhead, D., Armstrong, J., Schito, A. & Corrado, S. 2019. A thermal maturity map based on vitrinite reflectance of British coals. *Journal of the Geological Society*, **176**, 1136, http://doi.org/10.1144/jgs2019-055.

Burley, S. & Worden, R.H. 2003a. *Sandstone diagenesis: recent and ancient*. 1 ed. International Association of Sedimentologists, Blackwell Publishing Ltd, Oxford.

Burley, S.D. & Worden, R.H. 2003b. *Sandstone diagenesis. [electronic book] : recent and ancient*. Malden, MA ; Blackwell Publishing, 2003.

Burton, R., Kendall, C.G.S.C. & Lerche, I. 1987. Out of our depth: on the impossibility of fathoming eustasy from the stratigraphic record. *Earth-Science Reviews*, **24**, 237-277, http://doi.org/https://doi.org/10.1016/0012-8252(87)90062-6.

Butler, M. & Pullan, C.P. 1990. Tertiary structures and hydrocarbon entrapment in the Weald Basin of southern England. *Geological Society, London, Special Publications*, **55**, 371-391, http://doi.org/10.1144/gsl.sp.1990.055.01.19.

Byrnes, A.P. 1994. Empirical methods of reservoir quality prediction. *In*: M.D, W. (ed) *Reservoir quality assessment and prediction in clastic rocks*. SEPM Short Course 30, Tulsa, Oklahoma, 9-21.

Canfield, D. & Raiswell, R. 1991. Pyrite Formation and Fossil Preservation, 337-387.

Caracciolo, L. 2020. Sediment generation and sediment routing systems from a quantitative provenance analysis perspective: Review, application and future development. *Earth-Science Reviews*, **209**, 103226, http://doi.org/10.1016/j.earscirev.2020.103226.

Cardott, B. 2012. Introduction to vitrinite reflectance as a thermal maturity indicator. *Tulsa Geological Society luncheon, Tulsa*.

Carroll, D. 1953. Weatherability of zircon. *Journal of Sedimentary Research*, **23**, 106-116, http://doi.org/10.1306/d4269562-2b26-11d7-8648000102c1865d.

Castro, H.R., Figueiredo, F.T., Franco, L.S., Gomes, P.V., Soares, I.R., Andrade, L.L., Ramos, M.A. & Moraes, J.D. 2019. Facies distribution as a response to early rift tectonic activity in the Sergipe-Alagoas Basin, northeastern Brazil. *Sedimentary Geology*, **383**, 216-237.

Cecil, C.B. 2013. An overview and interpretation of autocyclic and allocyclic processes and the accumulation of strata during the Pennsylvanian–Permian transition in the central Appalachian Basin, USA. *International Journal of Coal Geology*, **119**, 21-31, http://doi.org/https://doi.org/10.1016/j.coal.2013.07.012.

Chadwick, R. 1985a. Permian, Mesozoic and Cenozoic structural evolution of England and Wales in relation to the principles of extension and inversion tectonics. *In*: Whittaker, A. (ed) *Atlas of onshore sedimentary basins in England and Wales: Post-Carboniferous tectonics and stratigraphy*. Blackie, Glasgow, 9-25.

Chadwick, R. 1985b. Cenozoic sedimentation, subsidence and tectonic inversion. *In*: Whittaker, A. (ed) *Atlas of Onshore Sedimentary Basins in England and Wales*. Blackie, Glasgow, 61-63.

Chadwick, R. 1993. Aspects of basin inversion in southern Britain. *Journal of the Geological Society*, **150**, 311-322.

Childs, C., Nicol, A., Walsh, J.J. & Watterson, J. 2003. The growth and propagation of synsedimentary faults. *Journal of Structural Geology*, **25**, 633-648, http://doi.org/10.1016/S0191-8141(02)00054-8.

Choquette, P.W. & Pray, L.C. 1970. GEOLOGIC NOMENCLATURE AND CLASSIFICATION OF POROSITY IN SEDIMENTARY CARBONATES. *American Association of Petroleum Geologists Bulletin*, **54**, 207-+.

Chuhan, F.A., Kjeldstad, A., Bjørlykke, K.O. & Høeg, K. 2002. Porosity loss in sand by grain crushin‡ experimental evidence and relevance to reservoir quality. *Marine and Petroleum Geology*, **19**, 39-53.

Chung, F.H. 1974. Quantitative interpretation of X-ray diffraction patterns of mixtures. I. Matrix-flushing method for quantitative multicomponent analysis. *Journal of Applied Crystallography*, **7**, 519-525, http://doi.org/https://doi.org/10.1107/S0021889874010375.

Cleary, W.J. & Conolly, J.R. 1971. Distribution and Genesis of Quartz in a Piedmont-Coastal Plain Environment. *GSA Bulletin*, **82**, 2755-2766, http://doi.org/10.1130/0016-7606(1971)82[2755:Dagoqi]2.0.Co;2.

Conybeare, C.E.B. 2013. *Lithostratigraphic analysis of sedimentary basins*. Academic Press, New York.

Crocker, M.E. & Marchin, L.M. 1988. Wettability and Adsorption Characteristics of Crude-Oil Asphaltene and Polar Fractions. *Journal of Petroleum Technology*, **40**, 470-474, http://doi.org/10.2118/14885-pa.

Dailly, G. 1975. Some remarks on regression and transgression in deltaic sediments. *In*: Yorath, C.J., Parker, E.R. & Glass, D.J. (eds) *Canada's Continental Margins and Offshore Petroleum Exploration*. Canadian Society of Petroleum Geologists, Calgary, Alberta, Canada, **Memoir, 4**, 791-820.

Damuth, J.E. & Fairbridge, R.W. 1970. Equatorial Atlantic Deep-Sea Arkosic Sands and Ice-Age Aridity in Tropical South America. *GSA Bulletin*, **81**, 189-206, http://doi.org/10.1130/0016-7606(1970)81[189:Eadasa]2.0.Co;2.

Daneshvar, E. & Worden, R.H. 2017. Feldspar alteration and Fe minerals: origin, distribution and implications for sandstone reservoir quality in estuarine sediments. *Geological Society, London, Special Publications*, **435**, SP435. 417.

Dapples, E.C., Krumbein, W.C. & Sloss, L.L. 1953. Petrographic and Lithologic Attributes of Sandstones. *The Journal of Geology*, **61**, 291-317.

de Wet, C.B. 1987. Deposition and diagenesis in an extensional basin: the Corallian Formation (Jurassic) near Oxford, England. *Geological Society, London, Special Publications*, **36**, 339-353, http://doi.org/10.1144/gsl.sp.1987.036.01.24.

de Wet, C.B. 1998. Deciphering the sedimentological expression of tectonics, eustasy, and climate: a basinwide study of the Corallian Formation, southern England. *Journal of Sedimentary Research*, **68**, 653-667.

Dickinson, W.R. 1985. Interpreting Provenance Relations from Detrital Modes of Sandstones. *In*: Zuffa, G.G. (ed) *Provenance of Arenites*. Springer Netherlands, Dordrecht, 333-361.

Dickinson, W.R. 1988. Provenance and sediment dispersal in relation to paleotectonics and paleogeography of sedimentary basins *New perspectives in basin analysis*. Springer, 3-25.

Dickinson, W.R. & Suczek, C.A. 1979. PLATE-TECTONICS AND SANDSTONE COMPOSITIONS. *Aapg Bulletin-American Association of Petroleum Geologists*, **63**, 2164-2182.

Dokuz, A. & Tanyolu, E. 2006. Geochemical constraints on the provenance, mineral sorting and subaerial weathering of Lower Jurassic and Upper Cretaceous clastic rocks of the eastern Pontides, Yusufeli (Artvin), NE Turkey. *Turkish Journal of Earth Sciences*, **15**, 181-209.

Downing, R.A., Allen, D.J., Barker, J.A., Burgess, W.G., Gray, D.A., Price, M. & Smith, I.F. 1983. Geothermal Exploration at Southampton in the UK: A Case Study of a Low Enthalpy Resource. *Energy Exploration & Exploitation*, **2**, 327-342.

Drake, H., Astrom, M., Tullborg, E.-L., Whitehouse, M. & Fallick, A.E. 2013. Variability of sulphur isotope ratios in pyrite and dissolved sulphate in granitoid fractures down to 1 km depth – Evidence for widespread activity of sulphur reducing bacteria. *Geochimica et Cosmochimica Acta*, **102**, 143–161, http://doi.org/10.1016/j.gca.2012.10.036.

Ebukanson, E.J. 1984. *An investigation of some potential Jurassic hydrocarbon source rocks of Southern England.* University of London.

Ebukanson, E.J. & Kinghorn, R.R.F. 1986. Oil and gas accumulations and their possible source rocks in southern England. *Journal of Petroleum Geology*, **9**, 413-427.

Ehrenberg, S., Nadeau, P.H. & Steen, Ø. 2009. Petroleum reservoir porosity versus depth: Influence of geological age. *Aapg Bulletin*, **93**, 1281-1296, http://doi.org/10.1306/06120908163.

Ehrenberg, S.N. 1993. Preservation of anomalously high porosity in deeply buried sandstones by grain-coating chlorite: examples from the Norwegian continental shelf. *American Association of Petroleum Geologists Bulletin*, **77**, 1260-1286.

Ehrenberg, S.N. 1997. Influence of depositional sand quality and diagenesis on porosity and permeability; examples from Brent Group reservoirs, northern North Sea. *Journal of Sedimentary Research*, **67**, 197-211.

Ehrenberg, S.N. & Nadeau, P.H. 1989. Formation of diagenetic illite in sandstones of the Garn Formation, Haltenbanken area, mid-Norwegian continental shelf. *Clay minerals*, **24**, 233-253.

Emery, D., Myers, K.J. & Young, R. 1990. Ancient subaerial exposure and freshwater leaching in sandstones. *Geology*, **18**, 1178-1181, http://doi.org/10.1130/0091-7613(1990)018<1178:Aseafl>2.3.Co;2.

Everett, P., Lister, T., Fordyce, F., Ferreira, A., Donald, A., Gowing, C. & Lawley, R. 2019. *Stream sediment geochemical atlas of the United Kingdom*. British Geological Survey.

Farrell, K.M., Harris, W.B., Mallinson, D.J., Culver, S.J., Riggs, S.R., Pierson, J., Self-Trail, J.M. & Lautier, J.C. 2012. Standardizing texture and facies codes for a process-based classification of clastic sediment and rock. *Journal of Sedimentary Research*, **82**, 364-378.

Fawad, M., Mondol, N., Jahren, J. & Bjørlykke, K. 2010. Microfabric and rock properties of experimentally compressed silt-clay mixtures. *Marine and Petroleum Geology - MAR PETROL GEOL*, **27**, 1698-1712, http://doi.org/10.1016/j.marpetgeo.2009.10.002.

Folk, R.L. 1956. The role of texture and composition in sandstone classification; discussion. *Journal of Sedimentary Research*, **26**, 166-171, http://doi.org/10.1306/74d70506-2b21-11d7-8648000102c1865d.

Folk, R.L. 1968. *Petrology of sedimentary rocks: the University of Texas geology 370K, 383L, 383M*. Austin: Hemphill, 1968.

Folk, R.L. 1980. *Petrology of sedimentary rocks*. Hemphill publishing company.

Fritz, S.J. & Toth, T.A. 1997. An Fe-berthierine from a Cretaceous laterite: Part II. Estimation of Eh, pH and pCO 2 conditions of formation. *Clays and Clay Minerals*, **45**, 580-586.

Fu, Y., van Berk, W., Schulz, H.-M. & Mu, N. 2015. Berthierine formation in reservoir rocks from the Siri oilfield (Danish North Sea) as result of fluid–rock interactions: part II. Deciphering organic–inorganic processes by hydrogeochemical modeling. *Marine and Petroleum Geology*, **65**, 317-326.

Gehring, A.U. 1990. Diagenesis of ferriferous phases in the Northampton ironstone in the Cowthick quarry near Corby (England). *Geological Magazine*, **127**, 169-176, http://doi.org/10.1017/S0016756800013856.

Gier, S., Worden, R.H. & Krois, P. 2015. Comparing clay mineral diagenesis in interbedded sandstones and mudstones, Vienna Basin, Austria. *Special Publication - Geological Society of London*, **435**, http://doi.org/10.1144/SP435.9.

Giles, M.R., Stevenson, S., Martin, S.V., Cannon, S.J.C., Hamilton, P.J., Marshall, J.D. & Samways, G. 1992. The reservoir properties and diagenesis of the Brent Group: a regional perspective. *Geological Society, London, Special Publications*, **61**, 289 - 327.

Glasmann, J.R. 1992. The fate of feldspar in Brent Group reservoirs, North Sea: A regional synthesis of diagenesis in shallow, intermediate, and deep burial environments. *Geological Society, London, Special Publications*, **61**, 329-350.

Glasmann, J.R., Lundegard, P.D., Clark, R.A., Penny, B.K. & Collins, I.D. 1989. Geochemical Evidence for the History of Diagenesis and Fluid Migration: Brent Sandstone, Heather Field, North Sea. *Clay minerals*, **24**, 255-284, http://doi.org/10.1180/claymin.1989.024.2.10.

Gluyas, J. & Cade, C.A. 1997. Prediction of porosity in compacted sands.

Gluyas, J. & Swarbrick, R. 2004. *Petroleum Geoscience*.

Goff, J.C., Demaison, G. & Murris, R.J. 1984. Hydrocarbon Generation and Migration from Jurassic Source Rocks in the East Shetland Basin and Viking Graben of the Northern North Sea *Petroleum Geochemistry and Basin Evaluation*. American Association of Petroleum Geologists, **35**, 0.

Goldhaber, M.B. 2003. Sulfur-rich Sediments. *In*: Mackenzie, F.T. (ed) *Treatise on Geochemistry*. Elsevier, Amsterdam, **7**, 257-289.

Goldring, R., Astin, T.R., Marshall, J.E.A., Gabbott, S. & Jenkins, C.D. 1998. Towards an integrated study of the depositional environment of the Bencliff Grit (Upper Jurassic) of Dorset. *In*: Underhill, J.R. (ed) *Development, Evolution and Petroleum Geology of the Wessex Basin*, **133**, 355-372.

Goldstein, R.H. & Reynolds, T.J. 1994. *Systematics of Fluid Inclusions in Diagenetic Minerals*. SEPM Society for Sedimentary Geology.

Goldstein, R.H. & Rossi, C. 2002. Recrystallization in quartz overgrowths. *Journal of Sedimentary Research*, **72**, 432-440.

Gowland, S. 1996. Facies characteristics and depositional models of highly bioturbated shallow marine siliciclastic strata: An example from the Fulmar Formation (Late Jurassic), UK Central Graben. *Geological Society, London, Special Publications*, **114**, 185-214, http://doi.org/10.1144/GSL.SP.1996.114.01.09.

Griffiths, J., Worden, R.H., Wooldridge, L.J., Utley, J.E.P. & Duller, R.A. 2018. Detrital clay coats, clay minerals, and pyrite: a modern shallow-core analogue for ancient and deeply buried estuarine sandstones. *Journal of Sedimentary Research*, **88**, 1205-1237.

Griffiths, J., Worden, R.H., Wooldridge, L.J., Utley, J.E.P. & Duller, R.A. 2019a. Compositional variation in modern estuarine sands: predicting major controls on sandstone reservoir quality. *American Association of Petroleum Geologists Bulletin*.

Griffiths, J., Worden, R.H., Wooldridge, L.J., Utley, J.E.P. & Duller, R.A. 2019b. Compositional variation in modern estuarine sands: Predicting major controls on sandstone reservoir quality. *American Association of Petroleum Geologists Bulletin*, **103**, 797-833, http://doi.org/10.1306/09181818025.

Griffiths, J., Worden, R.H., Wooldridge, L.J., Utley, J.E.P., Duller, R.A. & Edge, R.L. 2019c. Estuarine clay mineral distribution: Modern analogue for ancient sandstone reservoir quality prediction. *Sedimentology*.

Hallam, A. 1975. *Jurassic environments*. Cambridge University Press, Cambridge.

Hallam, A. 1977. Jurassic bivalve biogeography. *Paleobiology*, **3**, 58-73, http://doi.org/10.1017/S009483730000511X.

Hallam, A. 1978. Eustatic cycles in the Jurassic. *Palaeogeography, Palaeoclimatology, Palaeoecology*, **23**, 1-32, http://doi.org/https://doi.org/10.1016/0031-0182(78)90079-2.

Hallam, A. 1981. A revised sea-level curve for the early Jurassic. *Journal of the Geological Society*, **138**, 735-743.

Hallam, A. 1984. Continental humid and arid zones during the jurassic and cretaceous. *Palaeogeography, Palaeoclimatology, Palaeoecology*, **47**, 195-223, http://doi.org/https://doi.org/10.1016/0031-0182(84)90094-4.

Hallberg, J.A. 1984. A geochemical aid to igneous rock type identification in deeply weathered terrain. *Journal of Geochemical Exploration*, **20**, 1-8, http://doi.org/https://doi.org/10.1016/0375-6742(84)90085-2.

Hampson, G.J. & Storms, J.E. 2003. Geomorphological and sequence stratigraphic variability in wave-dominated, shoreface-shelf parasequences. *Sedimentology*, **50**, 667-701.

Hansen, D.L., Blundell, D.J. & Nielsen, S.B. 2002. A model for the evolution of the Weald Basin. *Bulletin of the Geological Society of Denmark*, **49, Part 2**, 109-118.

Haq, B.U. 2017. Jurassic sea-level variations: a reappraisal. *GSA Today*, **28**, 4-10.

Hardenbol, J., Thierry, J., Farley, M.B., Jacquin, T., De Graciansky, P.-C. & Vail, P.R. 1998. Mesozoic and Cenozoic sequence chronostratigraphic framework of European basins. *Society of Economic Paleontologists and Mineralogists Special Publication*, **60**, 3-13.

Hawkes, P.W., Fraser, A.J. & Einchcomb, C.C.G. 1998. The tectono-stratigraphic development and exploration history of the Weald and Wessex basins, Southern England, UK. *Geological Society, London, Special Publications*, **133**, 39-65, http://doi.org/10.1144/gsl.sp.1998.133.01.03.

Heald, M. & Baker, G. 1977. Diagenesis of the Mt. Simon and Rose Run sandstones in western West Virginia and southern Ohio. *Journal of Sedimentary Research*, **47**.

Heald, M.T. 1959. Significance of stylolites in permeable sandstones. *Journal of Sedimentary Research*, **29**, 251-253, http://doi.org/10.1306/74d708f3-2b21-11d7-8648000102c1865d.

Heasley, E.C., Worden, R.H. & Hendry, J.P. 2000. Cement distribution in a carbonate reservoir: recognition of a palaeo oil-water contact and its relationship to reservoir quality in the Humbly Grove field, onshore, UK. *Marine and Petroleum Geology*, **17**, 639-654, http://doi.org/10.1016/s0264-8172(99)00057-4.

Henares, S., Donselaar, M.E. & Caracciolo, L. 2020. Depositional controls on sediment properties in dryland rivers: Influence on near-surface diagenesis. *Earth-Science Reviews*, **208**, 103297, http://doi.org/https://doi.org/10.1016/j.earscirev.2020.103297.

Herwanger, J.V., Bottrill, A.D. & Mildren, S.D. 2015. Uses and abuses of the brittleness index with applications to hydraulic stimulation. *Unconventional Resources Technology Conference, San Antonio, Texas, 20-22 July 2015*. Society of Exploration Geophysicists, American Association of Petroleum Geologists, Society of Petroleum Engineers, 1215-1223.

Hiatt, E. & Pufahl, P. 2014. Cathodoluminescence petrography of carbonate rocks: a review of applications for understanding diagenesis, reservoir quality and pore system evolution. *Short Course*, **45**, 75-96.

Hillis, R., Holford, S., Green, P., Dore, A., Gatliff, R., Stoker, M., Thomson, K., Turner, J., *et al.* 2008a. Cenozoic exhumation of the southern British Isles. *Geology*, **36**, http://doi.org/10.1130/G24699A.1.

Hillis, R.R., Holford, S.P., Green, P.F., Doré, A.G., Gatliff, R.W., Stoker, M.S., Thomson, K., Turner, J.P., *et al.* 2008b. Cenozoic exhumation of the southern British Isles. *Geology*, **36**, 371-374, http://doi.org/10.1130/g24699a.1.

Ho, C. & Coleman, J.M. 1969. Consolidation and Cementation of Recent Sediments in the Atchafalaya Basin. *GSA Bulletin*, **80**, 183-192, http://doi.org/10.1130/0016-7606(1969)80[183:Cacors]2.0.Co;2.

Hogg, A.J.C., Mitchell, A.W. & Young, S. 1996. Predicting well productivity from grain size analysis and logging while drilling. *Petroleum Geoscience*, **2**, 1-15, http://doi.org/10.1144/petgeo.2.1.1.

Houseknecht, D.W. 1984. Influence of grain size and temperature on intergranular pressure solution, quartz cementation, and porosity in a quartzose sandstone. *Journal of Sedimentary Research*, **54**, 348-361.

Houseknecht, D.W. 1987. Assessing the relative importance of compaction processes and cementation to reduction of porosity in sandstones. *AAPG (Am. Assoc. Pet. Geol.) bulletin*, **71**, 633-642.

Hubert, J.F. 1962. A zircon-tourmaline-rutile maturity index and the interdependence of the composition of heavy mineral assemblages with the gross composition and texture of sandstones. *Journal of Sedimentary Research*, **32**, 440-450, http://doi.org/10.1306/74d70ce5-2b21-11d7-8648000102c1865d.

Ingersoll, R. 1990. Actualistic sandstone petrofacies: Discriminating modern and ancient source rocks. *Geology*, **18**, 733-736, http://doi.org/10.1130/0091-7613(1990)018<0733:ASPDMA>2.3.CO;2.

Japsen, P., Green, P.F. & Bonow, J.M. 2015. Investigation of the Burial and Exhumation History of East Greenland Based On Apatite-fission Track Analysis, Stratigraphic Landform Analysis and the Geological Record. *OTC Arctic Technology Conference*.

Johansen, T.E.S., Fossen, H. & Kluge, R. 2005. The impact of syn-faulting porosity reduction on damage zone architecture in porous sandstone: an outcrop example from the Moab Fault, Utah. *Journal of Structural Geology*, **27**, 1469-1485, http://doi.org/https://doi.org/10.1016/j.jsg.2005.01.014.

Jones, D.K. 1999a. On the uplift and denudation of the Weald. *In*: Smith, B.J., Whalley, B.W. & Warke, P.A. (eds) *Uplift, Erosion and Stability: Perspectives on Long-term Landscape Development*. Geological Society, London, Special Publications, London, **162**, 25-43.

Jones, D.K. (ed) 1999b. *On the uplift and denudation of the Weald*. Geological Society, London, Special Publications, London, **162**, 25-43.

Jordan, O.D., Gupta, S., Hampson, G.J. & Johnson, H.D. 2016. Preserved stratigraphic architecture and evolution of a net-transgressive mixed wave-and tide-influenced coastal system: the Cliff House Sandstone, northwestern New Mexico, USA. *Journal of Sedimentary Research*, **86**, 1399-1424.

Kamola, D.L. & Van Wagoner, J.C. (eds) 1995. *Stratigraphy and facies architecture of parasequences with examples from the Spring Canyon Member, Blackhawk Formation, Utah*. American Association of Petroleum Geologists memoir 64, Tulsa, Oklahoma, 27-54.

Kitamura, K., Takahashi, M., Mizoguchi, K., Masuda, K., Ito, H. & Song, S.-R. 2010. Effects of pressure on pore characteristics and permeability of porous rocks as estimated from seismic wave velocities in cores from TCDP Hole-A. *Geophysical Journal International*, **182**, 1148-1160, http://doi.org/10.1111/j.1365-246X.2010.04694.x.

Krauskopf, K. 1979. Introduction to Geochemistry, McGraw-Hill Book Co. *New York*.

Krissek, L. & Kyle, P. 2001. Geochemical Indicators of Weathering, Cenozoic Palaeoclimates, and Provenance from Fine-Grained Sediments in CRP-2/2A, Victoria Land Basin, Antarctica. *Terra Antartica*, **8**.

Kroonenberg, S. 1992. Effect of provenance, sorting and weathering on the geochemistry of fluvial sands from different tectonic and climatic environments. *Proc. 29th Int. Geol. Congr. Part A. Kyoto, Japan 1992, F. Kumon, K.M. Yu (eds.). VSP Publ., Utrecht (1994) 69-81.*

Kupecz, J.A., Gluyas, J.G. & Bloch, S. 1997a. *Reservoir Quality Prediction in Sandstones and Carbonates*. American Association of Petroleum Geologists (AAPG), Tulsa Oklahoma.

Kupecz, J.A., Gluyas, J.G., Bloch, S. & Geologists, A.A.o.P. 1997b. *Reservoir Quality Prediction in Sandstones and Carbonates*. American Association of Petroleum Geologists.

Lake, S.D. & Karner, G.D. 1987. The structure and evolution of the Wessex Basin, southern England: an example of inversion tectonics. *Tectonophysics*, **137**, 347-378, http://doi.org/https://doi.org/10.1016/0040-1951(87)90328-3.

Land, L.S. & Dutton, S.P. 1978. Cementation of a Pennsylvanian deltaic sandstone; isotopic data. *Journal of Sedimentary Research*, **48**, 1167-1176, http://doi.org/10.1306/212f761c-2b24-11d7-8648000102c1865d.

Lander, R.H. & Walderhaug, O. 1999. Predicting porosity through simulating sandstone compaction and quartz cementation. *American Association of Petroleum Geologists Bulletin*, **83**, 433-449.

Lander, R.H., Larese, R.E. & Bonnell, L.M. 2008. Toward more accurate quartz cement models: The importance of euhedral versus noneuhedral growth rates. *American Association of Petroleum Geologists Bulletin*, **92**, 1537-1563.

Law, A. 1998. Regional uplift in the English Channel: quantification using sonic velocity. *In*: Underhill, J.R. (ed) *Development, Evolution and Petroleum Geology of the Wessex Basin*. Geological Society, London, Special Publications, **133**, 187-197.

Lawrence, D.T. 1993. Evaluation of Eustasy, Subsidence, and Sediment Input as Controls on Depositional Sequence Geometries and the Synchroneity of Sequence Boundaries. *In*: Weimer, P. & Posamentier, H.W. (eds) *Siliciclastic Sequence Stratigraphy: Recent Developments and Applications*. American Association of Petroleum Geologists memoir 58, Tulsa, Oklahoma, **58**, 337-368.

Leeder, M.R., Harris, T. & Kirkby, M.J. 1998. Sediment supply and climate change: implications for basin stratigraphy. *Basin Research*, **10**, 7-18.

Lentz, N., Carr, R., Yarbrough, L., Neset, K., Lucero, B. & Kirst, T. 2014. *On-site XRF Analysis of Drill Cuttings in the Williston Basin*.

Lowe, D., Sylvester, P. & Enachescu, M. 2011. Provenance and paleodrainage patterns of Upper Jurassic and Lower Cretaceous synrift sandstones in the Flemish Pass Basin, offshore Newfoundland, east coast of Canada. *Aapg Bulletin*, **95**, 1295-1320, http://doi.org/10.1306/12081010005.

Lucas, J. & Prevot-Lucas, L. 1997. On the Genesis of Sedimentary Apatite and Phosphate-Rich Sediments *Soils and Sediments: Mineralogy and Geochemistry*. Springer Berlin Heidelberg, Berlin, Heidelberg, 249-268.

Machel, H.G. 2000. Application of Cathodoluminescence to Carbonate Diagenesis. *In*: Pagel, M., Barbin, V., Blanc, P. & Ohnenstetter, D. (eds) *Cathodoluminescence in Geosciences*. Springer Berlin Heidelberg, Berlin, Heidelberg, 271-301.

Mack, G.H. 2003. Tectonic control of sedimentation. *In*: Middleton, G.V., Church, M.J., Coniglio, M., Hardie, L.A. & Longstaffe, F.J. (eds) *Encyclopedia of Sediments and Sedimentary Rocks*. Springer Netherlands, Dordrecht, 729-734.

Macquaker, J.H.S., Taylor, K.G., Young, T.P. & Curtis, C.D. 1996. Sedimentological and geochemical controls on ooidal ironstone and 'bone-bed' formation and some comments on their sequence-stratigraphical significance. *Geological Society, London, Special Publications*, **103**, 97, http://doi.org/10.1144/GSL.SP.1996.103.01.07.

McBride, E. 1963. A Classification of Common Sandstones. *Journal of Sedimentary Research*, **33**, 664-669, http://doi.org/10.1306/74D70EE8-2B21-11D7-8648000102C1865D.

McBride, E.F. 1989. Quartz cement in sandstones: a review. *Earth-Science Reviews*, **26**, 69-112, http://doi.org/https://doi.org/10.1016/0012-8252(89)90019-6.

McKinley, J., Worden, R. & Ruffell, A. 2003a. Smectite in sandstones: a review of the controls on occurrence and behaviour during diagenesis. *In*: Worden, R.H. & Morad, S. (eds) *Clay mineral cements in sandstones*. International Association of Sedimentologists, Special Publications 34, 109-128.

McKinley, J.M., Worden, R.H. & Ruffell, A. 2003b. Smectite in sandstones: a review of the controls on occurrence and behaviour during diagenesis. *In*: Worden, R.H. & Morad, S. (eds) *Clay mineral cements in sandstones*. International Association of Sedimentologists, Special Publications 34, 109-128.

McLimans, R.K. & Videtich, P.E. 1989. Diagenesis and Burial History of Great Oolite Limestone, Southern England1. *AAPG (Am. Assoc. Pet. Geol.) bulletin*, **73**, 1195-1205, http://doi.org/10.1306/44b4aa00-170a-11d7-8645000102c1865d.

McPhee, C., Reed, J. & Zubizarreta, I. *Core analysis. [electronic book] : a best practice guide*.

Middelburg, J.J., van der Weijden, C.H. & Woittiez, J.R.W. 1988. Chemical processes affecting the mobility of major, minor and trace elements during weathering of granitic rocks. *Chemical Geology*, **68**, 253-273, http://doi.org/https://doi.org/10.1016/0009-2541(88)90025-3.

Middleton, G.V. 1960. Chemical Composition of Sandstones. *GSA Bulletin*, **71**, 1011-1026, http://doi.org/10.1130/0016-7606(1960)71[1011:Ccos]2.0.Co;2.

Miller & Tucker, M. 1988. Microscopical techniques: Slides, Slices, Stains, Peels. Pages 86-107 *Techniques in Sedimentology*, 86-107.

Milliken, K. 2003. Late Diagenesis and Mass Transfer in Sandstone Shale Sequences. *Treatise on Geochemistry*, **7**, 159-190, http://doi.org/10.1016/B0-08-043751-6/07091-2.

Milliman, J.D., Summerhayes, C.P. & Barretto, H.T. 1975. Quaternary Sedimentation on the Amazon Continental Margin: A Model. *GSA Bulletin*, **86**, 610-614, http://doi.org/10.1130/0016-7606(1975)86<610:Qsotac>2.0.Co;2.

Morad, S. & Adin, A., Ala. 1986. Alteration of detrital Fe-Ti oxides in sedimentary rocks. *GSA Bulletin*, **97**, 567-578, http://doi.org/10.1130/0016-7606(1986)97<567:Aodfoi>2.0.Co;2.

Morad, S. & De Ros, L. 1994. Geochemistry and diagenesis of stratabound calcite cement layers within the Rannoch Formation of the Brent Group, Murchison Field, North Viking Graben (northern North Sea)—comment. *Sedimentary Geology*, **93**, 135-141.

Morad, S., Ketzer, J.M. & De Ros, L.F. 2000. Spatial and temporal distribution of diagenetic alterations in siliciclastic rocks: implications for mass transfer in sedimentary basins. *Sedimentology*, **47**, 95-120, http://doi.org/10.1046/j.1365-3091.2000.00007.x.

Morad, S., Ketzer, J.M. & De Ros, L.F. 2013. Linking Diagenesis to Sequence Stratigraphy: An Integrated Tool for Understanding and Predicting Reservoir Quality Distribution *Linking Diagenesis to Sequence Stratigraphy*, 1-36.

Needham, S.J., Worden, R.H. & McILroy, D. 2005. Experimental production of clay rims by macrobiotic sediment ingestion and excretion processes. *Journal of Sedimentary Research*, **75**, 1028-1037.

Nesbitt, H., Young, G., McLennan, S.M. & Keays, R. 1996. Effects of Chemical Weathering and Sorting on the Petrogenesis of Siliciclastic Sediments, with Implications for Provenance Studies. *The Journal of Geology*, **104**, 525-542, http://doi.org/10.1086/629850.

Nesbitt, H.W. & Young, G. 1982. Early Proterozoic climates and plate motions inferred from major element chemistry of lutites. *Nature*, **299**, http://doi.org/10.1038/299715a0.

Neuzil, C.E. 2003. Hydromechanical coupling in geologic processes. *Hydrogeology Journal*, **11**, 41-83, http://doi.org/10.1007/s10040-002-0230-8.

Newell, A.J. 2000. Fault activity and sedimentation in a marine rift basin (Upper Jurassic, Wessex Basin, UK). *Journal of the Geological Society*, **157**, 83-92.

Nguyen, D., Jr, H. & Kaess, A. 2016. Diagenesis, plagioclase dissolution and preservation of porosity in Eocene and Oligocene sandstones at the Greeley oil field, southern San Joaquin basin, California, USA. *Geological Society, London, Special Publications*, **435**, SP435.414, http://doi.org/10.1144/SP435.14.

Odin, G.S. 1990. Clay mineral formation at the continent-ocean boundary: the verdine facies. *Clay minerals*, **25**, 477-483, http://doi.org/10.1180/claymin.1990.025.4.06.

Odom, I.E., Doe, T.W. & Dott, R.H. 1976. Nature of feldspar-grain size relations in some quartz-rich sandstones. *Journal of Sedimentary Research*, **46**, 862-870, http://doi.org/10.1306/212f7077-2b24-11d7-8648000102c1865d.

Orem, W. & Finkelman, R. 2003. Coal formation and geochemistry. *In*: Michael, W.D. (ed) *Treatise on Geochemistry*. Elsevier, Amsterdam, **7**, 191-223.

Palci, F., Fraser, A., Carles, M., Neumaier, M., Sanderson, S. & Wallace, R. 2018a. Unconventional Hydrocarbon Potential of the Weald Basin, Southern England, United Kingdom. *AAPG ACE 2018*. American Association of Petroleum Geologists, Salt Lake City, Utah.

Palci, F., Fraser, A., Carles, M., Neumaier, M., Sanderson, S. & Wallace, R. 2018b. Unconventional Hydrocarbon Potential of the Weald Basin, Southern England, United Kingdom. *AAPG (Am. Assoc. Pet. Geol.) ACE 2018*. American Association of Petroleum Geologists, Salt Lake City, Utah.

Parnell, J. 2002. Diagenesis and fluid flow in response to uplift and exhumation. *Geological Society of London, Special Publications*, **196**, 443-466.

Parnell, J., Doré, A.G., Cartwright, J.A., Stoker, M.S., Turner, J.P. & White, N. 2002. Diagenesis and fluid flow in response to uplift and exhumation *Exhumation of the North Atlantic Margin: Timing, Mechanisms and Implications for Petroleum Exploration*. Geological Society of London, **196**, 0.

Parrish, R., Parrish, C. & Lasalle, S. 2018a. Vein calcite dating reveals Pyrenean orogen as cause of Paleogene deformation in southern England. *Journal of the Geological Society*, **175**, jgs2017-2107, http://doi.org/10.1144/jgs2017-107.

Parrish, R.R., Parrish, C.M. & Lasalle, S. 2018b. Vein calcite dating reveals Pyrenean orogen as cause of Paleogene deformation in southern England. *Journal of the Geological Society*, **175**, 425-442, http://doi.org/10.1144/jgs2017-107.

Paxton, S., Szabo, J.O., Ajdukiewicz, J. & Klimentidis, R. 2002. Construction of an intergranular volume compaction curve for evaluating and predicting compaction and porosity loss in rigid-grain sandstone reservoirs. *Aapg Bulletin*, **86**, 2047-2067, http://doi.org/10.1306/61EEDDFA-173E-11D7-8645000102C1865D.

Pemberton, G., Maceachern, J., Dashtgard, S., Bann, K., Gingras, M. & Zonneveld, J.-P. (eds) 2012a. *Shorefaces*. Developments in Sedimentology, **64**, 563-603.

Pemberton, G., Maceachern, J., Dashtgard, S., Bann, K., Gingras, M. & Zonneveld, J.-P. 2012b. Shorefaces. *In*: Knaust, D. & Bromley, R.G. (eds) *Trace Fossils as Indicators of Sedimentary Environments*. Developments in Sedimentology, **64**, 563-603.

Pettijohn, F.J., Potter, P.E. & Siever, R. 1973. *Sand and sandstone*. Springer-Verlag, New York.

Pharaoh, T. 2018. The Anglo-Brabant Massif: Persistent but enigmatic palaeo-relief at the heart of western Europe. *Proceedings of the Geologists' Association*, **129**, 278-328, http://doi.org/https://doi.org/10.1016/j.pgeola.2018.02.009.

Pirrie, D., Butcher, A.R., Power, M.R., Gottlieb, P. & Miller, G.L. 2004. Rapid quantitative mineral and phase analysis using automated scanning electron microscopy (QemSCAN): Potential applications in forensic geoscience. *In*: Pye, K. & Croft, D.J. (eds) *Forensic Geoscience: Principles, Techniques and Applications*. Geological Society, Bath, **232**, 123-136.

Pittman, E.D., Larese, R.E. & Heald, M.T. 1992. Clay coats: Occurrence and relevance to preservation of porosity in sandstones.

Posamentier, H.W. & Vail, P.R. 1988. Eustatic Controls on Clastic Deposition II—Sequence and Systems Tract Models. *In*: Wilgus, C.K., Hastings, B.S., Ross, C.A., Posamentier, H.W., Van Wagoner, J. & Kendall, C.G.S.C. (eds) *Sea-Level Changes: An Integrated Approach*. Society for Sedimentary Geology, **42**, 125-154.

Potter, P.E. 1978. Petrology and Chemistry of Modern Big River Sands. *The Journal of Geology*, **86**, 423-449.

Potts, P.J. & Webb, P.C. 1992. X-ray fluorescence spectrometry. *Journal of Geochemical Exploration*, **44**, 251-296, http://doi.org/https://doi.org/10.1016/0375-6742(92)90052-A.

Pullan, C.P. & Butler, M. 2019. Paleozoic gas potential in the Weald Basin of southern England. *Geological Society, London, Special Publications*, **471**, 333-363.

Radley, J.D. 2006. A Wealden guide; I,; The Weald sub-basin. *Geology Today*, **22**, 109-118.

Rahman, M. & Worden, R.H. 2016a. Diagenesis and its impact on the reservoir quality of Miocene sandstones (Surma Group) from the Bengal Basin, Bangladesh. *Marine and Petroleum Geology*, **77**, http://doi.org/10.1016/j.marpetgeo.2016.07.027.

Rahman, M.J.J. & Worden, R.H. 2016b. Diagenesis and its impact on the reservoir quality of Miocene sandstones (Surma Group) from the Bengal Basin, Bangladesh. *Marine and Petroleum Geology*, **77**, 898-915, http://doi.org/10.1016/j.marpetgeo.2016.07.027.

Ramm, M. 1992. Porosity-depth trends in reservoir sandstones: theoretical models related to Jurassic sandstones offshore Norway. *Marine and Petroleum Geology*, **9**, 553-567, http://doi.org/https://doi.org/10.1016/0264-8172(92)90066-N.

Ramm, M. & Bjørlykke, K. 1994. Porosity/depth trends in reservoir sandstones: Assessing the quantitative effects of varying pore-pressure, temperature history and mineralogy, Norwegian Shelf data. *Clay minerals*, **29**, 475-490.

Ramm, M., Forsberg, A.W. & Jahren, J.S. 1997a. Porosity--Depth Trends in Deeply Buried Upper Jurassic Reservoirs in the Norwegian Central Graben: An Example of Porosity Preservation Beneath the Normal Economic Basement by Grain-Coating Microquartz. *In*: Kupecz, J.A., Gluyas, J.G. & Bloch, S. (eds) *Reservoir Quality Prediction in Sandstones and Carbonates*. AAPG (Am. Assoc. Pet. Geol.) Memoir, **69**, 177-200.

Ramm, M., Forsberg, A.W., Jahren, J.S., Kupecz, J.A., Gluyas, J. & Bloch, S. 1997b. Porosity-Depth Trends in Deeply Buried Upper Jurassic Reservoirs in the Norwegian Central Graben: An Example of Porosity Preservation Beneath the Normal Economic Basement by Grain-Coating Microquartz *Reservoir Quality Prediction in Sandstones and Carbonates*. American Association of Petroleum Geologists, **69**, 0.

Reinson, G.E., Bureau of Mineral Resources, G. & Geophysics. 2015. *Hydrology and sediments of a temperate estuary - Mallacoota Inlet, Victoria*. Bureau of Mineral Resources, Geology and Geophysics, http://catalogue.aodn.org.au/geonetwork/srv/eng/metadata.show?uuid=a05f7892-9cfe-7506-e044-00144fdd4fa6, https://researchdata.edu.au/hydrology-sediments-temperate-inlet-victoria

Renard, F. & Ortoleva, P. 1997. Water films at grain-grain contacts: Debye-Hückel, osmotic model of stress, salinity, and mineralogy dependence. *Geochimica et Cosmochimica Acta*, **61**, 1963-1970, http://doi.org/https://doi.org/10.1016/S0016-7037(97)00036-7.

Rice-Birchall, E., Faulkner, D. & Bedford, J. 2021. The manufacture, mechanical properties, and microstructural analysis of synthetic quartz-cemented sandstones. *International Journal of Rock Mechanics and Mining Sciences*, http://doi.org/10.1016/j.ijrmms.2021.104869.

Rider, M.H. 1986. *The geological interpretation of well logs*. John Wiley and Sons, Inc, United States.

Rijkers, R., Duin, E., Dusar, M. & Langenaeker, V. 1993. Crustal structure of the London–Brabant Massif, southern North Sea. *Geological Magazine*, **130**, 569-574, http://doi.org/10.1017/S0016756800020860.

Rowe, H., Hughes, N. & Robinson, K. 2012. The quantification and application of handheld energy-dispersive x-ray fluorescence (ED-XRF) in mudrock chemostratigraphy and geochemistry. *Chemical Geology*, **324-325**, 122-131, http://doi.org/https://doi.org/10.1016/j.chemgeo.2011.12.023.

Ruffell, A.H. & Rawson, P.F. 1994. Palaeoclimate control on sequence stratigraphic patterns in the late Jurassic to mid-Cretaceous, with a case study from Eastern England. *Palaeogeography, Palaeoclimatology, Palaeoecology*, **110**, 43-54, http://doi.org/https://doi.org/10.1016/0031-0182(94)90109-0.

Ruttenberg, K.C. & Berner, R.A. 1993. Authigenic apatite formation and burial in sediments from non-upwelling, continental margin environments. *Geochimica et Cosmochimica Acta*, **57**, 991-1007, http://doi.org/https://doi.org/10.1016/0016-7037(93)90035-U.

Salah, M.K., El Ghandour, M.M. & Abdel-Hameed, A.M.T. 2016. Effect of diagenesis on the petrophysical properties of the Miocene rocks at the Qattara Depression, north Western Desert, Egypt. *Arabian Journal of Geosciences*, **9**, http://doi.org/10.1007/s12517-015-2275-8.

Sano, Y., Shirai, K., Takahata, N., Hirata, T. & Sturchio, N.C. 2005. Nano-SIMS Analysis of Mg, Sr, Ba and U in Natural Calcium Carbonate. *Analytical Sciences*, **21**, 1091-1097, http://doi.org/10.2116/analsci.21.1091.

Scherer, M. 1987. Parameters influencing porosity in sandstones: a model for sandstone porosity prediction. *Aapg Bulletin*, **71**, 485-491.

Schmid, S., Worden, R.H. & Fisher, Q.J. 2004. Diagenesis and reservoir quality of the Sherwood Sandstone (Triassic), Corrib Field, Slyne Basin, west of Ireland. *Marine and Petroleum Geology*, **21**, 299-315, http://doi.org/10.1016/j.marpetgeo.2003.11.015.

Scholle, P.A. & Ulmer-Scholle, D.S. 2003. *A Color Guide to the Petrography of Carbonate Rocks: Grains, Textures, Porosity,Diagenesis*. American Association of Petroleum Geologists memoir, Tulsa, Oklahoma.

Schwab, F.L. 1975. Framework mineralogy and chemical composition of continental margin-type sandstone. *Geology*, **3**, 487-490, http://doi.org/10.1130/0091-7613(1975)3<487:Fmacco>2.0.Co;2.

Scotchman, I., Johnes, L. & Miller, R. 1989. Clay diagenesis and oil migration in Brent Group sandstones of NW Hutton Field, UK North Sea. *Clay minerals*, **24**, 339-374.

Scotese, C.R. 2001. *Atlas of earth history*. PALEOMAP project.

Seilacher, A. 1967. Bathymetry of trace fossils. *Marine geology*, **5**, 413-428.

Sellwood, B.W., Scott, J. & Lunn, G. 1986. Mesozoic basin evolution in Southern England. *Proceedings of the Geologists' Association*, **97**, 259-289, http://doi.org/http://dx.doi.org/10.1016/S0016-7878(86)80020-7.

Sellwood, B.W., Scott, J., Mikkelsen, P. & Akroyd, P. 1985. Stratigraphy and sedimentology of the Great Oolite Group in the Humbly Grove Oilfield, Hampshire. *Marine and Petroleum Geology*, **2**, 44-55, http://doi.org/http://dx.doi.org/10.1016/0264-8172(85)90047-9.

Senftle, J. & Landis, C.R. 1991. Vitrinite Reflectance as a Tool To Assess Thermal Maturity: Chapter 12: GEOCHEMICAL METHODS AND EXPLORATION.

Sheldon, H., Wheeler, J., Worden, R.H. & Cheadle, M. 2003. An Analysis of the Roles of Stress, Temperature, and pH in Chemical Compaction of Sandstones. *Journal of Sedimentary Research*, **73**, http://doi.org/10.1306/070802730064.

Sibley, D.F. & Blatt, H. 1976. Intergranular pressure solution and cementation of the Tuscarora orthoquartzite. *Journal of Sedimentary Research*, **46**, 881-896, http://doi.org/10.1306/212f7081-2b24-11d7-8648000102c1865d.

Siever, R. 1959. Petrology and geochemistry of silica cementation in some Pennsylvanian sandstones.

Sladen, C. & Batten, D. 1984. Source-area environments of Late Jurassic and Early Cretaceous sediments in southeast England. *Proceedings of the Geologists' Association*, **95**, 149-163.

Sun, S.Q. 1989. A new interpretation of the Corallian (Upper Jurassic) cycles of the Dorset coast, southern England. *Geological Journal*, **24**, 139-158.

Sun, S.Q. 1992. A storm-dominated offshore sandstone interval from the Corallian Group (Upper Jurassic), Weald Basin, southern England. *Marine and Petroleum Geology*, **9**, 274-286.

Surdam, R. & Crossey, L.J. 1985. Organic-inorganic reactions during progressive burial: key to porosity and permeability enhancement and preservation. *Philosophical Transactions of the Royal Society of London. Series A, Mathematical and Physical Sciences*, **315**, 135-156.

Swarbrick, R.E. 1999. Diagenesis in North Sea HPHT clastic reservoirs—Consequences for porosity and overpressure prediction. *Marine and Petroleum Geology*, **16**, 337-353.

Tada, R. & Siever, R. 2003. Pressure Solution During Diagenesis. *Annu. Rev. Earth Planet. Sci.*, **17**, 89-118, http://doi.org/10.1146/annurev.ea.17.050189.000513.

Talbot, M.R. 1973. Major sedimentary cycles in the corallian beds (Oxfordian) of Southern England. *Palaeogeography, Palaeoclimatology, Palaeoecology*, **14**, 293-317, http://doi.org/https://doi.org/10.1016/0031-0182(73)90014-X.

Taylor, A. & Goldring, R. 1993. Description and analysis of bioturbation and ichnofabric. *Journal of the Geological Society*, **150**, 141-148.

Taylor, K. 1990. Berthierine from the Non-Marine Wealden (Early Cretaceous) Sediments of South-East England. *Clay minerals*, **25**, 391-399, http://doi.org/10.1180/claymin.1990.025.3.13.

Taylor, S.P., Sellwood, B.W., Gallois, R.W. & Chambers, M.H. 2001. A sequence stratigraphy of the Kimmeridgian and Bolonian stages (late Jurassic): Wessex–Weald Basin, southern England. *Journal of the Geological Society*, **158**, 179-192, http://doi.org/10.1144/jgs.158.1.179.

Taylor, T., Kittridge, M., Winefield, P., Bryndzia, L. & Bonnell, L. 2015. Reservoir Quality and Rock Properties Modelling – Triassic and Jurassic Sandstones, Greater Shearwater Area, UK Central North Sea. *Marine and Petroleum Geology*, **65**, http://doi.org/10.1016/j.marpetgeo.2015.03.020.

Taylor, T.R., Giles, M.R., Hathon, L.A., Diggs, T.N., Braunsdorf, N.R., Birbiglia, G.V., Kittridge, M.G., Macaulay, C.I., *et al.* 2010. Sandstone diagenesis and reservoir quality prediction: Models, myths, and reality. *Aapg Bulletin*, **94**, 1093-1132.

The British Geological Survey 2020. The BGS Lexicon of Named Rock Units [online]. https://www.bgs.ac.uk/technologies/the-bgs-lexicon-of-named-rock-units/.

Thomson, A. & Ireland, H.A. 1959. Pressure Solution and Porosity *Silica in Sediments*. SEPM Society for Sedimentary Geology, **7**, 0.

Tiab, D. & Donaldson, E.C. 2012. *Petrophysics. [electronic book] : theory and practice of measuring reservoir rock and fluid transport properties*. Boston : Gulf Professional Pub./Elsevier, 2012.

3rd ed.

Tobin, R.C. & Schwarzer, D. 2013. Effects of sandstone provenance on reservoir quality preservation in the deep subsurface; experimental modelling of deep-water sand in the Gulf of Mexico. *Special Publication - Geological Society of London*, **386**, http://doi.org/10.1144/SP386.17.

Trueman, S. 2003a. The Humbly Grove, Herriard, Storrington, Singleton, Stockbridge, Goodworth, Horndean, Palmers Wood, Bletchingley and Albury Fields, Hampshire, Surrey and Sussex, UK Onshore. *In*: Gluyas, J.G. & Hichens, H.M. (eds) *United Kingdom Oil and Gas Fields Commemorative Millennium Volume*. Geological Society, Memoirs, London, **20**, 929-941.

Trueman, S. 2003b. The Humbly Grove, Herriard, Storrington, Singleton, Stockbridge, Goodworth, Horndean, Palmers Wood, Bletchingley and Albury Fields, Hampshire, Surrey and Sussex, UK Onshore. *Geological Society, London, Memoirs*, **20**, 929-941, http://doi.org/10.1144/gsl.mem.2003.020.01.79.

Tucker, M. 1981. *Sedimentary petrology: an introduction*. Blackwell Scientific Publications, Oxford.

Tucker, M. 1988. Techniques in Sedimentology. *Blackwell*.

Tucker, M.E. 1985. Shallow-marine carbonate facies and facies models. *Geological Society, London, Special Publications*, **18**, 147-169, http://doi.org/10.1144/gsl.sp.1985.018.01.08.

Vakarelov, B.K., Ainsworth, R.B. & MacEachern, J.A. 2012. Recognition of wave-dominated, tide-influenced shoreline systems in the rock record: Variations from a microtidal shoreline model. *Sedimentary Geology*, **279**, 23-41.

Valloni, R. & Maynard, J.B. 1981. Detrital modes of recent deep-sea sands and their relation to tectonic setting: a first approximation. *Sedimentology*, **28**, 75-83, http://doi.org/https://doi.org/10.1111/j.1365-3091.1981.tb01664.x.

Villagómez Díaz, D., Omodeo-Salé, S., Ulyanov, A. & Moscariello, A. 2021. Insights into the thermal history of north-eastern Switzerland—Apatite fission track dating of deep drill core samples from the Swiss Jura mountains and the Swiss Molasse Basin. *Geosciences*, **11**, 10.

Virolle, M., Brigaud, B., Beaufort, D., Patrier, P., Abdelrahman, E., Thomas, H., Portier, E., Samson, Y., *et al.* 2021. Authigenic berthierine and incipient chloritization in shallowly buried sandstone reservoirs: Key role of the source-to-sink context. *GSA Bulletin*, http://doi.org/10.1130/b35865.1.

Vuillemin, A., Wirth, R., Kemnitz, H., Schleicher, A., Friese, A., Bauer, K., Simister, R., Nomosatryo, S., *et al.* 2019. Formation of diagenetic siderite in modern ferruginous sediments. *Geology*, **47**, http://doi.org/10.1130/G46100.1.

Wagoner, J.C., Mitchum, R.M., Campion, K. & Rahmanian, V.D. 1990. Siliciclastic sequences in well logs, cores and outcrops: Concepts for High-Resolution Correlation of Time and Facies. *In*: Wagoner, J.C. (ed.) *Methods In Exploration Series*. American Association of Petroleum Geologists, Tulsa, Oklahoma.

Walderhaug, O. 1994a. Temperatures of quartz cementation in Jurassic sandstones from the Norwegian continental shelf; evidence from fluid inclusions. *Journal of Sedimentary Research*, **64**, 311-323, http://doi.org/10.1306/d4267d89-2b26-11d7-8648000102c1865d.

Walderhaug, O. 1994b. Precipitation rates for quartz cement in sandstones determined by fluid-inclusion microthermometry and temperature-history modeling. *Journal of Sedimentary Research*, **64**, 324-333.

Walderhaug, O. 2000. Modeling quartz cementation and porosity in Middle Jurassic Brent Group sandstones of the Kvitebjørn field, northern North Sea. *AAPG (Am. Assoc. Pet. Geol.) bulletin*, **84**, 1325-1339.

Walderhaug, O. & Bjørkum, P.A. 1998. Calcite Cement in Shallow Marine Sandstones: Growth Mechanisms and Geometry *Carbonate Cementation in Sandstones*, 179-192.

Walker, R.G. & Plint, G. 1992. Wave-and Storm-Dominated Shallow Marine Systems. *In*: Walker, R.G. & James, N.P. (eds) *Facies Models: A response to Sea Level Change*. Geological Association of Canada, Newfoundland, **1**, 219-238.

Walker, R.G. & James, N.P. 1992. Facies models: Response to sea-level change: Geological Association of Canada. *Geotext*, **1**, 409.

Waples, D. 1998. Basin modelling: how well have we done? In: Basin Modelling: Practice and Progress. *Geological Society, London, Special Publications*, **141**, 1-14, http://doi.org/10.1144/GSL.SP.1998.141.01.01.

Wentworth, C.K. 1922. A Scale of Grade and Class Terms for Clastic Sediments. *The Journal of Geology*, **30**, 377-392.

Weyl, P.K. 1959. Pressure solution and the force of crystallization: a phenomenological theory. *Journal of Geophysical Research (1896-1977)*, **64**, 2001-2025, http://doi.org/https://doi.org/10.1029/JZ064i011p02001.

Wilkinson, M. & Haszeldine, R.S. 2011. Oil charge preserves exceptional porosity in deeply buried, overpressured, sandstones: Central North Sea, UK. *Journal of the Geological Society*, **168**, 1285-1295.

Williams, M.E. 2003. The development of hiatal surfaces in the Osmington Mills ironstone member of the upper jurassic ringstead formation of south Dorset, England. *Proceedings of the Geologists' Association*, **114**, 193-210, http://doi.org/https://doi.org/10.1016/S0016-7878(03)80013-5.

Wilson, M.D. 1994. Reservoir quality assessment and prediction in clastic rocks.

Wilson, M.D. & Stanton, P.T. 1994. Diagenetic mechanisms of porosity and permeability reduction and enhancement.

Wilson, M.D., Houseknecht, D.W. & Pittman, E.D. 1992. Inherited Grain-Rimming Clays in Sandstones from Eolian and Shelf Environments: Their Origin and Control on Reservoir Properties *Origin, Diagenesis, and Petrophysics of Clay Minerals in Sandstones*. SEPM Society for Sedimentary Geology, **47**, 0.

Wooldridge, L.J., Worden, R.H., Griffiths, J. & Utley, J.E.P. 2017. Clay-Coated Sand Grains In Petroleum Reservoirs: Understanding Their Distribution Via A Modern Analogue. *Journal of Sedimentary Research*, **87**, 338-352.

Wooldridge, L.J., Worden, R.H., Griffiths, J. & Utley, J.E.P. 2018. The origin of clay-coated sand grains and sediment heterogeneity in tidal flats. *Sedimentary Geology*, **373**, 191-209, http://doi.org/10.1016/j.sedgeo.2018.06.004.

Worden, R., Allen, M., Faulkner, D., Utley, J., Bond, C., Alcalde, J., Heinemann, N., Haszeldine, R.S., *et al.* 2020a. Lower Cretaceous Rodby and Palaeocene Lista Shales: Characterisation and Comparison of Top-Seal Mudstones at Two Planned CCS Sites, Offshore UK. *Minerals*, **10**, 691, http://doi.org/10.3390/min10080691.

Worden, R.H. 1998. Dolomite cement distribution in a sandstone from core and wireline data: the Triassic fluvial Chaunoy Formation, Paris Basin. *Geological Society, London, Special Publications*, **136**, 197-211, http://doi.org/10.1144/GSL.SP.1998.136.01.17.

Worden, R.H. 2005. ANALYTICAL METHODS | Geochemical Analysis (Including X-ray), 54-76.

Worden, R.H. & Morad, S. 2000. Quartz Cementation in Oil Field Sandstones: A Review of the Key Controversies. *Spec. Publ. Int. Assoc. Sed.*, **29**, 1-20, http://doi.org/10.1002/9781444304237.ch1.

Worden, R.H. & Burley, S.D. 2003a. Sandstone diagenesis: the evolution of sand to stone. *Sandstone diagenesis: Recent and ancient*, **4**, 3-44.

Worden, R.H. & Burley, S.D. 2003b. Sandstone diagenesis: the evolution from sand to stone. *In*: Burley, S.D. & Worden, R.H. (eds) *Sandstone diagenesis, recent and ancient. International Association of Sedimentologists Reprint Series*, **4**, 3-44.

Worden, R.H. & Morad, S. 2003a. *Clay minerals in sandstones: controls on formation, distribution and evolution*. Wiley Online Library.

Worden, R.H. & Morad, S. 2003b. Clay Minerals in Sandstones: Controls on Formation, Distribution and Evolution. *In*: Worden, R.H. & Morad, S. (eds) *Clay mineral cements in sandstones*. International Association of Sedimentologists, **34**, 3-41.

Worden, R.H., Oxtoby, N.H. & Smalley, P.C. 1998. Can oil emplacement prevent quartz cementation in sandstones? *Petroleum Geoscience*, **4**, 129-137.

Worden, R.H., Bukar, M. & Shell, P. 2018a. The effect of oil emplacement on quartz cementation in a deeply buried sandstone reservoir. *Aapg Bulletin*, **102**, 49-75, http://doi.org/10.1306/02071716001.

Worden, R.H., Benshatwan, M.S., Potts, G.J. & Elgarmadi, S.M. 2016. Basin-scale fluid movement patterns revealed by veins: Wessex Basin, UK. *Geofluids*, **16**, 149-174, http://doi.org/10.1111/gfl.12141.

Worden, R.H., Morrall, G.T., Kelly, S., Mc Ardle, P. & Barshep, D.V. 2019. A renewed look at calcite cement in marine-deltaic sandstones: the Brent Reservoir, Heather Field, northern North Sea, UK. *Geological Society, London, Special Publications*, **484**, SP484-2018-2043, http://doi.org/10.1144/SP484-2018-43.

Worden, R.H., Utley, J.E.P., Butcher, A.R., Griffiths, J., Wooldridge, L.J. & Lawan, A.Y. 2018b. Improved imaging and analysis of chlorite in reservoirs and modern day analogues: new insights for reservoir quality and provenance. *Geological Society, London, Special Publications*, **484**, SP484.410, http://doi.org/10.1144/SP484.10.

Worden, R.H., Armitage, P.J., Butcher, A.R., Churchill, J.M., Csoma, A.E., Hollis, C., Lander, R.H. & Omma, J.E. 2018c. Petroleum reservoir quality prediction: overview and contrasting approaches from sandstone and carbonate communities. *Geological Society of London Special Publications*, **435**, 1, http://doi.org/10.1144/sp435.21.

Worden, R.H., Armitage, P.J., Butcher, A., Churchill, J., Csoma, A., Hollis, C., Lander, R.H. & Omma, J. 2018d. Petroleum reservoir quality prediction: overview and contrasting approaches from sandstone and carbonate communities. *In*: Armitage, P.J., Butcher, A., Churchill, J., Csoma, A., Hollis, C., Lander, R.H., Omma, J., *et al.* (eds) *Reservoir Quality of Clastic and Carbonate Rocks: Analysis, Modelling and Prediction. Special Publication*. Geological Society, London, **435**, 1-31.

Worden, R.H., Griffiths, J., Wooldridge, L.J., Utley, J.E.P., Lawan, A.Y., Muhammed, D.D., Simon, N. & Armitage, P.J. 2020b. Chlorite in sandstones. *Earth-Science Reviews*, **204**, 103105, http://doi.org/https://doi.org/10.1016/j.earscirev.2020.103105.

Worden, R.H., Griffiths, J., Wooldridge, L.J., Utley, J.E.P., Lawan, A.Y., Muhammed, D.D., Simon, N. & Armitage, P.J. 2020c. Chlorite in sandstones. *Earth Science-Reviews*, **204**, 103105, http://doi.org/10.1016/j.earscirev.2020.103105.

Worden, R.H., Allen, M.J., Faulkner, D.R., Utley, J.E., Bond, C.E., Alcalde, J., Heinemann, N., Haszeldine, R.S., *et al.* 2020d. Lower Cretaceous Rodby and Palaeocene Lista Shales: Characterisation and Comparison of Top-Seal Mudstones at Two Planned CCS Sites, Offshore UK. *Minerals*, **10**, 691.

Wright, J.K. 1981. The Corallian rocks of north Dorset. *Proceedings of the Geologists' Association*, **92**, 17-32.

Zahm, C. & Hennings, P. 2009. Complex fracture development related to stratigraphic architecture: Challenges for structural deformation prediction, Tensleep Sandstone at the Alcova anticline, Wyoming. *Aapg Bulletin*, **93**, 1427-1446, http://doi.org/10.1306/08040909110.

Zhang, H., Peng, J., Lin, X., Li, B. & Xia, Q. 2018. Diagenesis and its controlling factors of Lower Donghetang Formation tight sandstone reservoir in Bachu area, Tarim Basin, China. *Geosciences Journal*, **22**, 327-336, http://doi.org/10.1007/s12303-017-0055-z.

Zoback, M.D. & Kohli, A.H. 2019. *Unconventional Reservoir Geomechanics: Shale Gas, Tight Oil, and Induced Seismicity*. Cambridge University Press, Cambridge.

Appendix A

Calcite cement from all three wells were analysed using cathodolumiscence (CL) analysis to determine the generations of calcite cement. CL in carbonates occurs as a result of trace elements in solid solution; these elements act as activators, sensitisers or quenchers Table A1. Activators cause luminescence in calcite, sensitisers such as Pb^{2+}, Ce^{2+} or Zn^{2+} increase luminescence by activators while quenchers such as Fe reduce luminescence (Hiatt & Pufahl 2014). Mn^{2+} and Fe^{2+} are the most common activators and quenchers in carbonates due to their abundance in nature (Machel 2000). Mn at concentrations above 20-25ppm with Fe at concentrations less than 150ppm therefore causes a bright yellow luminescence in calcite and some dolomites and orange to red luminescence in dolomite (Budd et al. 2000; Machel 2000; Hiatt & Pufahl 2014). Increase in Fe in carbonates causes darker coloration from orange to pink to red and when concentrations rise above thousands of ppm, the luminescence turns dark-red to reddish-brown to non-luminescent (Budd et al. 2000).

Activators >10-20 ppm	Sensitisers >10 ppm	Quenchers >30-35 ppm
Mn^{2+}	Pb^{2+}	Fe^{3+}
Sm^{3+}	Ce^{3+}	Fe^{2+}
Tb^{3+}		Ni^{2+}
Dy^{3+}		Co^{2+}
Eu^{3+}		
Eu^{2+}		

Appendix A 1: possible CL activators sensitisers and quenchers in carbonate rocks modified from Machel (2000)

The CL analysis was carried out on polished thin sections from PW3, PW7 and BL5. CL analysis was carried out using a Cambridge Image Technology Mk5-2 CL microscope fitted with a Cambridge Instruments optical cathodoluminescence microscope stage, a Nikon Eclipse DS-Fi1c camera and an electron gun operating at 11 kV and 400 μA.

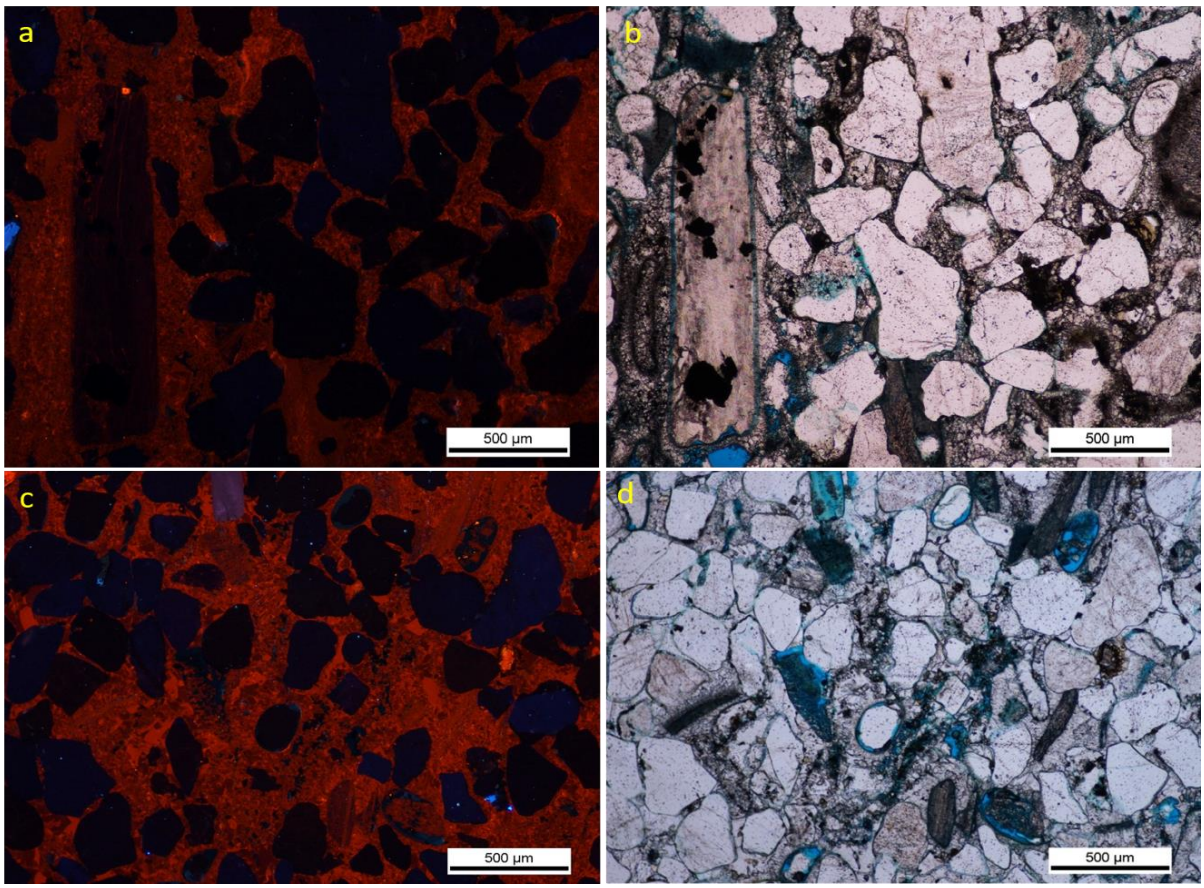

Appendix A 2: (A) PW3 (1085.09 m MD): the bivalve shell to the left is reddish brown to non-luminescent typical of deposition under oxidising conditions. At the top and to the right of it however is a dully luminescent calcite cement indicative of the gradual change in depositional conditions (c) two generations of calcite cement can be identified, both showing evidence of precipitation under suboxic conditions. Cement stratigraphy and open-framework grain texture suggests that the darker shades were deposited early with higher iron concentrations. The lighter shades are locally in the middle of pore spaces suggesting reduction in iron as diagenesis progresses.

CL analysis shows that calcite cement was deposited under sub-oxic conditions with significant iron input hence bright yellow luminescence is rare (Fig. A2). Cement stratigraphy in Figure A2 show evidence of early calcite cementation with A2a showing a predominant dark-red to reddish brown indicative of high iron content shortly after deposition. The dark coloration in the bivalve shells is typical of low manganese content in bivalves (compare bivalves in figure A2 a and A2b as well as aA2 c and A2d), however the gradation from a darker shade at grain

boundaries to a lighter shade in the middle of the pores is indicative of pore water geochemical evolution (Fig. A2c).

Appendix B

In the following paper, D.V.B carried out point counting analysis and interpretation and contributed critical feedback to the writing of the manuscript:

Worden R.H, Glenn T. Morall, Sean Kelly, Peter Mc Ardle, **Dinfa Vincent Barshep**, 2019: A renewed look at calcite cement in marine-deltaic sandstones: the Brent Reservoir, Heather Field, northern North Sea, UK (Published by the Geological Society, London, Special Publications, 484,305-335, 1 January 2019, https://doi.org/10.1144/SP484-2018-43)